8. SITE 637[1]

Shipboard Scientific Party[2]

HOLE 637A

Date occupied: 28 April 1985

Date departed: 4 May 1985

Time on hole: 6 days, 3 hr

Position: 42°05.3′N, 12°51.8′W

Water depth (sea level, corrected m, echo-sounding): 5307

Water depth (rig floor, corrected m, echo-sounding): 5317

Bottom felt (m, drill-pipe length from rig floor): 5321

Penetration (m): 285.6

Number of cores: 30

Total length of cored section (m): 285.6

Total core recovered (m): 93.0

Core recovery (%): 32

Deepest sedimentary unit cored:
Depth sub-bottom (m): 212
Nature: brown clay
Age: late Miocene(?), possibly older
Measured vertical sound velocity (km/s): 1.5 to 1.8

Igneous or metamorphic basement:
Depth sub-bottom (m): 212 (top); 285.6 (bottom of hole)
Nature: serpentinized peridotite (harzburgite)
Velocity range (km/s): 2.9 to 4.7

Principal Results: At Site 637, on the east flank of a buried ridge of basement rocks (Fig. 1) from which deeply weathered lherzolitic rocks had been dredged at a nearby outcrop, drilling established the presence of extensively serpentinized, foliated peridotite (harzburgite) beneath a cover of Neogene sediments. The main results of drilling are summarized in Figure 2.

The sedimentary section comprises three lithologic units:

1. 0–135 m: upper Pliocene to upper Pleistocene. Turbidites comprising clayey silt and olive-gray clay couplets, interbedded with nannofossil marl, which also shows evidence of redeposition.

2. 135–180 m: upper Miocene to lower Pliocene. Slumped brown clay and nannofossil marl. Interpreted as being pelagic sediment and weathering products from underlying basement, slumped off the basement hill.

3. 180–212 m: upper Miocene. Reddish brown and grayish brown clay with exotic lumps of light-colored clay. Interpreted as being mixture of pelagic clay, weathering products from underlying basement, and continental detritus brought to the site by dilute currents.

Crystalline rocks constitute the rest of the cored section. From 212 to 285.6 m, serpentinized peridotite is cut by veins of calcite. The rock is strongly foliated, the foliation being subhorizontal near the top of the basement and increasing to nearly vertical near the bottom of the hole. The dip is to the east, as determined from magnetic measurements on oriented specimens.

Standard Schlumberger logs were obtained from an interval that included about 35 m of basement rock and 110 m of the overlying sediments. The sonic log measured a nearly constant sound velocity of 1.6 km/s in the sediments; in the basement rock, velocities increased downward from 1.6 to 3.7 km/s.

Laboratory measurements of sound velocity in the peridotite yielded values ranging from 2.9 to 4.7 km/s, clustering around 3.7 km/s. Velocities are lower parallel to than normal to foliation.

BACKGROUND AND OBJECTIVES

The western Galicia margin is bounded to the west by a basement ridge trending north–south, which is approximately in line with magnetic anomaly M0, occurring to the south of the Leg 103 area (see "Introduction, Objectives, and Principal Results" chapter, this volume). The ridge is buried by sediment, except on Hill 5100, where a large sample of highly weathered peridotite was recovered by dredging (Boillot et al., 1980). This single sample seems to indicate that crustal rifting locally exposed the upper mantle along the basement ridge, which is interpreted as being along the ocean/continent boundary. Obtaining fresh samples by coring the ridge was important to verify this tentative conclusion (Fig. 3).

Studies of the mineralogy, chemistry, and structural petrology of cores were designed to address the following problems:

1. The mechanisms of rifting, e.g., crustal vs. lithospheric stretching.

2. The serpentization of upper mantle rocks near the ocean/continent boundary. When did this take place? Was it by hydro-

---

[1] Boillot, G., Winterer, E. L., Meyer, A. W., et al., *Proc., Init. Repts. (Pt. A), ODP*, 103.

[2] Gilbert Boillot (Co-Chief Scientist), Laboratoire de Géodynamique Sous-Marine, Université Pierre et Marie Curie, B. P. 48, 06230,Villefranche-sur-Mer, France; Edward L. Winterer (Co-Chief Scientist), Graduate Research Division A-012-W, Scripps Institution of Oceanography, La Jolla, CA 92093; Audrey W. Meyer (ODP Staff Scientist), Ocean Drilling Program, Texas A&M University, College Station, TX 77843-3469; Joseph Applegate, Department of Geology, Florida State University, Tallahassee, FL 32306; Miriam Baltuck, Department of Geology, Tulane University, New Orleans, LA 70118 (current address: NASA Headquarters, Code EEL, Washington, D.C. 20546); James A. Bergen, Department of Geology, Florida State University, Tallahassee, FL 32306; M. C. Comas, Departamento Estratigrafia y Paleontologia, Facultad de Ciencias, Universidad de Granada, 18001 Granada, Spain; Thomas A. Davies, Institute for Geophysics, University of Texas at Austin, 4920 North IH 35, Austin, TX 78751; Keith Dunham, Department of Atmospheric and Oceanic Sciences, University of Michigan, 2455 Hayward Avenue, Ann Arbor, MI 48109 (current address: P.O. Box 13, Pequat Lakes, MN 56478); Cynthia A. Evans, Department of Geology, Colgate University, Hamilton, NY 13346 (current address: Lamont-Doherty Geological Observatory, Palisades, NY 10964); Jacques Girardeau, Laboratoire de Materiaux Terrestres, I.P.G., 4 Place Jussieu, 75252 Paris Cedex 05, France; David Goldberg, Lamont-Doherty Geological Observatory, Palisades, NY 10964; Janet Haggerty, Department of Geology, University of Tulsa, 600 S. College Avenue, Tulsa, OK 74104; Lubomir F. Jansa, Atlantic Geoscience Center, Bedford Institute of Oceanography, Dartmouth, Nova Scotia B2Y 4A2, Canada; Jeffrey A. Johnson, Department of Earth and Space Sciences, University of California, Los Angeles, CA 90024 (current address: 9449 Briar Forest Drive, No. 3544, Houston, TX 77063); Junzo Kasahara, Earthquake Research Institute, University of Tokyo, 1,1,1 Yayoi, Bunkyo, Tokyo 113, Japan (current address: Nippon Schlumberger K.K., 2-1 Fuchinobe, 2-Chome, Sagamihara-shi, Kanagawa-ken, 229, Japan); Jean-Paul Loreau, Laboratoire de Géologie, Museum National D'Histoire Naturelle, 43 Rue Buffon, 75005 Paris, France; Emilio Luna, Hispanoil, Pez Volador No. 2, 28007 Madrid, Spain; Michel Moullade, Laboratoire de Géologie et Micropaleontologie Marines, Université de Nice, Parc Valrose, 06034 Nice Cedex, France; James Ogg, Geological Research Division A-012, Scripps Institution of Oceanography, La Jolla, CA 92093 (current address: Dept. Earth and Atmospheric Sciences, Purdue University, W. Lafayette, IN 47907); Massimo Sarti, Istituto di Geologia, Universitá di Ferrara, Corso Ercole d'Este, 32, 44100 Ferrara, Italy; Jürgen Thurow, Institut und Museum für Geologie und Paleontologie, Universität Tübingen, Sigwartstr. 10, D-7400 Tübingen, Federal Republic of Germany; Mark A. Williamson, Atlantic Geoscience Centre, Geological Survey of Canada, Bedford Institute of Oceanography, Box 1006, Dartmouth, Nova Scotia B2Y 4A2, Canada (current address: Shell Canada Ltd., P.O. Box 100, Stn. M, Calgary, Alberta T2P 2H5, Canada).

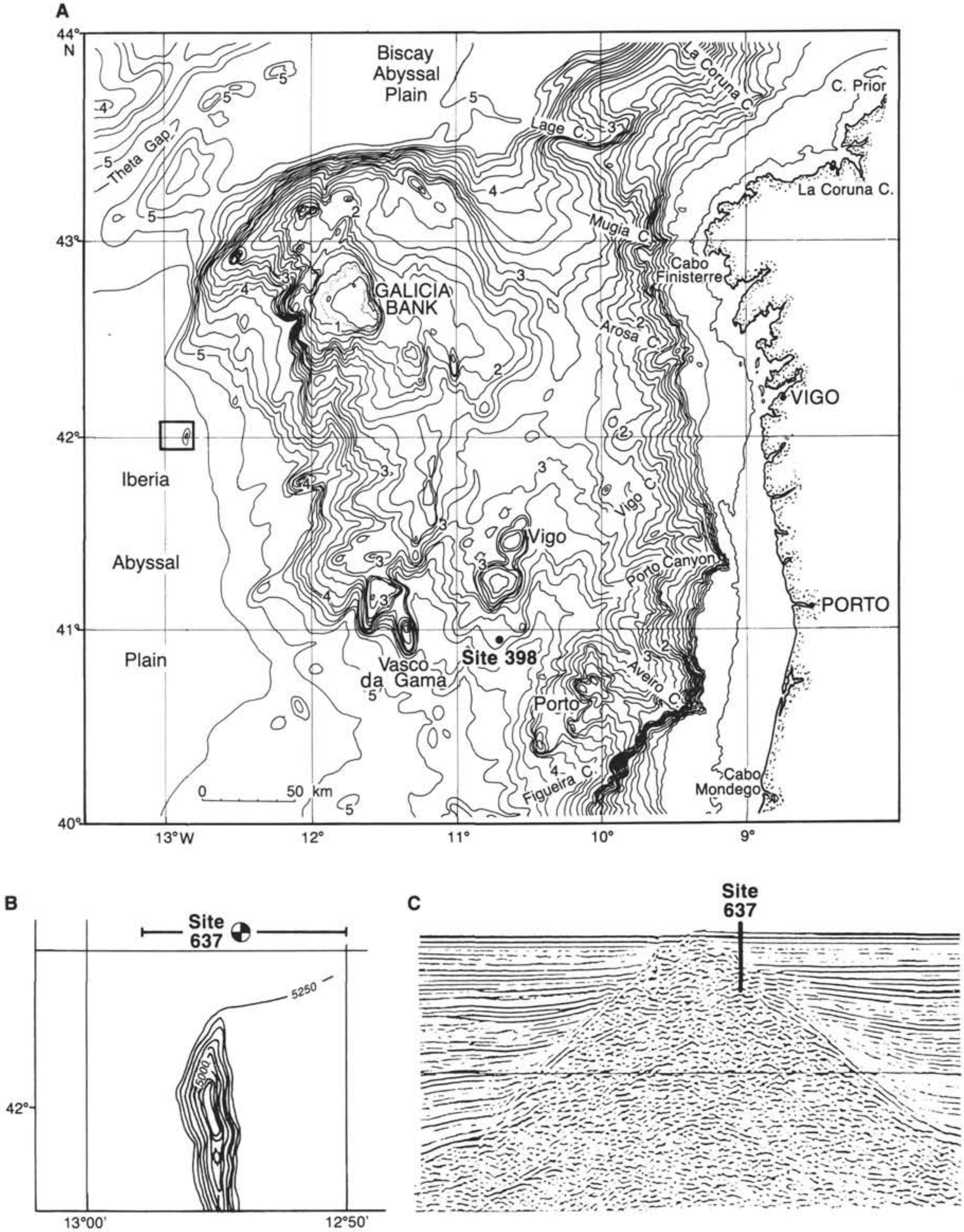

Figure 1. A. Bathymetric map of Galicia margin. Box outlines part of Sea Beam map shown in B. B. Sea Beam map showing bathymetry of basement ridge, location of Site 637, and location of profile shown in C. C. Multichannel seismic profile across Site 637. Location of profile is shown in B.

thermal processes at the beginning of oceanic accretion or was it mainly later?

3. The nature of diapiric structures at the foot of the margin. In some places, these are evaporites (Winterer and Hinz, 1984), but in other places, they may have resulted from serpentine mobility.

4. The significance in folded mountain belts of lower crustal ophiolites or mantle rocks, overlain directly by oceanic-pelagic sediments, lacking intervening gabbro and pillow basalt. In the Alpine chains, some serpentinites occur near what is thought to have been the ocean/continent boundary, as suggested for the occurrence of the serpentinites at the foot of the Galicia margin.

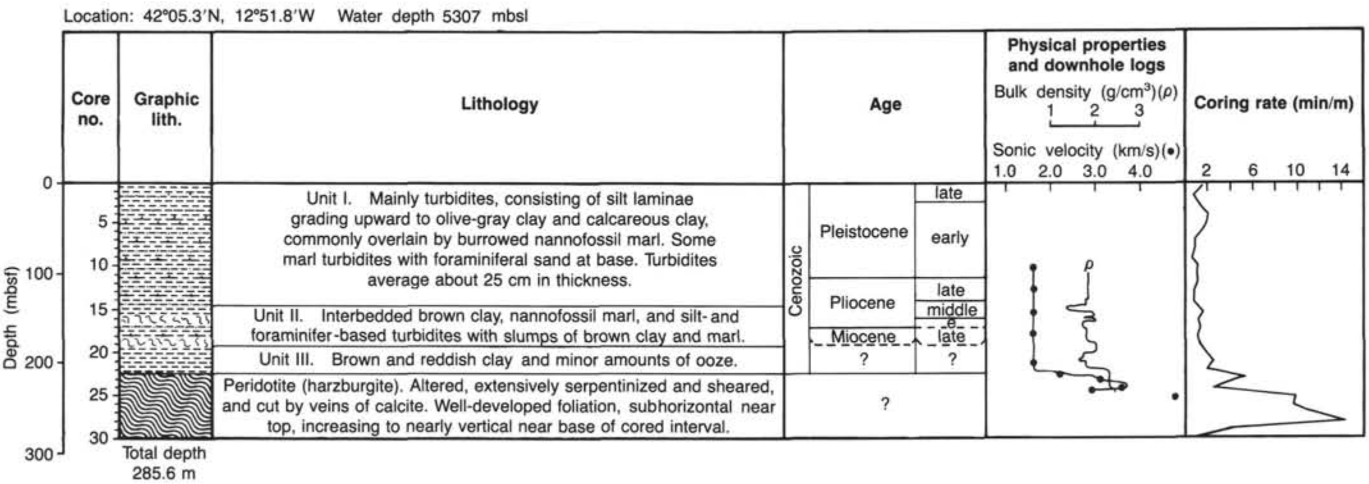

Figure 2. Stratigraphic summary log, Site 637 (Hole 637A).

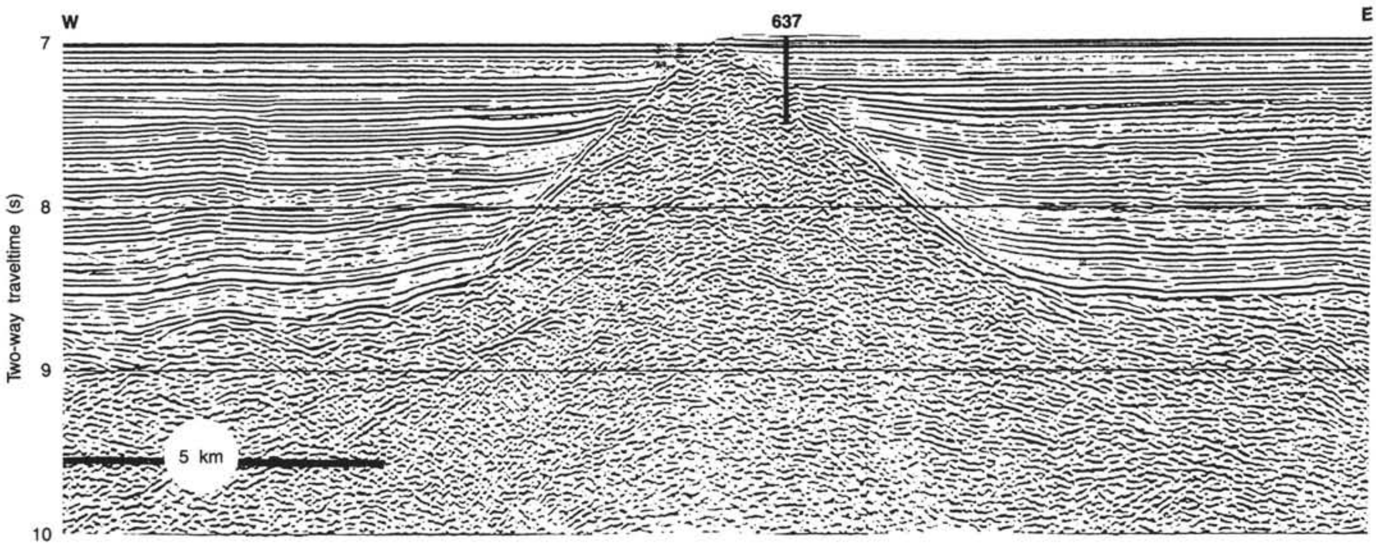

Figure 3. IFP processed multichannel seismic-reflection profile GP-12 across the buried peridotite ridge at Site 637. To the south, lherzolitic rocks have been dredged from the west flank of the ridge. Location of profile shown in Figure 4. Profile courtesy of L. Montadert.

OPERATIONS

Transit from Ponta Delgada and Approach to Site 637

Leg 103 began at 1900 hr (UTC) on 25 April 1985, when *JOIDES Resolution* sailed out of the Ponta Delgada harbor on the island of San Miguel in the Azores. The ship steamed at full speed toward a point at 47°N, 13°10′W to begin a seismic-reflection survey to locate target Site GAL-2B (later named Site 637). Unfavorable weather slowed the vessel to about 10.5 kt during much of the transit to the turning point.

During the night of 25 April, while the ship was under way at a speed of about 10 kt and the drilling crew was working on the derrick floor, the heave compensator moved from its normal secure position to its operating position; during this movement, one of the two high-pressure air hoses that service the compensator broke. Although no spare hose was on board, the SEDCO engineers assured us that the heave compensator should operate at nearly full efficiency for the rest of Leg 103.

On 27 April, we deployed two 80-in.^{3} water guns and a 100-m hydrophone streamer and began recording seismic-reflection profiles at 1400 hr. The records obtained from that time to the arrival at Site 637 are presented in the "Underway Geophysics" chapter (this volume). Because neither of the two magnetometers aboard was working, we obtained no magnetic data during Leg 103. The 3.5-kHz echo-sounder gave no useable data at speeds greater than about 8 kt, but when we slowed to about 6 kt during the approach to Site 637, the records were of normal quality. This difficulty appears to have stemmed from the location of the transducer, which is a little behind the open moon pool; at normal cruising speed, the moon pool is a maelstrom of turbulent water. The 12.5-kHz echo-sounder was inoperable during the transit from Ponta Delgada to Site 637.

At 1030 hr on 28 April, beginning at a point about 10 mi southwest of target site GAL-2B, we began a survey to locate the site. The ship was slowed to 6 kt to obtain useable 3.5-kHz data. As shown in Figure 4, the survey track took the ship along an easterly course across the small elongate hill where dredging had shown the presence of weathered serpentinized peridotite (Boillot et al., 1980). We adjusted the track to get a satellite position just before arriving at the planned location for the drill site, while steaming on a westerly course. In fact, wind and currents accelerated the ship so that we arrived over the buried hill

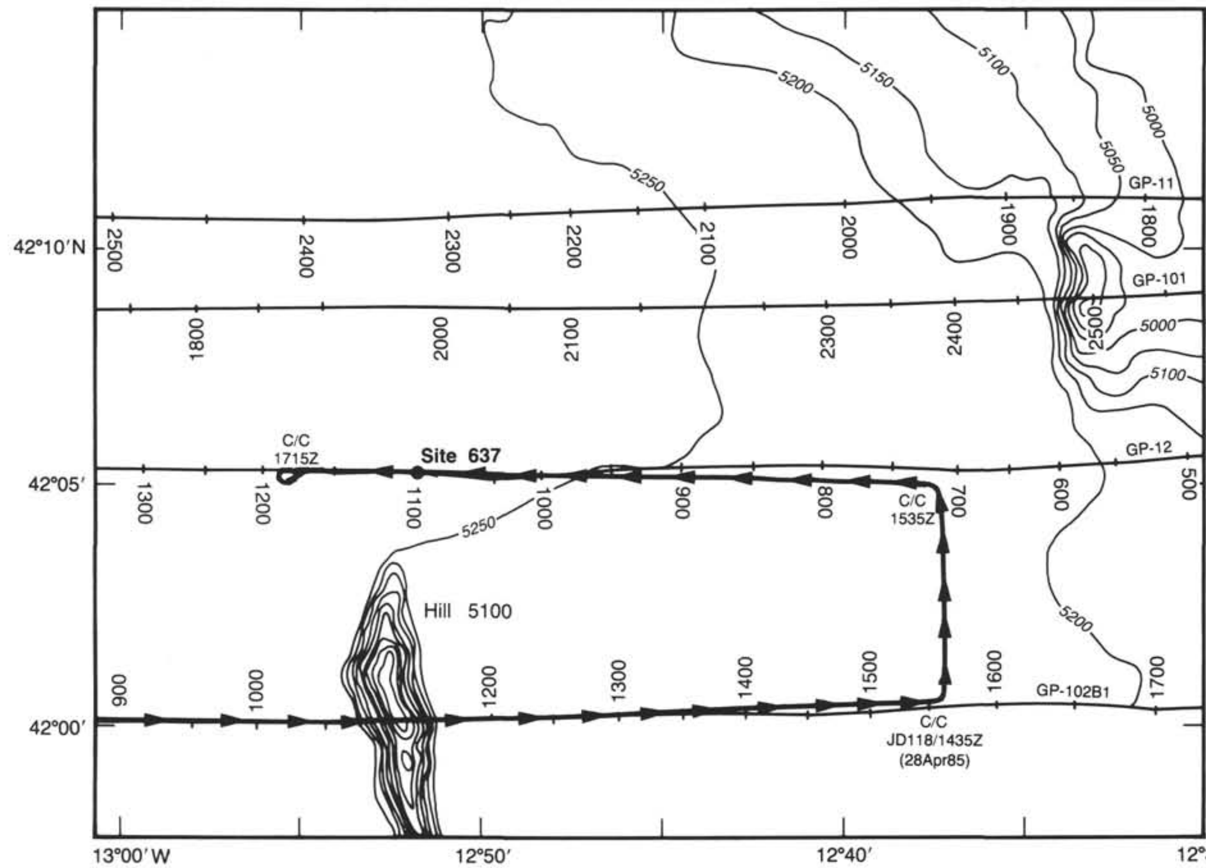

Figure 4. Approach to Site 637. The track of *JOIDES Resolution* is shown as a heavy line; arrows indicate direction of travel. The tracks for the multichannel seismic-reflection lines taken by the Institut Français du Petrole have numbered tick marks, indicating shotpoint locations. Base map from Sea Beam survey made from *Jean Charcot* during Seagal cruise, courtesy of J. C. Sibuet. Bathymetric contours in meters; contour interval, 50m.

at the drill site about 30 min earlier than expected. About 3 mi west of the summit of the buried hill, we turned the ship onto a reciprocal course and started back to find the drill site.

Inspection of the processed multichannnel seismic profiles taken across this hill by the Institut Français du Petrol, made available to us by L. Montadert (Fig. 3), and of the single-channel monitor record we made during our first crossing of the buried hill (Fig. 5) showed us that the hill was nearly symmetrical. Thus, we could position the site as well on one side of the hill as on the other if cover of soft sediments over the basement was sufficient (about 110 m) to provide support for the bottom-hole assembly (BHA). We planned to allow about 160 m, which we thought to be the equivalent of 0.2 s of sediment on the profiler records. To maintain operational simplicity, we elected to locate the site on the east flank of the hill, as explained in the following discussion.

To locate the buried hill, we had two sources of data: the seismic profiler and the 3.5-kHz recorder. Because the buried hill reaches just to the seafloor near the drill site, the hill has acted as a dam for sediments derived from the east, resulting in a seafloor level of about 30 m deeper on the west side of the hill than on the east. At our crossing, in fact, the basement itself apparently protrudes a little above the sediment cover (Fig. 6). To locate the site, we steamed east until we had crossed the hilltop and had just begun to see the reflections from the adjacent sediment-covered seafloor. From our previous study of the seismic data, we calculated that the average slope of the buried basement surface was about 15°. We calculated that, at our speed of 6 kt, the sediments should increase to a thickness of approximately 160 m by the time we had steamed 3 min eastward of the sediment pinch-outs near the hilltop. We, therefore, waited for 3 min and signaled the bridge to release the acoustic beacon at 1805 hr on 28 April (a discrepancy between lab clocks and the official ship's time, kept on the bridge, resulted in the geophysical records being marked to show the beacon release at 1807 hr).

To check the seismic picture at the point where we dropped the beacon, we steamed on eastward and marked the seismic profile 1 min 15 s after the drop, this being the time to travel the distance between the crane from which the beacon was dropped and a point halfway between the water guns and the hydrophone streamer. The record is in fact hard to read at this point, and the actual two-way reflection time to basement rock at the beacon is uncertain. We decided to prepare for drilling at the beacon and to move by a small offset from the beacon to drill a new hole should the sediments prove to be either too thin for safety or too thick for the time available to us.

Drilling and Coring Operations

For drilling and coring at Site 637, the BHA included three bumper subs, partly for extra heave compensation and partly to provide a jarring motion on the bit in hard rocks. The BHA measured about 110 m in length, the highest bumper sub being

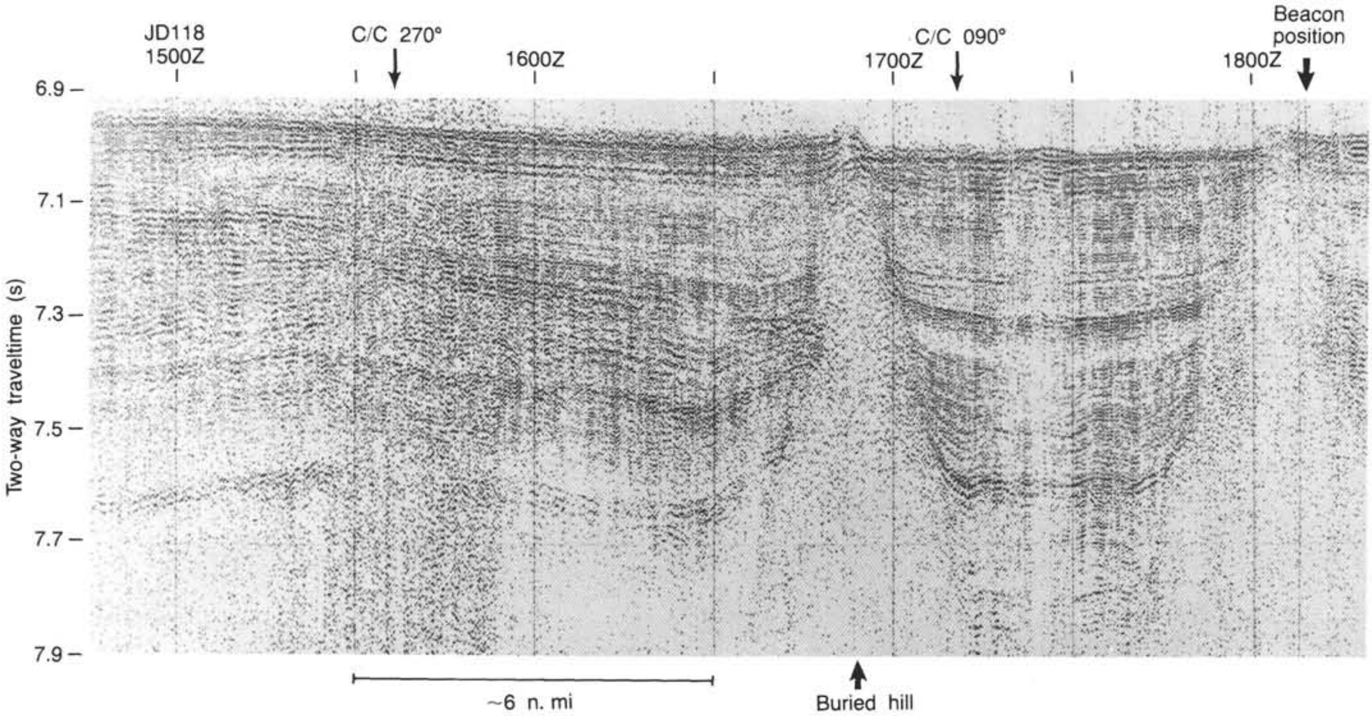

Figure 5. Seismic-reflection profile made from *JOIDES Resolution* during approach to Site 637. Location of profile shown in Figure 4. The first crossing of the buried hill was on a 270° course. Note the difference in level of the seafloor east and west of the hill, and note that the top of the hill has no apparent sediment cover. Vertical exaggeration at seafloor is about 23 ×. Buried flanks of the buried hill have roughly the same average slope of about 15°, after adjustments for the velocity of sound through the sedimentary cover. The acoustic beacon marking position of Site 637 was dropped where we thought the sediments would be about 160 m thick; drilling showed them to be 212 m thick.

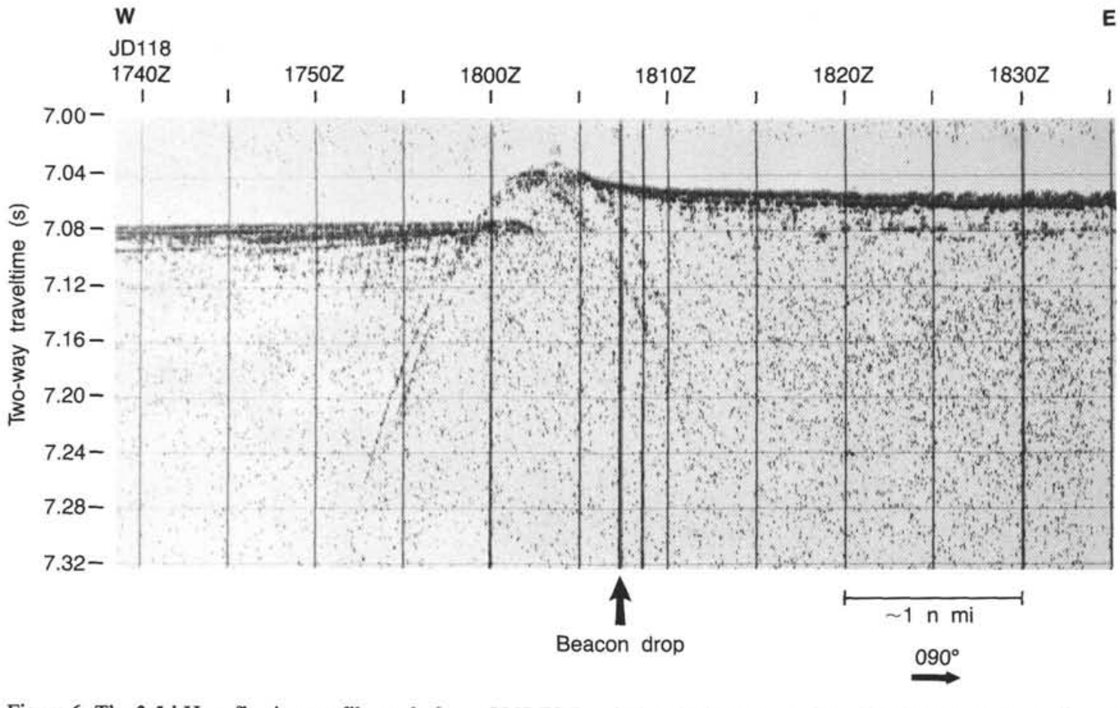

Figure 6. The 3.5-kHz reflection profile made from *JOIDES Resolution* during approach to Site 637. Note that sediments appear to pinch out on the east side of a hill slightly east of the summit.

about 73 m above the bit face. Making up the BHA and running in the drill pipe took about 19 hr because of the extra time necessary to measure the length and check the inside diameter of each piece of new drill pipe. Some minor mechanical problems developed in the alignment of the power unit that rotates the pipe and in the proper functioning of the automatic pipe racker; these also took extra time to fix.

After these adjustments, actual coring operations began. When the bit had reached a depth about 20 m shallower than the depth indicated by the 3.5-kHz echo-sounder (corrected for the velocity of sound in seawater), a core barrel was dropped into the drill string. When the barrel had been seated into the bit, the drill string was slowly lowered and new pipe added until the weight indicator showed a weight loss, signaling bit arrival at the seafloor. This depth was 5321 m below the derrick floor, according to the cumulative measured lengths of the drill-string components. The driller lowered the pipe another 3 m, to a depth of 5324 m, and lowered the overshot device, which latches onto and retrieves the core barrel, into the drill string on the sand line. At about 1840 on 29 April, the overshot device arrived back at deck level, without the core barrel, however. The device had failed to engage. To assure that no obstruction blocked the pipe, the driller circulated water freely through the bit. The overshot device was sent down again and returned with Core 103-637A-1R (Table 1). The core catcher contained about 50 cm^3 of gray silty marl, and the core barrel contained only muddy water. Despite this small recovery, we agreed to retain our decision to define the depth to the seafloor from the derrick floor as 5321 m.

The next several cores recovered almost nothing. For Core 103-637A-2R, the drill string was advanced another 12.7 m, to even out the spacing of pipe joints at the derrick floor. The coring took 19 min and required 40 rpm of bit rotation and about 50 strokes per min (spm) on the pumps. This, plus the 10,000 lb of weight on the bit, suggested that the sediments were firm. Again, the core barrel arrived empty, but a few lumps of gray marl remained in the catcher. The next three cores were likewise empty, except for traces in the core catcher. In all attempts, the actual core liner showed no trace of any sediment having been in the barrel at any time, despite our having used two different kinds of soft-sediment catchers and having cut Core 103-637A-5R without circulating water to the bit. We speculated that perhaps a stone was loose in the hole just ahead of the bit and was preventing sediment from entering the throat of the bit and passing up into the core barrel. We, therefore, elected to cut Core 103-637A-6R by circulating vigorously at about 90 spm for the upper 5 m and then reducing the pumping rate for the last 4.7 m of the 9.7-m cored interval. This procedure was designed to condition the hole and perhaps to push aside or remove any pebbles at the bottom.

Subsequently, Core 103-637A-6R recovered about 4.6 m of calcareous clay; from here throughout the rest of the sediment column, recovery rates ranged from about 17% to as much as 57%. Coring speed averaged slightly more than 1 min/m for the whole sedimentary section.

While cutting Core 103-637A-23R, at a sub-bottom depth estimated by the driller to be about 215 m, the bit encountered a hard layer, which cored at the rate of about 10 min/m. The lower part of this core contained serpentinized peridotite, and the following seven cores returned the same type of basement rock. Coring rates in this material averaged about 7 min/m. We continued coring ahead in the peridotite to try to obtain fresher samples and to provide an adequately long interval for significant downhole logging of the basement rocks. Because the coring rate for Core 103-637A-30R increased to about 1 min/m and because the recovered core contained mainly a drilling slurry of serpentinite fragments, we feared that the bit was entering a zone of potentially unstable hole conditions that could endan-

Table 1. Coring summary, Site 637 (Hole 637A).

Core no.	Date (mo./day) 1985	Time (hr)	Sub-bottom top (m)	Sub-bottom bottom (m)	Length cored (m)	Length recovered[a] (m)	Percentage recovered
1R	04/29	2045	0.0	3.0	3.0	TR	0.0
2R	04/30	0015	3.0	15.7	12.7	0.2	1.0
3R	04/30	0605	15.7	25.4	9.7	0.1	0.0
4R	04/30	0915	25.4	35.1	9.7	TR	0.0
5R	04/30	1230	35.1	44.9	9.8	TR	0.0
6R	04/30	1522	44.9	54.6	9.7	4.6	46.0
7R	04/30	1815	54.6	64.4	9.8	5.5	56.0
8R	04/30	2045	64.4	74.0	9.6	4.3	44.0
9R	04/30	2325	74.0	83.7	9.7	2.8	28.0
10R	05/01	0200	83.7	93.3	9.6	1.8	18.0
11R	05/01	0430	93.3	102.7	9.4	1.6	17.0
12R	05/01	0700	102.7	112.4	9.7	2.9	29.0
13R	05/01	0930	112.4	122.0	9.6	2.5	25.0
14R	05/01	1152	122.0	131.7	9.7	1.7	17.0
15R	05/01	1415	131.7	141.3	9.6	5.5	57.0
16R	05/01	1655	141.3	151.0	9.7	4.8	49.0
17R	05/01	1930	151.0	160.7	9.7	5.2	53.0
18R	05/01	2205	160.7	170.4	9.7	2.8	29.0
19R	05/02	0045	170.4	179.9	9.5	3.5	36.0
20R	05/02	0315	179.9	189.5	9.6	3.1	32.0
21R	05/02	0600	189.5	199.2	9.7	2.7	28.0
22R	05/02	0900	199.2	208.8	9.6	2.7	27.0
23R	05/02	1200	208.8	218.4	9.6	1.9	20.0
24R	05/02	1505	218.4	228.0	9.6	2.1	21.0
25R	05/02	1915	228.0	237.2	9.2	7.5	75.0
26R	05/02	2245	237.2	246.9	9.7	4.8	49.0
27R	05/03	0300	246.9	256.6	9.7	8.7	89.0
28R	05/03	0730	256.6	266.3	9.7	5.1	52.0
29R	05/03	1010	266.3	275.9	9.6	2.8	28.0
30R	05/03	1450	275.9	285.6	9.7	1.8	18.0

[a] TR = trace recovery.

ger not only the drilling operations but also the logging tools. Additionally, our alloted time for drilling at Site 637 was running out; therefore, we elected to terminate drilling the hole at this point, at a total depth of 285.6 m below the seafloor (mbsf). The last core was on deck at 1450 hr on 3 May 1985.

Downhole-Logging Operations

After circulating to clear the hole of cuttings, filling the hole with drilling mud, dropping the bit, and positioning the BHA within the uppermost part of the hole, logging began. For the first run, we lowered a caliper, a natural gamma, and a sonic velocity tool. The lowest 39 m of the hole had filled with cavings, so that this set of logs began at a depth of 248 m and continued to the bottom of the BHA, 100 mbsf. The second run employed natural gamma-ray spectrometry and lithodensity tools, but because of continued caving of the hole, the logs could be run only over the interval from 211 to 100 mbsf. All logs showed a marked change in properties, corresponding to the top of serpentinite basement at a depth of 212 mbsf. We, therefore, used this depth for the sediment/basement contact, rather than the depth of 215 m estimated more crudely from the change in coring rate.

We had hoped to make a third logging run, using the multichannel sonic device, but because our main interest in this tool was to learn more about the properties of the basement rocks, and because the second logging run had shown that the basement was virtually buried in cavings, we terminated the logging program at Site 637.

The logging tools were retrieved, the pipe tripped, and the ship made ready to get under way for Site 638. *JOIDES Resolution* departed Site 637 at 2105 hr on 4 May 1985.

SEDIMENT LITHOLOGY

The sedimentary section at Site 637 consists of 212 m of clay, marl, and clayey ooze; terrigenous silt layers are common in the upper part. The section can be divided into three sedimentary units, which are resting on Unit IV, the basement rock (Table 2).

Unit I (0–135 m; Core 103-637A-1R through Sample 103-637A-15R)

Unit I is 135 m thick. It can be subdivided into three subunits, although the same sediment types are present throughout. The upper part of the section, Subunit IA, is represented by only a few cubic centimeters of light- and dark-gray marl and clay recovered from the core catchers of Cores 103-637A-1R through 103-637A-5R. Although designated a separate interval, Subunit IA is most likely lithologically the same as Subunit IB.

Subunit IB, represented by Cores 103-637A-6R through 103-637A-9R, consists of olive-gray clay and nannofossil marl interbedded with thick clayey silt layers. Typically, the silt and olive-gray clay occur as couplets, or cycles, consisting of a graded silt layer, structureless or with parallel laminae, passing upward into olive-gray clay. The silt layer has a sharp basal contact with the underlying sediment, and the clay shows evidence of burrowing in its upper part. The clay may be succeeded by nannofossil marl or by another silt/clay cycle. A typical cycle is shown in Figure 7. The silt layers are as much as 20 cm thick, although in some cycles the basal coarse unit is restricted to only a few silty laminae. A few silty to fine sand layers as much as 60 cm thick occur in Cores 103-637A-7R through 103-637A-9R. These same cores contain indications that significant amounts of silt and fine sand have been washed by drilling. Compositionally, the silty layers consist of terrigenous detrital minerals having only minor amounts of carbonate (10%–15%). These cycles are interpreted as being turbidites, bringing terrigenous material from the Iberian mainland via pathways such as the Nazaré Canyon, to the southeast of the site, or south of Galicia Bank, where smaller distributary systems are recognizable in the slope morphology.

The nannofossil marl is light and pale gray, homogeneous, and mostly structureless. Compositionally, the marl consists principally of nannofossils and clay, with relatively few foraminifers (>50% carbonate). Where present, foraminifers are dispersed through the marl. Bioturbation has generally mixed the marl with the adjacent sediment, blurring the depositional contacts. Except for the few unambiguous layers described in the following discussion, the origin of the calcareous units is not entirely clear. The water depth at the site is near the carbonate compensation depth (CCD), generally estimated to lie at 4.5–5.0 km in this area of the North Atlantic. Nevertheless, the fossils show little evidence of dissolution. This, coupled with the persistent occurrence of a small percentage of reworked older (Cretaceous–Oligocene) species, suggests that a significant fraction of the carbonate was transported from shallower depths, perhaps as a nepheloid layer. Accumulation at the site was rapid enough to prevent dissolution but slow enough for a burrowing benthic fauna to survive. However, the calcareous sediments could represent *in-situ* pelagic sedimentation. The carbonate-free pelagic clay sedimentation that might be expected at these water depths is not apparent.

In a few layers throughout Subunits IB and IC, foraminiferal sand occurs at the base of the marl (e.g., Section 103-637A-7R-2) and sharply contacts the underlying sediment. In these places, the foraminiferal sands are clearly concentrations of material transported from the shallow slopes of the adjacent Galicia Bank.

Subunit IC (Core 103-637A-10R through Sample 103-637A-15R-3, 3 cm) is similar to Subunit IB except that the silty layers

Table 2. Lithologic units recovered at Site 637.

Lithologic unit/subunit		Lithology	Cores	Sub-bottom depth (m)
I	IA	Poorly recovered turbidites and marl	103-637A-1R-1.0 cm–103-637A-5R,CC	0–44.9
	IB	Terrigenous turbidites with thick silty layers and marl	103-637A-6R-1, 0 cm–103-637A-9R,CC	44.9–83.7
	IC	Terrigenous turbidites with thin silty layers and marl	103-637A-10R-1, 0 cm–103-637A-15R-3, 3 cm	83.7–135.0
II		Slumped brown clay	103-637A-15R-3, 3 cm–103-637A-20R-1	135.0–[a]181.5
III		Reddish brown clay	103-637A-20R-6, 0 cm–103-637A-23R-2, 135 cm	[a]187.5–[b]212.0
IV		Serpentinite/peridotite	103-637A-23R-2, 135 cm–103-637A-30R,CC	212.0–285.6

[a] Sections 2–5 of Core 103-637A-20R are empty. The boundary between Units II and III falls within this interval.
[b] Depth to basement determined from downhole logs.

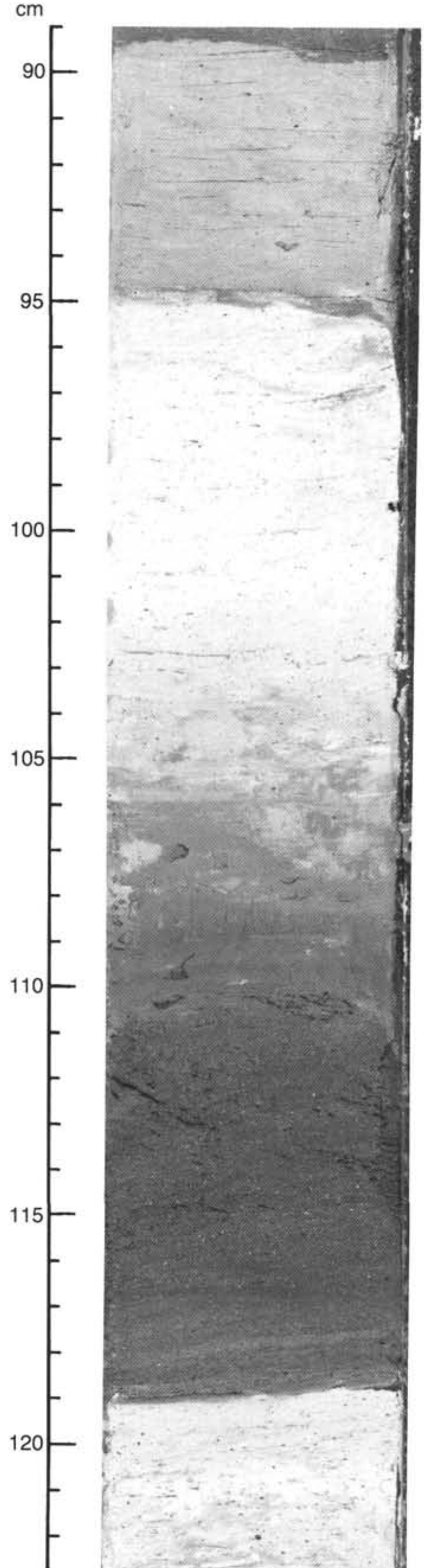

Figure 7. Sample 103-637A-8R-2, 89–123 cm. Typical turbidite bed. Basal silty layers grade up into clay and nannofossil marl.

are much less common and are restricted to less than 5 cm in thickness. The unit consists of olive-gray clay and white or gray nannofossil marl and is interpreted as being interbedded terrigenous turbidites and calcareous units. Individual cycles are generally less than 25 cm thick. Ferromanganese-rich, purplish dark-gray laminae with diffuse boundaries are common in the calcareous parts of Subunit IC. These may indicate a pause in sedimentation or may be a product of early, shallow subsurface diagenesis.

Despite poor core recovery, a general upward-thickening and -coarsening trend can be recognized in Subunits IB and IC. Figure 8 shows the frequency and thickness of turbidites throughout the section.

Unit II (135–180 m; Sample 103-637A-15R-3, 3 cm through Section 103-637A-20R-1)

Unit II, strikingly different from the overlying turbidite unit, consists of slumped brown clay and nannofossil marl. Slump structures are seen in the bottom part of Core 103-637A-15R, in Core 103-637A-16R, in the bottom part of Core 103-637A-18R, and in Core 103-637A-l9R. At least two episodes of slumping are recorded. Core 103-637A-17R and the upper part of Core 103-637A-18R show interbedded and bioturbated brown clay and nannofossil marl. These could result from settling of material thrown into suspension by slumping nearby. The brown clay is pure, having little detrital or carbonate material. Fish debris and iron oxide granules, indicative of slow sedimentation, are not common. The nannofossil marl is similarly pure. Gray and olive-gray clay is noticeably less common in Unit II. The late Miocene boundary, suggested by the foraminiferal biostratigraphy to lie at a depth of 80 cm below the top of Core 103-637A-l8R, is not evident in the sediments, although the brown clay laminations become noticeably finer below 110 cm in Core 103-637A-18R. A slight color change to darker shades of yellowish brown, variegated clay occurs in Section 103-637A-18R-2.

A notable feature of Unit II, seen in Cores 103-637A-17R and 103-637A-18R, is the occurrence of several thin layers of foraminiferal sand containing shallower water benthonic foraminifers. The nannofossil marl and foraminiferal sand could represent material deposited by turbidity currents descending from the slopes of neighboring banks and overriding Hill 5100, then subsequently being incorporated into the slumps.

Unit III (180–212 m; Section 103-637A-20R-6 through Sample 103-637A-23R-2, 135 cm)

Unit III, overlying the basement, consists of reddish brown and grayish brown clay with some exotic slumps of light-colored clay. The boundary between Unit II and Unit III falls below Section 103-637A-20R-1, which consists of slumps and displaced material of Unit II, and above Section 103-637A-20R-6, which has a lithology typical of Unit III. Unit III consists dominantly of recrystallized clay particles, with some zeolites, volcanic glass, and iron oxide granules. A few specimens of deep-water, arenaceous foraminifers, which were recovered in core catchers, may be from cavings rather than from the *in-situ* sediment. A small but persistent percentage of detrital silt particles composed of quartz, mica(?), and other minerals indicates a granitic or metamorphic source. Typically, these occur as aggregates coated with a fine layer of iron-manganese(?) oxide. A single pebble of mica schist(?) encountered in Core 103-637A-20R may be an exotic caving from higher in the hole because it appears not to have influenced sediment accumulation and to be out of place. (If this is true, the unsampled intervals must have contained some very coarse pebbly material.) Many dark-gray or black horizons rich in organic matter are in Cores 103-637A-20R and 103-637A-21R. Near the contact with the basement rock, the red clay grades into yellowish brown clay (Sample 103-637A-23R-2, 123 cm), which overlies two fragments of calcite crust interlayered with dark laminae (sulfide?). The calcite crust rests on fragments of deeply weathered serpentinite.

Unit III is interpreted as being a mixture of pelagic clay, weathering products from the underlying basement, and continental material brought to the site by contour currents, as a nepheloid layer, or in the "tails" of turbidity currents. Because the emplacement of the basement is probably Mesozoic in age and the overlying turbidites of Unit I are no older than Pliocene, Unit III clearly accumulated slowly, and Units II and III may contain significant hiatuses in sediment accumulation.

In summary, Site 637 shows an intensely weathered serpentinite basement overlain by a 35-m-thick layer of recrystallized red clay with an admixture of continentally derived material (Unit III). Slow accumulation of this clay was followed by the addition of a further 45 m of similar, though not so strongly recrystallized, material slumped from nearby slopes (Unit II). During the Pliocene, sediments encroaching on Hill 5100 buried the site in a 135-m sequence of nannofossil marls from the slopes of the banks to the east and silty terrigenous turbidites composed of material from the Iberian mainland (Unit I). Many similarities exist between this sequence and that drilled at Site 118 in the Bay of Biscay, where Mesozoic basement rock is overlain by a sequence of Paleocene-Eocene red clay and Neogene marl and silty clay (Laughton, Berggren, et al., 1972).

BASEMENT ROCKS

The Iberian margin comprises many north-trending bathymetric highs. On the basis of recovery of serpentinized lherzolite in a dredge haul, Boillot et al. (1980) proposed that one of the outermost ridges, including Hill 5100, represents a mantle-derived diapir, emplaced during the last stage of continental rifting during the Mesozoic at the ocean/continent boundary.

Site 637 is on the northward subsurface extension of Hill 5100, on its eastern side about 700–900 m from the top of the ridge. Altered peridotite was recovered beneath a 212-m-thick sedimentary cover of Miocene to Pleistocene age. The drill penetrated 73.6 m into the peridotite, of which 35.9 m was recovered as core sample.

General Lithologic Description

The peridotite is homogeneous in lithology and structure. It displays porphyroclastic to mylonitic textures, and the rocks have a well-developed foliation. The original mineralogy of the rock was olivine, orthopyroxene, and clinopyroxene in variable abundances, with rare plagioclase and chromium spinel. The clinopyroxene content is generally less than 5%, and orthopyroxene composes from 10% to 20% of the rock. The peridotite can thus be characterized as harzburgite.

The entire section of peridotite is altered, but the alteration is more pervasive in the upper 60 cm. The rock has a leached appearance (Fig. 9), and the alteration involves serpentinization and veining by serpentine and calcite (Fig. 10). The peridotite generally is yellow to pale green, but local sections are black (Samples 103-637A-26R-4, 60 cm, to 103-637A-27R-2, 15 cm; 103-637A-27R-4, 45–120 cm; 103-637A-29R-1, 35–125 cm). Rock color is an indication of the extent of alteration.

Thin bands (1–3 mm) of clinopyroxene occur locally, as well as changes in the relative abundance of orthopyroxene (e.g., Samples 103-637A-25R-4, 100–142 cm; 103-637A-25R-5, 1–20 cm; 103-637A-26R-4, 60–70 cm; and 103-637A-27R-2, 106–124 cm). In all places, the zones between pyroxene-rich and pyroxene-poor facies are extremely gradational (Fig. 11).

The peridotite everywhere shows a strong foliation marked by the elongation of pale-white orthopyroxene and spinel crystals (Fig. 10). Foliation dip can be directly measured on sections cut perpendicularly to the horizontal plane and parallel to the lineation direction. From 212 to 259 m sub-bottom depth, the dip of the main foliation is remarkably constant at 30°. Near the base of the hole, the foliation steepens to 75° (Fig. 12). Locally, the peridotite is extremely sheared, as evidenced by the extreme elongation of orthopyroxene crystals (e.g., Sample 103-637A-25R-4, 110–115 cm). In these places, the dip of the foliation in the shear zones is generally steeper (about 10°) than in the adjacent intervals (Figs. 12 and 13). Some of these shear zones include late-formed serpentine breccia, serpentine rubble (Samples 103-637A-26R-3, 75–150 cm; 103-637A-26R-4, 0–75 cm; 103-637A-29R-1, 0–125 cm), pieces with slickensides (Samples 103-637A-25R-5, 92–100 cm), and fibrous serpentine veins (Samples 103-637A-28R-3, 80–95 cm).

Another prominent feature of the peridotite is the occurrence of abundant cross-cutting white calcite veins of variable thicknesses (<1 mm to 4–5 cm). Microscopic veins are pervasive. The veins generally show two specific orientations: subparallel or subperpendicular to the main foliation (Fig. 14). The widest (2–4 cm) calcite veins have comb structures and in some places include coarse black crystals of calcite and magnetite at their center (Fig. 15). These veins commonly brecciate the rock, and the calcite veins include angular serpentine (e.g., Sample 103-637A-25R-5, 124–126 cm). Cross-cutting relationships indicate that the calcite veining was a late-stage alteration event, relative to serpentinization.

The development of serpentine veins is also ubiquitous. Both thin serpentine veinlets less than 1 mm thick (Sample 103-637A-28R-3, 100–110 cm) and larger massive pale-green serpentine veins (Sample 103-637A-25R-2, 104–112 cm) occur. Like the calcite veins, the serpentine veins are generally subparallel or subperpendicular to the main foliation in the peridotite. Intervals of serpentine breccia also occur (Fig. 16; Samples 103-637A-28R-3, 68–80 cm; 103-637A-28R-4, 0–94 cm; and 103-637A-28R-5, 0–46 cm).

Petrographic and Textural Data

Primary Mineralogy

The data presented here result from preliminary study of 60 thin sections. All the thin sections indicate high degrees of peridotite alteration; at best, 5% of the primary mineral phases (olivine, orthopyroxene, clinopyroxene, and chromium-spinel) are preserved (Figs. 17A through 17C). A few samples contain plagioclase rims around spinel (Fig. 17D).

In most of the thin sections, olivine is almost totally transformed into serpentine. However, a few samples contain olivine; the initial modal content of olivine ranges from 70% to 90% of the whole rock.

Although orthopyroxenes are generally completely replaced by secondary products (serpentine or calcite), their initial shapes are often recognizable. The orthopyroxene is enstatite and displays abundant thin exsolution lamellae (Fig. 17C), which may be curved or bent. The primary modal abundance of the orthopyroxene is variable, ranging between 10% and 15%.

Clinopyroxene (diopside) is relatively fresh relative to other primary phases but is replaced by calcite in the most altered samples. It typically appears either as equant isolated crystals within the serpentine or at the periphery of orthopyroxene crystals. Locally, clinopyroxene occurs in small granulated aggregates or layers (0.1–0.5 cm to 1 cm) that parallel the foliation. Some crystals show small, thin exsolution lamellae. The clinopyroxene modal abundance of the peridotite ranges from 0% to 5%.

Chrome-rich spinel crystals are commonly embayed or irregularly shaped, fractured, and slightly elongated (0.1–1 mm in size). The spinel is yellow-brown to reddish, sometimes rimmed by magnetite, and its modal content is from 1% to 2%.

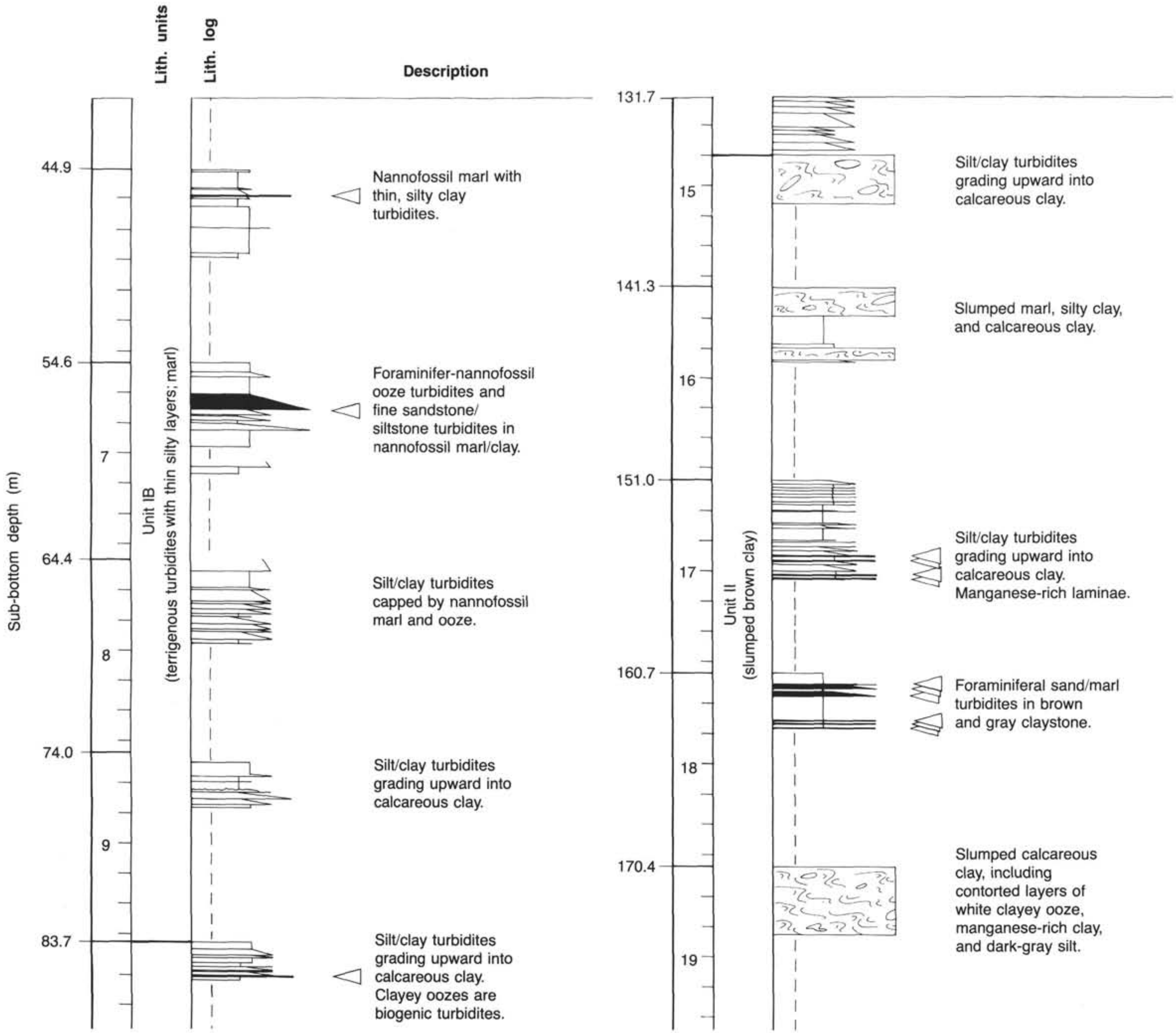

Lith. units
Lith. log
Description
Sub-bottom depth (m)
44.9
54.6
64.4
74.0
83.7
7
8
9
Unit IB
(terrigenous turbidites with thin silty layers; marl)
Nannofossil marl with thin, silty clay turbidites.
Foraminifer-nannofossil ooze turbidites and fine sandstone/ siltstone turbidites in nannofossil marl/clay.
Silt/clay turbidites capped by nannofossil marl and ooze.
Silt/clay turbidites grading upward into calcareous clay.
Silt/clay turbidites grading upward into calcareous clay. Clayey oozes are biogenic turbidites.
131.7
141.3
151.0
160.7
170.4
15
16
17
18
19
Unit II
(slumped brown clay)
Silt/clay turbidites grading upward into calcareous clay.
Slumped marl, silty clay, and calcareous clay.
Silt/clay turbidites grading upward into calcareous clay. Manganese-rich laminae.
Foraminiferal sand/marl turbidites in brown and gray claystone.
Slumped calcareous clay, including contorted layers of white clayey ooze, manganese-rich clay, and dark-gray silt.

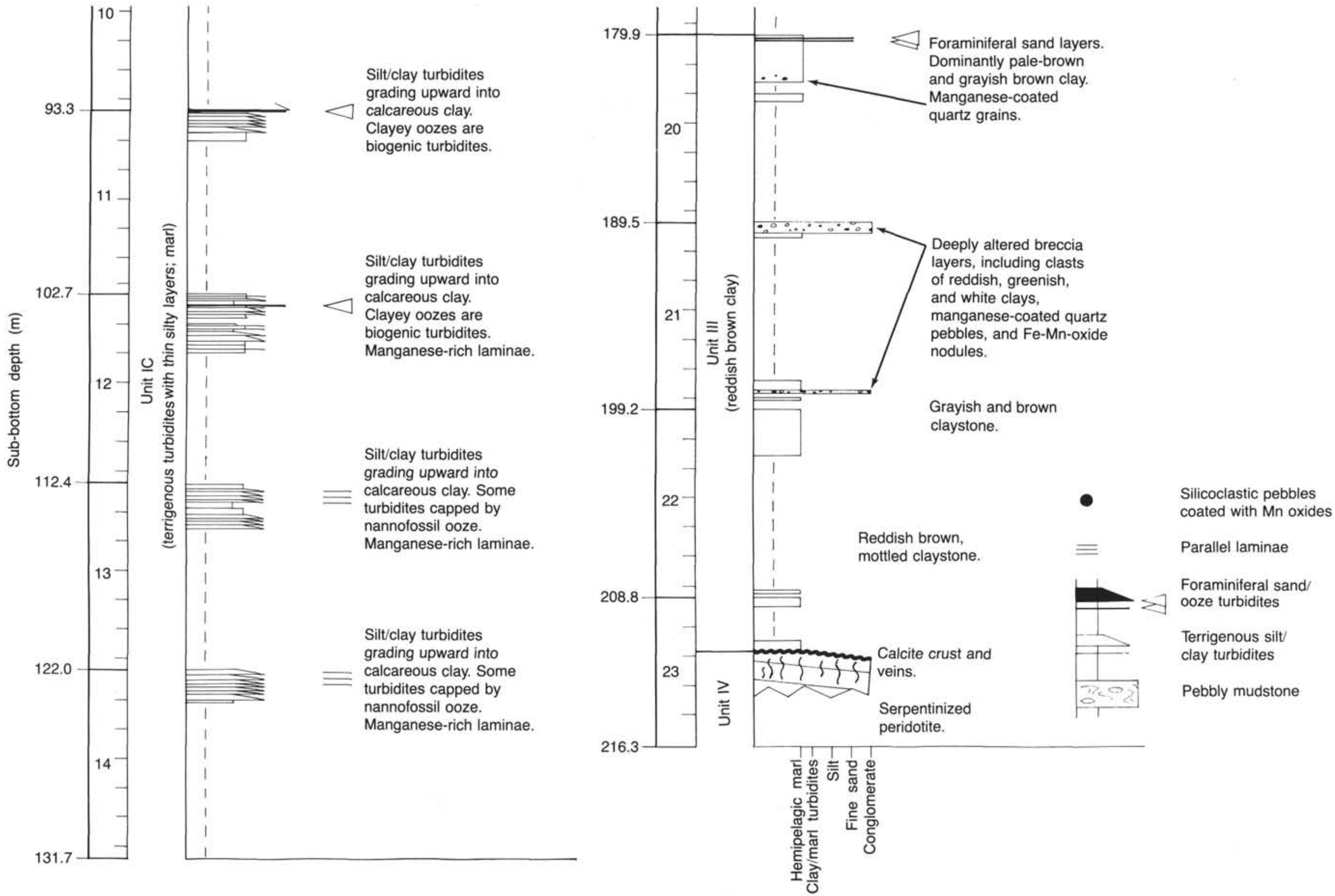

Figure 8. Lithologic log of the sedimentary column at Site 637.

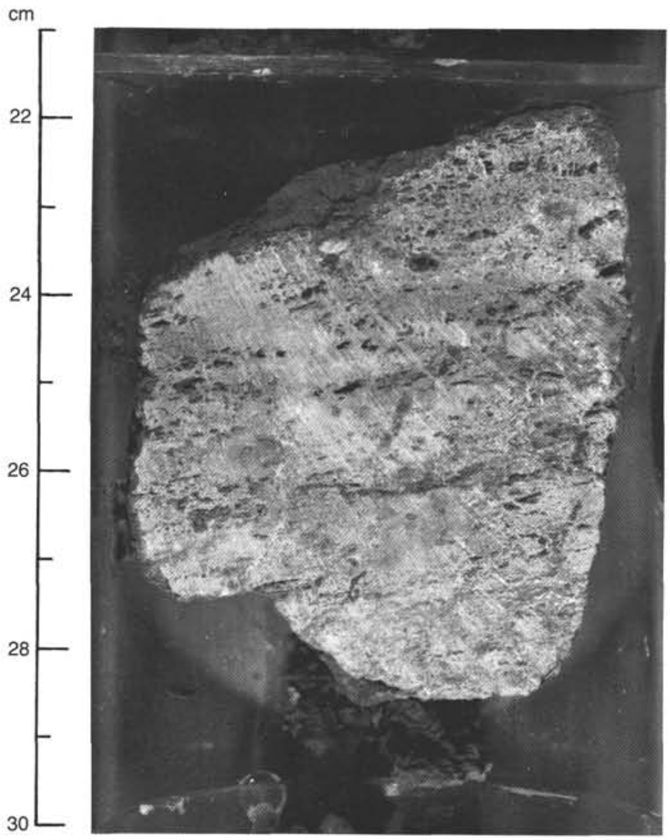

Figure 9. Sample 103-637A-23R-3, 21–30 cm. Uppermost peridotite recovered at Hole 637A. The peridotite is highly leached and includes dissolution cavities parallel to the rock foliation.

Plagioclase was observed in only a few samples, but where present, is fresh and rims spinel grains.

Alteration Mineralogy

Secondary products compose, by volume, the major phases present in the peridotite (Figs. 17A, 17E, and 17F). These include serpentine, opaque minerals (hematite, magnetite, and amorphous oxide phases), and amphibole.

Amphibole

Amphibole occurs along the rims of orthopyroxene crystals and is sometimes found within altered orthopyroxene or as small veinlets. Amphibole is also associated in some places with the diopside microbands. Tremolite is the most common amphibole, but hornblende is also present, an indication that metamorphic crystallization began at high temperatures. The opaque minerals are disseminated throughout the rock and are products of the serpentinization process.

Serpentine

Several generations of serpentine formation are evident from textural relationships in these rocks. Most of the peridotite is a meshwork of thin serpentine veinlets, characteristic of the alteration of olivine to serpentine. Orthopyroxene crystals are partly or completely serpentinized. Grain outlines of the original orthopyroxene crystals are obvious, making it possible to assess the original modal abundances. The altered pyroxene crystals are commonly rimmed or partly replaced by calcite (Fig. 17E).

Veins, bands, and lenses of more massive serpentine, formed during brittle deformation, also dissect the rock. They may parallel and highlight the foliation produced by shearing. Other

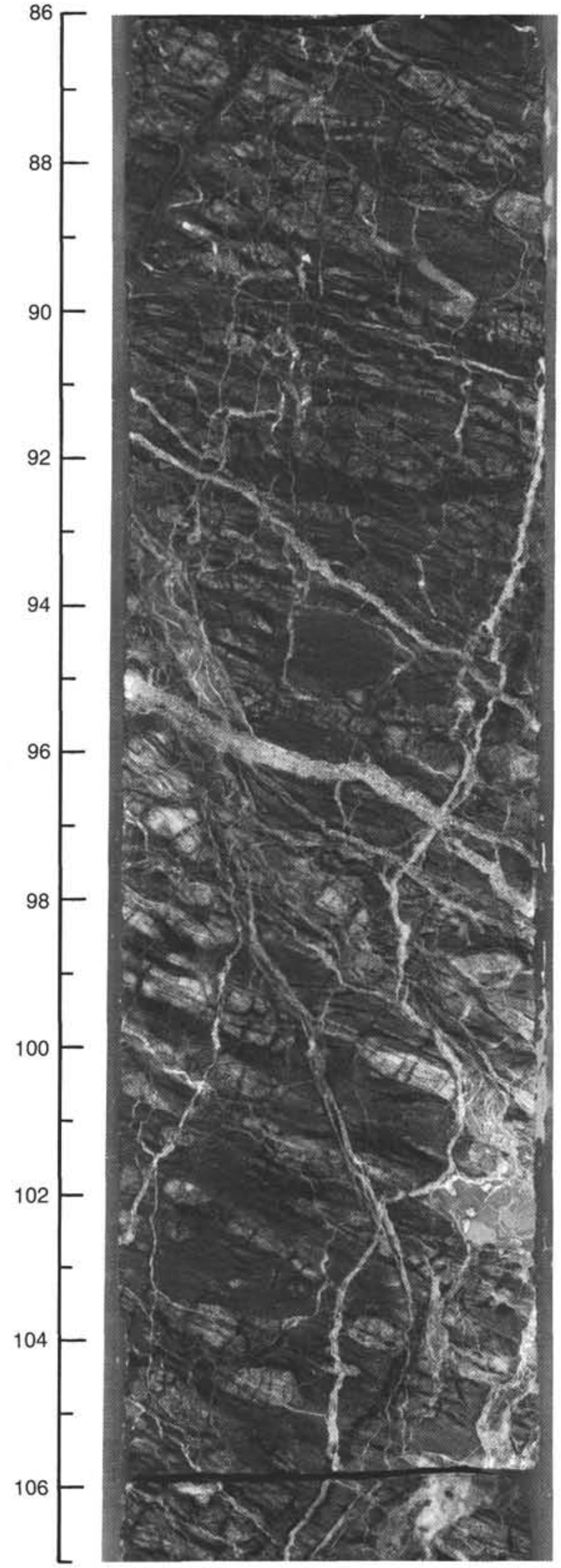

Figure 10. Sample 103-637A-26R-2, 86–107 cm. Altered and foliated peridotite typical of basement rocks recovered from Hole 637A. Foliation is defined by elongation of pyroxene crystals and bands of serpentine. Veins are calcite and serpentine and are generally subperpendicular or subparallel to the main foliation.

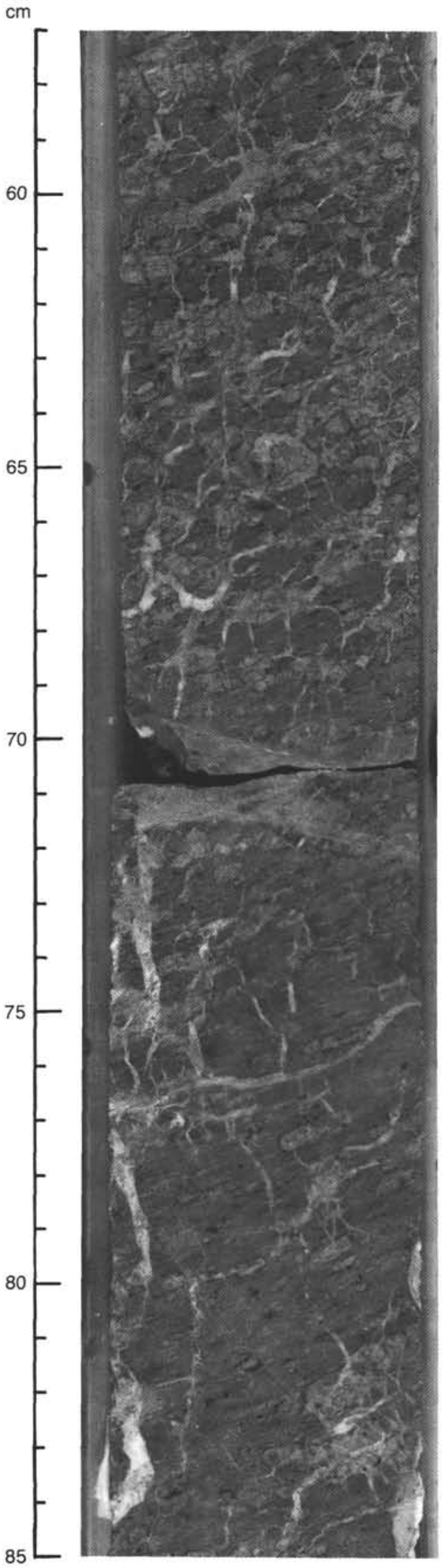

Figure 11. Sample 103-637A-25R-1, 57–85 cm. Peridotite displaying variable pyroxene abundances. Pyroxene content decreases downward.

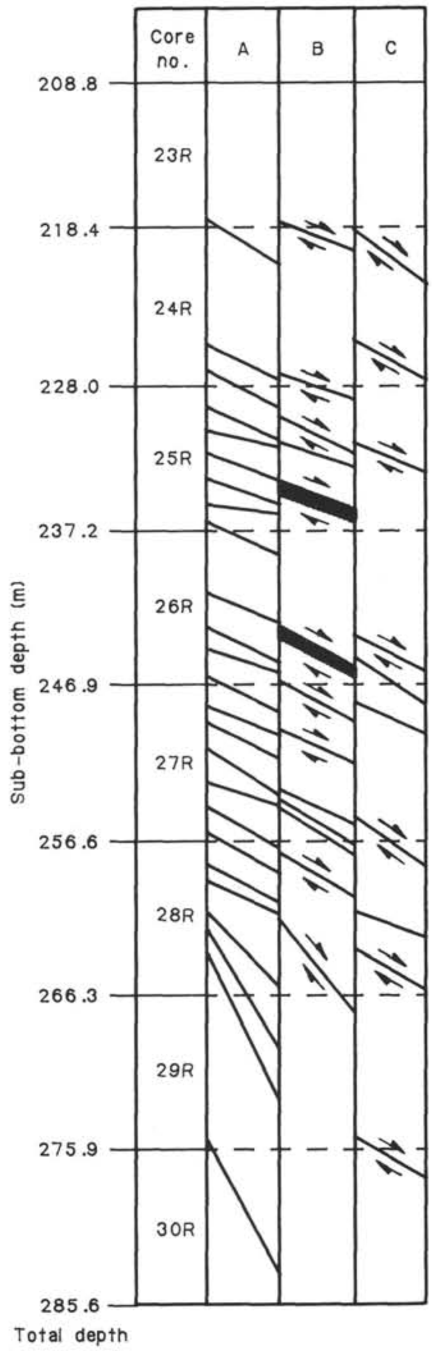

Figure 12. Schematic cross section of peridotite in Cores 103-637A-23R through 103-637A-30R, showing the attitude of main structures measured. Column A: attitude of main porphyroclastic foliation; Column B: attitude of mylonitic foliation of primary sense of shear determined in thin sections; Column C: attitude of large brittle microfaults and sense of displacement along the faults. Top of basement is at 212 m sub-bottom depth.

discordant bands and veins were formed during later deformation, as, for example, serpentine veins that enclose angular fragments and serpentine-filled tension gashes.

The serpentine minerals include chrysotile and lizardite, identified by x-ray diffraction (XRD). No antigorite was unequivocally detected, although minor amounts might be present. The presence of amphibole suggests that antigorite may have been formed at an early, higher temperature stage of alteration. If

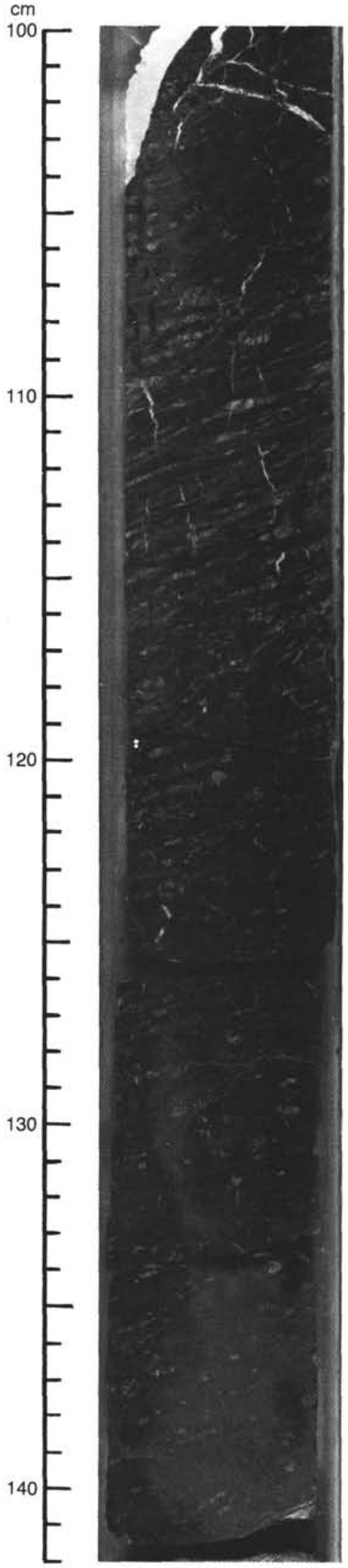

Figure 13. Sample 103-637A-25R-4, 100–142 cm. Shear zone (109–114 cm) slightly oblique to the main foliation in the peridotite. Note also the differences in pyroxene content of the peridotite from top (poor) to base (rich).

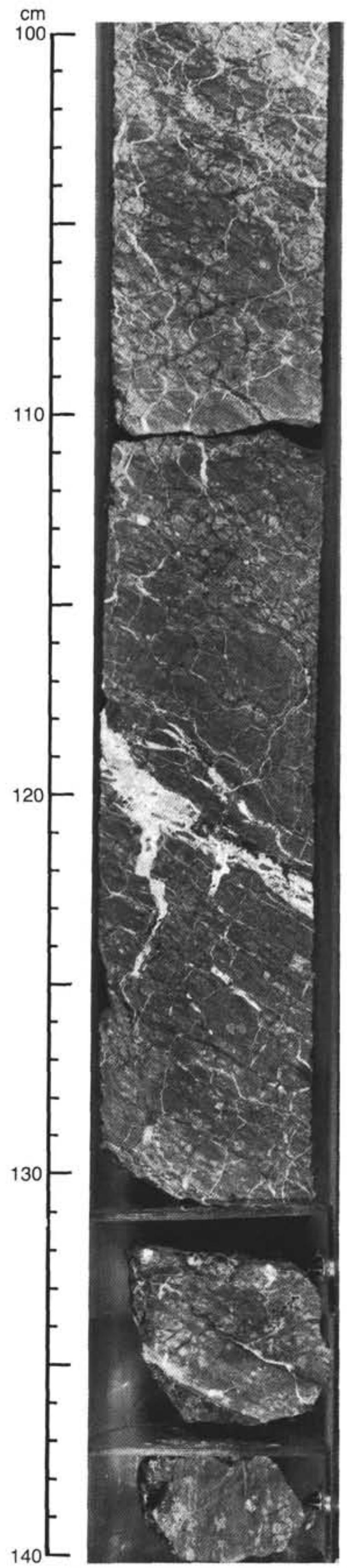

Figure 14. Sample 103-637A-27R-1, 100–140 cm. Calcite veins dominantly in fractures subperpendicular or subparallel to the foliation.

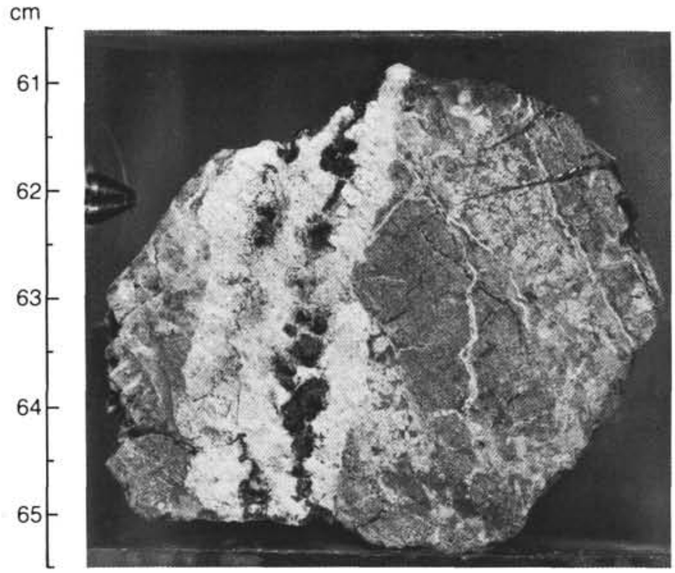

Figure 15. Sample 103-637A-26R-3, 60–65 cm. Large calcite veins with comb structures and black calcite crystals in center.

this is true, the antigorite has been almost completely recrystallized to the lower temperature serpentine polymorphs.

Calcite

The most altered samples (e.g., Sample 103-637A-23R-3, 20–70 cm) are pervasively impregnated by microscopic, anastamosing veinlets of calcite (0.1–0.5 mm thick; Fig. 17F). Calcite composes as much as 50% of the rock in these samples and is generally coarsely crystalline; in the largest veins (e.g., Fig. 15), individual crystals are several mm in size. Calcite also commonly replaces pyroxene.

Peridotite color is roughly related to calcite content; peridotite with the least amount of calcite is black, whereas the most altered samples with large amounts of calcite tend to be yellow. These altered samples also contain larger amounts of ferric iron oxides, which lend the rock a yellow-red color.

The extensive replacement of the rock by calcite tends to obscure much of the primary structure in the peridotite. The degree of replacement, especially the amount of calcite replacement, correlates well with the seismic velocities measured on individual samples of peridotite. Samples with the lowest velocities (as little as 2.9 km/s) are either brecciated or heavily replaced by calcite. The highest seismic velocities (as much as 4.7 km/s) were measured from samples with the least amount of calcite veining (see "Physical Properties" section, this chapter).

Calcite replacement and veining was the last alteration stage of these rocks. Calcite veins cross cut, brecciate, or replace existing structures. Geochemical and isotopic studies will probably place better constraints on the conditions of the different generations of alteration. This, in turn, may lend insight into the timing and conditions of peridotite emplacement.

Textural and Structural Data

Two types of peridotite texture can be clearly distinguished: porphyroclastic and mylonitic. The most common texture in the peridotite is porphyroclastic (Fig. 17A and 17C). The orthopyroxene porphyroclasts and spinel elongation define the main foliation throughout the entire interval sampled. Although determining the size of initial olivine porphyroclasts is usually impossible because of serpentinization, the original grain size of porphyroclastic samples was probably coarse (larger than 5 mm), as seen in a few unaltered samples. The large size and shape of

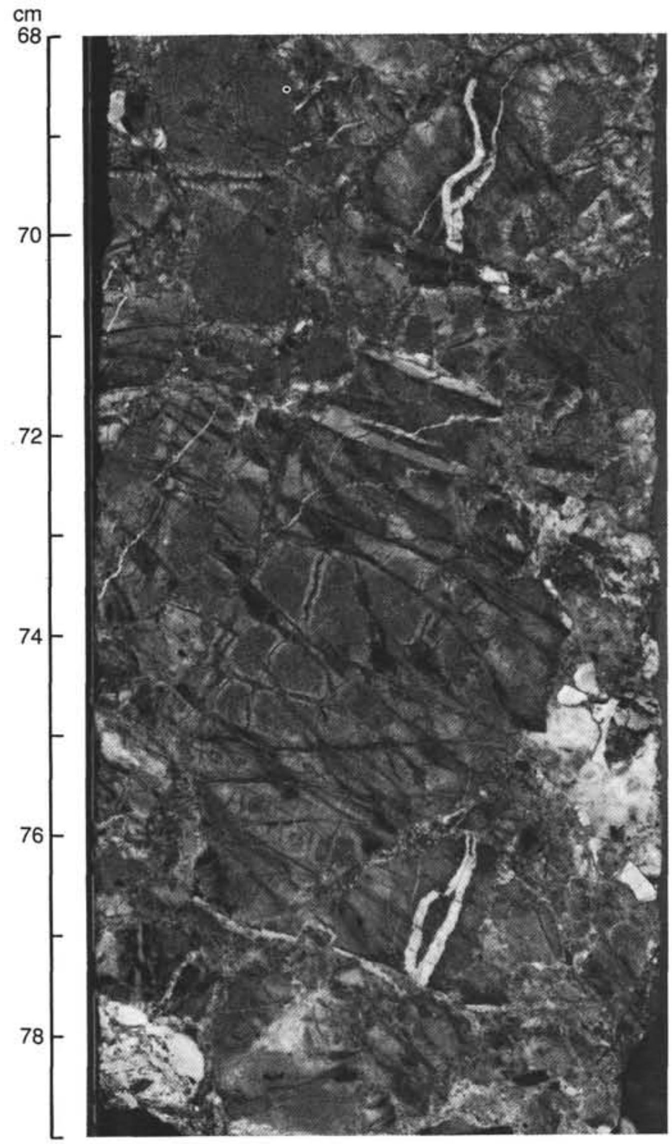

Figure 16. Sample 103-637A-28R-3, 68–79 cm. Serpentine breccia.

orthopyroxene crystals, which are round to elongate and between 4 and 8 mm in size, also supports this conclusion. Spinel crystals also have relatively large sizes (0.5–2 mm). These textures are common in oceanic-mantle peridotites and result from high-temperature–low-stress plastic deformation during asthenospheric flow (Nicolas et al., 1980; Mercier, 1984).

Mylonitic textures, less abundant than porphyroclastic textures and occurring only in the shear zones, are characterized by the presence of stretched orthopyroxene crystals, which show extremely large elongation ratios, in some places greater than 1:15 (Fig. 17G). The olivine grain size was small in these mylonites, indicative of large deviatoric stresses during deformation. Mylonitic textures such as these are well documented in other peridotite localities and result from high-stress–"low"-temperature deformation generally ascribed to transform-fault movements or to primary thrusting of mantle slices during orogenesis.

Discussion

The occurrence of the peridotite ridge near the transition between oceanic and continental crustal domains raises several questions concerning the nature and mechanism of uplift of mantle

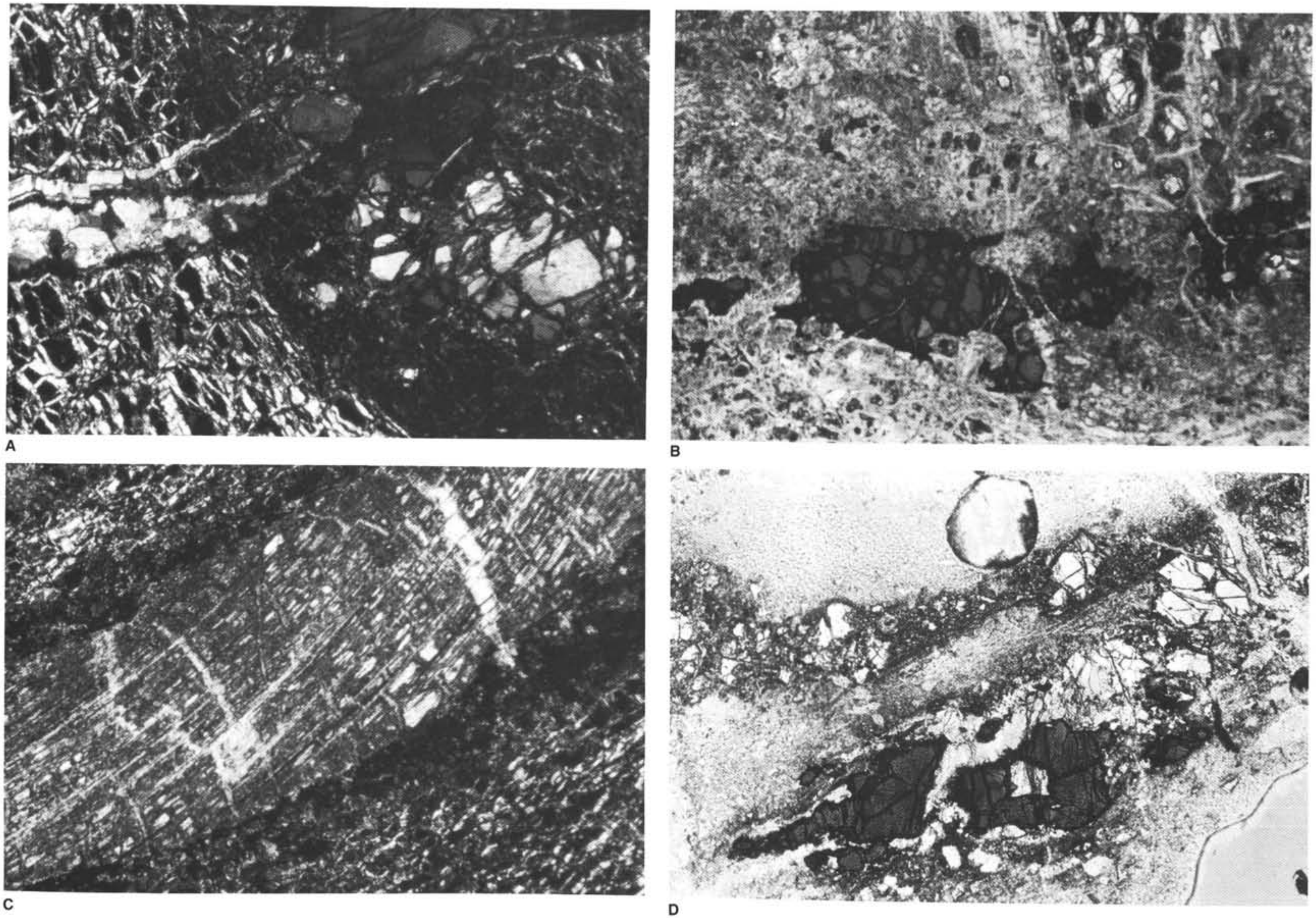
A
B
C
D

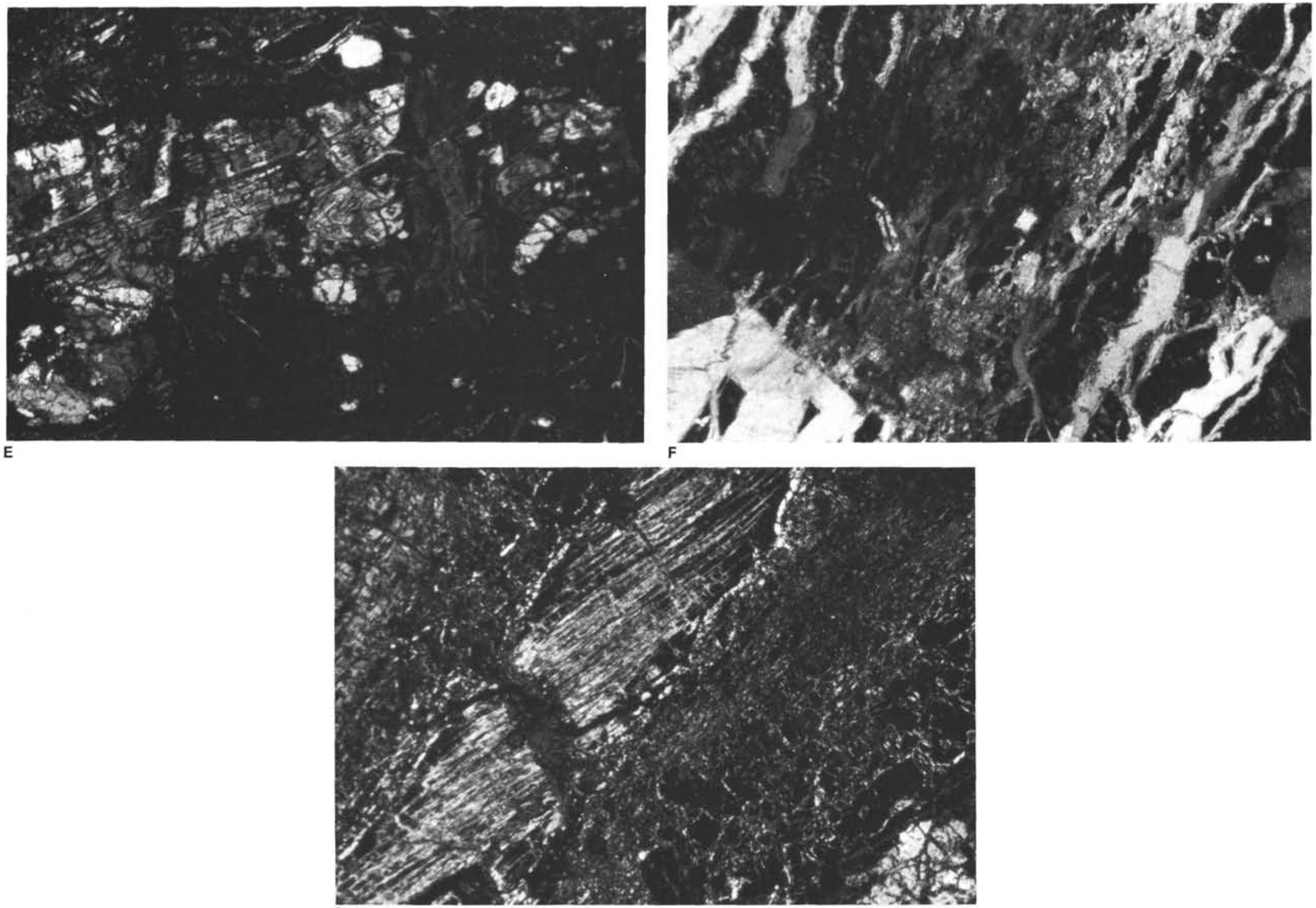

E F G

Figure 17. Photomicrographs of representative features in peridotite. The field of view of 2.4 × 3.6 mm. A. Sample 103-637A-25R-5, 119–121 cm. Photograph displays relict clinopyroxene grains with thin exsolution Iamellae (top center), surrounded by serpentine. The white vein to the left is calcite. B. Sample 103-637A-26R-4, 67–69 cm. Elongate and embaed chromite grain (plane polarized light) in serpentinized peridotite. The brighter grain fragments in the upper right are unaltered orthopyroxene fragments. C. Sample 103-637A-25R-4, 146–148 cm. Elongate orthopyroxene porphycroclast with slightly bent cleavage traces. Small calcite veins cut the grain at a high angle to the cleavage. D. Sample 103-637A-25R-5, 141–144 cm. Spinel grain (dark mineral) is rimmed by plagioclase (light mineral). E. Sample 103-637A-24R-2, 82–85 cm. Pyroxene porphyroclasts replaced by calcite. Surrounding material is serpentine. F. Sample 103-637A-25R-2, 61–63 cm. Calcite veinlets (bright) in altered peridotite. Dark background is serpentine. G. Sample 103-637A-26R-4, 62–64 cm. Stretched orthopyroxene grain. Only about one-third of the length of the grain is shown in this photography; the grain is actually about 1 cm long. Pyroxene is heavily serpentinized and rimmed by a small vein of calcite.

material. The peridotite could represent either suboceanic or subcontinental mantle emplaced during the latest stage of Mesozoic continental rifting. Its emplacement could result from stretching and diapiric processes, as suggested by Boillot et al. (1980), or from transform faulting or thrusting. Differences in the composition of peridotites from Site 637 and those from the Cabo Ortegal area in Spain (e.g., the presence of plagioclase vs. garnet, respectively; Ibarnuchi and Girardeau, pers. comm., 1985) indicate that these peridotites have not undergone similar metamorphic histories; therefore, Site 637 peridotites are probably not remnants of a dismembered slice of Hercynian ophiolite.

Evident mineralogic phases, which suggest that the peridotite samples recovered from drilling are harzburgites, are similar to most of the peridotite samples recovered from the ocean basins and trenches (e.g., Site 395, Shipboard Party, 1978; equatorial Mid-Atlantic Ridge, Bonatti et al., 1970; Vema, Romanche, and St. Paul fracture zones, Honnorez et al., 1984; Bonatti et al., 1979). However, the plagioclase that rims spinel in a few samples, as also previously observed by Boillot et al. (1980), indicates that these rocks have been equilibrated at low pressure (<3 Kb) as peridotites emplaced in rift areas (e.g., Bonatti et al., 1986).

Site 637 peridotites may represent the suboceanic mantle, which is less depleted than most oceanic peridotites because it was not included in the extensive partial melting that caused the generation of oceanic basalts. Compositional data on individual mineral phases will provide the basis for comparison of the peridotites from Site 637 with other peridotites from oceanic environments, Pyrenean lherzolites, and ophiolitic peridotites.

On the basis of textural data, we can show that serpentinization of the peridotite occurred after its mylonitization and, therefore, after its emplacement at shallow levels. The serpentine is not schistose, and all primary deformation textures have been preserved. This precludes emplacement of Site 637 peridotites as a serpentinite diapir, as proposed for the schistose serpentinites in oceanic fracture zones (Bonatti et al., 1979).

The attitudes of foliation and lineation in the peridotite from Site 637 indicate that the peridotites were not emplaced in a transform-fault environment, which would have produced horizontal lineation in the foliation. Instead, steeply dipping lineation is observed.

On the other hand, the attitudes of the main foliation and shear zones and of the corresponding stretching lineations indicate tangential shear along a slightly inclined plane. The present direction of the foliation dip, determined through shipboard magnetic measurements, is to the east. Therefore, the stretching lineation should have a nearly east–west orientation. The sense of shear, as determined in thin sections, clearly indicates an eastward transport of the overlying block relative to the underlying material. This geometry is compatible with a large diapiric emplacement of mantle rocks at shallow lithospheric levels during crustal thinning.

In summary, the ridge appears to consist only of serpentinized harzburgite, similar to most oceanic peridotites. The emplacement of peridotite at the boundary between oceanic and continental crust is probably the result of crustal thinning during rifting. It may have occurred along low-angle conjugate normal faults or along a single normal fault (Boillot, 1986) in a manner suggested by Wernicke (1985).

BIOSTRATIGRAPHY

At Site 637, we proposed to penetrate a north–south ridge of ultramafic basement rock near the ocean/continent crust boundary off the Iberian margin. Approximately 212 m of sediment were recovered overlying a serpentinite basement. Core-catcher and some core-section samples were examined for nannofossils and planktonic foraminifers to determine a working biozonation. Radiolarians and other siliceous microfossils were absent, except for a few isolated specimens.

A nearly continuous sequence of upper Miocene through upper Pleistocene sediments are present at this site. The upper part of the section (lithologic Unit I; see "Sediment Lithology" section, this volume) is dated as late Pliocene through late Pleistocene. Planktonic foraminifers and nannofossils indicate a minor hiatus in the upper Pliocene. The preservation quality of the planktonic foraminifers decreases downhole within this interval. Calcareous nannofossils are moderately to well preserved in both the clastic and the pelagic sediment in lithologic Unit I. Unit II is late Miocene through middle Pliocene; planktonic foraminifers are better preserved in this unit. The calcareous nannofossils are well preserved within the calcareous-rich sediment but are poorly preserved in the brown clays, which are prominent in the lower part of lithologic Unit II. Planktonic foraminifers indicate that the lowermost Pliocene Subzones PL1A and PL1B may be missing between Samples 103-637A-17R, CC, and 103-637A-18R, CC; however, the calcareous nannofossils confirm the presence of the lowermost Pliocene (Subzone CN-10B) in Section 103-637A-18R-1. At the base of the section, 35 m of red clay (lithologic Unit III) are unfossiliferous. Early Pliocene ages determined for isolated calcareous-ooze clasts are doubtful because these clasts are most likely cavings from higher in the drill hole.

Trace amounts of reworked calcareous nannofossils occur in every sample; reworked planktonic foraminifers occur in most samples. These reworked microfossils are Late Cretaceous to Pliocene in age.

Foraminifers

Core-catcher samples from the sediments overlying basement rock at Hole 637A were examined to establish a preliminary planktonic foraminiferal biozonation. Most of these samples yielded an abundant, moderately to well-preserved planktonic foraminiferal assemblage.

According to foraminiferal preservation, the sedimentary section can be divided into two parts. An upper part comprising Samples 103-637A-1R, CC, to 103-637A-14R, CC (lithologic Unit I), exhibits a progressive downhole decrease in preservation quality of the planktonic fauna. More obvious signs of dissolution are seen downhole beginning with Samples 103-637A-11R, CC. The lower part (i.e., Samples 103-637A-15R, CC, to 103-637A-24R, CC; lithologic Units II and III) generally yields a better preserved, and commonly more diverse, planktonic assemblage. Several levels, for instance Sample 103-637A-18R, CC, show a significant increase in the proportion of benthic specimens.

The biostratigraphic interpretation based on the vertical distribution of selected planktonic foraminiferal species (Fig. 18) was constructed using the works of Stainforth et al. (1975), Berggren (1977), Berggren et al. (1983, in press), Kennett and Srinivasan (1983), Moullade (1983, in press), and Ma'alouleh and Moullade (in press).

Samples 103-637A-1R, CC, to 103-637A-12R, CC, are given a Quaternary age because of the regular (rare to common) occurrence of *Globorotalia truncatulinoides*. This mid-latitude marker occurred at this site, together with relatively cold-water planktonic forms, *G. inflata, Neogloboquadrina pachyderma*, and *Globigerina bulloides* being dominant species. The low-latitude warmer water taxa, such as menardiiform globorotalias, *Sphaeroidinella dehiscens, Globigerinoides trilobus, Pulleniatina*, etc., appear to be absent.

The relatively constant occurrence of *Globorotalia tosaensis* and *G. truncatulinoides* in this interval is particularly noteworthy and enables a precise age determination of early Pleistocene (Zone N22) for lithologic Unit I. Similarly, the sporadic occur-

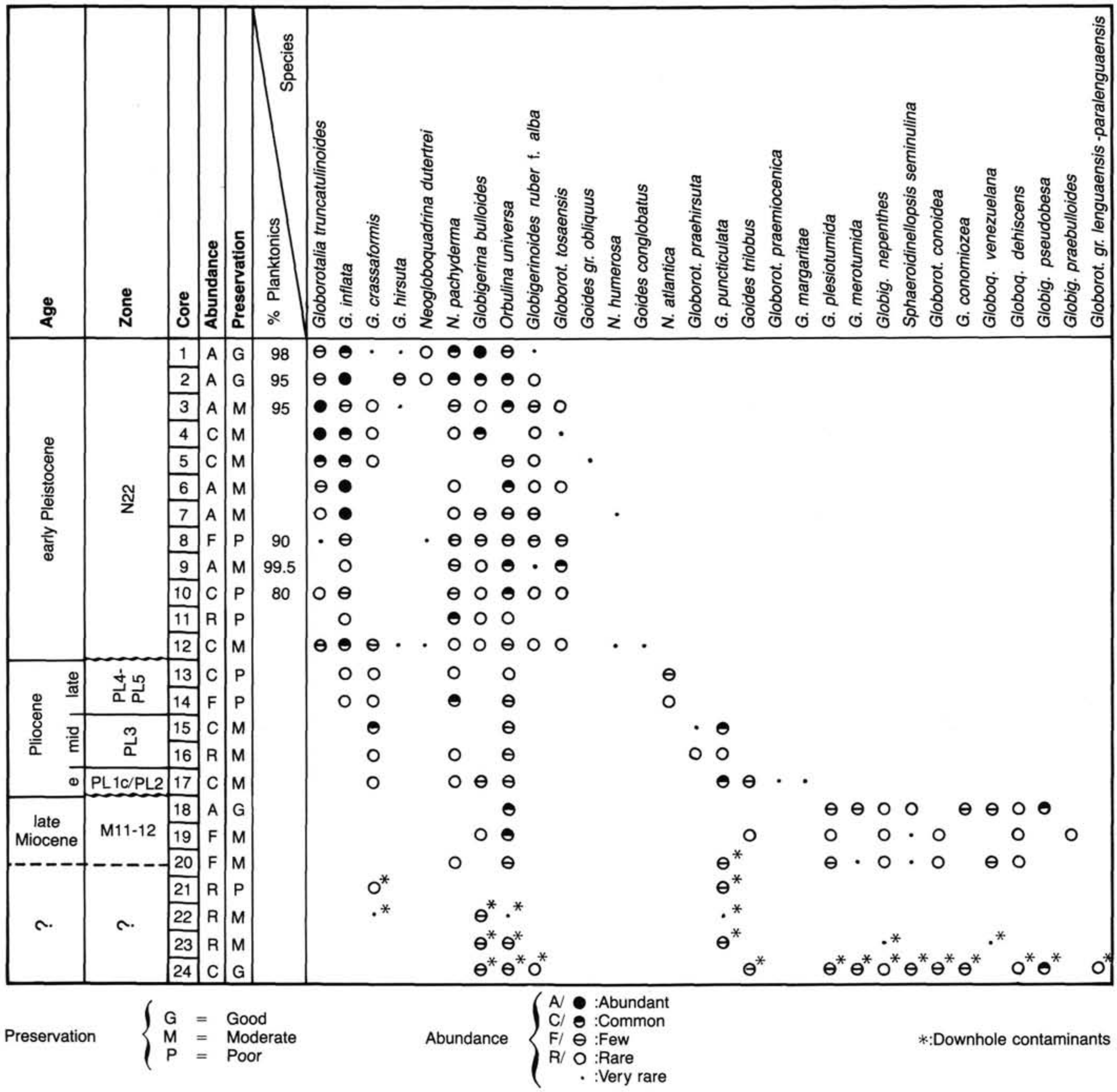

Figure 18. Vertical distribution of selected planktonic foraminiferal species, Hole 637A.

rence of *Globigerinoides obliquus* in Sample 103-637A-5R, CC, and *Neogloboquadrina humerosa* in Samples 103-637A-7R, CC, and 103-637A-12R, CC (two species known to extend up to the lowermost Pleistocene), enhances this designation. At the top of the recovered sequence, the absence of *Globigerinoides ruber* f. *rosea*, having a first-appearance datum (FAD) calibrated at approximately 0.9 Ma, confirms that most if not all the late Pleistocene is not represented in Site 637.

Some difficulties arise when determining a consistent succession of age assignments for the pre-Quaternary sediments recognized in Hole 637A. An obvious gap, possibly exaggerated by poor core recovery, appears between Samples 103-637A-12R, CC, and 103-637A-13R, CC. Samples 103-637A-13R, CC, and 103-637A-14R, CC, yield a rather impoverished and poorly preserved assemblage, dominated by *N. pachyderma, Globortalia crassaformis, G. inflata*, and *N. atlantica*. The co-occurrence of the last two species defines an interval that comprises Pliocene Zones PL4 and PL5. Thus, the uppermost Pliocene Zone PL6 is possibly missing in this hole. Samples 103-637A-15R, CC, and 103-637A-16R, CC, contain a more abundant and better preserved mid-Pliocene (Zone PL3) planktonic foraminiferal assemblage, including *G. crassaformis, G. praehirsuta*, and *G. puncticulata*. Sample 103-637A-17R, CC, yields a relatively more diverse and warmer-water microfauna, in which *G. crassaformis* and *G. puncticulata* are accompanied by rare *Globigerinoides trilobus, Globorotalia praemiocenica*, and *G. margaritae*. Co-occurrence of these two species enables the determination of Zones PL1C and PL2, corresponding to the upper part of the lower Pliocene.

Another gap in the sequence of about 1.0 m.y. duration (Berggren, 1977) is possibly indicated by the absence of planktonics signifying the lowermost Pliocene Subzone PL1A. The lower Pliocene of Core 103-637A-17R is underlain in Cores 103-637A-18R to 103-637A-20R by a rich, well-preserved Miocene assemblage including *G. conoidea, G. conomiozoa, G. merotumida, G. plesiotumida, Globoquadrina dehiscens, Globigerina praebulloides* and is devoid of *G. margaritae*, which indicates the upper Miocene M11 through M12 Zones.

Samples taken from Cores 103-637A-21R to 103-637A-24R are either barren or contain rare non-age-diagnostic primitive agglutinated forms. In this interval, core-catcher samples are commonly enriched by Quaternary and Pliocene downhole contaminants.

Sample 103-637A-20R-1, 122–129 cm, also contains Miocene ichthyoliths, and Sample 103-637A-23R-2, 111–118 cm, yields Paleocene/Eocene(?) and possibly reworked Cretaceous specimens (P. Doyle, pers. comm., 1985).

Nannofossils

Late Miocene through late Pleistocene nannofossil assemblages were recovered from sediments drilled at Site 637. For age determinations, we used Gartner's (1977) zonation for the Pleistocene and that of Okada and Bukry (1980) for the Miocene through Pliocene. Low core recoveries from this hole limit biostratigraphic interpretations, especially in Cores 103-637A-1R through 103-637A-5R. In these five cores, 0.4 m of sediment was recovered. The abundance and preservation of recovered assemblages varies with lithology. Nannofossils are generally better preserved in the nannofossil-rich sediment than in the brown clay, where only poorly preserved, solution-resistant assemblages were encountered. Trace amounts of reworked material of Late Cretaceous to Oligocene age are present in all samples examined.

Samples from Core 103-637A-1R through Section 103-637A-15R-2, corresponding to lithologic Unit I, are dated as late Pleistocene (*Emiliania huxleyi* Zone) to late Pliocene (*Discoaster surculus* Subzone, CN-12B). Sediments from these cores consist predominantly of turbidites that grade from silt or silty clay layers at the base to clay at the top and commonly include overlying bioturbated calcareous clays and marls. Whether the calcareous sediments overlying these turbidites are of pelagic or transported origin is uncertain. Principal evidence of the calcareous sediments being deposited by a transported mode is their association with clastic turbidites, the general abundance of well-preserved calcareous microfossils at such great water depth, and the continual presence of trace amounts of reworked species.

Examination of assemblages recovered from lithologic Unit I indicates a nearly complete section, lacking any evidence of extensive reworking. All the Pleistocene zones indicated by Gartner (1977) were recognized. *Pseudoemiliania lacunosa* is not present in core-catcher samples from Cores 103-637A-1R and 103-637A-2R. Sample 103-637A-1R, CC, contains *Emiliania huxleyi*, whereas Sample 103-637A-2R, CC, does not; these samples are assigned to the upper Pleistocene *Emiliania huxleyi* and *Gephyrocapsa oceanica* Zones, respectively. The *Pseudoemiliania lacunosa* Zone was determined for the three core-catcher samples examined from Cores 103-637A-3R through 103-637A-5R, where the nominative species is present in the absence of abundant small *Gephyrocapsa* spp. Samples 103-637A-6R-1, 50–51 cm, through 103-637A-8R-3, 60–61 cm, contain abundant small *Gephyrocapsa* spp. and *Pseudoemiliania lacunosa* and are placed in the small *Gephyrocapsa* Zone. The *Helicosphaera sellii* Zone was recognized for Samples 103-637A-8R, CC, through 103-637A-10R, CC, by the occurrence of the nominative species in the absence of *Calcidiscus macintyrei*. The lowermost Pleistocene *Calcidiscus macintyrei* Zone is determined for Core 103-637A-11R, the top of which has the highest occurrence of *C. macintyrei*. The last occurrence of the genus *Discoaster*, which defines the base of this zone, was used to determine the Pliocene/Pleistocene boundary, which falls between Samples 103-637A-11R, CC, and 103-637A-12R-1, 43–44 cm. The lowest occurrence of *Gephyrocapsa oceanica* in Sample 103-637A-10R, CC, provides a first-occurrence datum in the lower Pleistocene.

Samples 103-637A-12R-1, 43–44 cm, through 103-637A-13R-1, 72–73 cm, contain both *Discoaster brouweri* and *D. triradiatus* and are placed in the upper Pliocene *Calcidiscus macintyrei* Subzone (CN-12D) of Okada and Bukry (1980). The highest occurrences of both *D. pentaradiatus* and *D. surculus* were observed in Sample 103-637A-13R-2, 46–47 cm. The presence of these two species in the absence of *D. tamalis* down to Sample 103-637A-15R-2, 82–83 cm, dates the base of lithologic Unit I in the *Discoaster surculus* Subzone (CN-12B). A minor hiatus was detected between Samples 103-637A-13R-1, 72–73 cm, and 103-637A-13R-2, 46–47 cm, where the entire *Discoaster pentaradiatus* Subzone (CN-12C) and possibly parts of the two adjacent subzones are absent.

Lithologic Unit II (the bottom of Core 103-637A-15R through the top of Core 103-637A-20R) consists of slumped brown clay and nannofossil marl. Nannofossil assemblages indicate a late Miocene (*Discoaster berggrenii* Subzone CN-9A) through late Pliocene (*Discoaster tamalis* Subzone CN-12A) age for this interval. Slumping or extensive reworking of noncontemporaneous material was not observed in this unit. Samples 103-637A-15R-4, 48–49 cm, through 103-637A-16R-1, 23–24 cm, contain *D. tamalis* but not *Reticulofenestra pseudoumbilica* and are placed in the upper Pliocene *Discoaster tamalis* Subzone (CN-12A). An early Pliocene age was determined down to Sample 103-637A-18R-1, 96–97 cm, where the lowest occurrence of *Ceratolithus acutus* was observed. The first occurrence of this species closely approximates the Miocene/Pliocene boundary. Samples 103-637A-16R-1, 147–148 cm, through 103-637A-17R-3, 39–40 cm, contain *R. pseudoumbilica* but no members of the genus *Amaurolithus* and are assigned to the *Reticulofenestra pseudoumbilica* Zone (CN-11). Sample 637A-17R-4, 39–40 cm, containing the genus *Amaurolithus* as well as *Ceratolithus rugosus*, was placed in the *Ceratolithus rugosus* Subzone (CN-10C). Rare specimens of *Ceratolithus acutus* were observed in three of four samples between Sample 103-637A-17R, CC, through 103-637A-18R-1, 96 cm; this interval is placed in the *Ceratolithus acutus* Subzone (CN-10B), on the basis of the entire range of the nominitive species. The *Triquetrorhabdulus rugosus* Subzone (CN-10A) was not recognized at this site because of the sporadic occurrence of the *D. quinqueramus*, which defines the base of this zone. Samples 103-637A-18R-2, 27–28 cm, through 103-637A-19R-2, 45–46 cm, contain amauroliths but no ceratoliths; the upper Miocene *Amaurolithus primus* Subzone (CN-9B) is determined for these samples. Samples 103-637A-19R-2, 80–81 cm, through 103-637A-20R-1, 57–58 cm, contain *D. surculus* but no amauroliths. These samples are placed within the *Discoaster berggrenii* Subzone (CN-9A). The occurrence of *D. loeblichii* and *Minylitha convalis*, two species having their last occurrences within this subzone (Perch-Nielsen, 1985), were also noted.

Samples taken from the red-brown clay of lithologic Unit III at the base of the sedimentary section are barren. The only nannofossils recovered within this lithologic unit came from isolated clasts of calcareous ooze (Samples 103-637A-20R, CC, 103-637A-21R, CC, and 103-637A-21R-5, 14–15 cm). These clasts contain well-preserved assemblages and indicate an early Pliocene age. Since two of these samples are from core catchers and the third from an interval of drilling breccia, they are most likely cavings from uphole.

The trace amounts of reworked material, detected in every sample, are constant and never exceed 1% of the total assemblage. Common solution-resistant Late Cretaceous forms, such as *Micula staurophora, Eiffellithus turriseiffeli, Cribrosphaerella ehrenbergii, Zygolithus diplogramus*, and *Prediscospaera cretacea*, are the most prevalent. *Ceratolithoides aculeous, Arkhangelskiella cymbiformis, Parhabdolithus asper*, and *Eiffellithus eximius* were also encountered. Many samples contain reworked Eocene species such as *Discoaster saipanensis* and *Discoaster barbadiensis. Dictyoccites bisectus* and *Dictyoccites abisectus*, common to early Oligocene assemblages, were also found in many samples. Pleistocene sediments commonly contain reworked Pliocene forms; similarly, Miocene forms occur in the Pliocene samples. The trace, yet persistent, amount of reworking is indicative of erosion and resuspension of material by bottom currents throughout the period of deposition at Site 637.

Radiolarians

Radiolarian preparations were made for all core-catcher samples from Hole 637A, together with an additional 50 samples from Cores 103-637A-6R to 103-637A-24R. The samples were treated with Calgon and, where necessary, with H_2O_2. In a second preparation phase, they were treated with diluted HCl.

The noncalcareous fraction (more than 62 μm) is dominated by detrital mineral grains, mainly mica and quartz and in some samples glauconite. Samples 103-637A-18R, CC, to 103-637A-24R, CC, contain aggregates from basement rocks.

Two nondiagnostic specimens of radiolarians (*Cenosphaera* sp., *Axoprunum* [?] sp.) and rare sponge spicules were observed in Sample 103-637A-1R, CC. Radiolarians and other siliceous microfossils are absent in samples prepared from the interval 103-637A-2R, CC, to 103-637A-24R-2, 90–92 cm.

The presence of detrital material suggests that many of the samples are allochthonous. The position of the drill site, near a basement high that acts as sediment trap, allows the accumulation of large amounts of redistributed and reworked material. Therefore, whether the absence of siliceous microfossils is the result of dissolution or of strong dilution with detrital material is unclear. Sedimentological observations somewhat indicate that the red clays of Samples 103-637A-19R, CC, to 103-637A-22R, CC, are products of alteration processes in the uppermost part of the basement rocks; this may account for the absence of siliceous microfossils from this interval.

The conclusions of Hole 637A radiolarian studies agree with those of nearby Hole 398D (Leg 47B, Vigo Seamount; Sibuet, Ryan, et al., 1979), where no radiolarians or other siliceous microfossils were recovered from strata younger than early Miocene. Furthermore, Sites 118 and 119 (Laughton, Berggren, et al., 1972) and Sites 399 through 402 (Montadert, Roberts, et al., 1979), situated farther north in the Bay of Biscay, were also barren of radiolarians during these times.

Summary

Foraminiferal and nannofossil assemblages recovered from Hole 637A allowed age determinations of late Miocene to late Pleistocene for lithologic Units I through III. Table 3 integrates foraminiferal and nannofossil age data with these lithologic units. Preservation and abundance was generally good for both nannofossils and foraminifers, though some core-catcher samples show evidence of drilling contamination. Reworking of older sediments compounded the contamination problems, making it difficult to establish a reliable age for some samples.

PALEOMAGNETICS

Two types of analyses were made on the sediments and crystalline rocks recovered at Site 637: whole-core measurements on Cores 103-637A-2R through 103-637A-15R and discrete sample

Table 3. Integrated zonation of Site 637.

Core no.	Foraminifers		Nannofossils		Lithologic units
	Age	Zone	Age	Zone	
1R				*Emiliania huxleyi*	I / IA
2R			Pleistocene, late	*Gephyrocapsa oceanica*	
3R					IA
4R				*Pseudoemiliania lacunosa*	
5R					
6R		N22	Pleistocene		IB
7R				*Gephyrocapsa* small	
8R	Pleistocene				I
9R				*Helicosphasera sellii*	
10R			early		IC
11R				*Calcidiscus macintyrei*	
12R			Pliocene	CN-12D	
13R	Pliocene, late	PL4/5	late	CN-12B	
14R					
15R	Pliocene	PL3		CN-12A	II
16R	mid		early	CN-11	
17R	early	PL1C/2		CN-10C CN-10B	
18R	late Miocene	M11-12	late Miocene	CN-9B	
19R				CN-9A	
20R					III
21R					
22R	?	?	?	?	
23R					IV
24R					

analyses on undisturbed sediment intervals in Cores 103-637A-9R through 103-637A-22R and on serpentinite basement in Cores 103-637A-23R through 103-637A-28R. The results are useful for magnetostratigraphic studies of only some of the discrete samples from marls or upper parts of turbidites in Cores 103-637A-9R through 103-637A-17R; all other analyses suggest major overprinting, acquisition of viscous magnetization, or disruption of the primary magnetization either during drilling or as a byproduct of magnetic mineralogy and postdepositional chemical alteration.

In this report, centimeter/gram/second (CGS) units are used instead of Standard International (SI) units because these are the metric units currently used by the shipboard laboratory equipment and computer programs and because CGS units are better suited than SI units for discussions of total and unit magnetization of sample volumes measured in cm^3 rather than in m^3.

Discrete Samples (Late Miocene–Pleistocene Sediments)

Discrete samples were collected as oriented cubes or thin slabs and were progressively demagnetized in an alternating field (AF) of as much as 100 oersteds. These data were also collected using the pass-through cryogenic magnetometer, although a computer program for accurate analysis of discrete samples has not yet been written. Furthermore, the peak of intensity on the Z-axis (up–down component of magnetization) is offset by about 5 cm from the peaks on the X- and Y-axes (horizontal components) during the conveyer movement of the discrete sample through the sensor region, which leads to an inherent uncertainty of several degrees in the computed inclination. In Table 4, the data were selected at the step displaying the maximum *total* intensity. As a result, the polarity of the samples were determined from the Z-axis component of magnetization as shown on the graphic display; the quantitative values of inclination and intensity in Table 4 should not be used for computation of mean inclination or paleolatitudes.

Samples were collected at a density of as much as four per section wherever the recovered cores showed relatively undisturbed sedimentary structures. The poor recovery (rarely more than 15%) and even poorer recovery of intact sediments generally limited discrete sampling to about six per core, which was inadequate to derive a magnetostratigraphy.

Cores 103-637A-1R through 103-637A-7R were too disturbed to allow discrete sampling. Cores 103-637A-8R through 103-637A-17R yielded mixed polarity upon AF demagnetization, though thermal demagnetization could possibly provide more reliable data. Cores 103-637A-18R through 103-637A-23R are dominated by brownish clay; the results of predominantly normal polarity are probably due entirely to an overprint of present-day field carried by goethite-bearing clay. Thermal demagnetization can remove overprints carried by goethite; the present laboratory lacks the necessary shielded oven required for such treatment.

A predominantly reversed interval occurs from Sample 103-637A-10R-1, 65 cm, to Sample 103-637A-13R-1, 96 cm. The biostratigraphy indicates that this reversed interval is the Matuyama Reversed Chron of early Pleistocene and latest Pliocene age. One normal sample, representing the interval between Sample 103-637A-12R-1, 83 cm, and 103-637A-12R-2, 65 cm, could be all that was recovered of the Olduvai Normal Event, but this is speculative. The interval from the lower part of Core 103-637A-13R through the upper part of Core 103-637A-17R displays normal polarity during AF demagnetization, which is inconsistent with the mixed polarity expected for the late through early Pliocene age interval; this could either arise by chance or indicate an overprint carried by goethite and/or other secondary iron minerals. The lower part of Core 103-637A-17R displays reversed polarity upon AF demagnetization above 50 oersteds, as does the upper part of Core 103-637A-19R; however, it is impossible to make a correlation to the magnetic polarity time scale of the Pliocene. The polarity interpretations are tabulated in Table 4.

Serpentinite Basement: Orientation of Foliation and Intensity of Magnetization

Nine oriented small slabs (thin-section billets or petrographic samples) of the serpentinized peridotite basement were analyzed using progressive demagnetization. These slabs from Cores 103-637A-25R to 103-637A-27R were selected from blocks displaying a 20°–40° apparent dip of foliation (indicated by lighter streaks, deformed phenocrysts, and other textures).

The dip-direction orientation of the foliation with respect to the "X-axis" of the magnetometer coordinate system was recorded for each sample. A sample having a direction/magnetization in the (+X, Z) plane has a declination of 0° in this coordinate system. Therefore, if this sample has a foliation dip direction of 90° clockwise to the X axis, then the relative declination of the dip direction with respect to the 0° declination of magnetization is 90°. If the direction of magnetization has other apparent declinations in the magnetometer coordinate system, then the foliation dip direction with respect to the magnetization direction is the difference measured clockwise from the magnetization direction between the two (e.g., if foliation dip direction is toward 180° or in −X direction and magnetization direction is toward 135° declination, then the relative direction of the dip of foliation is at +45° with respect to the magnetization). If the magnetization has normal polarity, as indicated by position inclinations, then the *actual* direction of magnetization is north, or at 0° declination in the paleogeographic coordinate system; therefore, the relative declination of foliation dip direction with respect to the magnetization is the same as its actual orientation with respect to paleogeographic north.

All samples were treated by progressive AF demagnetization to 100 oersteds; most of the samples displayed a fairly stable direction of magnetization. The results are shown in Table 5.

All nine pieces yielded normal polarity with the dip direction of the foliation oriented approximately 90° clockwise to the declination of the magnetization. Two samples yielding a magnetization significantly different from eastward are considered to be spurious.

Regardless of whether these normal-polarity magnetization directions are due to a primary Cretaceous direction during the period of the Cretaceous Normal Quiet Zone (the presumed age of the uplift of the serpentinite ridge) or to an overprint of present-day normal polarity, the orientations of either magnetic "north" are within 30° declination of each other. Therefore, the direction of magnetic "north" relative to the direction of foliation indicates that the foliation must dip toward the *east*.

The mean inclination of the samples in the 100-oersted AF demagnetization step is 40°–55°, which would imply a paleolatitude of approximately 25°–35°. Although this inclination is consistent with a Cretaceous latitude, we do not consider these samples to provide a reliable mean inclination, owing to the lack of stable directions during AF demagnetization.

The mean intensity of natural remanent magnetization (NRM) is approximately 1.2×10^{-3} emu/cm^3 for the less-altered samples, although the rapid decrease of intensity in some samples when AF demagnetization was applied suggests that a large part of the NRM is a viscous remanent magnetization. The average NRM intensity of this serpentinized peridotite is one-third of the average intensity of basaltic rocks recovered at DSDP sites in the Atlantic (Lowrie, 1979). Why the "serpentinized peridotite ridge" displays no magnetic anomaly cannot be answered without knowing the thickness of the body and the intensity of magnetization at depth. Some possible explanations could be that (1) the body is thin; hence, it has a negligible net magnetization; (2) the underlying part of the body has an even lower magnetization; (3) the surrounding crust has a relatively high net magnetization; hence there is no contrast; and (4) removal of basement-rock topographic effects from the magnetic anomaly charts would reveal a large negative anomaly associated with this ridge, which is not apparent in the total magnetic field charts currently being used. These possibilities could be narrowed if the nature and magnetization of the adjacent crust were known.

ORGANIC GEOCHEMISTRY

Carbon, Hydrogen, and Nitrogen Analysis

Twenty-nine sediment samples were taken from Hole 637A for organic carbon (C), hydrogen (H), and nitrogen (N) determination using the Perkin Elmer elemental analyzer. Results of the organic carbon percentage on a dry-sediment weight basis are plotted vs. depth in Figure 19. In general, preservation of organic matter is poor at Site 637. Excluding the uppermost sample, organic carbon averages 0.25%. This is below the 0.3% average for ancient deep-ocean sediments (McIver, 1975). Because of technical problems, reliable determination of elemental nitrogen was impossible. Since atomic carbon-to-nitrogen ratios were unavailable, the type of organic matter (marine vs. terrestrial) was based on Rock-Eval interpretation.

Rock-Eval Analysis

Twenty-one sediment samples representing all the various lithologic units recovered were analyzed using the Rock-Eval. The organic matter at Site 637 is composed mostly of terrigenous (Type III) kerogen and small amounts of marine (Type II) kerogen. The hydrogen index (HI) and the oxygen index (OI) average 87 and 1251, respectively. High OI values such as these may indicate highly oxidized, reworked organic matter. With such high oxidation or reworking, the original character of the organic matter may have been obscured by diagenetic alterations. The temperature of the S2 peak maximum (T_{max}) indicates the maturity of the organic matter (Espitalie et al., 1977). T_{max} values for the 21 samples average 349°C, a low value indicating a low thermal history for the organic matter.

Organic Carbon Isotope Analyses

Organic carbon isotopes were run onshore after the cruise. Procedures for collecting these data are given in the "Explanatory Notes" chapter (this volume); the data are listed in Table 6.

INORGANIC GEOCHEMISTRY

Interstitial-Water Chemistry

Six sediment samples were taken from the cores recovered by rotary drilling at Site 637 to extract interstitial-water samples. These 340-cm^3 sediment samples were squeezed aboard ship, and the interstitial waters were analyzed for pH, alkalinity, chlorinity, salinity, calcium, and magnesium. Wet-chemical titrations were used for analysis of calcium, magnesium, and chloride ions, following the procedures of Gieskes (1974) and Gieskes and Peretsman (1986). A semiautomatic titration using a Metrohm titrator was implemented for the pH and alkalinity analyses. Salinity was determined using a Goldberg refractometer. The primary standard used for calibration of the water analyses was IAPSO standard seawater. A sample of the surface seawater was obtained at Site 637 and chemically analyzed for comparison with other samples.

The results, as listed in Table 7 and graphed in Figure 20, show little variation with increasing depth. The alkalinity decreases downward, as expected (Gieskes, 1981). Salinity, chlorinity, and pH show no significant changes with depth.

The slight variation in the calcium and magnesium cations with depth is enhanced for comparison by plotting the values obtained by analysis of surface seawater from Site 637 (Fig. 21). A small minimum occurs in the calcium plot in Core 103-637A-9R (75.4–75.5 m sub-bottom depth) where the lithology changes from terrigenous turbidites having thick, silty layers and marls (lithologic Subunit IB) to underlying terrigenous turbidites having thin, silty layers and marls (lithologic Subunit IC). Below Core 103-637A-9R, the calcium concentration increases to approximately double the minimum value immediately above basement rock in Core 103-637A-23R. Magnesium concentrations show no distinct downhole trend and fluctuate around 47.0 mmol/L.

Calcium Carbonate

Concentrations of $CaCO_3$ in dried sediment samples determined by the shipboard carbonate bomb (Müller and Gastner, 1971) are graphed with respect to depth in Figure 22 and listed in Table 8. The chaotic pattern of highs and lows above 180 m sub-bottom depth (Core 103-637A-20R) are the consequence of the interbedded terrigenous and calcareous turbidite deposits in lithologic Unit I and interbedded slumped brown clay and nannofossil marl in lithologic Unit II. Below 180 m sub-bottom depth, in samples from reddish brown clay of lithologic Unit III, carbonate-content values are consistently low.

PHYSICAL PROPERTIES

Physical-property measurements were made on sediment and basement samples from Core 103-637A-6R to Core 103-637A-30R. Unsplit cores were processed through the shipboard Gamma Ray Attenuation Porosity Evaluator (GRAPE), analyzed for magnetic properties, and then allowed to equilibrate with room temperature for 4 hr. After waiting 4 hr for Core 103-637A-6R to reach thermal equilibrium with the ambient temperature of the laboratory, sediment from the core was tested for thermal drift to assure that the core temperature had stabilized. Upon confirming that 4 hr was sufficient time for temperature stabilization, we adopted the convention of allowing this much time to pass between the first appearance of a core on deck and the measurement of thermal conductivity of the core contents.

After thermal-conductivity measurements, the core sections were surrendered to shipboard technicians for splitting before we began the next series of physical-properties measurements. These included measurement of shear strength on the vane apparatus, compressive seismic velocity on the Hamilton Frame velocimeter, and index properties (bulk and grain density, water content, and porosity) calculated on the basis of weights obtained from a triple-beam balance and volumes obtained using the shipboard Penta-Pyncnometer densitometer. Index-property samples were also used for determination of carbonate content using the carbonate bomb (Müller and Gastner, 1971).

Thermal Conductivity

Thermal-conductivity measurements were performed on Cores 103-637A-6R to 103-637A-23R (Fig. 23A). Values increase slightly with depth from lithologic Unit I (only drilling-disturbed material was available for measurements in Subunit IB) through the brown clay of lithologic Unit II and decrease slightly through the reddish brown clay of lithologic Unit III. Values range from 2.00 to 3.71 $\times 10^{-3}$ cal $\times$ °$C^{-1} \times cm^{-1} \times s^{-1}$ (calories/degree Celsius/centimeter/second). If sections that are suspect because of visible drilling disturbance are omitted, the low value in this range increases to 2.50 $\times 10^{-3}$ cal $\times$ °$C^{-1} \times cm^{-1} \times s^{-1}$, and average thermal conductivity for the sedimentary section becomes 2.94 $\times 10^{-3}$ cal $\times$ °$C^{-1} \times cm^{-1} \times s^{-1}$.

Table 4. Paleomagnetic data from discrete samples of late Miocene–Pleistocene sediments, Hole 637A.

Sample	Treatment	Decl.	Incl.	Intensity ($\times 10^{-7}$ emu/cm^3)	Polarity
103-637A-8R-2, 93 cm	AF 100	350°	56.0°	0.6	N? weak
103-637A-8R-2, 126 cm	AF 100	227°	29.2°	10.8	N
	AF 101	208°	19.0°	15.6	
103-637A-8R-3, 87 cm	AF 100	289°	21.6°	3.1	N
103-637A-9R-1, 73 cm	AF 100	44°	14.8°	5.2	N
103-637A-9R-2, 79 cm	AF 100	1°	44.5°	3.0	N
103-637A-10R-1, 19 cm	AF 100	70°	58.9°	14.2	N
103-637A-10R-1, 65 cm	AF 100	160°	−13.5°	10.3	R
103-637A-10R-1, 142 cm	AF 100	105°	14.9°	8.7	N
103-637A-11R-1, 65 cm	AF 100	160°	−53.5°	5.1	R
103-637A-11R-1, 87 cm	AF 100	105°	14.9°	8.7	N?
103-637A-11R-1, 139 cm	AF 100	196°	−14.1°	6.8	R
103-637A-12R-1, 44 cm	AF 100	297°	−19.8°	9.7	R
103-637A-12R-1, 83 cm	AF 100	12°	−21.1°	5.6	R
	2nd try	8°	−27.4°	4.6	
103-637A-12R-2, 21 cm	AF 50	281°	19.3°	7.8	N
103-637A-12R-2, 65 cm	AF 50	97°	−57.8°	3.1	R
	AF 80	131°	−63.6°	4.6	
103-637A-13R-1, 54 cm	AF 70	42°	−2.2°	16.4	R
	AF 90	40°	−6.0°	16.3	
103-637A-13R-1, 82 cm	AF 70	184°	−3.1°	3.6	R?
	AF 90	171°	−13.2°	3.0?	
103-637A-13R-1, 96 cm	AF 70	15°	−31.2°	9.5	R
	AF 90	14°	−30.9°	9.8	
103-637A-13R-1, 115 cm	AF 70	177°	52.6°	12.3	N
	AF 90	176°	51.9°	11.6	
103-637A-13R-2, 48 cm	AF 70	75°	11.0°	13.0	N
	AF 90	74°	9.1°	12.6	
103-637A-13R-2, 74 cm	AF 70	75°	48.0°	26.6	N
	AF 90	55°	46.6°	20.1	
103-637A-14R-1, 46 cm	AF 50	4°	25.4°	13.7	N
	AF 70	1°	23.6°	12.0	
103-637A-14R-1, 64 cm	AF 50	37°	5.6°	16.5	N?
	AF 70	38°	0.9°	16.2	
103-637A-14R-1, 78 cm	AF 50	44°	38.5°	8.4	N
	AF 70	49°	37.0°	7.2	
103-637A-14R-1, 149 cm	AF 50	113°	8.5°	14.1	N
	AF 70	117°	4.7°	14.3	
103-637A-15R-1, 9 cm	NRM	263°	?	60? off scale	
	AF 50	264°	65.4°	42.9	N
	AF 80	262°	65.9°	38.7	
103-637A-15R-1, 37 cm	NRM	213°	43.8°	46.8	N
	AF 50	219°	68.2°	27.6	
	AF 80	217°	67.6°	25.4	
103-637A-15R-1, 72 cm	NRM	305°	65.2°	15.4	N
	AF 50	300°	59.8°	10.0	
	AF 80	304°	55.2°	8.2	
103-637A-15R-1, 132 cm	NRM	12°	62.4°	60? off scale	
	AF 50	14°	64.5°	30.3	N
	AF 80	15°	63.6°	27.4	
103-637A-15R-2, 31 cm	NRM	323°	58.7°	27.0	N
	AF 50	320°	59.0°	22.3	
	AF 80	317°	57.7°	20.0	
103-637A-15R-2, 58 cm	NRM	18°	60.0°	37.1	N
	AF 50	23°	62.0°	30.1	
	AF 80	21°	61.8°	26.6	
103-637A-15R-2, 91 cm	NRM	296°	75.0°	20.2	?
	AF 50	284°	70.6°	14.9	
	AF 80	286°	66.4°	13.1	
103-637A-16R-2, 87 cm	NRM	137°	75.9°	26.1	?
	AF 50	149°	75.1°	15.7	
	AF 80	147°	80.9°	10.9	
103-637A-16R-3, 64 cm	NRM	81°	65.4°	41.9	N
	AF 50	85°	64.6°	35.6	
	AF 80	78°	62.1°	32.0	
103-637A-16R-4, 3 cm	NRM	246°	84.3°	42.0	?
	AF 50	315°	82.2°	38.7	
	AF 80	261°	83.5°	34.7	
103-637A-17R-1, 19 cm	NRM	298°	67.6°	41.9	N
	AF 50	297°	65.3°	35.9	
	AF 80	290°	38.2°	14.9	
103-637A-17R-1, 131 cm	NRM	122°	64.4°	10.0	N
	AF 50	116°	59.4°	5.5	
	AF 80	108°	54.1°	3.9	

Table 4 (continued).

Sample	Treatment	Decl.	Incl.	Intensity ($\times 10^{-7}$ emu/cm^3)	Polarity
103-637A-17R-2, 51 cm	NRM	82°	56.6°	35.0	N weak
	AF 50	83°	52.7°	28.0	
	AF 80	83°	50.9°	23.6	
103-637A-17R-3, 24 cm	NRM	344°	6.8°	1.3	? weak
	AF 50	322°	66.8°	0.7	
	AF 80	343°	5.8°	1.0	
103-637A-17R-3, 67 cm	NRM	353°	24.3°	1.9	R? weak
	AF 50	357°	−1.7°	1.1	
	AF 80	357°	−21.1°	1.6	
103-637A-17R-3, 131 cm	NRM	24°	29.7°	7.3	R
	AF 50	25°	−1.4°	6.4	
	AF 80	22°	−10.5°	7.0	
103-637A-17R-4, 15 cm	NRM	62°	66.7°	17.7	R
	AF 50	63°	12.4°	7.7	
	AF 80	59°	−13.4°	8.4	
103-637A-18R-1, 49 cm	NRM	37°	71.3°	35.4	N
	AF 20	40°	72.2°	35.2	
	AF 50	35°	69.1°	33.4	
103-637A-18R-1, 84 cm	NRM	82°	57.0°	22.4	N
	AF 20	83°	56.7°	22.1	
	AF 50	83°	54.7°	21.5	
103-637A-18R-1, 121 cm	NRM	136°	78.2°	48.0	N?
	AF 20	19°	62.7°	49.1	
	AF 50	18°	60.1°	35.5	
103-637A-18R-2, 5 cm	NRM	55°	65.3°	38.5	N
	AF 20	59°	62.0°	32.4	
	AF 50	74°	54.4°	16.9	
103-637A-18R-2, 49 cm	NRM	185°	64.0°	56.2	?
	AF 20	327°	86.0°	35.3	
	AF 50	260°	81.6°	14.9	
103-637A-18R-2, 99 cm	NRM	130°	59.7°	20.2	N
	AF 20	122°	60.0°	18.6	
103-637A-19R-1, 37 cm	NRM	203°	28.2°	38.6	R
	AF 20	206°	18.0°	31.4	
	AF 50,80	Data missing, plots indicate reversed			
103-637A-19R-1, 84 cm	NRM	294°	54.7°	18.8	R
	AF 20	301°	38.8°	13.9	
	AF 50,80	Data missing, plots indicate reversed			
103-637A-19R-1, 122 cm	NRM	330°	52.4°	23.1	?
	AF 20	334°	44.3°	19.5	
103-637A-19R-2, 11 cm	NRM	178°	61.5°	25.1	N
	AF 20	172°	59.1°	19.4	
	AF 50	170°	16.1°	25.0	
103-637A-19R-2, 71 cm	NRM,AF20,AF50	Polarity determined from graphs			N
103-637A-19R-2, 115 cm	NRM,AF20,AF50	Polarity determined from graphs			N
103-637A-19R-3, 11 cm	NRM,AF20,AF50	Polarity determined from graphs			N
103-637A-20R-1, 13 cm	NRM,AF20,AF50	Polarity determined from graphs			N
103-637A-20R-1, 63 cm	NRM,AF20,AF50	Polarity determined from graphs			N
103-637A-20R-1, 83 cm	NRM	261°	71.6°	30.6	N
	AF 20	281°	68.5°	24.4	
	AF 50	321°	41.8°	8.8	
103-637A-20R-1, 118 cm	NRM	108°	63.8°	43.9	N
	AF 20	107°	60.1°	38.2	
	AF 50	104°	59.4°	15.9	
103-637A-20R-2, 26 cm	NRM	191°	79.1°	53.3	N? steep
	AF 20	186°	77.6°	44.5	
	AF 50	196°	75.8°	20.2	
103-637A-20R-2, 61 cm	NRM	0°	81.1°	28.7	? steep
	AF 20	7°	82.2°	22.5	
	AF 50	120°	87.8°	8.4	
103-637A-20R-3, 26 cm	NRM	237°	75.8°	21.1	N
	AF 20	227°	70.3°	17.3	
	AF 50	241°	52.2°	8.3	
103-637A-21R-1, 59 cm	NRM	346°	61.3°	63.5	N
	AF 20	342°	55.9°	54.0	
	AF 50	338°	49.4°	36.4	
103-637A-21R-6, 111 cm	NRM	194°	81.6°	44.8	N
	AF 20	186°	82.3°	41.0	
	AF 50	127°	78.1°	27.3	
103-637A-22R-1, 95 cm	NRM	Data missing, polarity from graph			N

Note: Polarity of brownish clays in Cores 103-637A-17R through 103-637A-22R often appeared to be normal, but these require thermal demagnetization to obtain the primary polarity.

Table 5. Paleomagnetic data from serpentinite basement samples, Hole 637A.

Sample	Treatment	Decl.[a]	Incl.	Intensity ($\times 10^{-4}$ emu/cm^3)
103-637A-25R-1, piece no. 8E	NRM	196°	30°	3.1
	AF 20	193°	37°	2.4
	AF 40	189°	45°	2.1
	AF 70	190°	35°	1.5
	AF 100	191°	35°	1.3
Relative orientation in magnetometer coordinate system of maximum dip of foliation ~270° clockwise implies declination = 101° (east) with respect to magnetic "north."				
103-637A-25R-2, piece no. 1D	NRM	145°	46°	14.5
	AF 20	153°	47°	10.1
	AF 40	161°	44°	3.4
	AF 70	171°	48°	1.9
	AF 100	170°	47°	1.5
Relative orientation of maximum dip of foliation ~270° clockwise implies declination = 80° (east).				
103-637A-25R-5, 1-3 cm	NRM	39°	66°	8.0
	AF 20	43°	79°	6.7
	AF 40	22°	67°	3.0
	AF 70	6°	62°	0.2
	AF 100	356°	57°	0.1
Relative orientation of maximum dip of foliation ~90° clockwise implies declination = 86° (east).				
103-637A-26R-1, 145-147 cm	NRM	348°	39°?	12.0 (off scale)
	AF 20	344°	58°	6.4
	AF 40	343°	60°	2.4
	AF 70	348°	68°	1.5
	AF 100	359°	75°	0.8
Relative orientation of maximum dip of foliation ~270° clockwise implies declination = 269° (west), thus being inconsistent with other results. Sample is very altered.				
103-637A-26R-2, piece no. 1E	NRM	157°	62°	15.0
	AF 20	162°	64°	10.2
	AF 40	151°	65°	3.9
	AF 70	9°	54°	1.5
	AF 100	0°	57°	0.3
Relative orientation of maximum dip of foliation ~90° clockwise implies declination = 90° (east).				
103-637A-27R-2, 113-117 cm	NRM	177°	36°	12.6
	AF 20	173°	39°	10.5
	AF 40	164°	39°	7.5
	AF 70	150°	40°	4.3
	AF 100	141°	39°	2.5
Relative orientation of maximum dip of foliation ~270° clockwise implies declination = 60°-50° (~northeast).				
103-637A-27R-3, 31-33 cm	NRM	340°	56°	9.3
	AF 20	345°	54°	8.7
	AF 40	346°	49°	7.1
	AF 70	343°	46°	5.8
	AF 100	341°	44°	4.5
Relative orientation of maximum dip of foliation ~0° implies declination = 341° (northwest, inconsistent with other results).				
103-637A-27R-4, 99-102 cm	NRM	191°	74°	12.7
	AF 20	202°	75°	10.2
	AF 40	208°	75°	5.9
	AF 70	199°	75°	0.7
	AF 100	179°	74°?	0.4
Relative orientation of maximum dip of foliation ~270° clockwise implies declination = 89° (east).				
103-637A-27R-5, 13-16 cm	NRM	176°	58°?	16.0? off scale
	AF 20	220°	60°?	12.0? off scale
	AF 40	198°	60°?	10.0? off scale
	AF 70	177°	60°?	8.0? off scale
	AF 100	179°	60°?	7.0? off scale
Relative orientation of maximum dip of foliation ~270° clockwise implies declination = 89° (east).				

[a] Declinations of magnetization and relative orientations of foliation are given with respect to the +X direction in the coordinate system of the magnetometer.

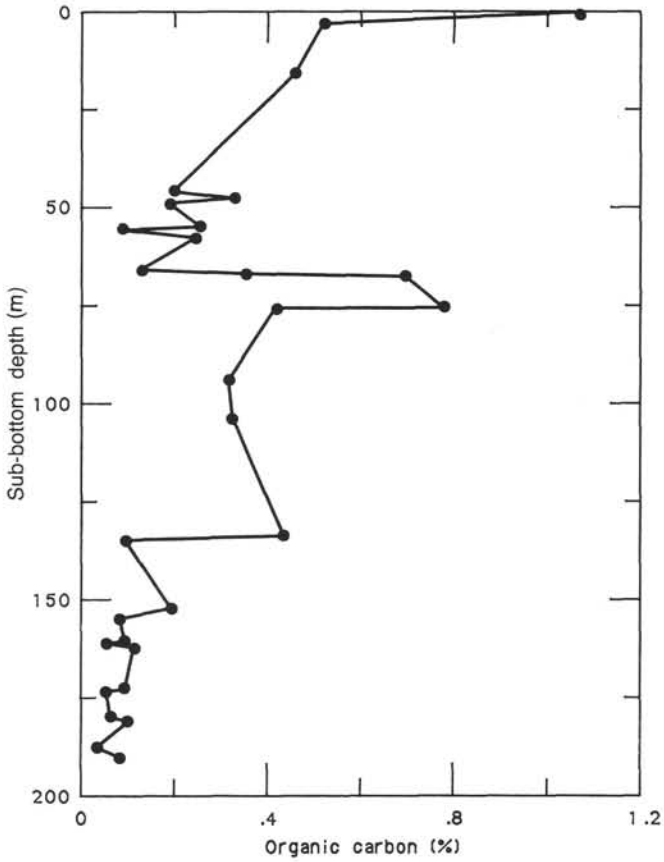

Figure 19. Organic carbon percentage vs. sub-bottom depth (m).

Vane-Shear Strength

Vane-shear-strength measurements were performed on sediments from Cores 103-637A-6R through 103-637A-10R (Fig. 23B). Undrained shear strength ranges from 10 to 30 kiloPascals (kPa) in Cores 103-637A-6R to 103-637A-9R (45–84 m sub-bottom); these sediments were moderately disturbed by drilling (see "Sediment Lithology" section, this chapter), and shear-strength measurements on this interval are probably conservative indicators of *in-situ* values.

An abrupt increase in shear strength was measured between Cores 103-637A-9R and 103-637A-10R; Sample 103-637A-10R-1, 100 cm (84.7 m sub-bottom), showed a shear strength of 72 kPa. No further measurements of shear strength were made at this site because the shear strength of this last sample twisted the blades of the vane. The increase in shear strength between Cores 103-637A-9R and 103-637A-10R may correspond to differences in the physical properties of lithologic Subunit IB (Cores 103-637A-6R through 103-637A-9R) and Subunit IC (Cores 103-637A-10R to 103-637A-15R). More likely, the increase is a simple reflection of the greater degree of drilling disturbance observed in the first nine cores drilled at this site.

Compressional Seismic Velocities

Seismic velocities of sediments from Hole 637A measured on the Hamilton Frame velocimeter were commonly lower than those used in interpreting the site-survey seismic profiles before drilling. Predrilling calculations assumed a seismic velocity in the sediments of about 1.60 kilometers per second (km/s), and laboratory measurements on sediments cored at Site 637 yielded values clustering around 1.50 km/s. Reported velocities reflect a

Table 6. Organic carbon isotope values, Hole 637A. HI = hydrogen index; OI = oxygen index.

Sample (interval in cm)	Sub-bottom depth (m)	Age	Organic carbon (%)	$CaCO_3$ (%)	$\delta^{13}C$	HI	OI
103-637A-6R-1, 129–131	46.19	Pleistocene	0.2	31	−23.8	na	na
103-637A-8R-3, 20–23	67.6	Pleistocene	0.36	4.4	−23.9	na	na
103-637A-11R-1, 97–99	94.28	Pleistocene	0.32	14.9	−24.5	na	na
103-637A-15R-2, 50–52	133.7	Pliocene	0.44	16.3	−26	31	525
103-637A-18R-2, 34–36	162.54	Pliocene	0.12	4.4	−27.5	na	na
103-637A-21R-1, 35–38	189.95	Miocene	0.09	4.4	−25.8	844	111

na = not available.

Table 7. Shipboard interstitial-water analyses, Site 637.

Sample (interval in cm)	Sub-bottom depth (m)	pH	Alkalinity (meq/kg)	Salinity (‰)	Chlorinity (‰)	Ca^{++} (mmol/L)	Mg^{++} (mmol/L)
103-637A-6R-2, 140–150	47.8–47.9	7.42	8.92	34.5	19.56	6.68	47.16
103-637A-7R-2, 140–150	57.9–58.0	7.45	7.61	34.6	19.75	6.08	46.56
103-637A-9R-1, 140–150	75.4–75.5	7.51	7.82	34.3	18.25	5.80	47.56
103-637A-15R-3, 140–150	136.1–136.2	7.54	4.38	34.5	19.45	8.67	46.53
103-637A-18R-1, 140–150	162.1–162.2	7.49	3.71	33.8	18.43	9.27	47.52
103-637A-23R-3, 0–10	211.8–211.9	7.78	2.49	35.6	17.82	11.83	46.82

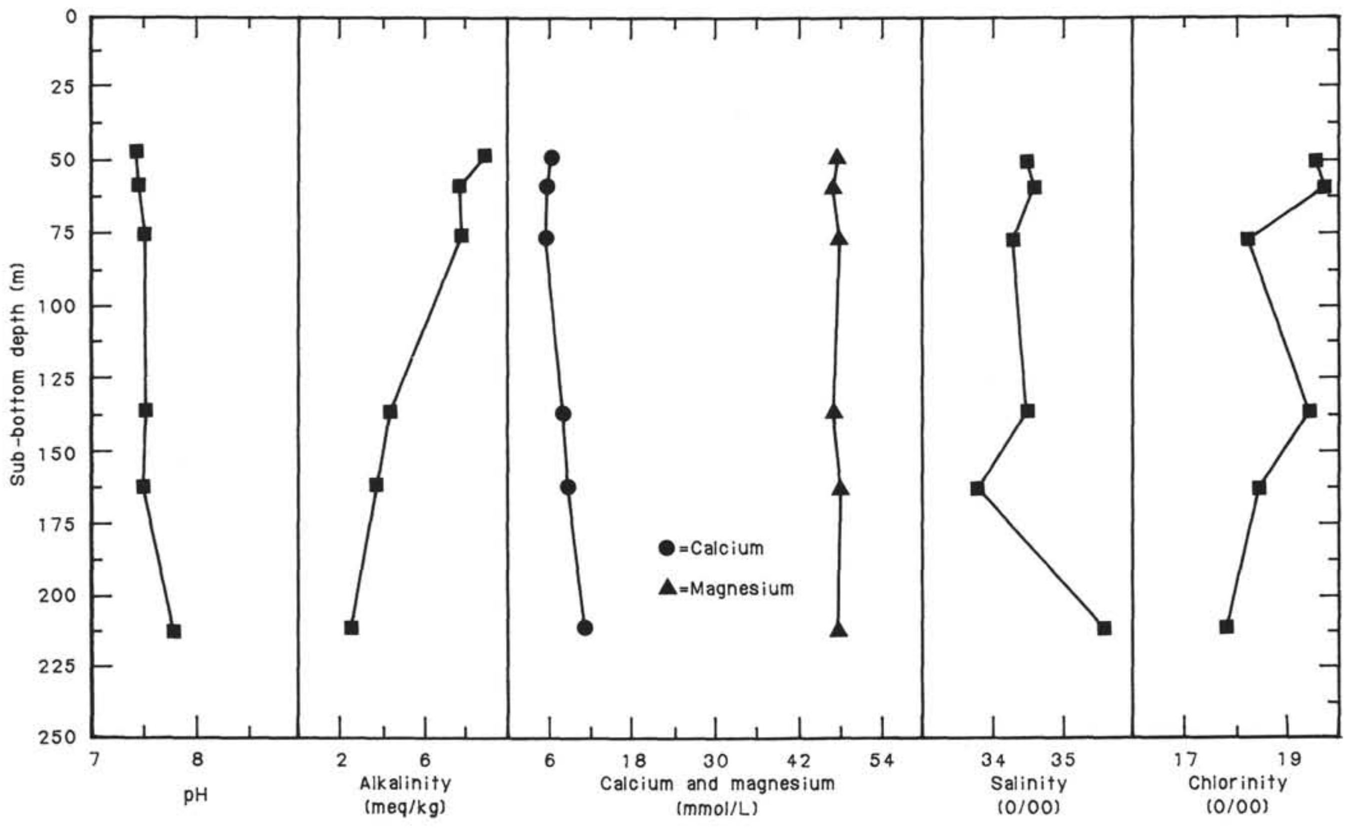

Figure 20. Summary of interstitial-water data from Site 637. Data are given in Table 7.

precision of ±0.04 km/s in the upper 75 m of section and ± 0.02 km/s in materials below this.

A few trends can be observed in Figure 23C, which shows compressional seismic velocity plotted against sub-bottom depth. The scattered low velocity values in the upper 75 m reflect the disruption of the sediment as a result of rotary drilling. Cores 103-637A-9R through 103-637A-17R show slightly less variability and a slight increase in velocity. A reversal in this trend occurs between about 160 and 190 m sub-bottom (Cores 103-637A-18R to 103-637A-21R), and velocities decrease slightly. Below about 190 m sub-bottom, velocity again increases with depth. The increase at 190 m corresponds to approximately the boundary between lithologic Units II and III (about 180 m sub-bottom; see "Sediment Lithology" section, this chapter). From about 190 m sub-bottom to basement (roughly corresponding to lithologic Unit III; see "Sediment Lithology" section, this chapter), veloc-

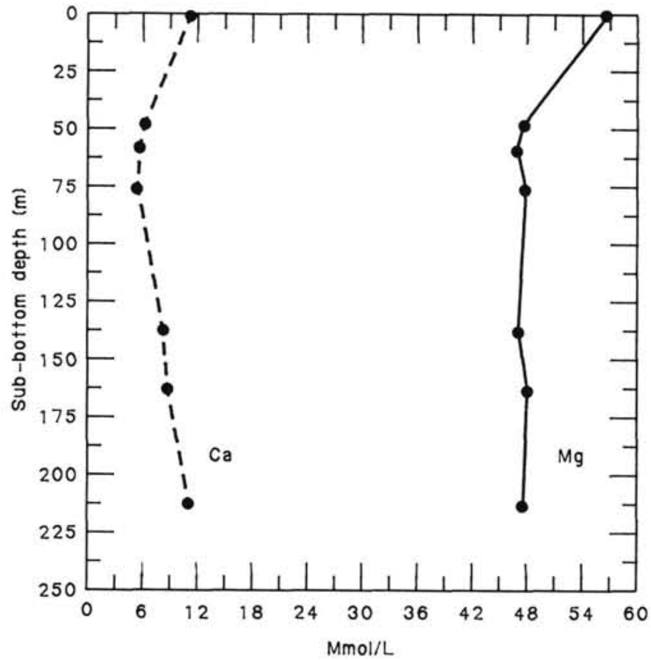

Figure 21. Calcium and magnesium cation concentrations in interstitial-water samples compared with surface seawater values (plotted at 0-m depth) at Site 637.

ities again increase with depth to about 1.80 km/s. Marl and mudstone velocities are slightly greater than velocities in carbonate ooze.

Although systematic compressional velocity anisotropy is not apparent in the sediment samples, the ultramafic nature of the basement rock suggests that it might exhibit anisotropy. Foliation planes are clear in fresher (greenish) rocks having attitudes ranging from several degrees to 45°. More-altered rocks (darker green or black serpentinite; see "Basement Rocks" section, this chapter) exhibit weak to no foliation. In fresh peridotite, compressional seismic velocities range from 8.0 to 8.9 km/s and commonly show a strong preferred orientation of olivine crystals (Kasahara et al., 1968). Seismic velocities for basement material at Site 637 range from 2.9 to 4.7 km/s and cluster around 3.7 km/s. On the assumption that the fresher basement material might preserve some of this orientation, we analyzed 15 basement samples in three directions: (1) perpendicular to the foliation plane (a-direction; dots in Fig. 23C), (2) parallel to the split core face and perpendicular to a-direction (b-direction; triangles in Fig. 23C), and (3) perpendicular to both of these directions (c-direction; squares in Fig. 23C). Ten of the 15 samples analyzed exhibited weak to strong foliation-related anisotropy even in samples that are altered from peridotite to serpentinite; velocities are lower in the a-direction (foliation-perpendicular). The weak anisotropy observed in more altered rocks suggests that alteration of olivine-rich peridotite to serpentinite distorts preexisting preferred orientation, resulting in a more random structure. According to empirical evaluation of birefringence and velocity anisotropy, minerals of the serpentine group should retain

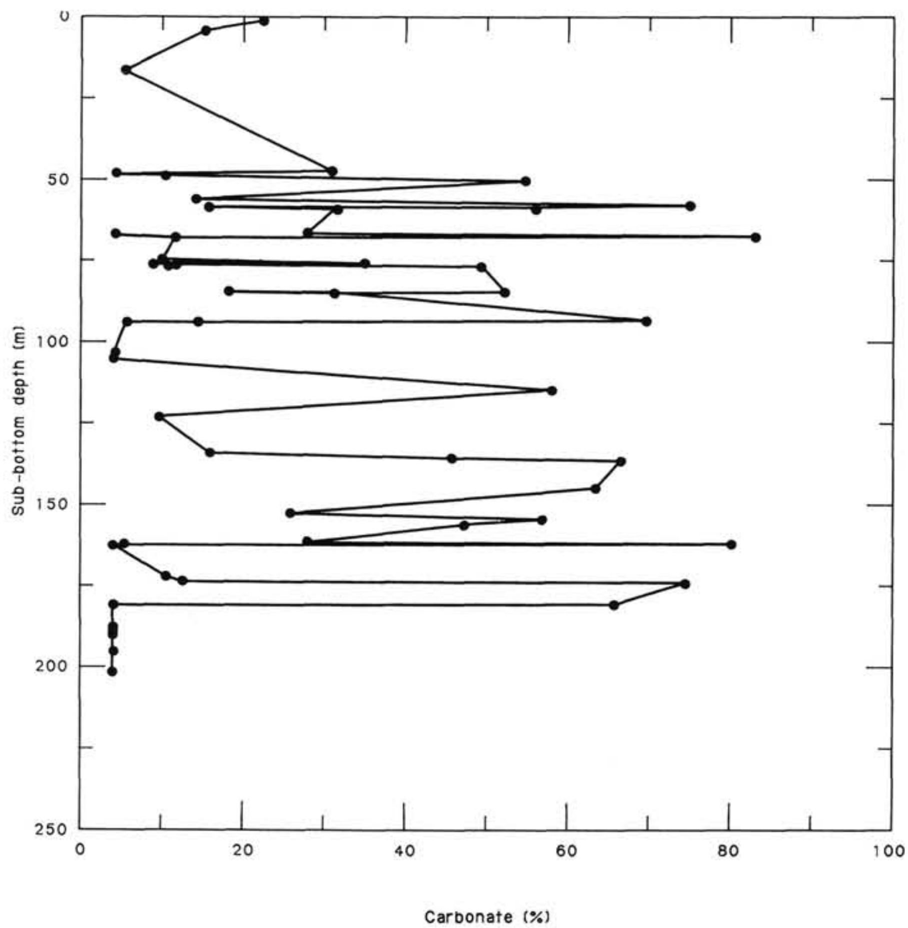

Figure 22. Percentage of calcium carbonate in dried sediment samples from Site 637. Data are given in Table 8.

Table 8. Carbonate-bomb analyses, Site 637.

Sample (interval in cm)	Sub-bottom depth (m)	Carbonate (%)	Lithology[a]
103-637A-1R-CC, 5-6	0.05	22.4	Calcareous clay
103-637A-2R-1, 5-6	3.05	15.4	Calcareous clay
103-637A-3R-CC	15.70	5.4	Clay
103-637A-6R-1, 129-131	46.19	30.97	Foraminiferal sand
103-637A-6R-2, 129-131	47.69	4.36	Muddy dark-gray silt
103-637A-6R-3, 129-131	49.19	54.6	Marl
103-637A-7R-1, 85-87	55.45	14.40	Clay nannofossil marl
103-637A-7R-2, 61-63	56.71	74.7	White nannofossil ooze
103-637A-7R-3, 66-68	58.26	31.5	Nannofossil marl
103-637A-8R-2, 26-27	66.16	28.0	Nannofossil marl
103-637A-8R-2, 96-98	66.86	82.7	Nannofossil ooze
103-637A-8R-3, 20-22	67.60	4.4	Olive clay
103-637A-8R-3, 43-45	67.81	11.9	Sandy silt
103-637A-9R-1, 67-68	74.67	10.4	Calcareous clay
103-637A-9R-1, 133-134	75.33	35.0	Mottled nannofossil marl
103-637A-9R-2, 42-43	75.92	11.9	Micaceous silty sand
103-637A-9R-2, 56-58	76.06	10.9	Clayey silt
103-637A-9R-2, 72-74	76.22	9.4	Micaceous silty sand
103-637A-9R-2, 82-83	76.32	49.6	Nannofossil marl
103-637A-10R-1, 74-75	84.44	52.6	Nannofossil marl
103-637A-10R-1, 81-82	84.51	18.4	Nannofossil calcareous clay
103-637A-10R-1, 97-99	84.67	31.5	Nannofossil marl
103-637A-11R-1, 7-8	93.37	69.6	Foraminifer nannofossil ooze
103-637A-11R-1, 97-99	94.28	14.9	Silt layer
103-637A-11R-1, 103-104	94.33	5.9	Clay
103-637A-12R-1, 102-104	103.72	4.4	Greenish gray silty mud
103-637A-12R-2, 82-84	106.04	4.4	Clay
103-637A-13R-2, 51-53	114.41	58.1	Olive-gray marl
103-637A-14R-1, 100-102	123.0	9.9	Olive-gray clay
103-637A-15R-2, 50-52	133.7	16.3	Silty calcareous clay
103-637A-15R-4, 50-52	135.2	46.0	Clayey nannofossil marl
103-637A-16R-2, 51-53	144.3	63.6	White nannofossil marl
103-637A-17R-1, 138-140	152.38	26.0	Nannofossil clay
103-637A-17R-2, 138-140	153.38	57.1	Nannofossil marl
103-637A-17R-3, 138-140	155.38	47.5	Gray marl
103-637A-18R-1, 34-36	161.04	28.0	Nannofossil-rich calcareous claystone
103-637A-18R-1, 92-93	161.62	80.2	White foraminiferal ooze
103-637A-18R-2, 34-36	162.54	4.4	Variegated brown clay
103-637A-19R-1, 140-142	171.82	10.9	Nannofossil-rich claystone
103-637A-19R-2, 140-142	173.32	12.9	Nannofossil-rich claystone
103-637A-19R-3, 33-37	173.73	74.7	Nannofossil ooze
103-637A-20R-1, 50-52	180.4	66.1	Nannofossil marl
103-637A-20R-1, 110-112	181.00	4.4	Claystone
103-637A-20R-6, 50-52	187.9	4.4	Brown claystone
103-637A-20R-7, 30-32	189.2	4.4	Brown claystone
103-637A-21R-1, 35-38	189.95	4.4	Brown reddish claystone
103-637A-21R-1, 65-68	190.25	4.4	Claystone
103-637A-22R-2, 52-55	201.22	4.4	Reddish brown clay

[a] Lithologic names are those used on the visual-core-description forms.

about one-third of the anisotropy of the original peridotite (Kasahara and Kumazawa, 1969).

Index Properties

Figures 23D and 23E illustrate the values obtained for bulk density and porosity plotted against sub-bottom depth. As expected, sediment bulk density increases with burial depth. Porosity correspondingly decreases rather abruptly from high values of 59% to 69% in the drilling-disturbed upper interval of the section (Cores 103-637A-6R through 103-637A-9R; 45–84 m sub-bottom). Porosity then decreases more slowly from percentages in the upper 50's to those in the lower 50's in Cores 103-637A-10R through 103-637A-20R (84–190 m sub-bottom). A reversal in both the bulk-density and the porosity trends occurs in Cores 103-637A-21R and 103-637A-22R (190–212 m sub-bottom) within the same interval where the velocity reversal was measured. Porosity values increase to a range of from 61% to 73%, and bulk densities decrease to a range of from 1.52 to 1.74 g/cm^3. Basement porosities (Cores 103-637A-23R to 103-637A-29R) are generally low, ranging from 5% to 28%. Basement-rock bulk densities range from 2.4 to 2.9 g/cm^3 and average 2.62 g/cm^3.

Grain densities obtained from sediment samples range from 2.7 to 3.0 g/cm^3 and cluster around 2.8 g/cm^3, as expected for sediment composed predominantly of felsic silicates and carbonates. Grain density of the basement rocks, which ranges from 2.3 to 3.2 g/cm^3 and clusters around 2.6 g/cm^3, is typical of highly altered peridotite.

Figure 24 illustrates the positive correlation expected between bulk density and velocity as a function of decreasing porosity downhole. The data points in the higher velocity and density range correspond to basement-rock samples.

Acoustic Impedances and Basement Reflectivity

In predrilling planning, we assumed that the major reflector in the seismic profile at Site 637 represented the sediment/basement interface (see "Seismic Stratigraphy" section, this chapter); we, therefore, calculated the reflectivity of this interface and that of any other possible reflector using data obtained from cored material. A seismic reflector is generated by a large

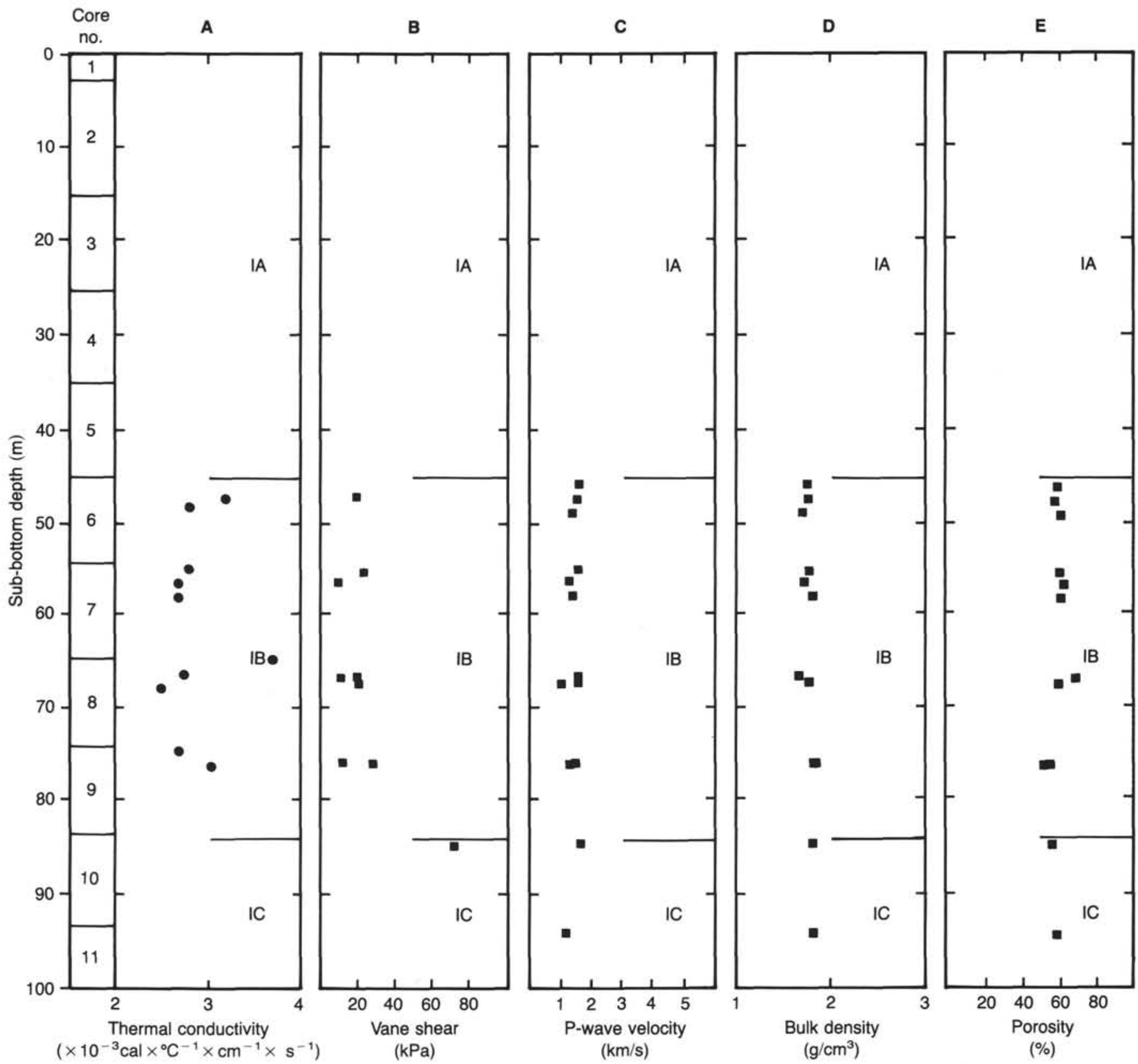

Figure 23. A. Thermal-conductivity values ($\times 10^{-3}$ cal $\times$ °C^{-1} $\times$ cm^{-1} $\times$ s^{-1}) obtained from sediments of Hole 637A plotted against sub-bottom depth. Data points plotted as dots indicate values that are probably inaccurate because they were obtained from drilling-disturbed sediments. Lithologic units as described in the "Sediment Lithology" section (this chapter) are indicated on right side of the figure. B. Vane-shear strength (in kiloPascals) plotted against sub-bottom depth in Hole 637A. Lithologic units noted on right side of Figure. C. Compressional velocity (kilometers per second) obtained from sediments and rocks of Hole 637A plotted against sub-bottom depth. Square data points indicate velocities measured in the plane of the core diameter perpendicular to the cut face of the core (c-direction), triangular data points indicate velocities measured in the plane of the core diameter and parallel to the cut face of the core (b-direction), and dots indicate velocities measured perpendicular to the plane of the core diameter (perpendicular to the plane of foliation; a-direction). Lithologic units noted on right side of figure. D. Bulk density (grams per cubic centimeter) of sediments and basement rocks from Hole 637A plotted against sub-bottom depth. Lithologic units noted on right side of figure. E. Porosity (percent) of sediments and basement rocks from Hole 637A plotted against sub-bottom depth. Lithologic units noted on right side of figure.

contrast in acoustic impedance of adjacent layers on the seafloor. Acoustic impedance is the product of compressional velocity (V_p) and bulk density (ρ_b); reflectivity (R) is defined as the quotient of the difference between acoustic impedances over the sum of acoustic impedances of two adjacent layers:

$$\frac{V_{p1}\rho_{b1} - V_{p2}\rho_{b2}}{V_{p1}\rho_{b1} + V_{p2}\rho_{b2}} .$$

The velocity and bulk-density data in Figures 23C and 23D show a large increase in values between basement at about 212 mbsf (Core 103-637-23R; V_p = 3.7 km/s, ρ_b = 2.60 g/cm^3) and overlying clay of lithologic Unit III (Cores 103-637A-21R and 103-637A-22R; basal V_p = 1.8 km/s, and basal ρ_b = 1.7 g/cm^3). The reflectivity coefficient R calculated for this interface is 0.51. This reflector probably corresponds to the basement reflector discussed in the "Seismic Stratigraphy" section (this chapter).

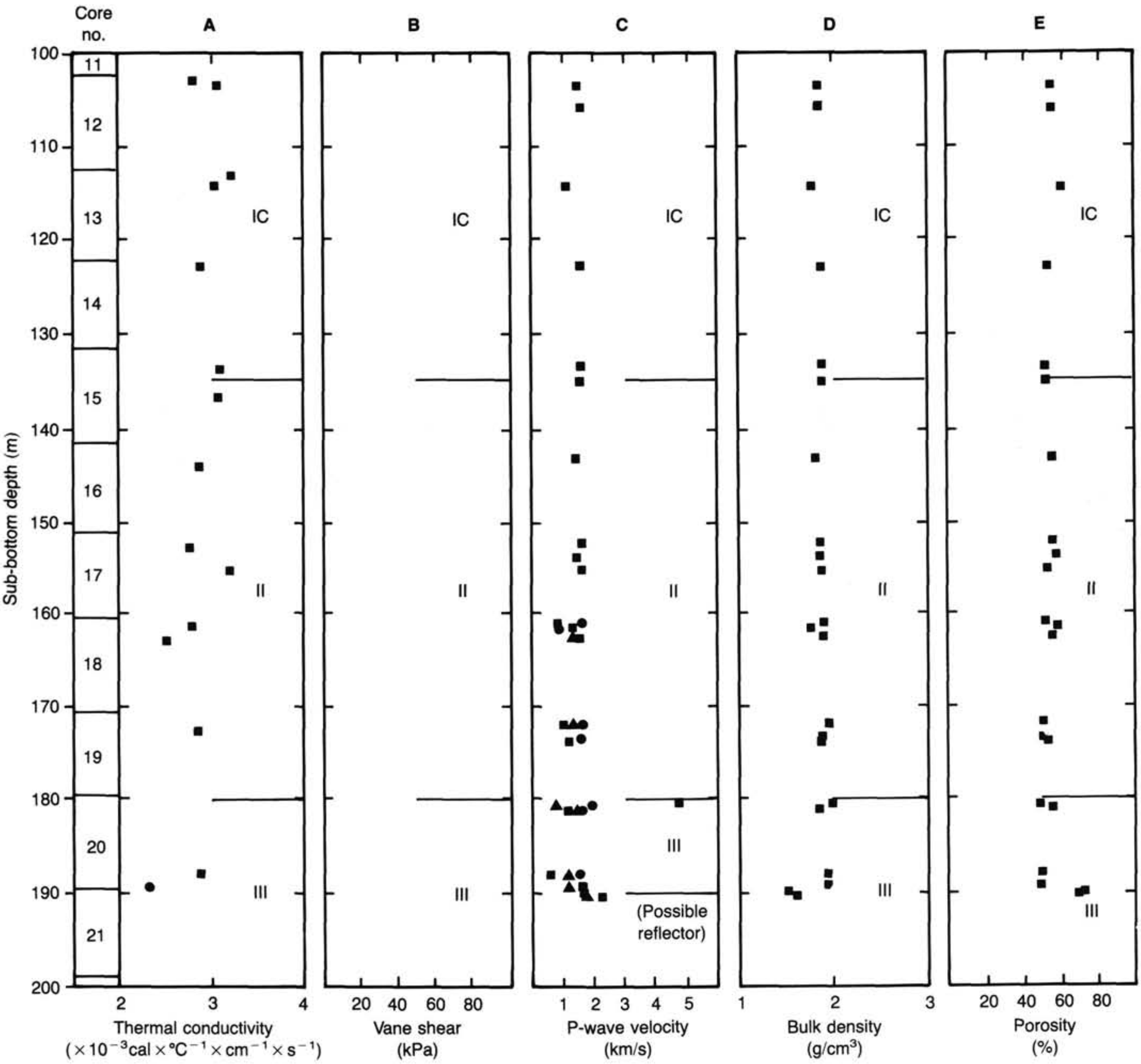

Figure 23 (continued).

A less distinct break in velocity and density trends occurs between lithologic Units II and III at about 180 m sub-bottom between Cores 103-637A-20R and 103-637A-21R. Using values of V_p = 1.6 km/s and ρ_b = 1.9 g/cm³ for the base of lithologic Unit II and V_p = 1.7 km/s and ρ_b = 1.5 g/cm³ for the top of lithologic Unit III, we calculated a reflection coefficient R of 0.07. Although this impedence contrast would be expected to generate a much weaker reflector than the sediment/basement interface, and no significant change in sonic velocity shows on the downhole sonic log over this depth (see "Logging Results" section, this chapter), a reflector (R1) is observed at about 180 m sub-bottom, where laboratory-derived physical-properties data predicted (see "Seismic Stratigraphy" section, this chapter).

Correlation of GRAPE Scan and Section Lithology

GRAPE measurements were routinely made on sediments and hard rocks recovered from Hole 637A. A clear correlation between sediment lithology and GRAPE-derived bulk densities was observed. One example of this is shown in Figure 25, in which GRAPE data for Section 103-637A-15R-1 is plotted alongside the shipboard graphic visual-core description of that section. Beds that grade upward from silty bases to calcareous clay tops are observed from 0 to 30 cm, 30 to 60 cm, 60 to 90 cm, and 95 to 115 cm in the visual-core description and are clearly indicated by decreases in bulk density from about 1.8 g/cm³ at the base to 1.6 g/cm³ at the top of each graded sequence.

Summary

Thermal-conductivity and vane-shear-strength values both increase between lithologic Subunits IB and IC (Cores 103-637A-9R and 103-637A-10R; 84 m sub-bottom). Thermal conductivity increases slightly, and vane-shear strength increases by a factor of about 4 to 7, more likely a reflection of the greater degree of drilling disturbance upsection than of a change in lithology.

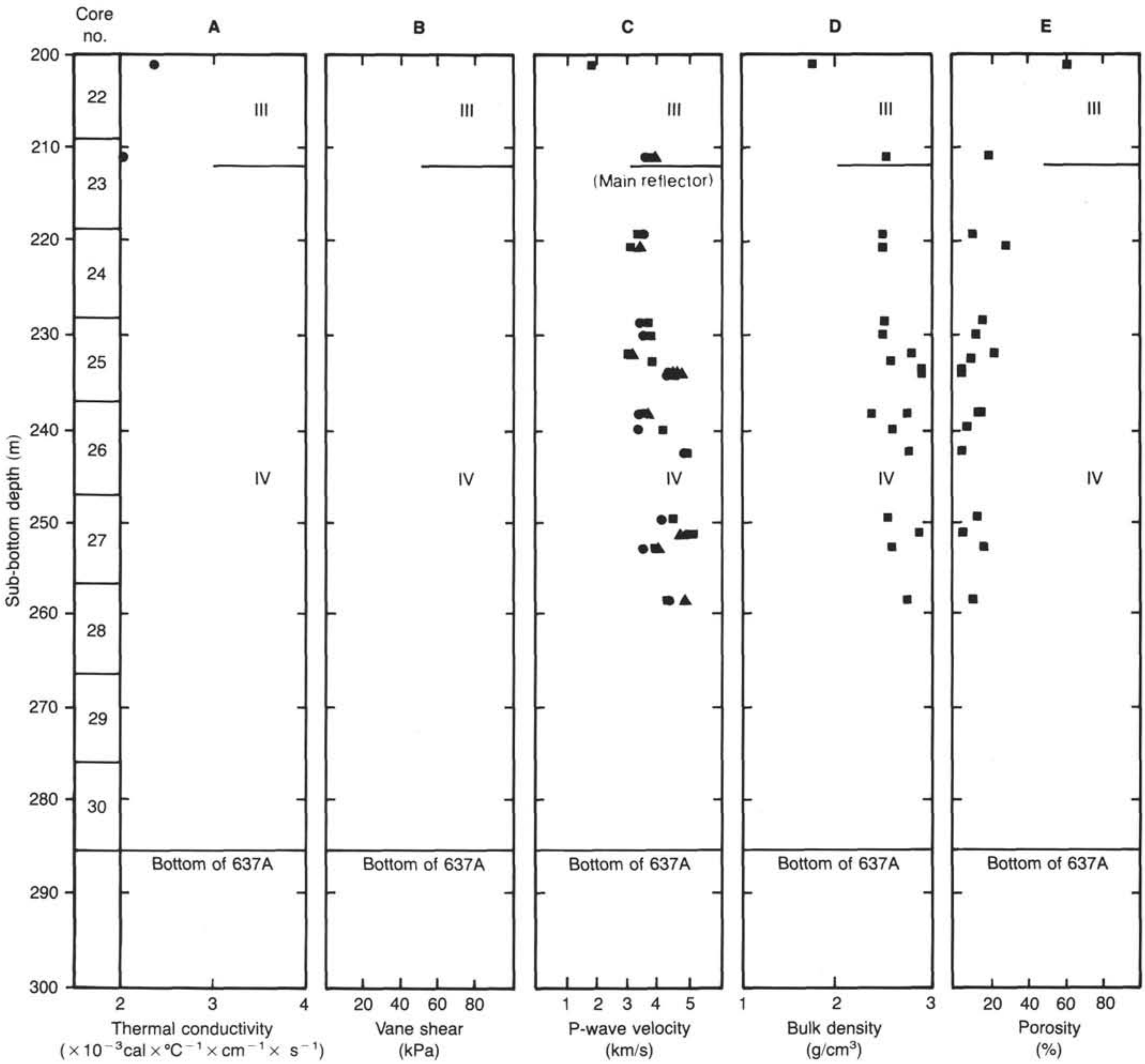

Figure 23 (continued).

Although measured sediment seismic velocities are lower than anticipated, the calculated depths to reflectors and results of logging corroborate the low sediment compressional velocities measured in the lab. Scattered low velocities in the upper 75 m of the section partly reflect drilling disruption. Sediment velocities are more consistent and increase slightly with depth to about 160 m sub-bottom. From about 160 to 190 m sub-bottom, the trend reverses, and sediment velocities decrease with depth. From about 190 m sub-bottom to basement rock at about 212 m sub-bottom, velocities again increase with depth.

About two-thirds of the basement ultramafic rocks analyzed show weak to strong seismic velocity anisotropy, the lower velocity being associated with the direction of foliation. Foliation and anisotropy are most pronounced in the freshest peridotite samples analyzed; the randomization of olivine orientation that occurs as peridotite is altered to serpentinite has probably caused the decreased foliation and anisotropy in more altered rocks. Basement-rock velocities average around 3.7 km/s.

Bulk-density and porosity values predictably reflect the decreasing water content with sub-bottom depth. Bulk density increases as porosity decreases greatly between the drilling-disturbed upper part of the section; below about 80 m sub-bottom depth, bulk density slowly increases. A reversal in the bulk-density trend occurs in the interval where the velocity reversal was measured, i.e., from about 160 to 190 m sub-bottom. The increase with depth resumes below about 190 m sub-bottom to basement at about 212 m sub-bottom, where bulk density jumps to an average of about 3.6 g/cm^3.

The reversals in bulk density and velocity and the abrupt change in these values imply that acoustic-impedance contrasts exist at the sediment/basement interface and possibly at a sub-bottom depth of about 180 m. Although the reflection coeffi-

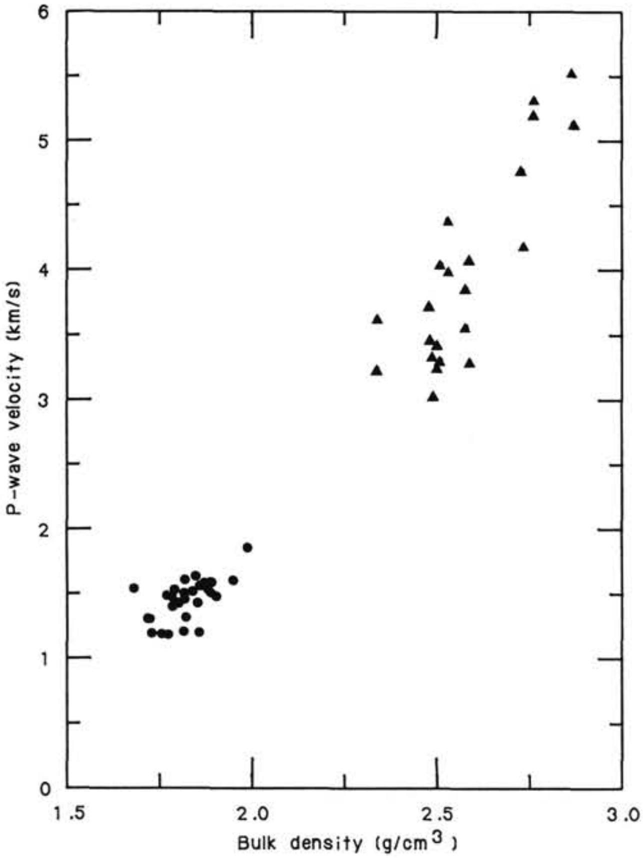

Figure 24. Bulk density (g/cm³) plotted against compressional seismic velocity V_p (km/s) from Hole 637A samples. Data points in the high-velocity range (>3.00 km/s) represent basement samples. Open and shaded circles correspond to velocities measured on the same sample (same density) in different orientations.

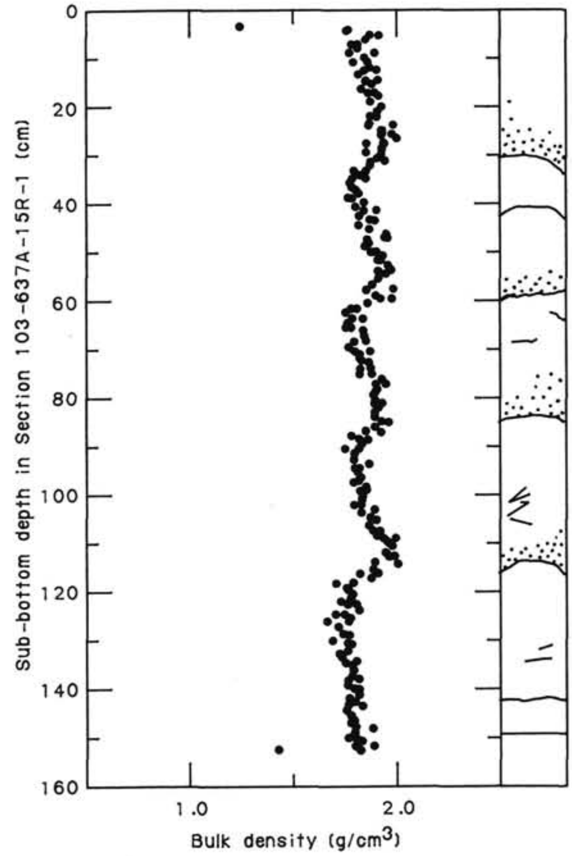

Figure 25. Continuous GRAPE scan bulk-density plot of Section 103-637A-15R-1 and graphic representation column of the shipboard visual core description of the same section. Note the close correspondence of GRAPE bulk-density variation with the graded beds in this section (stippled area indicates silty base of graded beds).

cient calculated for the interface at about 180 mbsf is small, a reflector R1 can be observed in seismic profiles near this depth (see "Seismic Stratigraphy" section, this chapter).

Continuous bulk-density values measured by the GRAPE showed a remarkable correlation with graded beds in lithologic Unit I. The presence of normally graded beds on the order of 30 cm thick can be inferred from shifts in density values before core splitting.

AGE-VS.-DEPTH AND ACCUMULATION-RATE CURVES

As shown on Figure 26A, the curve drawn through the biostratigraphic-control limits illustrates a general increase in sedimentation rates during the Pliocene and early Pleistocene, followed by a decrease in the late Pleistocene. When converted to accumulation rates in g/cm²/1000 yr (Fig. 26B), accounting for the measured bulk density and porosity of the sediments, the rate calculated for the late Miocene is about 2 g/cm²/1000 yr, for the Pliocene about 4 g/cm²/1000 yr, and for the Pleistocene about 10 g/cm²/1000 yr. Because of the uncertainties in the ties of the biostratigraphic zones to the radiometric scale and because of the width of the bars and boxes in Figure 26A that constrain the age-vs.-depth curve, the values calculated for accumulation rates are considerably uncertain. On the other hand, even with large error bars, the general trends are probably valid.

LOGGING RESULTS

Geophysical logs were obtained at Hole 637A from 100 to 248 mbsf in two different runs using Schlumberger tools. The first run successfully recorded long-spaced sonic, induction, gamma-ray, and caliper logs. In the second run, lithodensity, compensated neutron, and natural gamma-ray logs were recorded. Run 2 was terminated about 21 m shallower than was run 1 because of cave-in of the hole between logging runs. For this reason, additional logging runs were not attempted.

The total depth of the hole was 285.6 mbsf. The borehole was cut with a 9⅞-in. bit and filled with 9.5-lb drilling mud; then the 4¼-in.-inner-diameter drill pipe was pulled up to 100 mbsf before logging. The logs were recorded as the tools were pulled uphole at approximately 900–1000 ft/hr.

The long-spacing sonic tool measures the vertical slowness (inverse velocity) of the formation by timing the difference between compressional wave arrival times at different receiver separations. Microseconds/foot is the typical unit of measure for slowness (DT). The induction tool measures deep (ILD), shallow (SFL), and proximal (ILM) resistivities in ohm-meter from changes in the electrolytic properties of the formation pore fluids. The natural gamma-ray tool measures the radioactivity (SGR) of the formation, including potassium (POTA), thorium (THOR), and uranium (URAN) contributions. The API standard unit of measurement is scaled relative to the weight percentage of the radioactive elements. Using a three-arm bowspring, the caliper tool measures the mean diameter (CAL) of the borehole in inches. The lithodensity tool captures the energy of scattered high-energy gamma rays emitted into the formation, and hence, the electron density, photoelectric effect (PEF) with which to calculate the bulk density (RHOB). Bulk-density units are in g/cm³. The compensated neutron tool measures the hydrogen ion con-

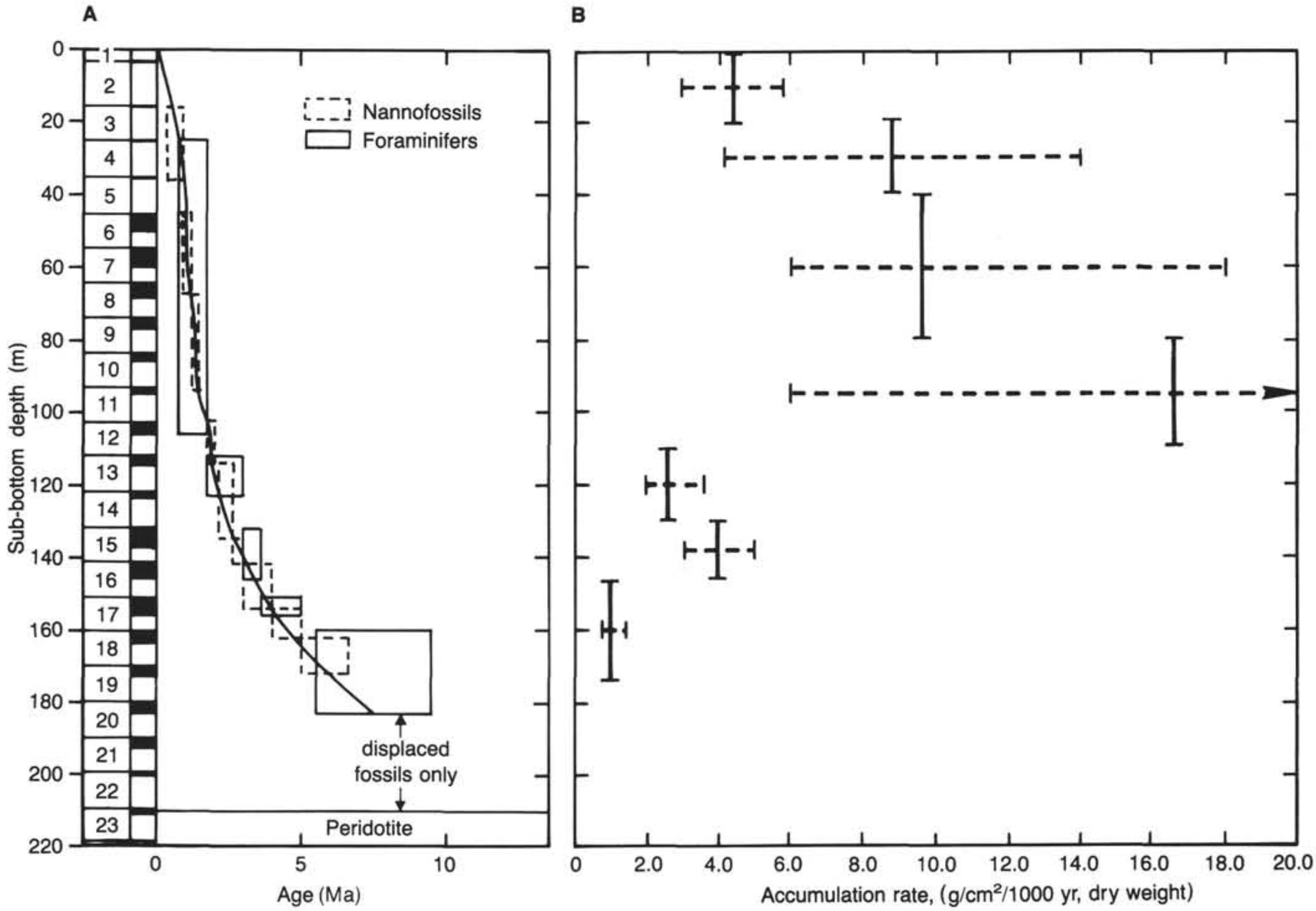

Figure 26. A. Depth vs. age, Hole 637A. B. Sediment-accumulation rates, Hole 637A. Horizontal error bars indicate the uncertainties in drawing a line through the biostratigraphic data shown on Figure 26A.

centration of the formation pore fluids by the proportion of thermal neutrons captured at a sensor. Neutron-count units are calibrated and converted to porosity (NPHI) units.

Log Analysis

Relative tool responses in the logged interval distinguish four different "log-lithologic" units, identified by discrete changes in the velocity, density, and gamma-ray logs shown in Figures 27 through 30. Their maximum and minimum values are summarized in Table 9. The mean caliper log is relatively constant at 9.8 in. over the logged interval. Potassium, thorium, and uranium contributions to the gamma-ray log can be analyzed for clay mineralogy.

In general, Unit A (Table 9) has a homogeneous log character with high gamma-ray values (mostly K and Th) that correspond to clay intervals (Fig. 27). Intervals showing decreased log values may correspond to thin (1-2 m) clay-poor layers. Having at least two different log-lithologic types, Unit B, in contrast, is generally heterogeneous (Fig. 28). These two types are distinguished by alternating low and high log values (both shown in Table 9) in 2- to 10-m-thick intervals. Unit B log values in the clay intervals are similar to those observed in Unit A. Unit C has high gamma-ray values, similar to those of Unit A, again indicative of homogeneous clay (Fig. 29). The log responses are significantly different in Unit D, indicating a major change in composition (Fig. 30). In Unit D, gamma-ray values are lower, and sonic velocity, density, and resistivity values are higher than in any of the overlying log-lithologic units.

Lithostratigraphic Correlation

The correlation is good between the four log-lithologic units and the lithostratigraphic section described from the recovered core (see "Sediment Lithology" section, this chapter). Summarized in Table 10, the correlation suggests that intervals of nannofossil marl, clay, and serpentinite can be identified by the log responses. In the sediments, low gamma-ray and density values correspond to intervals of nannofossil marl, whereas high values correspond to clay. Within the measurement and depth uncertainties, laboratory physical-property measurements of core samples (see "Physical Properties" section, this chapter) reasonably agree with the logging results. As expected from the lab measurements, the serpentinized peridotite in the basement has dramatically higher density, sonic velocity, and resistivity values than does the overlying sediments. The log-response variations in Unit D probably relate to different degrees of serpentinization and calcite content.

Preliminary Seismic Correlation

A synthetic seismogram was calculated from a simplified model of the lithologic column. Bulk-density and sonic-velocity values were averaged from the log responses in intervals determined by the foregoing log analysis. The resulting 19-layer model is shown in Table 11. Sonic traveltime was converted to velocity (km/s); depths correspond to the top of each interval. A zero-phase wavelet centered at 20 Hz was used to approximate the source function and was convolved with the velocity/density

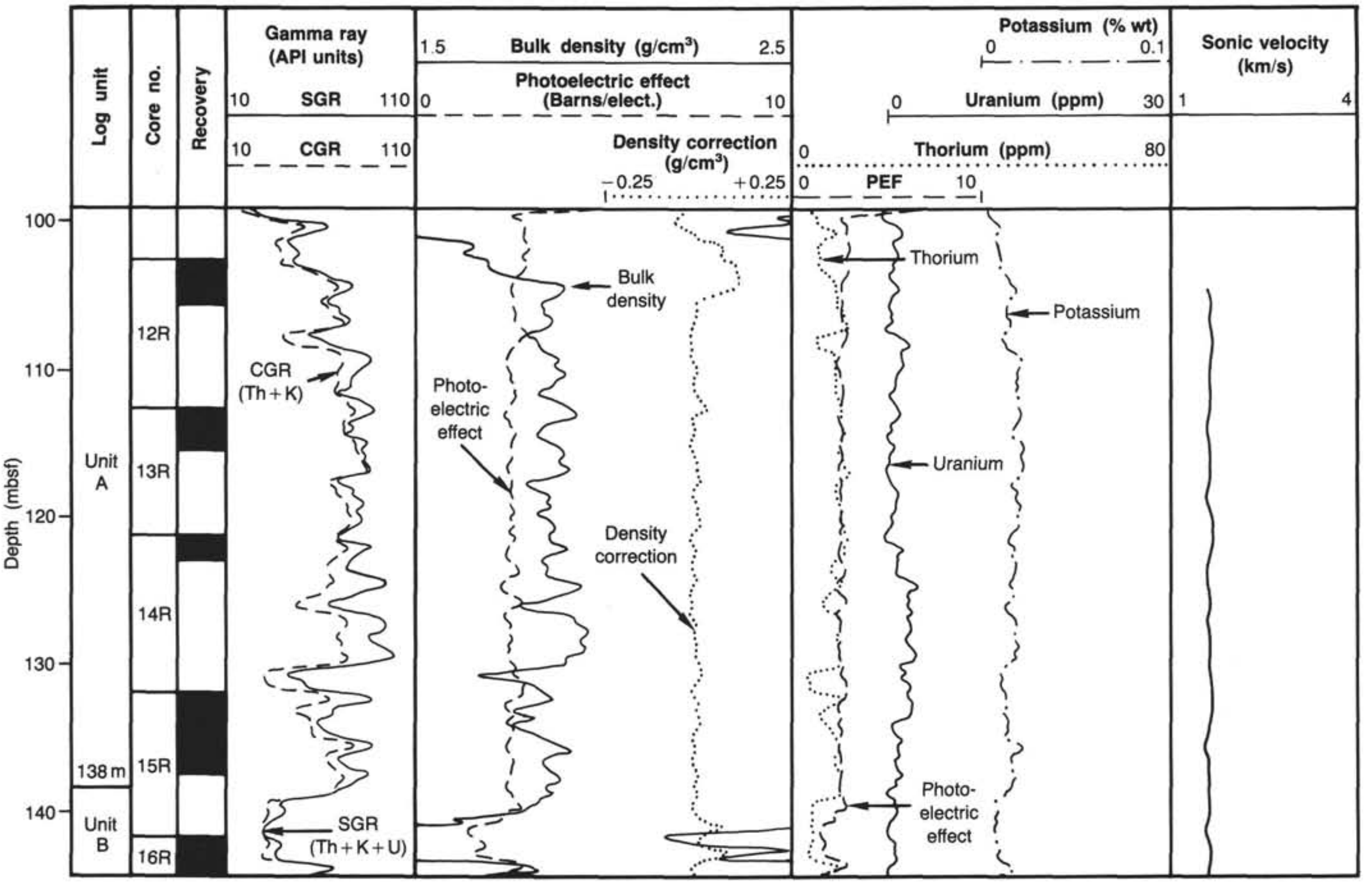

Figure 27. Composite log and core recovery in log-lithologic Unit A. See text for description of logs.

model. The resulting acoustic seismogram is shown in Figure 31; relative seismic amplitude is plotted vs. two-way traveltime. The high-amplitude phases between 0.2 and 0.3 s correspond to reflections from impedance contrasts in the sediments at the depths shown in Table 11. These contrasts, however, may be exaggerated by the simplicity of the model. The basement reflector corresponds to the latest high-amplitude arrival. Note, however, that these phases are strongly influenced by internally reflected energy and assumptions about the source signature. Caution is therefore advised in making interpretations using this correlation.

SEISMIC STRATIGRAPHY

Seismic Stratigraphy of the Sedimentary Sequence

East of the basement ridge, three strong reflectors appear on the seismic line recorded from *JOIDES Resolution* during the site survey to locate Site 637; these are labeled R1, R2, and R3 on Figure 32. The depth of the reflectors is somewhat different on the west side of the ridge, where only two reflectors, R′1 and R′2, are recorded (Figs. 5 and 32), and the acoustic response of sediments, although comparable, is not identical. For this reason, we do not propose correlations between reflectors R and R′. The differences probably result from the ridge having acted as a dam for sediments transported by bottom currents from the east.

The interval between the seafloor and R1 is well stratified. Judging from the flatness of the layers and the results of drilling at Site 637, we assume it to be mainly a sequence of turbidites.

R1, which is about 250 ms beneath the seafloor, where it is last clearly identifiable about 400 m east of Site 637, was probably reached by drilling at Site 637. It most plausibly is correlated with the transition between lithologic Units II and III, assuming an average sound velocity in the sediments of 1.5 km/s. This lithologic change is near the Miocene/Pliocene boundary. The downhole logs show a slight downward increase in sound velocity and a pronounced increase in bulk density at about 182 mbsf, at the top of an 8-m-thick interval having high gamma-ray counts. This combination of properties can produce a seismic reflector.

In terms of the regional seismic stratigraphy (Groupe Galice, 1979), R3 would be the boundary between acoustic Units 1 and 2 (upper Eocene). Near the buried ridge, this reflector also marks a slight unconformity, possibly resulting from a small amount of uplift of the ridge during the late Eocene (Boillot et al., 1980). Below R3, reflections are weak but consistent with the pattern of reflections from older layers seen clearly on the multichannel line over Site 637 (Fig. 3).

Morphology of the Basement Rock

The roughness of the basement surface, given the large impedance contrast between the serpentinite of the acoustic basement and the overlying water and low-velocity sediment, produces diffractions that are expressed by hyperbolic-reflection traces on the seismic record and that mask the true form of the ridge. The migrated multichannel record (Fig. 3) better depicts the basement slope, which, when corrected for the speed of sound in the sediments and the vertical exaggeration of the seismic profiles (Fig. 32), has an average inclination of only about 15° from the summit outward about 5 km on both sides (Fig. 33).

SUMMARY AND CONCLUSIONS

Drilling accomplished the main objective at Site 637, which was to obtain fresh samples of the basement rock that forms a long north-trending ridge close to the ocean/continent bound-

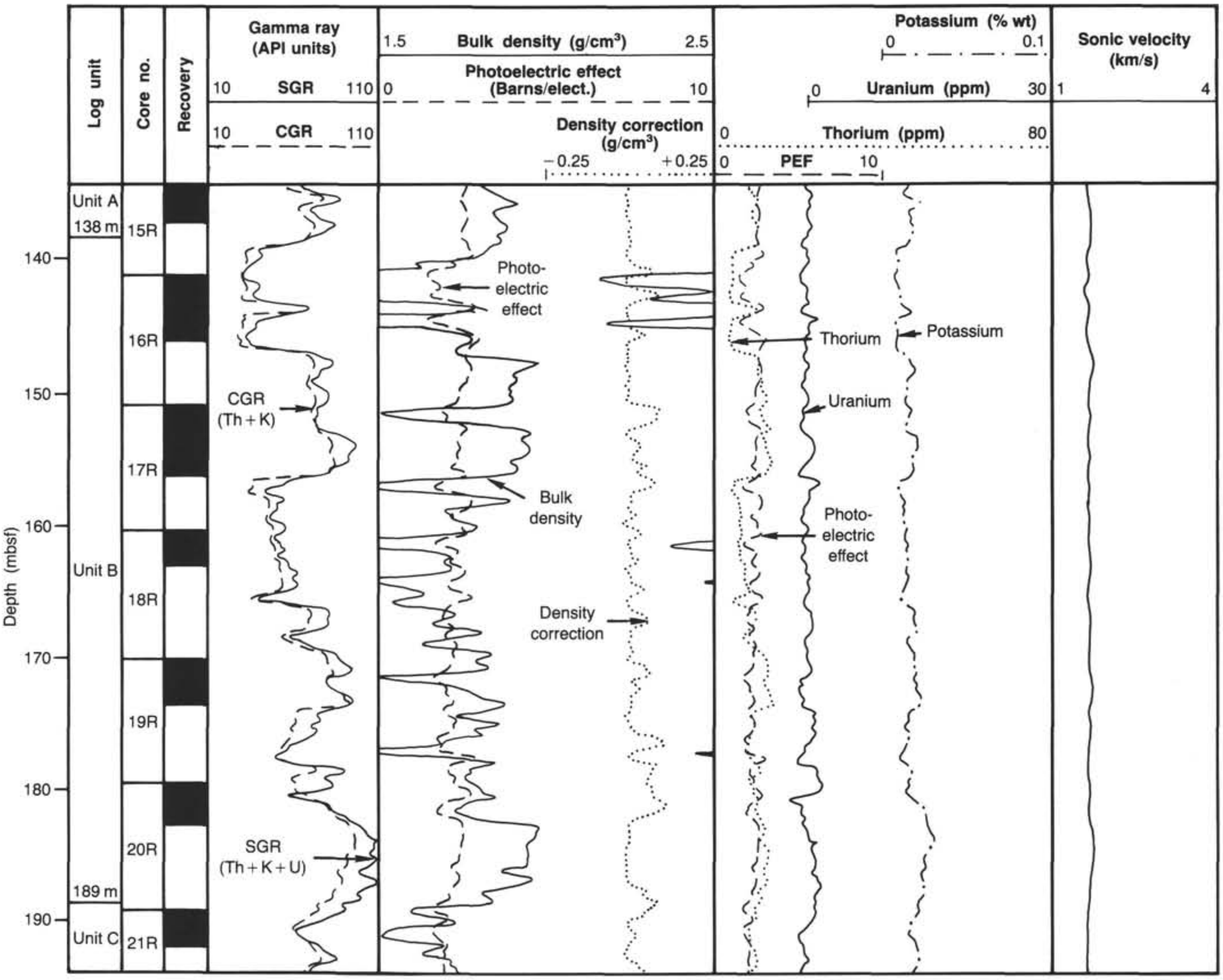

Figure 28. Composite log and core recovery in log-lithologic Unit B. See text for description of logs.

ary near the foot of the Galicia margin. On the basis of samples dredged from outcrops along the ridge about 10 km south of the drill site, we expected to recover samples of peridotite. The main questions to answer are (1) do the rocks represent suboceanic or subcontinental mantle, and (2) what was the mechanism of their emplacement? The drill penetrated about 74 m of serpentinized peridotite lying beneath a cover of Neogene clay and turbidite sands about 212 m thick. The major features of the lithology, petrology, biostratigraphy, and physical and logging properties of the cored sequence are shown summarily in Figure 2 and in more detail in Figure 34.

Crystalline Basement Rocks

From the bottom of the drill hole, at a depth of 285.6 m, to the base of the overlying Neogene sediments, at a depth of 212 m, the drill sampled serpentinized peridotite, with enough relict original minerals to establish that the original mineralogy was generally that of spinel-harzburgite: about 70%-90% olivine, 10%-20% orthopyroxene, less than 5% clinopyroxene, plus about 1% or 2% chromium spinel. A few samples, however, contain spinel rimmed by plagioclase. The olivine is almost totally transformed into serpentine. Orthopyroxene (enstatite) crystals and pseudomorphs of serpentine or calcite have abundant exsolution lamellae. The clinopyroxene (diopside) and spinel are commonly less altered than are the other primary phases. Where present, plagioclase is fresh.

Several generations of serpentine, which occurs as both chrysotile and lizardite, are present. Olivine and enstatite have been altered into a meshwork of serpentine. A second generation of serpentine also occurs as veins, bands, and lenses formed after the deformations that produced the foliation characterizing the cored sequence.

Calcite extensively replaced the peridotite during the last stages of peridotite alteration; in some samples, about 80% of the rock is now calcite, as both replacements and cross-cutting veins.

The common texture in the peridodite is porphyroclastic, with large, equant orthopyroxene crystals and a foliation well defined by spinel elongation. Such textures are common in oceanic peridotites and are thought to result from high-temperature, low-stress plastic deformation during asthenospheric flow at an oceanic-spreading center at a depth of about 5-10 km.

True mylonitic textures occur in shear zones, which are slightly oblique to the prophyroclastic foliation. These rocks have stretched orthopyroxene crystals, within a fine-grained, recrystallized olivine matrix. Mylonitic textures such as these form in high-stress conditions at relatively lower temperatures than those prevailing

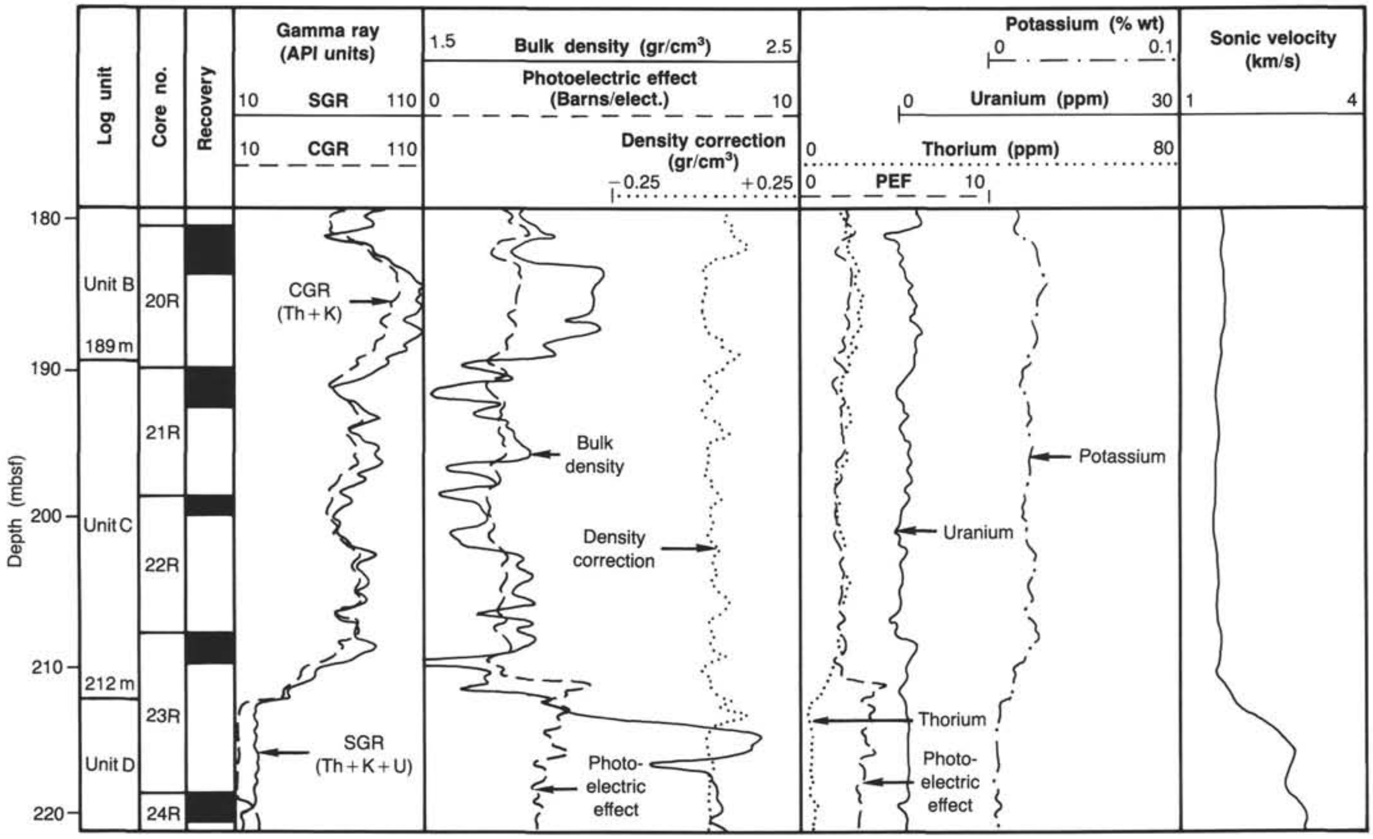

Figure 29. Composite log and core recovery in log-lithologic Unit C. See text for description of logs.

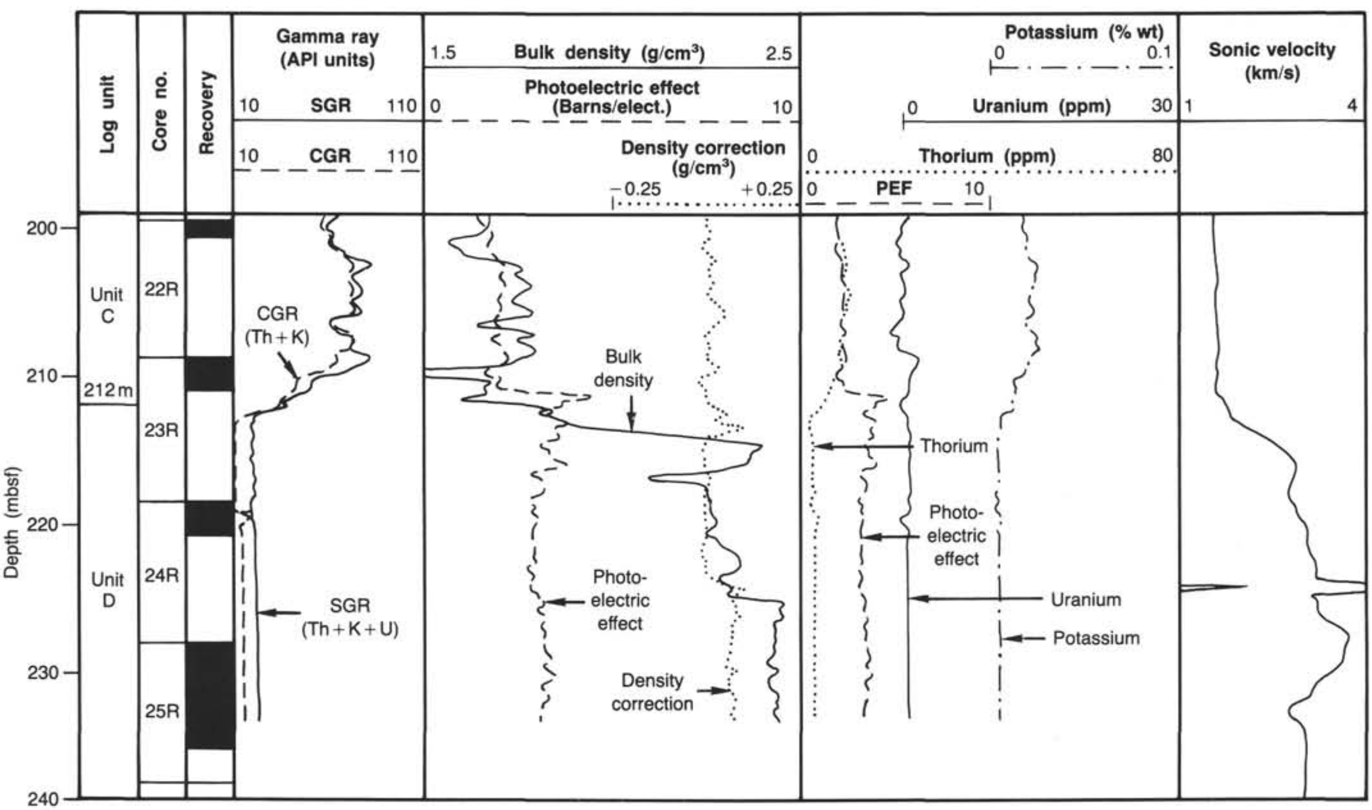

Figure 30. Composite log and core recovery in log-lithologic Unit D. See text for description of logs.

Table 9. Minimum/maximum values in log-lithologic units. GR = gamma ray (API units); VEL = sonic velocity (km/s); ILD = deep induction (ohmm); SFLU = spherical focused induction (ohmm); RHOB = bulk density (g/cm^3); PEF = photoelectric effect (barns/electron); POTA = potassium (% wt); THOR = thorium (ppm); URAN = uranium (ppm); NPHI = neutron porosity (%).

	Unit A	Unit B	Unit C	Unit D
Depth	100–138	138–189	189–212	212–278
GR	35/86	20/100	40/70	10/15
VEL	1.56	1.56/1.95	1.85/1.95	3.05/4.00
ILD	1	0.9/1.2	0.7/1	4/80
SLFU	0.9/1.1	0.7/1.2	0.8/1.1	5/2000
RHOB	1.78/1.95	1.4/2.0	1.5/1.8	2.1/2.45
PEF	2.2/3	1.6/3	1.6/2.4	2.7/3.8
POTA	0.01/0.023	0.005/0.03	0.01/0.025	0/0.005
THOR	3/12	3/14	5/10	0/2.2
URAN	0/3.2	0/2.7	0/2	0/1.2
NPHI	46/62	50/70	55/68	46/60

Table 10. Summary correlation between Hole 637A logs and lithology.

Log unit	Lithologic unit	Cores	Lithology
Unit A	Unit 1 (Subunit 1C)	103-637A-15R	Terrigenous turbidites with thin silty layers; marl
Unit B	Unit 2	103-637A-20R	Slumped brown clay and nannofossil marl
Unit C	Unit 3	103-637A-23R	Reddish brown clay
Unit D	Basement	103-637A-30R	Serpentinite

Table 11. Average velocity (V_p) and density (RHOB) values calculated in log-lithologic intervals determined by log analysis (see text). Values shown correspond to the interval below each depth.

Depth (mbsf)	V_p (km/s)	RHOB (g/cm^3)
0	1.525	1.77
46	1.563	1.77
67	1.563	1.79
79	1.563	1.82
103	1.563	1.85
125	1.646	1.80
140	1.563	1.40
147	1.676	1.90
160	1.554	1.70
171	1.615	1.80
181	1.646	1.95
189	1.554	1.70
195	1.554	1.65
201	1.563	1.75
212	2.743	2.25
221	3.048	2.35
227	3.810	2.45
230	3.383	2.45
232	3.048	2.45

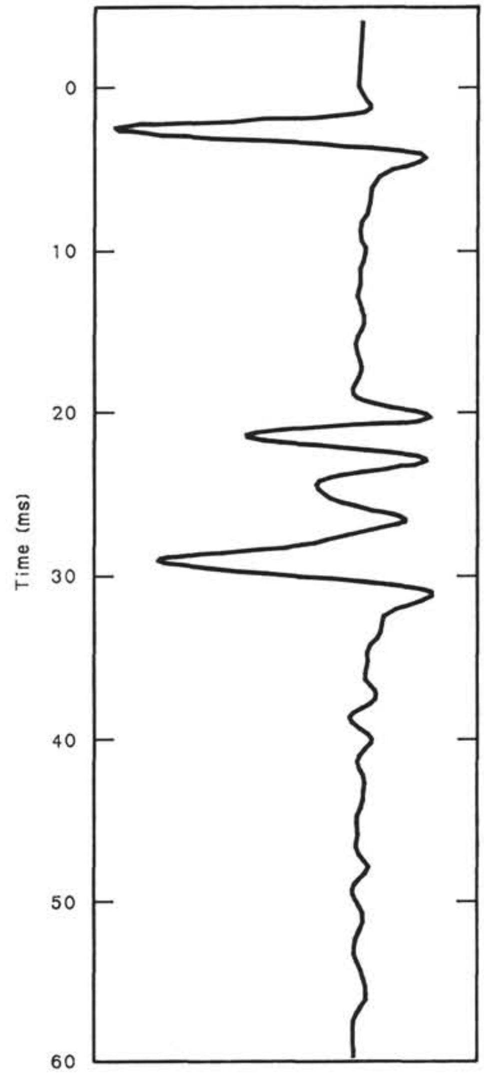

Figure 31. Preliminary synthetic seismogram calculated from data in Table 11. A zero-phase source function centered about 20 Hz was used for the calculation. The high-amplitude basement reflection arrives about 0.3 s after the seafloor-reflection arrival (see text).

during lithospheric accretion, as for example along thrust or transform faults.

The pervasive foliation of the peridotite has a nearly uniform dip of about 35°, except near the base of the cored section, where the dip steepens to about 75°. The lineation is everywhere at a high angle to the strike of the foliation. Measurements of the magnetization direction of magnetic minerals in peridotite show that the foliation strike is north and the dip is east. Therefore, the lineation trends east–west.

Concerning the main questions about the provenance and emplacement of the peridotite: the harzburgitic composition of the rocks from Site 637 is similar to the composition of samples recovered from ocean basins, particularly in rift environments, because of the presence of the plagioclase-spinel association. Site 637 peridotite may represent suboceanic mantle that has been less depleted than most oceanic peridotites.

The structural data are consistent with emplacement of the peridotite by eastward-directed tangential (low-angle normal) faults. Tectonic denudation of the mantle might have resulted from low-angle faulting during the stretching and rifting of the continental lithosphere associated with the events leading to the Early Cretaceous formation of North Atlantic oceanic crust. That the peridotite is a slice of Hercynian basement rock, related to the Galicia mainland peridotite, is a possibility we consider unlikely; Site 637 peridotite was formed under high-temperature, low-pressure conditions, whereas the Hercynian rocks reflect lower temperature, higher pressure conditions.

Neogene Sediments

The overlying Neogene sediments compose three lithologic units. From oldest to youngest these are as follows:

Unit III (180–212 m): brown and reddish clay, with zeolites, glass, and iron oxide particles. A small percentage of silt-sized

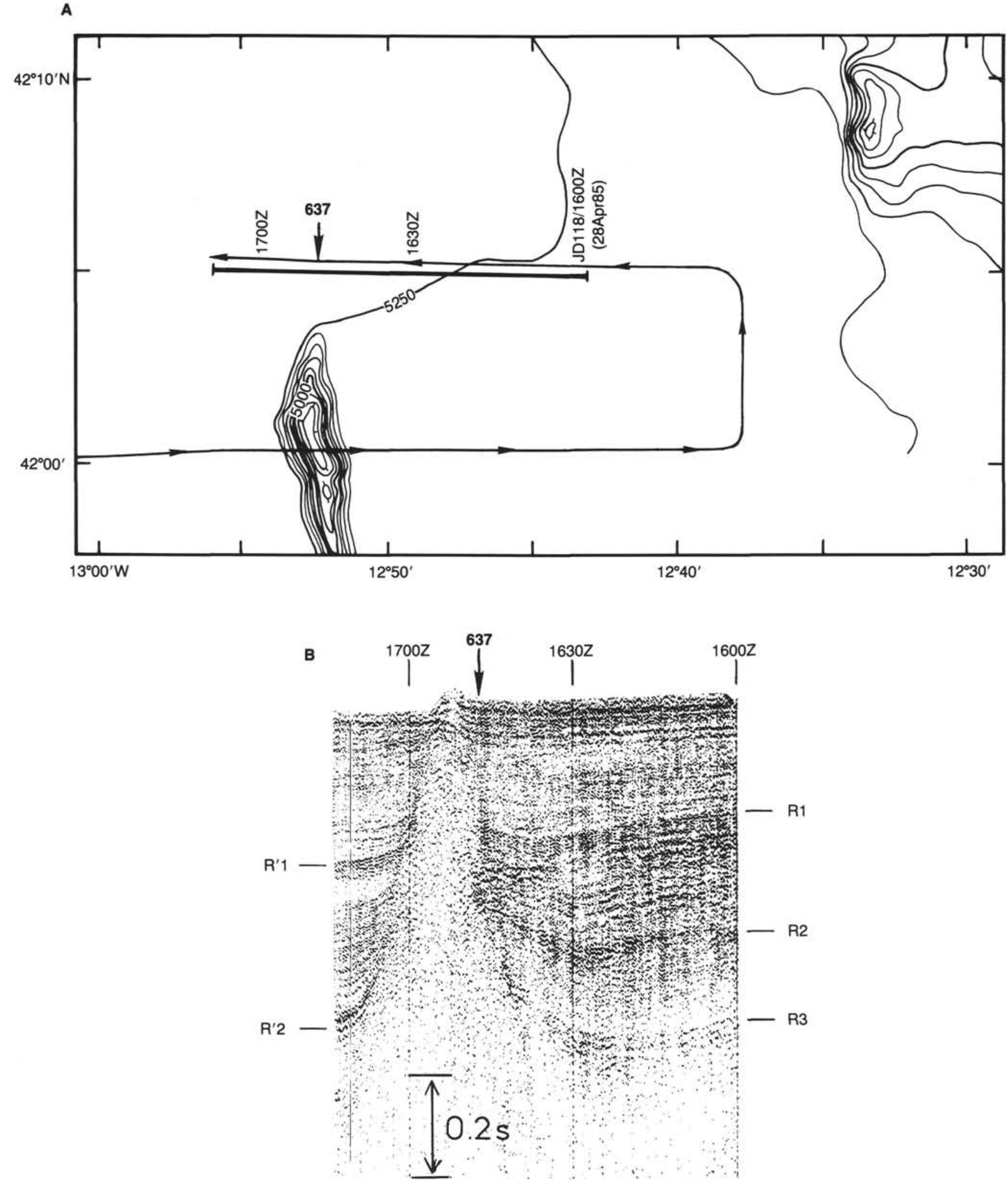

Figure 32. A. Bathymetric chart showing the track of *JOIDES Resolution* during the approach to Site 637. Sea Beam bathymetry from Figure 4. B. Seismic-reflection profile taken during this approach showing reflectors described in text. The times along the trackline correspond to the times indicated on the seismic-reflection profile.

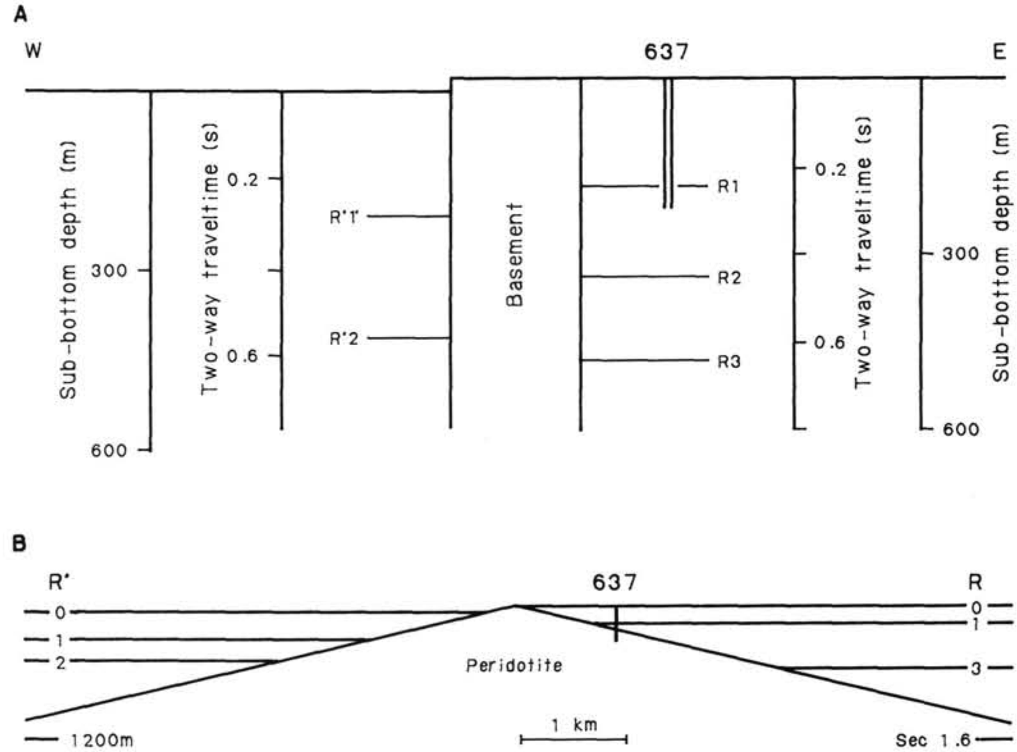

Figure 33. A. Diagrammatic representation of the prominent reflectors on either side of the basement ridge at Site 637, showing time and depth from the seafloor to these reflectors. Reflectors shown in Figure 32. Note the differences in the depths to these reflectors on either side of the ridge. Vertical scales are two-way traveltime in seconds, and the corresponding depths below the seafloor are in meters. B. Diagrammatic depth section across the serpentinized peridotite ridge drilled at Site 637, showing approximate angle of basement slope and depth to prominent reflectors, with no vertical exaggeration.

terrigenous sediment appears throughout the unit. The only *in-situ* fossils are rare ichthyoliths. According to P. Doyle (pers. comm., 1985), these are of middle or early Miocene age at 181 m and of either Cretaceous or Paleocene/Eocene age at 211 m. Accumulation rates, indicated by the deep-water, pelagic character of the clays, were probably much slower than the 2 g/cm^2/1000 yr estimated for the overlying, less pelagic sediments of lithologic Unit II.

A special feature of this unit is the presence in one core of an interval about 30 cm thick that contains finely disseminated organic matter showing a high degree of thermal maturity and algal-amorphous kerogen. The available evidence does not allow a choice between the two most plausible hypotheses: (1) *in-situ* thermal alteration from high heat flow at Site 637 or (2) thermal alteration at some distant site before redeposition at Site 637.

The brown clays of Unit III were most likely deposited on the slopes of the peridotite hill and were derived partly from weathering of the basement rocks, partly from slow pelagic accumulation below the CCD, and partly from fine detritus carried to the site in thermohaline currents or nepheloid layers.

Unit II (135–180 m): upper Miocene to middle Pliocene interbedded brown clay, nannofossil marl, and calcareous turbidites, including some slumped intervals of clay and marl. Sonic velocities are about 1.6 km/s. Accumulation rates averaged about 2 g/cm^2/1000 yr.

Slump structures are conspicuous in at least two intervals in this unit and may signal eastward downslope mass movement of material from the hill west of the drill site. The clay may represent redeposition of submarine-weathering products of the peridotite basement outcrop, exposed on the seafloor a short distance west of the site. The occurrence of turbidites along with the slumped beds and the brown clay suggests a location at the junction of the hill slope and the abyssal plain to the east.

Unit I (0–135 m): middle Pliocene to upper Pleistocene turbidites, typically about 25 cm thick, grading from silt to clay, which are commonly overlain by nannofossil marl. Sonic velocities are near 1.6 km/s. Accumulation rates were variable, from a maximum of about 16 g/cm^2/1000 yr near the beginning of the Pleistocene to only about 4 g/cm^2/1000 yr during the late Pleistocene.

Most of the turbidites have a terrigenous provenance and were probably delivered to the area of Site 637 via submarine valleys and canyons that extend to the Iberian mainland. A few turbidite layers have foraminiferal sand at the base. The nannofossil marl, despite a water depth near the CCD, contains relatively undissolved fossils, including persistent trace amounts of reworked Cretaceous–Oligocene species. Therefore, some of the marly material could have been transported from somewhat shallower depths, perhaps in nepheloid layers.

REFERENCES

Berggren, W. A., 1977. Late Neogene planktonic foraminiferal biostratigraphy of the Rio Grande Rise (South Atlantic. *Mar. Micropaleontol.*, 2:265–313.

Berggren, W. A., Aubry, M. P., and Hamilton, N., 1983. Neogene magnetobiostratigraphy of Deep Sea Drilling Project Site 516 (Rio Grande Rise, South Atlantic). *In* Barker, P. F., Carlson, R. L., Johnson, D. A., et al., *Init. Repts. DSDP*, 72: Washington (U.S. Govt. Printing Office), 675–713.

Berggren, W. A., Kent, D. V., Flynn, J. J., and Van Couvering, J. A., in press. Cenozoic Geochronology. *In* Snelling, N. J. (Ed.), *Geochronology and the Geologic Time Scale:* Geol. Soc. London, Spec. Pap.

Boillot, G., Grimaud, S., Mauffret, A., Mougenot, D., Mergoil-Daniel, J., Kornprobst, J., and Torrent, G., 1980. Ocean-continent boundary off the Iberian margin: a serpentinite diapir west of the Galicia Bank. *Earth Planet. Sci. Lett.*, 48:23–34.

Boillot, G., et al., 1986. Thinning of the continental crust and tectonic denudation of the upper mantle beneath passive margins: a model. The example of the western Galicia Margin (Spain). *Bulletin des Centres des Recherches Exploration-Production Elf-Aquitaine*, 10(1): 95–104.

Boillot, G., 1986. Comparison between the Galicia and Aquitaine margins. *Tectonophysics,* 129:243–255.

Bonatti, E., Chermark, A., and Honnorez, J., 1979. Tectonic and igneous emplacement of crust in oceanic transform zones. *In* Talwani, M., Harrison, C. G., and Hayes, D. E. (Eds.), *Deep Drilling Results in the Atlantic Ocean: Oceanic Crust, Maurice Ewing Series*: Washington (Am. Geophys. Union), 2:239–248.

Bonatti, E., Honnorez, J., and Ferrara, G., 1970. Equatorial Mid-Atlantic Ridge: petrologic and Sr isotopic evidence from an alpine-type rock assemblage. *Earth Planet. Sci. Lett.*, 9:247–256.

Bonatti, E., Ottonello, G., and Hamlyn, P. R., 1986. Peridotites from the island of Zabargad (St. John), Red Sea: petrology and geochemistry. *J. Geophys. Res.*, 91:599–631.

Espitalie, J., Madec, M., and Tissot, B., 1977. Source rock characterization method for petroleum exploration. *Ninth Annual Offshore Technology Conference Proceedings*, 399–404.

Gartner, S., 1977. Calcareous nannofossil biostratigraphy and revised zonation of the Pleistocene. *Mar. Micropaleont.*, 2:1–25.

Gieskes, J. M., 1974. Interstitial water studies, Leg 25. *In* Simpson, E. S. W., Schlich, R., et al., *Init. Repts. DSDP*, 25: Washington (U.S. Govt. Printing Office), 361–394.

———, 1981. Deep-sea drilling interstitial water studies: implications for chemical alteration of the oceanic crust, Layer I and II. *Soc. Econ. Paleontol. Mineral., Spec. Publ.*, 32:149–167.

Gieskes, J. M., and Peretsman, G., 1986. Water-Chemistry Procedures Aboard the JOIDES Resolution—Some Comments, *ODP Tech. Note 5.*

Groupe Galice, 1979. The continental margin off Galicia and Portugal: acoustical stratigraphy, dredge stratigraphy, and structural evolution. *In* Sibuet, J. C., and Ryan, W. B. F., et al., *Init. Repts. DSDP*, 47, Pt. 2: Washington (U.S. Govt. Printing Office), 633–662.

Honnorez, J., Mevel, C., and Montigny, R., 1984. Geotectonic significance of gneissic amphibolites from the Vema Fracture Zone, equatorial Mid-Atlantic Ridge. *J. Geophys. Res.*, 89:11379–11400.

Kasahara, J., and Kumazawa, M., 1969. An empirical relation between velocity anisotropy and optical anisotropy. *J. Seismol. Soc. Japan.*

Kasahara, J., Kumazawa, M., Suzuki, I., and Iida, K., 1968. P-wave anisotropy in Hidaka dunite. *J. Seismol. Soc. Japan*, 222–228.

Kennett, J. P., and Srinivasan, S., 1983. *Neogene Planktonic Foraminifera. A Phylogenetic Atlas*: Stroudsburg (Hutchison-Ross).

Laughton, A. S., Berggren, W. A., et al., 1972. *Init. Repts. DSDP*, 12: Washington (U.S. Govt. Printing Office).

Laughton, A. S., Berggren, W. A., Benson, R. N., Davies, T. A., Franz, U., Musich, L. F., Perch-Nielsen, K., Ruffman, A. S., van Hinte, J. E., Whitmarsh, R. B., Aumento, F., Clarke, A. D., Ryall, P. J. C., Cann, J. R., Bryan, W. B., and Bukry, D., 1972. Site 118. *In* Laughton, A. S., Berggren, W. A., et al., *Init. Repts. DSDP*, 12: Washington (U.S. Govt. Printing Office), 673–751.

Lowrie, W., 1979. Geomagnetic reversals and ocean crust magnetization. *In* Talwani, M., Harrison, C. G., and Hayes, D. E. (Eds.), *Deep Drilling Results in the Atlantic Ocean: Ocean Crust, Maurice Ewing Series:* Washington (American Geophysical Union), 2:135–150.

Ma'alouleh, K., and Moullade, M., in press. Biostratigraphic and paleoceanographic study of Neogene and Quaternary planktonic foraminifers from the lower continental rise of the New Jersey Margin (western North Atlantic), DSDP Leg 93, Site 603. *Init. Repts. DSDP*, 93: Washington (U.S. Govt. Printing Office).

McIver, R., 1975. Hydrocarbon occurrence from JOIDES Deep Sea Drilling Project. *Proceedings, Ninth World Petroleum Congress*, 269–280.

Mercier, J. C., 1984. Olivine and pyroxenes. *In* Wenk, H. R. (Ed.), *Preferred Orientation in Deformed Metals and Rocks: an Introduction to Modern Texture Analysis*. New York (Academic Press), 407–430.

Montadert, L., Roberts, D.G., et al., 1979. *Init. Repts. DSDP*, 48: Washington (U.S. Govt. Printing Office).

Montadert, L., Roberts, D. G., De Charpal, O., and Geunnoc, P., 1979. Rifting and subsidence of the northern continental margin of the Bay of Biscay. *In* Montadert, L., Roberts, D. B., et al., *Init. Repts. DSDP*, 48: Washington (U.S. Govt. Printing Office), 1025–1060.

Moullade, M., 1983. Upper Neogene and Quaternary planktonic foraminifera from the Blake Outer Ridge and Blake Bahama Basin (western North Atlantic). *In* Sheridan, P. E., Gradstein, F. M., et al., *Init. Repts. DSDP*, 76: Washington (U.S. Govt. Printing Office), 511–535.

———, in press. Distribution of Neogene and Quaternary planktonic foraminifers from the upper continental rise of the New Jersey margin (western North Atlantic), DSDP Site 604: biostratigraphical analysis, sedimentary and paleoceanographic implications. *Init. Repts. DSDP*, 93: Washington (U.S. Govt. Printing Office).

Müller, G., and Gastner, M., 1971. The "Karbonate-Bombe," a simple device for determination of the carbonate content in sediments, soils, and other materials. *Neues Jahrb. Mineral. Monatsch.*, 10: 466–469.

Nicolas, A., Boudier, F., and Bouchez, J. L., 1980. Interpretation of peridotite structures from ophiolitic and oceanic environments. *Ann. J. Sci.*, 279A:2–15.

Okada, H., and Bukry, D., 1980. Supplementary modification and introduction of code numbers to the low latitude coccolith biostratigraphic zonation. *Mar. Micropaleontol.*, 5:321–325.

Perch-Nielsen, K., 1985. Cenozoic calcareous nannofossils. *In* Saunders, J. B., Bolli, H., and Perch-Nielsen, K. (Eds.), *Plankton Stratigraphy:* Cambridge University Press, 427–554.

Shipboard Party, 1978. Site 395: 23°N, Mid-Atlantic Ridge. *In* Melson, W. G., Rabinowitz, P. D., et al., *Init. Repts. DSDP*, 45: Washington (U.S. Govt. Printing Office), 131–267.

Sibuet, J. C., Ryan, W. B. F., et al., 1979. *Init. Repts. DSDP*, 47, Pt. 2: Washington (U.S. Govt. Printing Office).

Stainforth, R. M., Lamb, J. L., Luterbacher, H., Beard, J. M., and Jeffords, R. M., 1975. Cenozoic planktonic foraminiferal zonation and characteristics of index forms. *The University of Kansas Paleontological Contributions, Article 62.*

Wernicke, B., 1985. Uniform-sense normal simple shear of the continental lithosphere. *Can. J. Earth Sci.*, 22(1):108–125.

Winterer, E. L., and Hinz, K., 1984. The evolution of the Mazagan continental margin: a synthesis of geophysical and geological data with results of drilling during Deep Sea Drilling Leg 79. *In* Hinz, K., Winterer, E. L., et al., *Init. Repts. DSDP*, 79: Washington (U.S. Govt. Printing Office), 893–919.

Location: 42°05.3′N, 12°51.8′W Water depth: 5321 m below derrick floor (5311 mbsl)

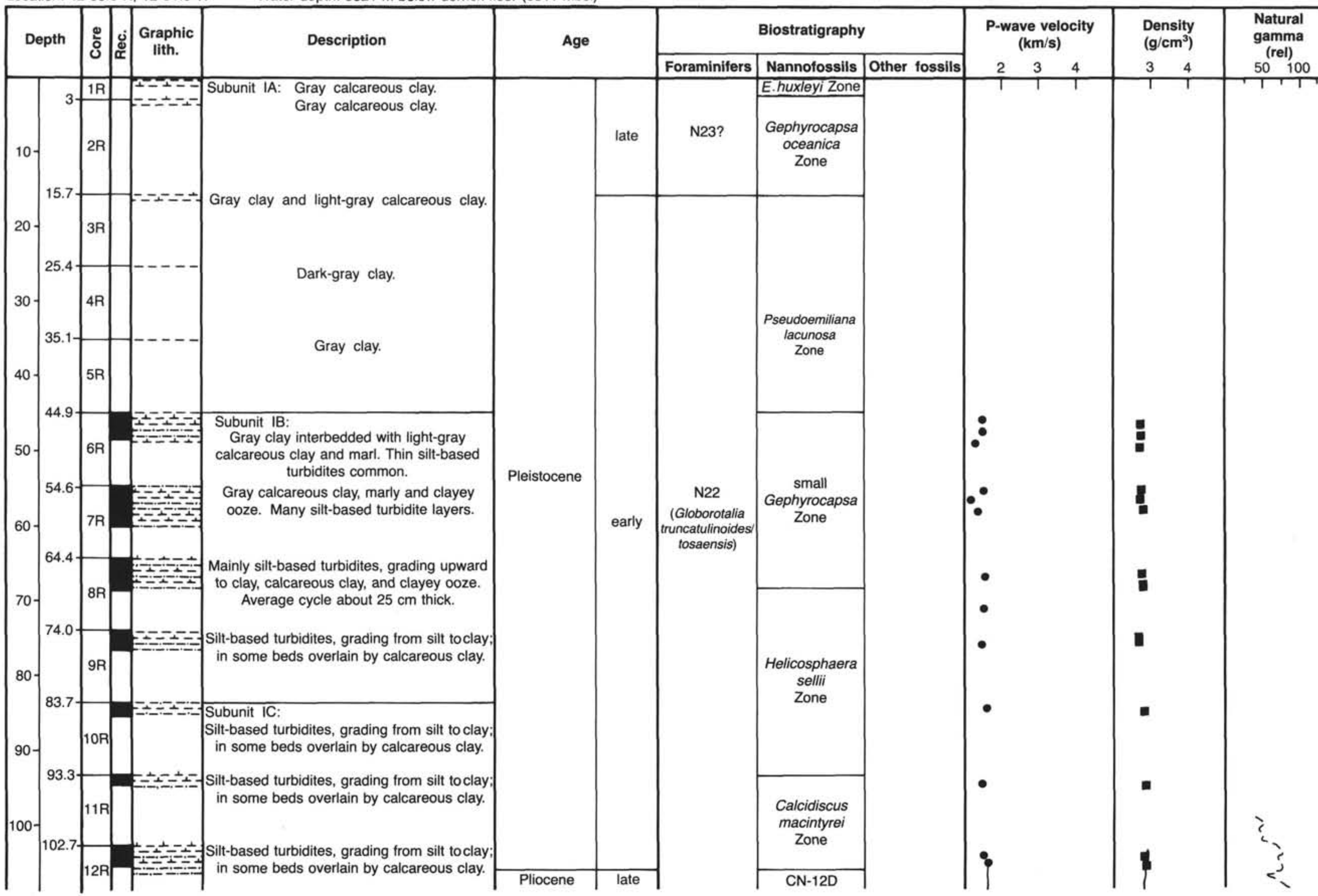

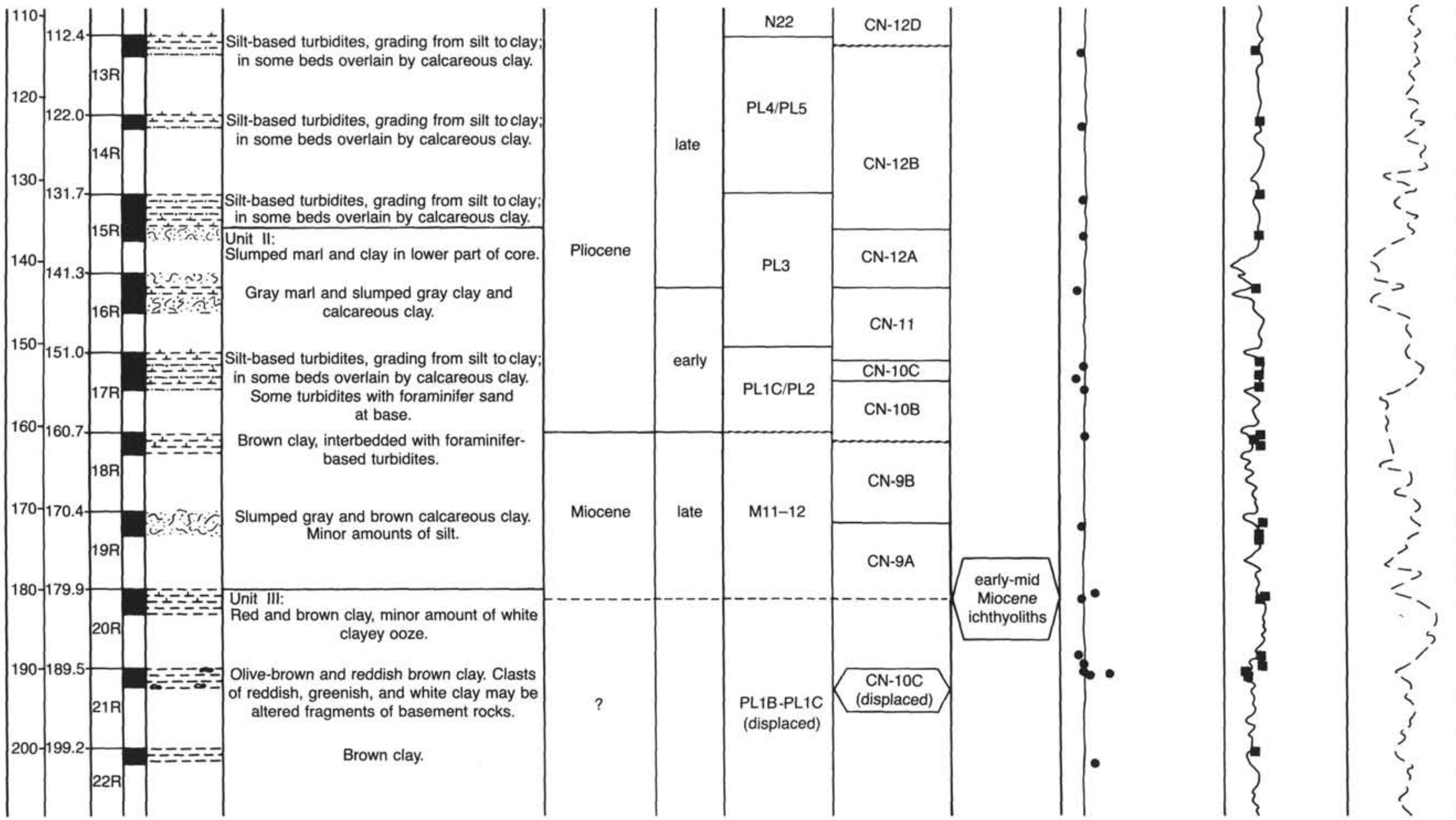

Figure 34. Summary logs, Site 637 (Hole 637A).

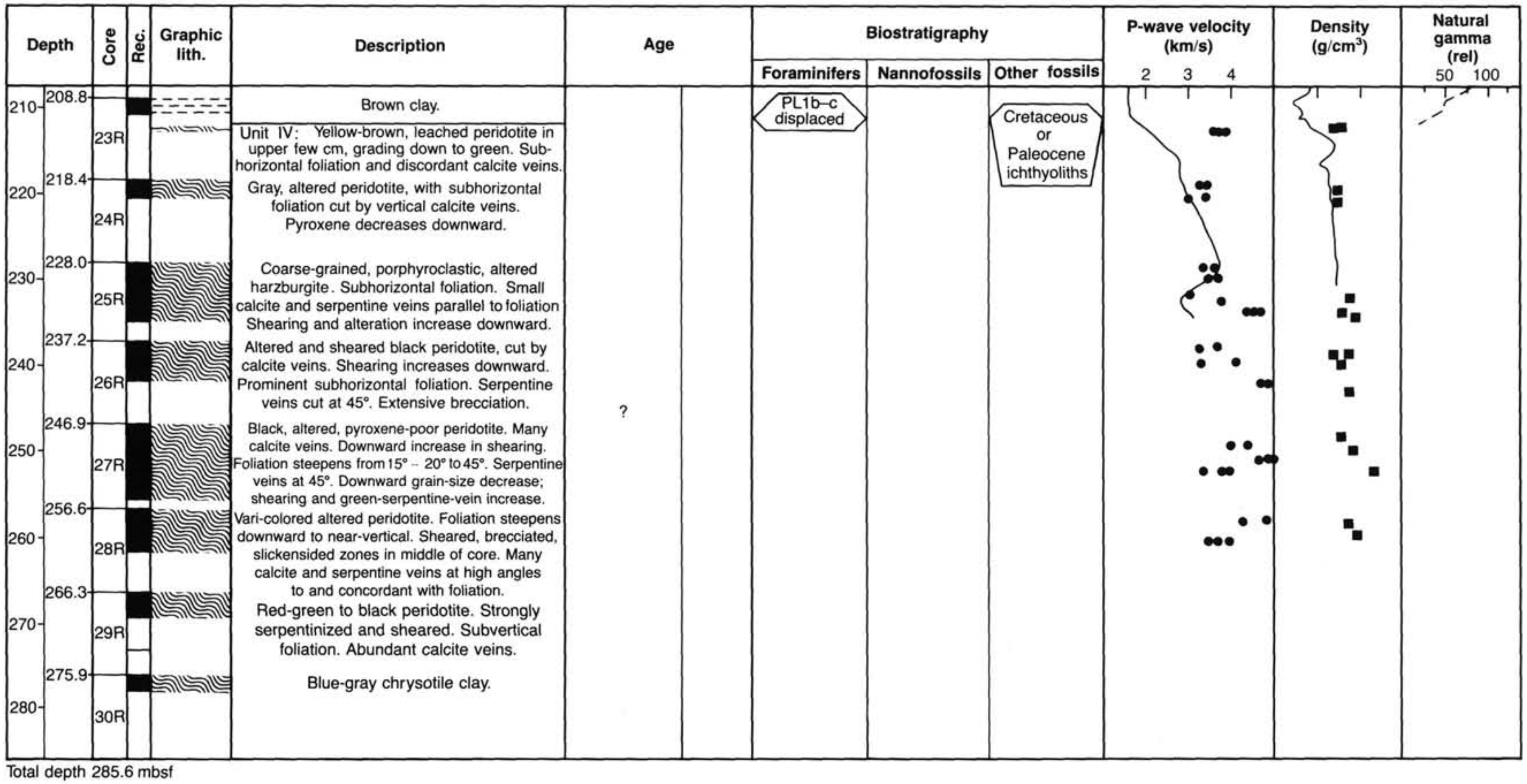

Figure 34 (continued).

SITE 637 HOLE A CORE 1 R CORED INTERVAL 5310.5–5313.5 mbsl; 0.0–3.0 mbsf

TIME-ROCK UNIT	BIOSTRAT. ZONE/ FOSSIL CHARACTER: FORAMINIFERS	NANNOFOSSILS	RADIOLARIANS	DIATOMS	PALEOMAGNETICS	PHYS. PROPERTIES	CHEMISTRY	SECTION	METERS	GRAPHIC LITHOLOGY	DRILLING DISTURB.	SED. STRUCTURES	SAMPLES
LATE PLEISTOCENE	N22-23 *Globorot. truncatulinoides* Zone A/G	*Emiliania huxleyi* Zone A/M	B				• 22 %	CC					*

LITHOLOGIC DESCRIPTION

GRAY CALCAREOUS CLAY.

This core is empty except for 7 cm of highly disturbed, gray (5Y5/1) calcareous clay in the CC.

SMEAR SLIDE SUMMARY (%):

	CC D
TEXTURE:	
Sand	10
Silt	14
Clay	76
COMPOSITION:	
Quartz	15
Feldspar	Tr
Mica	3
Clay	20
Volcanic Glass	Tr
Calcite/Dolomite	Tr
Accessory Minerals	2
Foraminifers	4
Nannofossils	56
Sponge Spicules	Tr
Fish Remains	Tr
Bioclasts	Tr

Information on Core Description Forms, for ALL sites, represents field notes taken aboard ship. Some of this information has been refined in accord with post-cruise findings, but production schedules prohibit definitive correlation of these forms with subsequent findings. Thus the reader should be alerted to the occasional ambiguity or discrepancy.

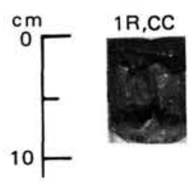

SITE 637 HOLE A CORE 2 R CORED INTERVAL 5315.5–5326.2 mbsl; 3.0–15.7 mbsf

TIME-ROCK UNIT	FORAMINIFERS	NANNOFOSSILS	RADIOLARIANS	DIATOMS	PALEOMAGNETICS	PHYS. PROPERTIES	CHEMISTRY	SECTION	METERS	GRAPHIC LITHOLOGY	DRILLING DISTURB.	SED. STRUCTURES	SAMPLES
LATE PLEISTOCENE	A/G N 22–23	C/G *Gephyrocapsa Oceanica* Zone	B				● 15 %	1 CC					*

BIOSTRAT. ZONE/ FOSSIL CHARACTER

LITHOLOGIC DESCRIPTION

GRAY CALCAREOUS CLAY.

This core is empty except for highly disturbed, gray (5Y5/1) calcareous clay in Section 1 and the CC.

SMEAR SLIDE SUMMARY (%):

	CC D	CC D
TEXTURE:		
Sand	10	0
Silt	40	13
Clay	50	87
COMPOSITION:		
Quartz	5	10
Feldspar	5	1
Mica	5	Tr
Clay	40	35
Accessory Minerals: Glauconite, Zircon, & Opaques	–	3
Foraminifers	5	1
Nannofossils	40	50
Fish Remains	–	Tr

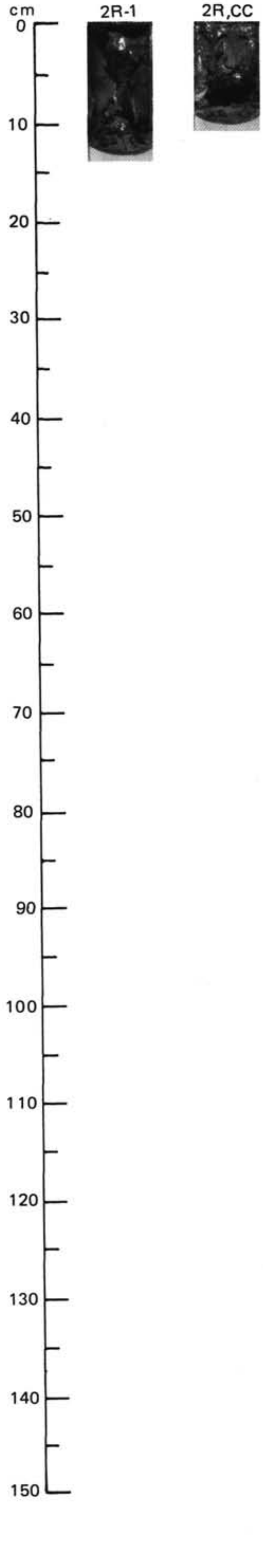
cm
0
10
20
30
40
50
60
70
80
90
100
110
120
130
140
150
2R-1
2R,CC

SITE 637 HOLE A CORE 3 R CORED INTERVAL 5326.2-5335.9 mbsl; 15.7-25.4 mbsf

TIME-ROCK UNIT	FORAMINIFERS	NANNOFOSSILS	RADIOLARIANS	DIATOMS	PALEOMAGNETICS	PHYS. PROPERTIES	CHEMISTRY	SECTION	METERS	GRAPHIC LITHOLOGY	DRILLING DISTURB.	SED. STRUCTURES	SAMPLES
EARLY PLEISTOCENE	N 22 *Glt. truncatulinoides/tosaensis* Zone A/M	*P. lacunosa* Zone A/G	B				● 5 %	CC					*

BIOSTRAT. ZONE/ FOSSIL CHARACTER

LITHOLOGIC DESCRIPTION

GRAY CLAY and LIGHT GRAY CALCAREOUS CLAY.

This core is empty except for 8 cm of highly disturbed, varigated gray (5Y5/1) clay and light gray (5Y7/1) calcareous clay in the CC.

SMEAR SLIDE SUMMARY (%):

	CC D
TEXTURE:	
Sand	5
Silt	7
Clay	88
COMPOSITION:	
Quartz	4
Feldspar	Tr
Mica	Tr
Clay	60
Accessory Minerals:	
Glauconite & Opaques	1
Foraminifers	10
Nannofossils	25
Fish Remains	Tr

SITE 637 HOLE A CORE 4 R CORED INTERVAL 5335.9-5345.6 mbsl; 25.4-35.1 mbsf

TIME-ROCK UNIT	FORAMINIFERS	NANNOFOSSILS	RADIOLARIANS	DIATOMS	PALEOMAGNETICS	PHYS. PROPERTIES	CHEMISTRY	SECTION	METERS	GRAPHIC LITHOLOGY	DRILLING DISTURB.	SED. STRUCTURES	SAMPLES
EARLY PLEISTOCENE	N 22 C/M	*P. lacunosa* Zone A/G	B					1	0.5, 1.0				

BIOSTRAT. ZONE/ FOSSIL CHARACTER

LITHOLOGIC DESCRIPTION

This core was empty, except for traces of dark gray (5Y4/1) clay given to the shipboard paleontologists for dating.

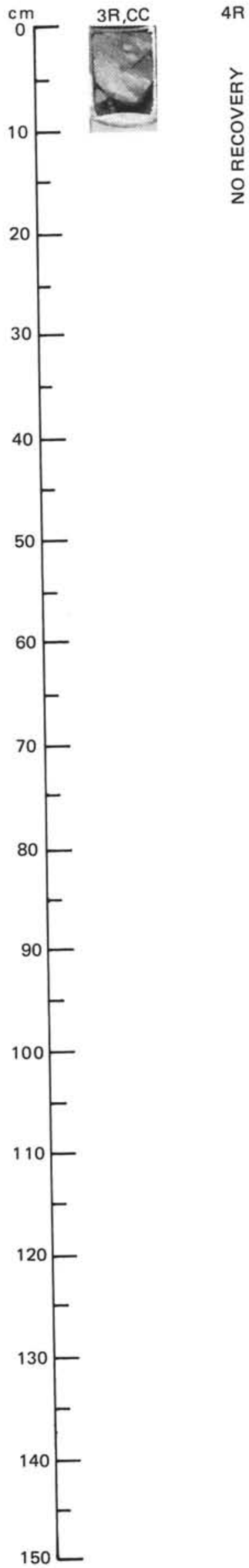
cm
3R,CC
4R
NO RECOVERY
0
10
20
30
40
50
60
70
80
90
100
110
120
130
140
150

SITE 637 HOLE A CORE 5 R CORED INTERVAL 5345.6-5355.4 mbsl; 35.1-44.9 mbsf

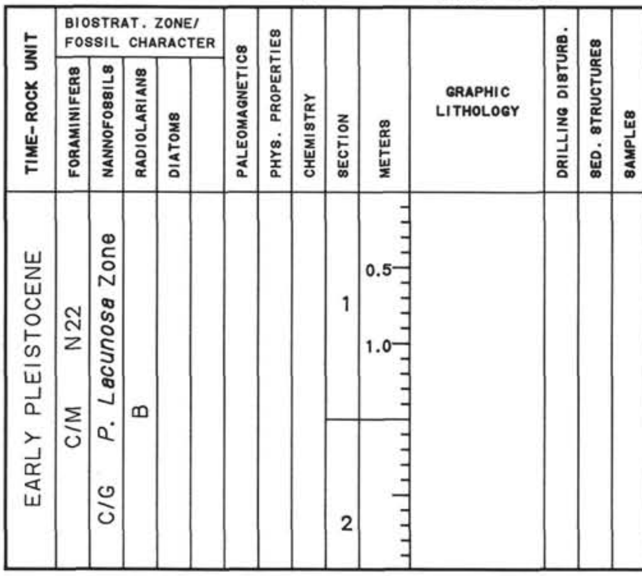

LITHOLOGIC DESCRIPTION

This core was empty, except for traces of gray (5Y5/1) clay given to the shipboard paleontologists for dating.

SITE 637 HOLE A CORE 6 R CORED INTERVAL 5355.4-5365.1 mbsl; 44.9-54.6 mbsf

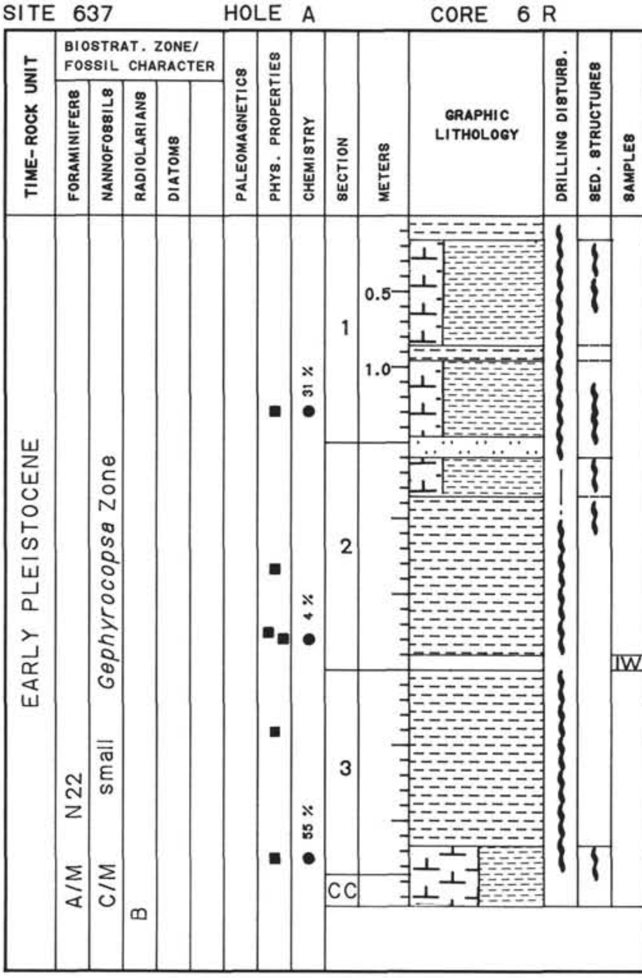

LITHOLOGIC DESCRIPTION

CLAY interbedded with CALCAREOUS CLAY and MARLS.

This core consists dominantly of highly deformed, gray (5Y5/1) clay, found in Section 1, 0-15 cm and 87-92 cm and in Section 2, 36 cm through Section 3, 116 cm. The clay contains pockets and thin layers of gray (5Y5/1) silty clay in Section 1, 13-15 cm, in Section 2 at 53 cm, 119-120 cm, and 136-141 cm, and in Section 3 at 30-32 cm, 100-102 cm, and 115-119 cm. These silts are interpreted to be the base of turbidite layers. Upper portion of the clay in Section 2, 36-53 cm is slightly more calcareous, olive (5Y5/3), and contains light gray (5Y7/2) burrows and mottles. Contact with overlying layer in Section 2 is marked by a diffuse dark, thin manganese-stained layer.

Light brownish gray (2.5Y6/2) and light gray (10YR6/1, 10YR7/1, 10YR7/2), highly deformed, mottled calcareous clays occur in Section 1, 15-92 cm and 97-150 cm and in Section 2, 10-35 cm. Light gray (10YR7/1), highly deformed, mottled marl occurs in Section 3, 117-136 cm and in the CC. Highly deformed marls in the CC also include slightly darker, intermixed calcareous clays.

PHYSICAL PROPERTIES DATA:

	1,130	2,84	2,125	2,130	3,39	3,130
V_p (c)	1.50	–	–	1.48	–	132
ρ_b	1.77	–	–	1.79	–	1.72
γ	–	–	18.33	–	–	–
T_c	–	3.17	–	–	2.79	–

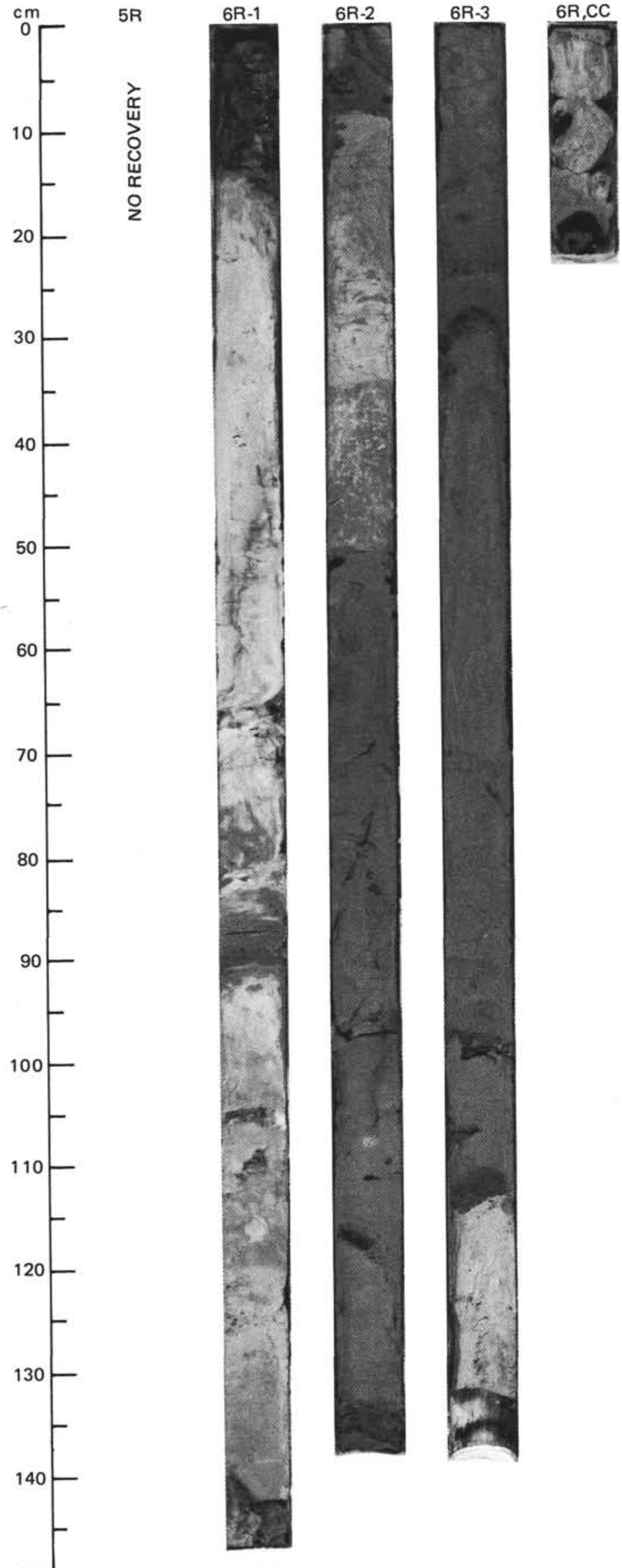
cm
0
10
20
30
40
50
60
70
80
90
100
110
120
130
140
150
5R
NO RECOVERY
6R-1
6R-2
6R-3
6R,CC

SITE 637 HOLE A CORE 7 R CORED INTERVAL 5365.1-5374.9 mbsl; 54.6-64.4 mbsf

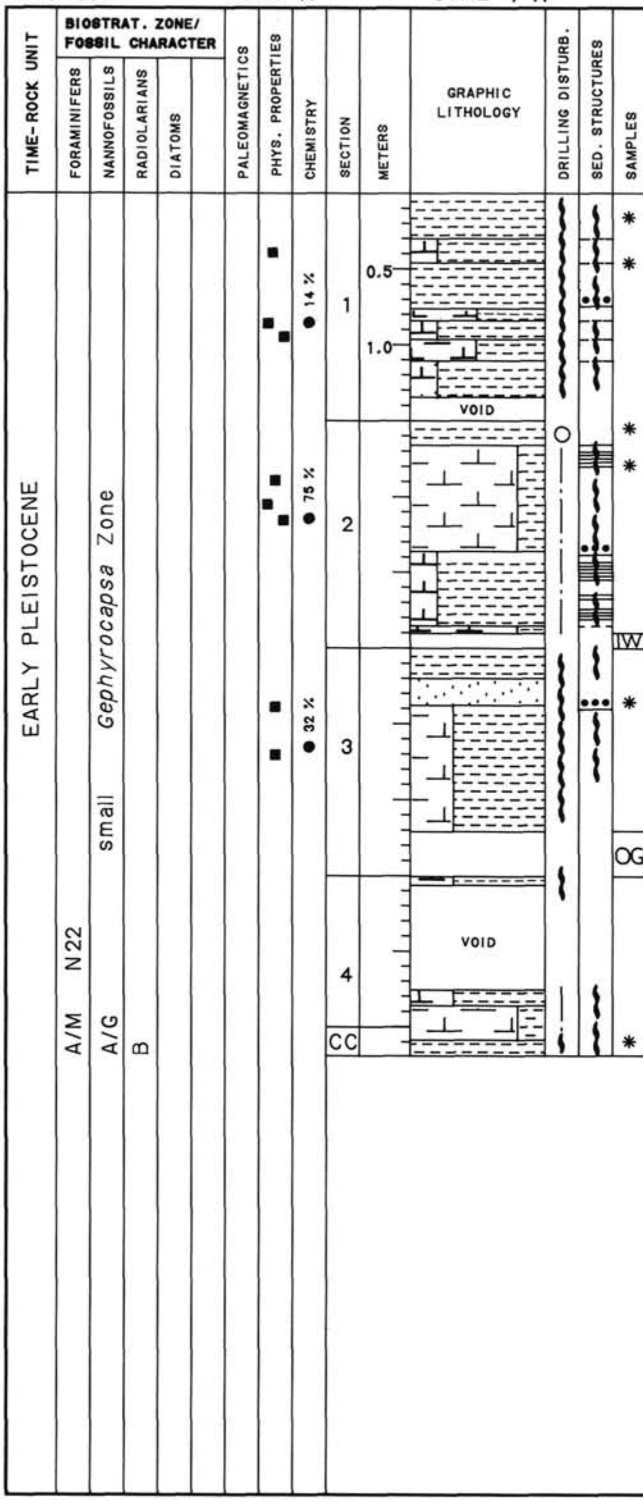

LITHOLOGIC DESCRIPTION

TURBIDITES, CALCAREOUS CLAYS, MARLS, and CLAYEY OOZES.

This core contains moderately to very deformed, bioturbated, gray (5Y5/1) clays, gray (5Y5/1 - 6/1) calcareous clays, light gray (5Y 6/1 - 7/1) marls, and white (5Y8/1) clayey ooze. Thin silt layers and deformed silt patches underlie many of the clays, and are interpreted to represent the base of terrigenous turbidite beds. The mode of deposition of the more bioturbated calcareous sediments is not entirely certain, but they may represent a combination of resedimented and pelagic deposits.

SMEAR SLIDE SUMMARY (%):

	1,16 D	1,43 D	2,5 D	2,32 D	3,34 D	CC D
TEXTURE:						
Sand	–	–	20	5	5	Tr
Silt	6	20	50	45	25	10
Clay	94	80	30	50	70	90
COMPOSITON:						
Quartz	5	10	30	2	20	Tr
Feldspar	Tr	–	–	–	Tr	–
Mica	Tr	Tr	Tr	–	1	Tr
Clay	74	20	20	3	59	15
Volcanic Glass	Tr	–	Tr	–	Tr	–
Calcite/Dolomite	–	Tr	Tr	–	–	1
Accessory Minerals:						
Glauconite & Zeolites	1	Tr	10	Tr	5	Tr
Foraminifers	–	10	30	5	5	12
Nannofossils	20	60	10	90	10	72
Fish Remains	–	–	Tr	–	Tr	–

PHYSICAL PROPERTIES DATA:

	1,40	1,86	1,90	2,40
V_p (c)	–	1.50	–	–
ρ_b	–	1.79	–	–
γ	–	–	22.76	–
T_c	2.80	–	–	2.69

	2,55	2,62	3,40	3,67
V_p (c)	–	1.19	–	1.33
ρ_b	–	1.73	–	1.82
γ	8.17	–	–	–
T_c	–	–	2.63	–

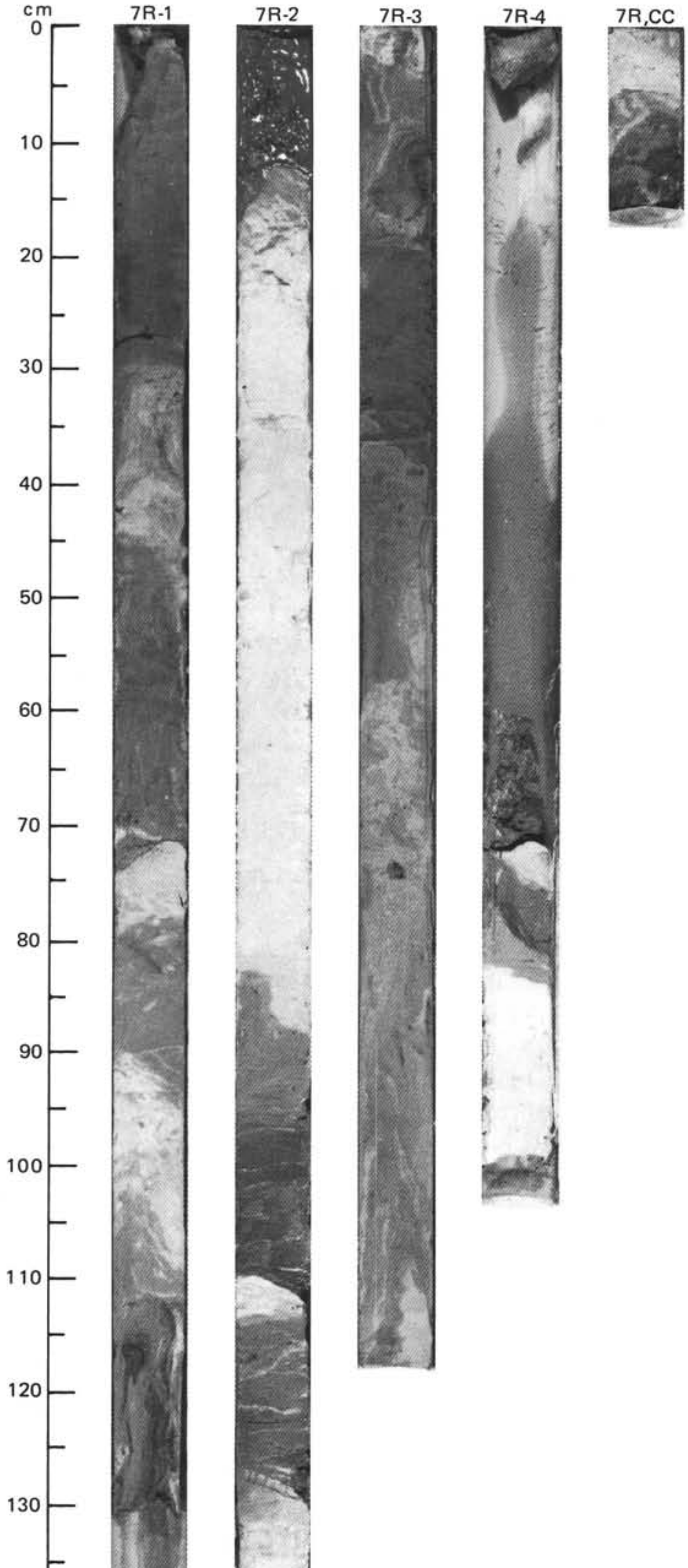
cm
0
10
20
30
40
50
60
70
80
90
100
110
120
130
140
150
7R-1
7R-2
7R-3
7R-4
7R,CC

SITE 637 HOLE A CORE 8 R CORED INTERVAL 5374.9-5384.5 mbsl; 64.4-74.0 mbsf

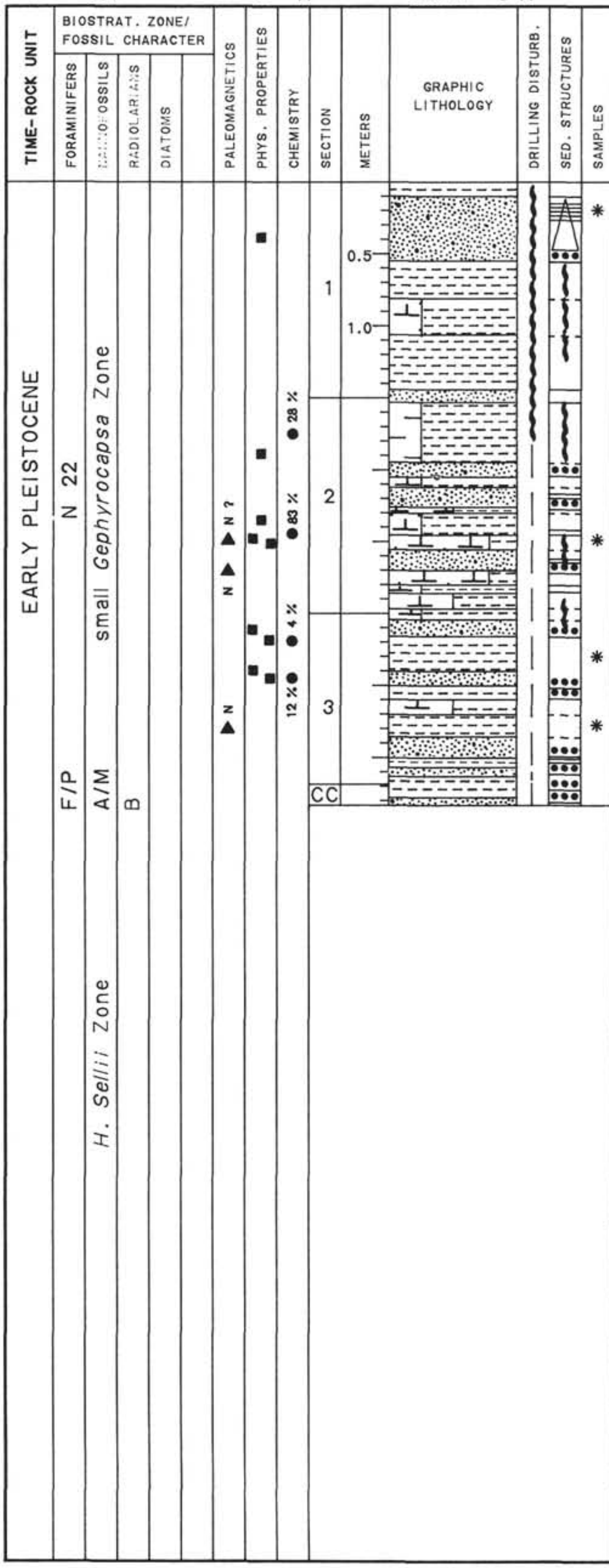

LITHOLOGIC DESCRIPTION

SILTY TURBIDITES.

This core contains a series of turbidite beds that typically grade from sandy silt, to clay, to calcareous clay, to marl upsection. A few of these cycles are topped by clayey oozes. The turbidite cycles range from 2-100 cm in thickness, averaging about 25 cm.

The sandy silts marking the base of the turbidites are normally graded, dark gray to gray (5Y4/1-5Y5/1) and sometimes appear laminated at the top. The clays overlying the sandy silts are dark gray to gray (5Y4/1-5Y6/1) and bioturbated. The calcareous clays, marls, and clayey oozes are gray to light gray (5Y6/1-5Y7/1) and bioturbated.

Section 1 and the top of Section 2 were highly deformed by drilling. There is some suggestion of thin silt layers within the clay section in Section 1, 130-140 cm, though the drilling deformation has obscured them.

SMEAR SLIDE SUMMARY (%):

	1,25 D	2,101 D	3,31 D	3,73 D
TEXTURE:				
Sand	6	–	–	–
Silt	5	10	80	15
Clay	94	90	20	85
COMPOSITION:				
Quartz	10	Tr	59	10
Feldspar	Tr	–	20	Tr
Mica	1	Tr	Tr	Tr
Clay	30	5	20	85
Calcite/Dolomite	Tr	–	–	–
Accessory Minerals: (Glauconite,Zircon, Opaques)	Tr	Tr	1	5
Foraminifers	–	10	–	–
Nannofossils	59	85	–	–
Sponge Spicules	Tr	–	–	–
Fish Remains	–	Tr	–	–

PHYSICAL PROPERTIES DATA:

	1,40	2,40	2,86	2,97	2,100
V_p (c)	–	–	–	1.56	–
ρ_b	–	–	–	1.68	–
γ	–	–	19.20	–	11.23
T_c	3.71	2.75	–	–	–

	3,14	3,21	3,40	3,44
V_p (c)	–	–	–	1.51
ρ_b	–	1.79	–	1.79
γ	20.01	–	–	–
T_c	–	–	2.50	–

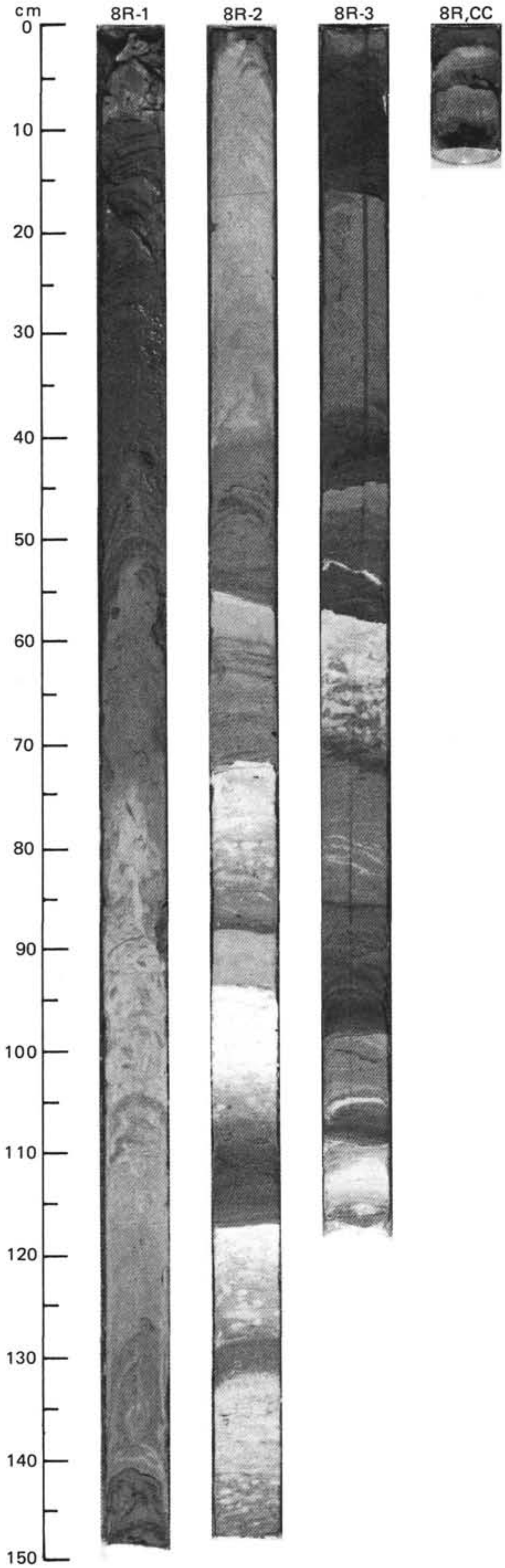
cm
0
10
20
30
40
50
60
70
80
90
100
110
120
130
140
150
8R-1
8R-2
8R-3
8R,CC

SITE 637 HOLE A CORE 9 R CORED INTERVAL 5384.5-5394.2 mbsl; 74.0-83.7 mbsf

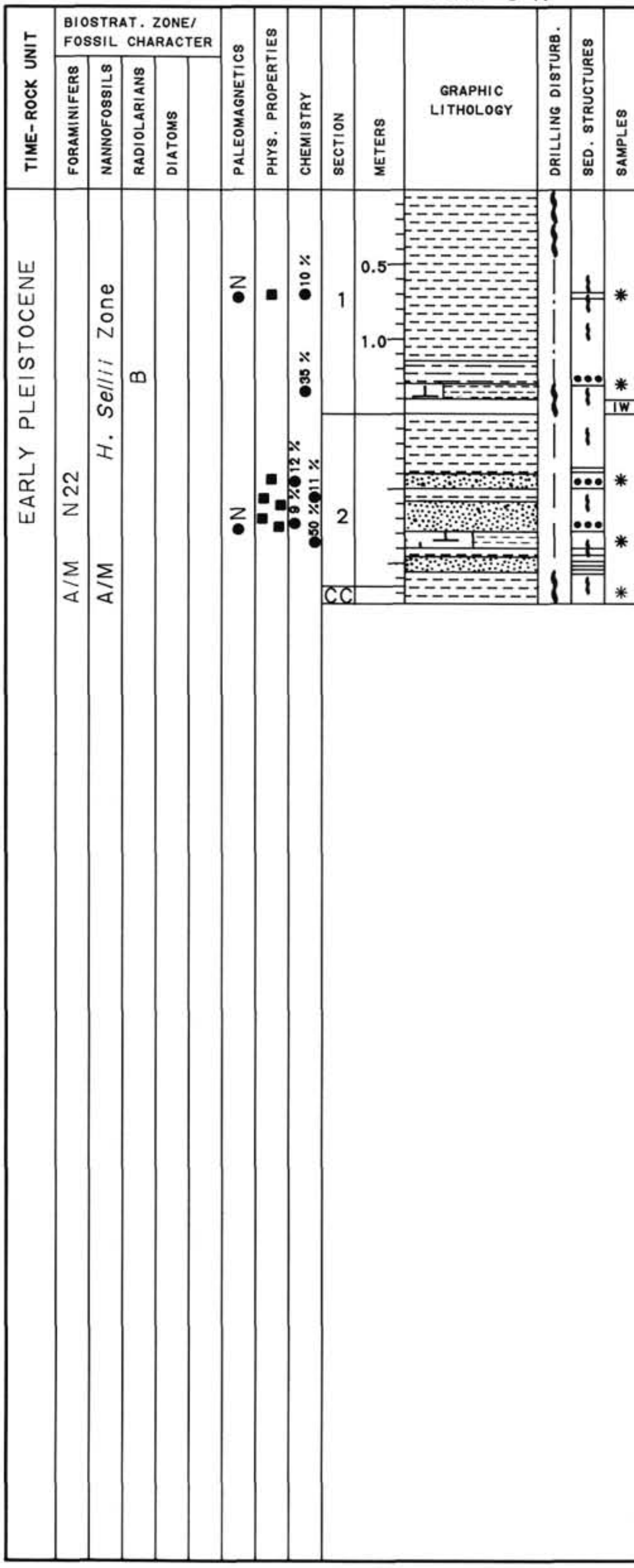

LITHOLOGIC DESCRIPTION

SILTY TURBIDITES.

This core contains a series of turbidite beds that typically grade from sandy silt or clayey silt at the base to clay at the top. Several of the turbidite beds have calcareous clays overlying the clay sections. The sandy silts and clayey silts are normally graded, dark gray (5Y4/1), sometimes laminated, and have either gradational or sharp contacts with the overlying clays. The clays are gray (5Y5/1) and primarily structureless. Calcareous clays and marls are light gray to white (5Y6/1 - 8/1) and bioturbated. Two thin manganese-stained laminae occur in Section 1 at approximately 73-77 cm.

Section 1, 0-50 cm is very deformed and contains drilling slurry. The rest of the core appears to be only slightly deformed by drilling, except for a small interval of highly deformed material at the base of Section 1.

SMEAR SLIDE SUMMARY (%):

	1,68 D	1,133 D	2,44 D	2,82 D	CC D
TEXTURE:					
Sand	–	Tr	50	–	–
Silt	5	10	30	40	5
Clay	95	90	20	50	95
COMPOSITION:					
Quartz	2	Tr	40	–	5
Feldspar	–	–	10	–	–
Mica	8	Tr	10	–	–
Clay	50	10	20	10	30
Accessory Minerals: Opaques, Zircon, & Glauconite	Tr	Tr	10	–	5
Foraminifers	–	10	5	10	Tr
Nannofossils	40	80	5	80	60

PHYSICAL PROPERTIES DATA:

	1,70	2,45	2,53	2,57	2,70	2,73
V_p (c)	–	–	–	1.47	–	1.29
ρ_b	–	–	–	1.82	–	1.86
γ	–	12.25	28.39	–	–	–
T_c	2.69	–	–	–	3.04	–

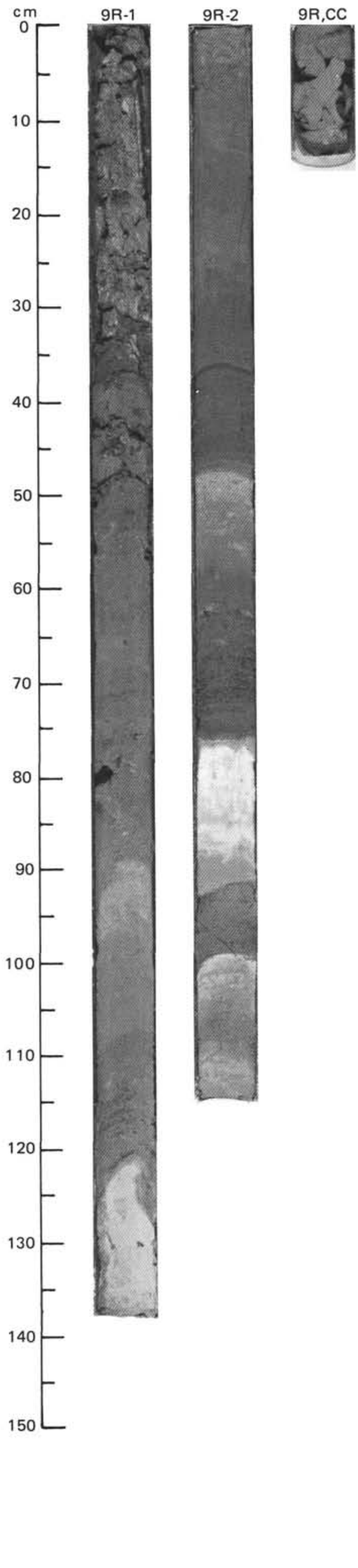
cm
9R-1
9R-2
9R,CC
0
10
20
30
40
50
60
70
80
90
100
110
120
130
140
150

SITE 637 HOLE A CORE 10 R CORED INTERVAL 5394.2-5403.8 mbsl; 83.7-93.3 mbsl

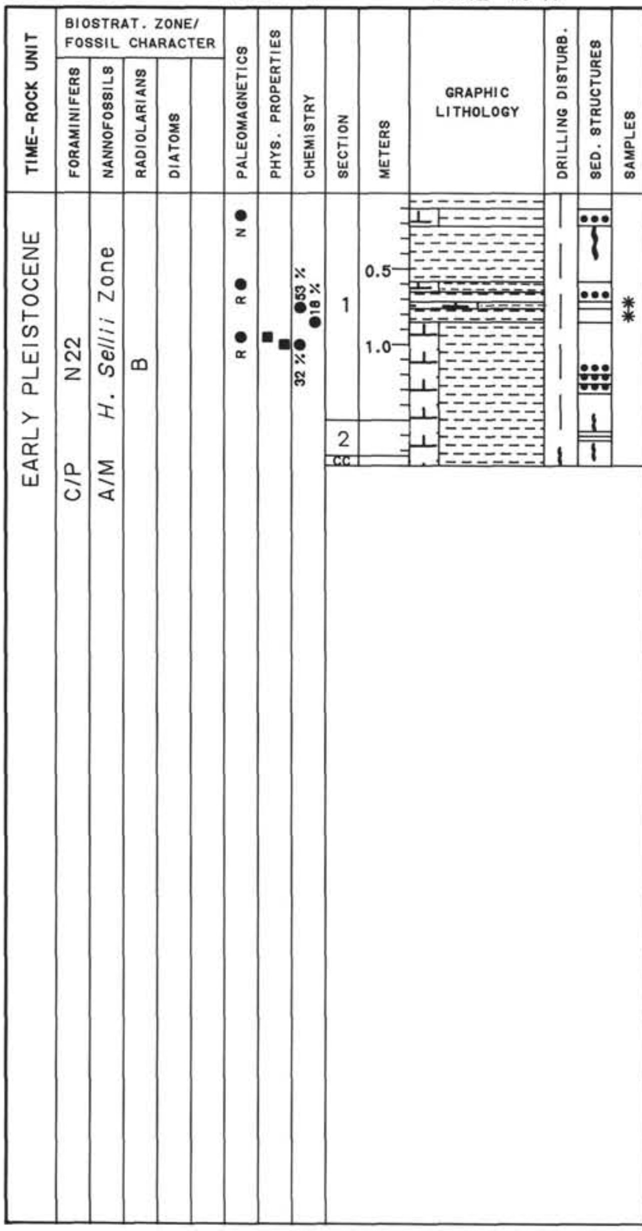

LITHOLOGIC DESCRIPTION

TURBIDITES and CALCAREOUS CLAYS.

This core consists of turbidites that typically grade from thin, dark gray to gray (5Y4/1 - 5/1) silts at the base to gray (5Y5/1) clays and bioturbated, light gray (5Y6/1) calcareous clays at the top. Other similar calcareous clays and a light gray (5Y7/1) marl in Section 1, 73-77 cm that do not appear to be immediately contiguous with an underlying graded silt and clay layer also occur. Because of the low recovery in this core and the 'biscuited' appearance of some of the bedding contacts, it is impossible to determine whether or not these isolated calcareous sediments overlie unrecovered clays and silts.

SMEAR SLIDE SUMMARY (%):

	1,74 D	1,82 D
TEXTURE:		
Silt	40	3
Clay	60	97
COMPOSITION:		
Quartz	Tr	2
Feldspar	–	Tr
Mica	–	Tr
Clay	5	50
Accessory Minerals	Tr	Tr
Foraminifers	5	1
Nannofossils	90	47

PHYSICAL PROPERTIES DATA:

	1,98	1,100
V_p (c)	1.60	–
ρ_b	1.82	–
γ	–	71.88

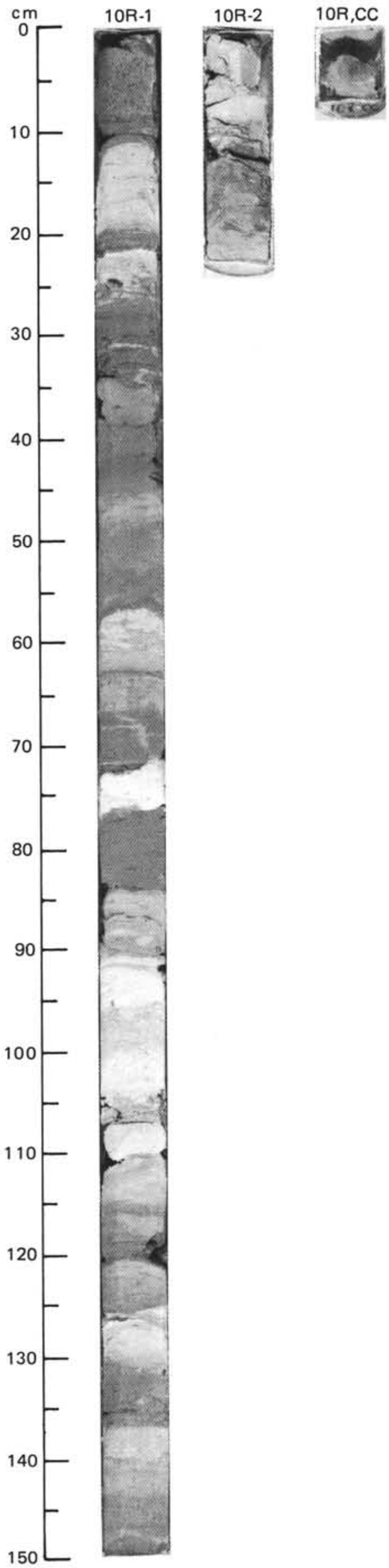
cm
10R-1
10R-2
10R,CC
0
10
20
30
40
50
60
70
80
90
100
110
120
130
140
150

SITE 637 HOLE A CORE 11 R CORED INTERVAL 5403.8-5413.2 mbsl; 93.3-102.7 mbsf

TIME-ROCK UNIT	FORAMINIFERS	NANNOFOSSILS	RADIOLARIANS	DIATOMS	PALEOMAGNETICS	PHYS. PROPERTIES	CHEMISTRY	SECTION	METERS
EARLY PLEISTOCENE	N22 R/P	*C. macintyrei* Zone F/P	B		●N ●R ●R	■	70 % ● 15 % ●● 6 % ●	1, CC	0.5, 1.0

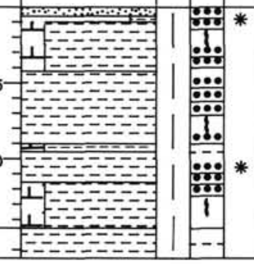

LITHOLOGIC DESCRIPTION

TURBIDITES and CALCAREOUS CLAYS.

This core consists of turbidites that grade from thin, dark gray and gray (5Y4/1 - 5/1) silts at the base to gray (5Y5/1) clays and bioturbated, light gray (5Y6/1 - 7/1) calcareous clays at the top. The upper boundary of some of these turbidites is delineated by a thin, dark, manganese-rich layer (Section 1, 7-8 cm, 110, 123 cm, and 139 cm). Separate calcareous clays and one clayey ooze in Section 1, 3-7 cm also occur, sometimes appearing graded, and likely represent biogenic turbidites.

SMEAR SLIDE SUMMARY (%):

	1,7 D	1,104 D
TEXTURE:		
Sand	10	–
Silt	15	13
Clay	75	87
COMPOSITION:		
Quartz	Tr	10
Mica	–	3
Clay	5	50
Accessory Minerals: Zircon, Glauconite & Opaques	Tr	Tr
Foraminifers	25	–
Nannofossils	70	37
Fish Remains	Tr	–

PHYSICAL PROPERTIES DATA:

	1,98
V_p (a)	0.88
V_p (b)	1.49
V_p (c)	1.20
ρ_b	1.82

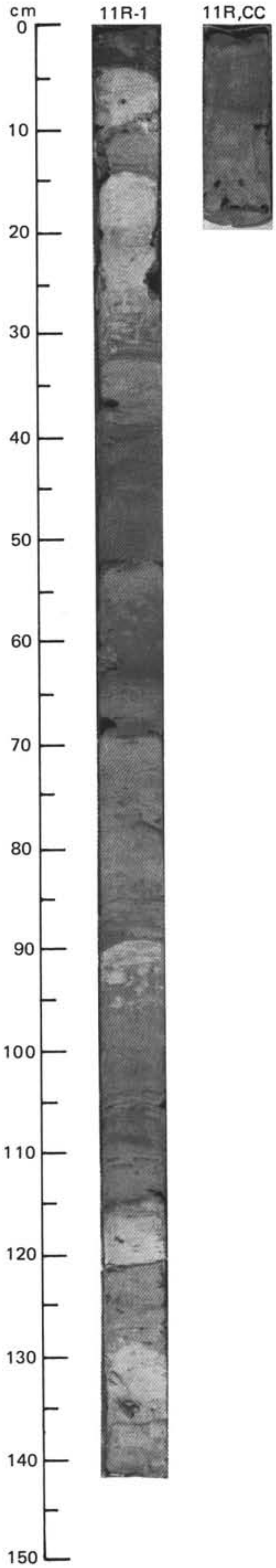
cm
0
10
20
30
40
50
60
70
80
90
100
110
120
130
140
150
11R-1
11R,CC

SITE 637 HOLE A CORE 12 R CORED INTERVAL 5413.2-5422.9 mbsl; 102.7-112.4 mbsf

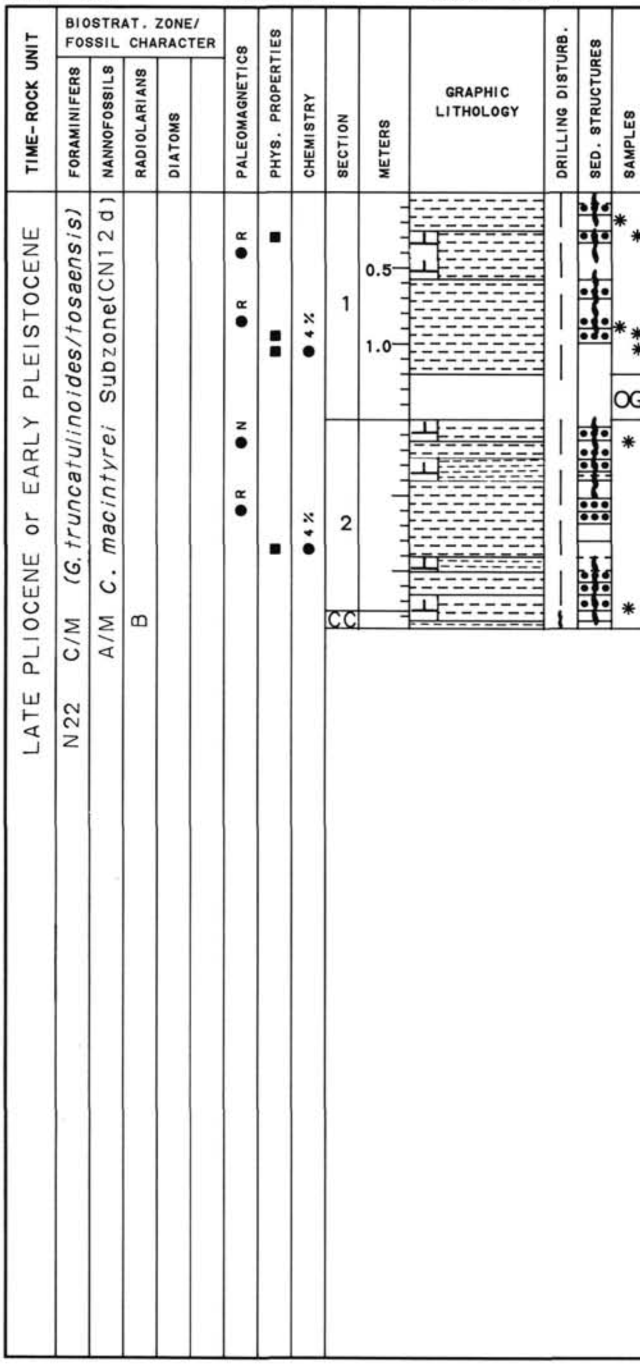

LITHOLOGIC DESCRIPTION

TURBIDITES, CALCAREOUS CLAYS and MARLS.

This core consists dominantly of turbidites that grade from thin, dark gray to olive gray (5Y4/1 - 5/2) silts at the base to gray to light olive gray (5Y5/1 - 6/2) clays and bioturbated, light gray (5Y6/1 - 7/2) calcareous clays at the top. Manganese-rich laminae occur in Section 2, 21 cm, 31-32 cm, 64 cm, 80 cm, and 127 cm.

SMEAR SLIDE SUMMARY (%):

	1,19 D	1,27 D	1,87 D	1,88 D	1,103 D	2,16 D	2,122 M
TEXTURE:							
Sand	Tr	–	–	Tr	–	–	–
Silt	5	1	42	46	5	3	20
Clay	95	99	58	54	95	97	80
COMPOSITION:							
Quartz	Tr	–	40	35	5	1	4
Feldspar	Tr	–	–	–	–	Tr	–
Mica	1	–	Tr	4	10	1	1
Clay	65	60	40	54	82	95	45
Calcite/Dolomite	1	Tr	3	3	1	Tr	Tr
Accessory Minerals: Opaques, Glauconite, Zircon & Zeolites?	1	Tr	Tr	1	Tr	Tr	Tr
Foraminifers	Tr	Tr	2	Tr	–	1	10
Nannofossils	32	40	15	3	2	2	40
Fish Remains	–	Tr	–	–	Tr	–	–

PHYSICAL PROPERTIES DATA:

	1,30	1,95	1,103	2,83
V_p (c)	–	–	1.52	1.65
ρ_b	–	–	1.84	1.85
T_c	2.83	3.10	–	–

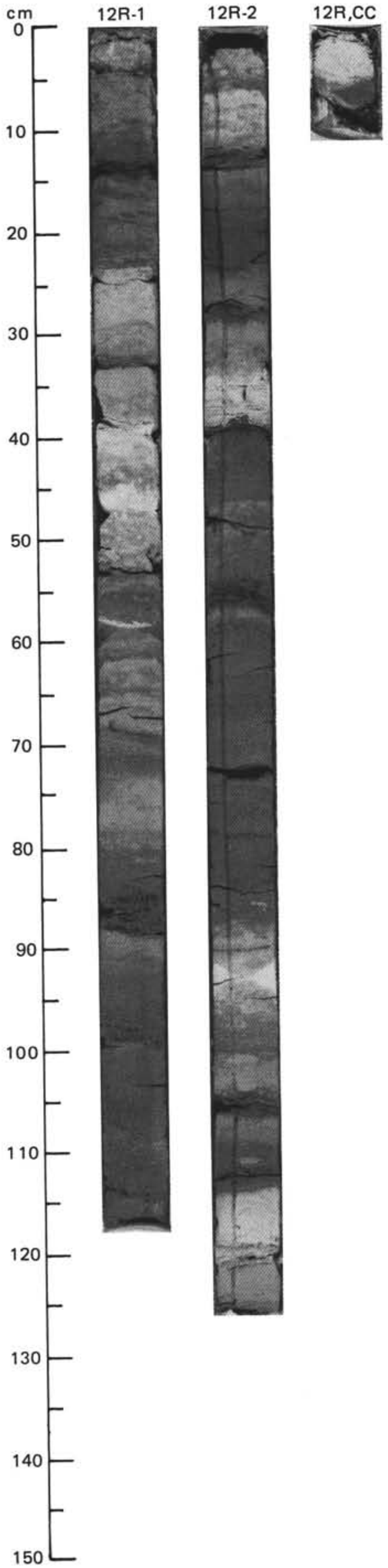
cm
0
10
20
30
40
50
60
70
80
90
100
110
120
130
140
150
12R-1
12R-2
12R,CC

SITE 637 HOLE A CORE 13 R CORED INTERVAL 5422.9-5432.5 mbsl; 112.4-122.0 mbsf

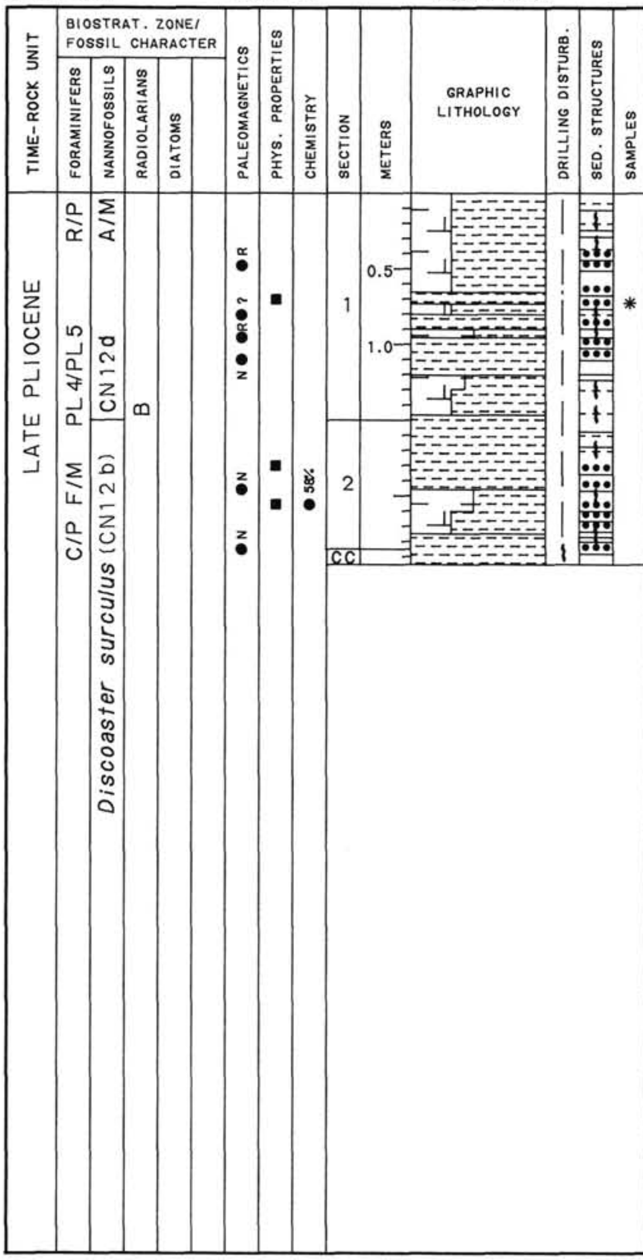

LITHOLOGIC DESCRIPTION

TURBIDITES, CALCAREOUS CLAYS AND MARLS.

This core consists dominantly of turbidites that grade from thin, very dark gray to gray (5Y3/1-4/1) silts and silty clays at the base to gray (5Y5/1) clays that are bioturbated in their upper parts. Bioturbated, light gray (5Y6/1-7/1), grayish brown (2.5Y5/2) and olive gray (5GY5/2) calcareous clays and marls often overlie the clays at the top of the turbidites. Usually bioturbation has mixed the marls with the underlying clays and blurred the depositional contacts, hence the origin of the calcareous units is not entirely clear. Diffuse manganese-rich laminae and blebs occur in Section 1 at 15-17 cm, 54-55 cm, 124 cm, and 135-140 cm.

SMEAR SLIDE SUMMARY (%):

	1,74
	M
TEXTURE:	
Clay	100
COMPOSITION:	
Clay	8
Calcite/Dolomite	Tr
Accessory Minerals	Tr
Foraminifers	2
Nannofossils	90

PHYSICAL PROPERTIES DATA:

	1,70	2,30	2,52
V_p (c)	–	–	1.18
ρ_b	–	–	1.76
T_c	3.24	3.06	–

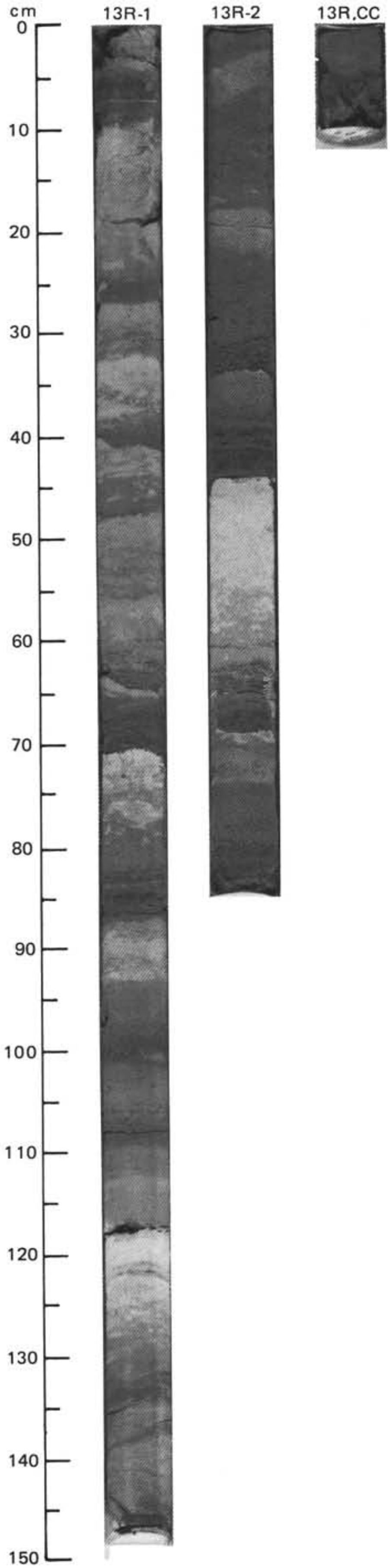
cm
0
10
20
30
40
50
60
70
80
90
100
110
120
130
140
150
13R-1
13R-2
13R,CC

SITE 637 HOLE A CORE 14 R CORED INTERVAL 5432.5-5442.2 mbsl; 122.0-131.7 mbsf

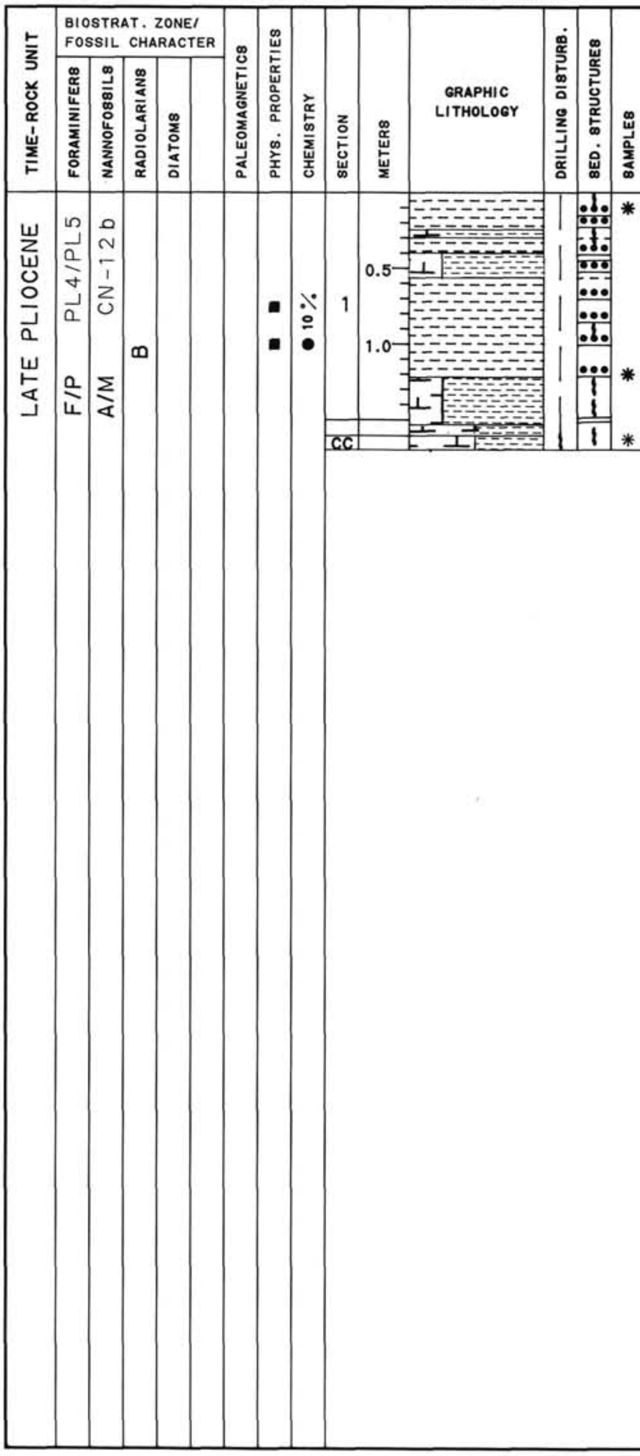

LITHOLOGIC DESCRIPTION

TURBIDITES, CALCAREOUS CLAYS, and MARLS

This core consists dominantly of turbidites that grade from very thin, dark gray to gray (5Y4/1-5/1) silts and silty clays at the base to gray and olive gray (5Y5/1-5/2) clays that are bioturbated in their upper parts. Bioturbated, light gray and light olive gray (5Y6/2-7/2) calcareous clays and marls overlie some of clays at the top of the turbidites. Bioturbation has mixed the marls with the underlying clays and blurred the depositional contacts, hence the origin of the minor calcareous units is not entirely clear.

SMEAR SLIDE SUMMARY (%):

	1,5 D	1,118 D	CC D
TEXTURE:			
Silt	3	10	25
Clay	97	90	75
COMPOSITION:			
Quartz	Tr	4	20
Feldspar	–	–	2
Mica	1	1	–
Clay	36	71	30
Calcite/Dolomite	1	3	–
Accessory Minerals (Zeolites?, Opaques, Glauconite, Hematite, & Magnetite)	1	1	3
Foraminifers	1	Tr	–
Nannofossils	60	20	45
Fish Remains	–	–	Tr

PHYSICAL PROPERTIES DATA:

	1,75	1,101
$V\rho$ (c)	–	1.58
ρ_b	–	1.88
T_c	2.90	–

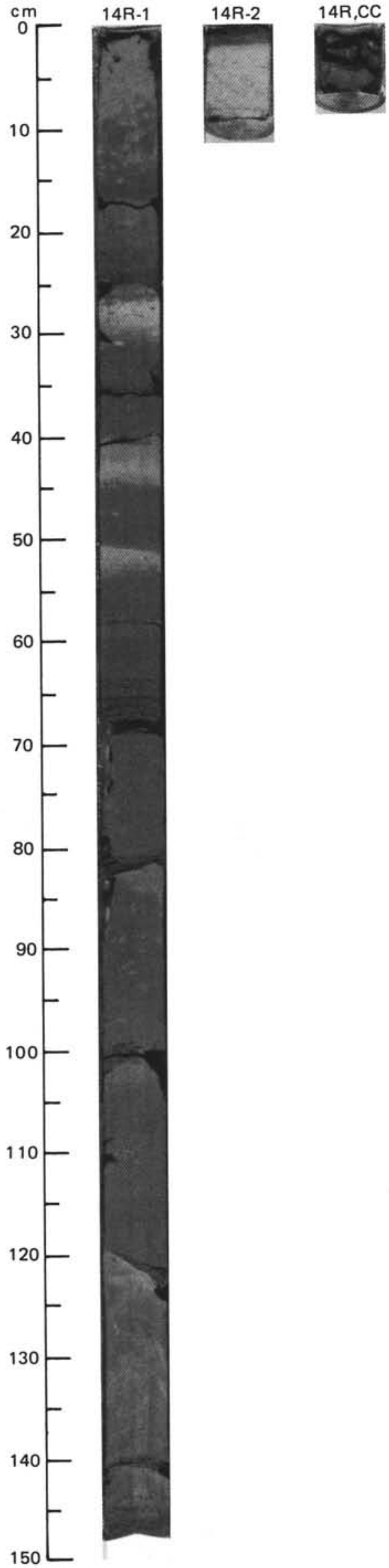
cm
0
10
20
30
40
50
60
70
80
90
100
110
120
130
140
150
14R-1
14R-2
14R,CC

SITE 637 HOLE A CORE 15 R CORED INTERVAL 5442.2-5451.8 mbsl; 131.7-141.3 mbsf

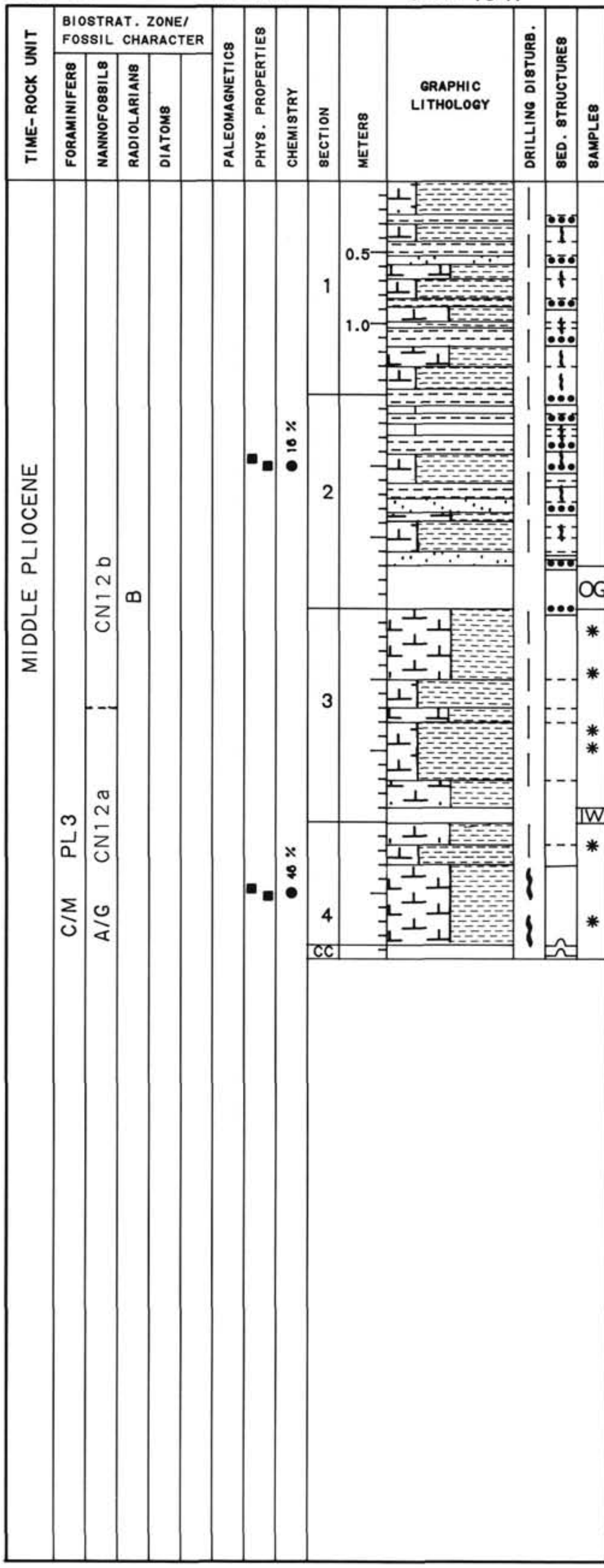

LITHOLOGIC DESCRIPTION

TURBIDITES, CALCAREOUS CLAYS, and CALCAREOUS SLUMPS.

Section 1 through Section 3, 3 cm of this core consists dominantly of turbidites with sharp bases that grade from very thin, very dark gray to dark gray (5Y3/1-4/1) silts and silty clays at the base to olive gray (5Y4/2-5/2) clays that are bioturbated in their upper parts. Bioturbated, olive gray to light olive gray (5Y5/6-6/2) calcareous clays and marls overlie the clays at the top of the turbidites. Bioturbation has mixed the marls with the underlying clays and blurred the depositional contacts, hence the origin of the calcareous units is not entirely clear. The turbidite-marl sequences average about 25 cm in thickness. A Zoophycus type burrow occurs in Section 1, 102-107 cm.

Section 3, 3 cm through the CC consist of contorted, convoluted, and swirled light gray (5Y7/1-7/2) and white (5Y8/1) marls and olive gray to light olive gray (5Y4/2-6/2) calcareous clays. We interpret these calcareous clays and marls to be slumped material.

SMEAR SLIDE SUMMARY (%):

	3,15 M	3,43 D	3,83 M	3,99 M	4,20 M	4,72 D
TEXTURE:						
Silt	5	5	5	2	10	–
Clay	95	95	95	98	90	100
COMPOSITION:						
Quartz	1	2	3	1	6	–
Feldspar	–	–	Tr	–	–	–
Mica	Tr	–	3	–	–	–
Clay	60	7	12	60	28	30
Calcite/Dolomite	1	Tr	–	4	–	–
Accessory Minerals (Iron Oxides, Glauconite, Apatite?) (Pyrite)	8	1	Tr	Tr	Tr	–
Foraminifers	Tr	1	–	1	2	–
Nannofossils	30	89	78	34	64	30
Fish Remains	–	–	Tr	–	Tr	–
Micrite	–	–	4	–	–	40

PHYSICAL PROPERTIES DATA:

	2,50	2,51	4,50	4,51
V_p (c)	–	1.58	–	1.56
ρ_b	–	1.88	–	1.88
T_c	3.10	–	3.07	–

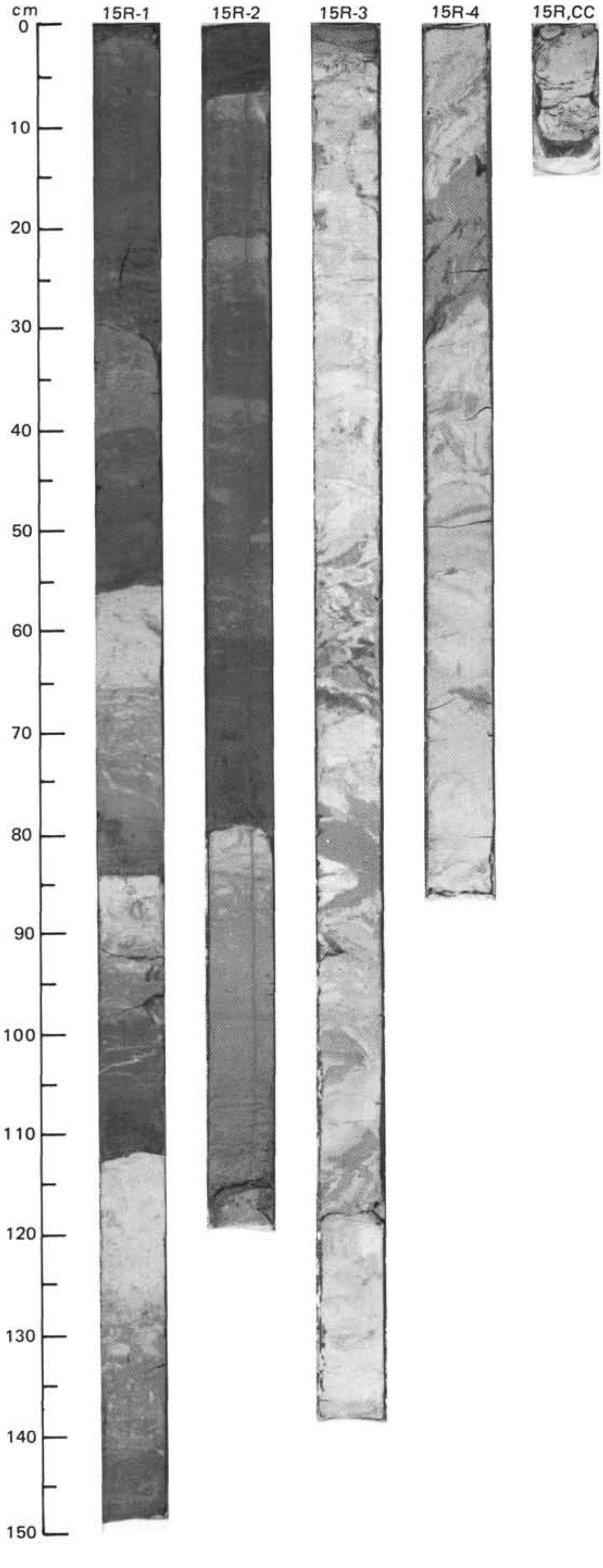
cm
0
10
20
30
40
50
60
70
80
90
100
110
120
130
140
150
15R-1
15R-2
15R-3
15R-4
15R,CC

SITE 637 HOLE A CORE 16 R CORED INTERVAL 5451.8-5461.5 mbsl; 141.3-151.0 mbsf

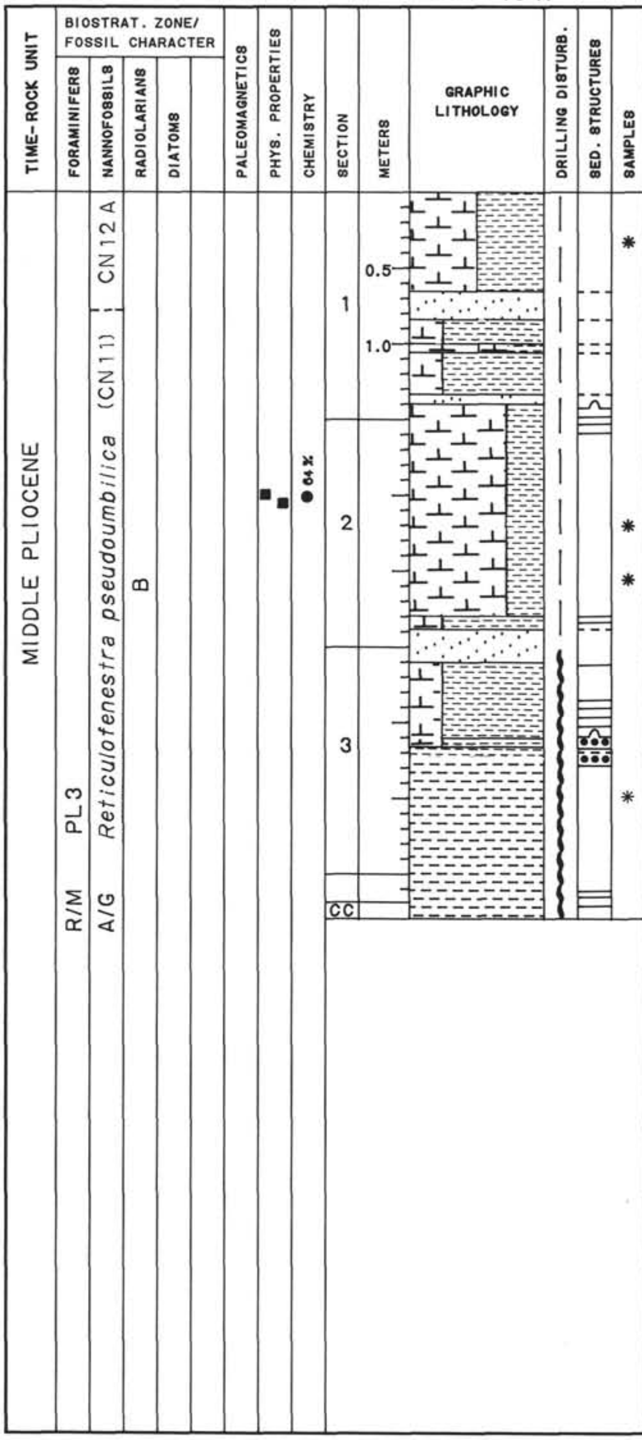

LITHOLOGIC DESCRIPTION

MARL, CLAY and CALCAREOUS CLAY.

Section 1, 0-140 cm and Section 2, 135 cm through the CC consist of contorted, convoluted, and swirled olive gray (5Y5/2) and light gray (5Y5/1-2.5Y7/2) calcareous clays, gray (5Y5/1) and brown (10YR5/3) clays, and olive gray (5Y5/2) to dark gray (5Y4/1-5/1) silty clays. We interpret these as slumped material. Below Section 3, 70 cm, this material consists of slurry very deformed by drilling.

Section 1, 140 cm through Section 2, 135 cm consist of light gray to white (5Y7/2-5Y8/1), slightly mottled marl.

SMEAR SLIDE SUMMARY (%):

	1,35	2,68	3,109
	D	D	D
TEXTURE:			
Silt	20	1	5
Clay	80	99	95
COMPOSITION:			
Quartz	15	Tr	Tr
Feldspar	–	–	Tr
Mica	2	Tr	Tr
Clay	30	10	64
Calcite,Dolomite	2	2	–
Accessory Minerals (Glauconite, Opaques, Zeolite, Zircon, Rutile Needles?)	1	Tr	Tr
Foraminifers	–	Tr	–
Nannofossils	50	88	35
Fish Remains	–	–	Tr

PHYSICAL PROPERTIES DATA:

	2,50	2,52
V_p (c)	–	1.43
ρ_b	–	1.80
T_c	2.86	–

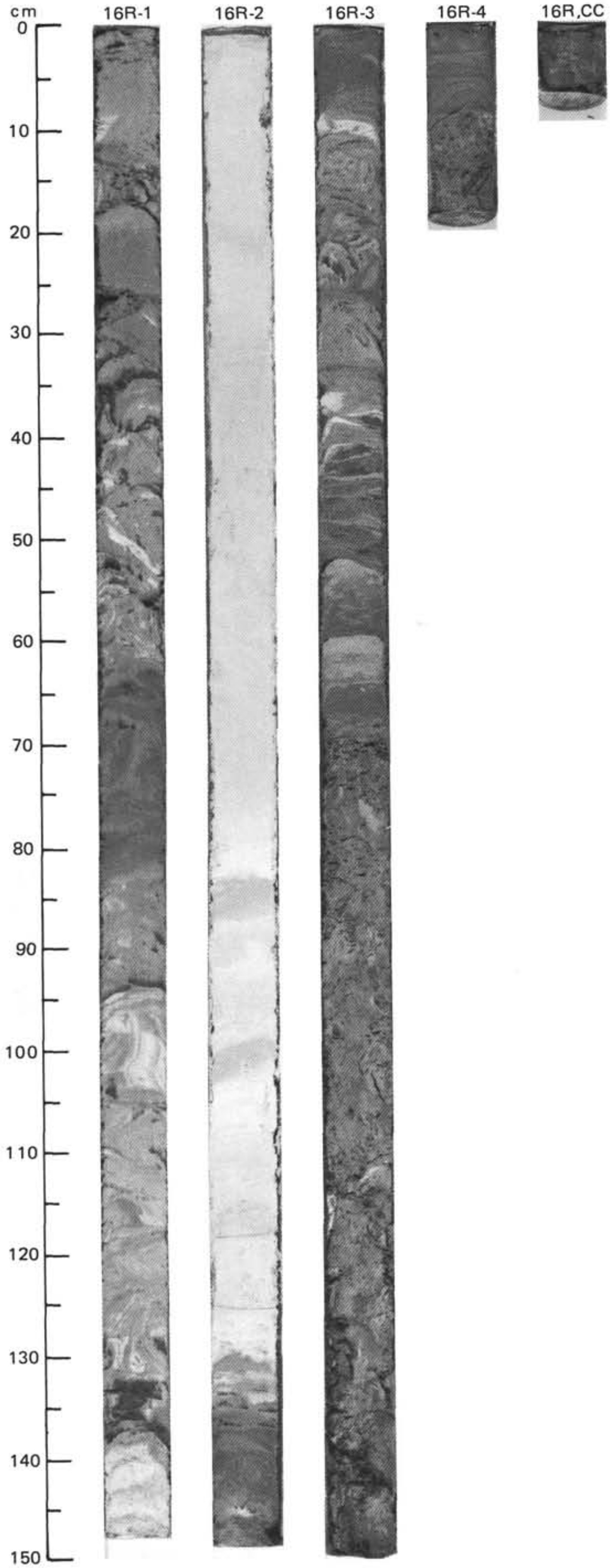
cm
0
10
20
30
40
50
60
70
80
90
100
110
120
130
140
150
16R-1
16R-2
16R-3
16R-4
16R,CC

SITE 637 HOLE A CORE 17 R CORED INTERVAL 5461.5-5471.2 mbsl; 151.0-160.7 mbsf

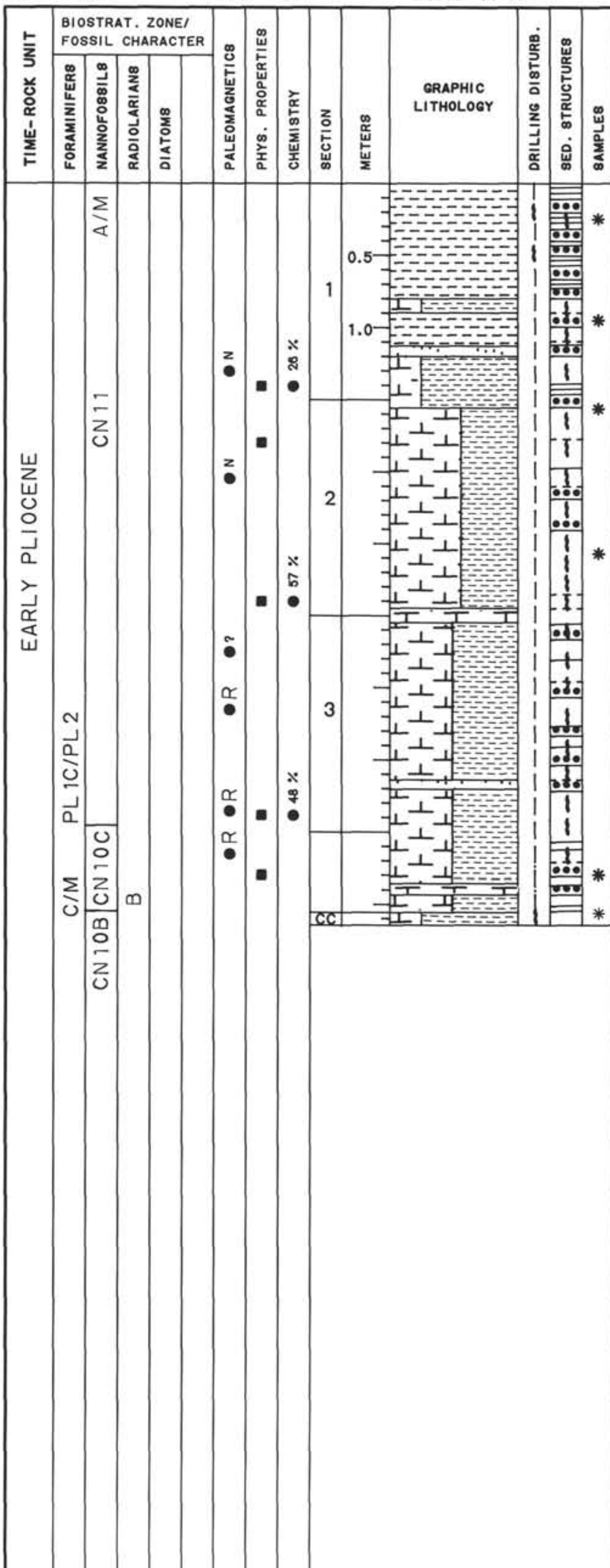

LITHOLOGIC DESCRIPTION

CLAYS, CALCAREOUS CLAYS, and MARLS.

Section 1 through Section 2, 6 cm of this core consists of turbidites interbedded with minor calcareous clays. The turbidites range from approximately 15-20 cm in thickness; they grade from structureless or faintly laminated, dark gray (5Y4/1) silt upward to bioturbated, gray (5Y5/1) and olive gray (5Y5/2) clays. Most of the silts at the base of the turbidite layers have been highly deformed by drilling. The calcareous clays, found at the top of the more complete turbidite sequences, are bioturbated and light olive gray (5Y6/2).

Section 2, 6 cm through the CC contain bioturbated, light gray (5Y6/1, 5Y7/1-7/2), white (5Y8/1), and pale olive (5Y6/3) marls interbedded with grayish green (10GY5/2) silts and white (5Y8/1) foram sands. The foram sand layers overlain by marls may represent biogenic turbidites. Burrowing has not entirely homogenized the sediment, and distinct layering defined by color changes is clearly visible. Thin, manganese-rich horizons are present in Section 2 at 19, 35, 45, 52, 71, and 90 cm.

SMEAR SLIDE SUMMARY (%):

	1,30 D	1,93 D	2,5 D	2,110 D	4,27 D	CC D
TEXTURE:						
Sand	—	—	5	10	5	—
Silt	5	Tr	85	40	30	Tr
Clay	95	100	10	50	65	100
COMPOSITION:						
Quartz	1	Tr	50	5	20	Tr
Feldspar	—	—	Tr	—	—	—
Rock Fragments	—	—	Tr	—	—	—
Mica	Tr	—	5	—	Tr	Tr
Clay	85	90	30	10	25	40
Calcite/Dolomite	—	—	Tr	—	—	—
Accessory Minerals (Fe Oxides, Zircon, Opaques)	4	Tr	5	—	Tr	Tr
Foraminifers	—	—	Tr	5	10	—
Nannofossils	10	10	10	80	45	60
Fish Remains	—	—	—	—	Tr	—

PHYSICAL PROPERTIES DATA:

	1,139	2,30	2,139	3,139	4,30
V_p (c)	1.58	—	1.42	1.59	—
ρ_b	1.86	—	1.86	1.87	—
T_c	—	2.76	—	—	3.18

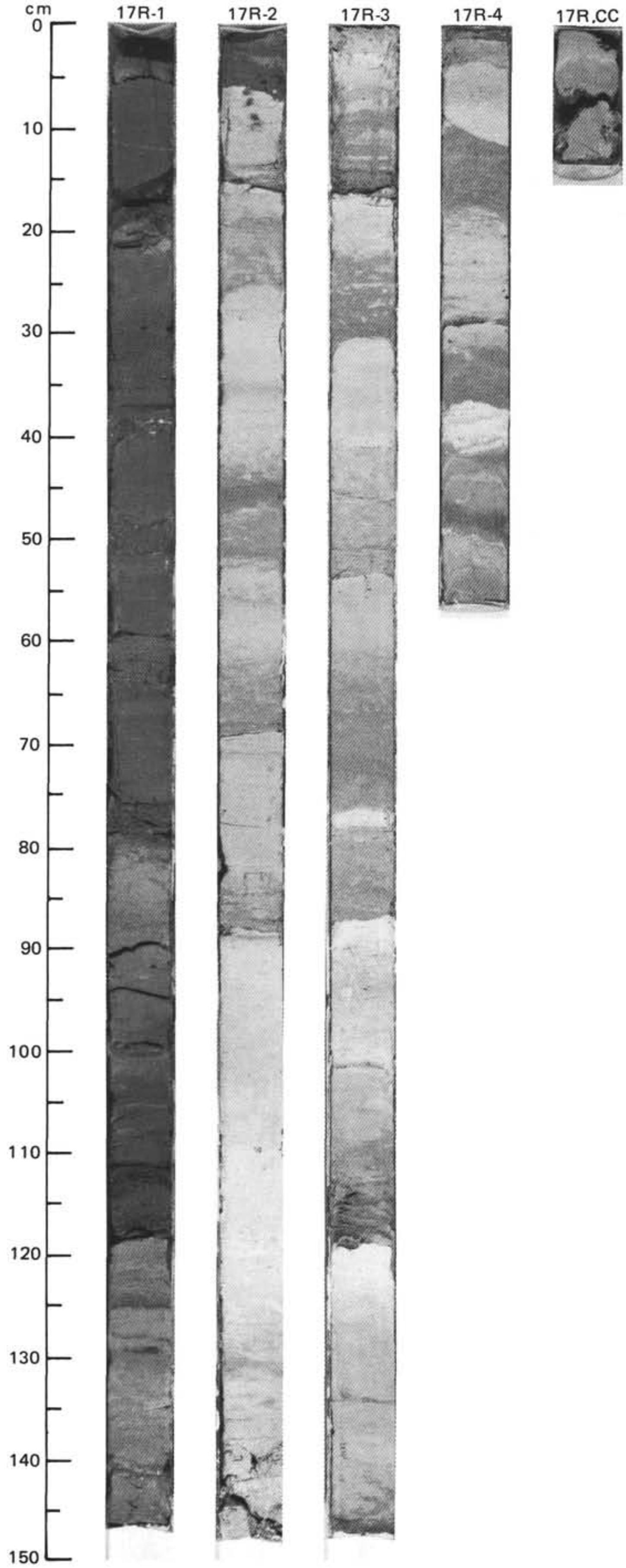
cm
0
10
20
30
40
50
60
70
80
90
100
110
120
130
140
150
17R-1
17R-2
17R-3
17R-4
17R,CC

SITE 637 HOLE A CORE 18 R CORED INTERVAL 5471.2-5480.9 MBSL; 160.7-170.4 mbsf

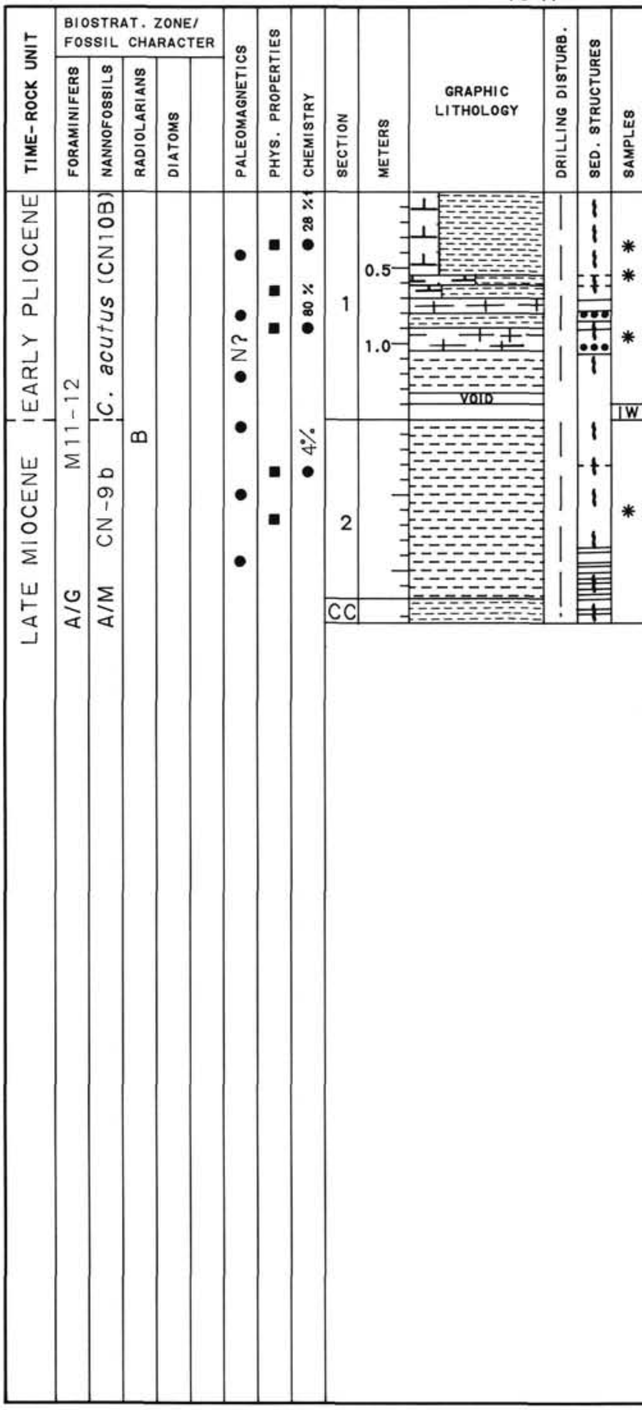

LITHOLOGIC DESCRIPTION

CLAYS, CALCAREOUS CLAYS, and MARLS.

This core consists dominantly of bioturbated, layered, varigated dark grayish brown (10YR4/2), brown (10YR5/3), pale brown (10YR6/3), and light yellowish brown (10YR6/4, 2.5Y6/4) clay that has been slightly disturbed by drilling. These clays are interbedded with white (5Y8/1) foraminiferal ooze layers, some of which grade upward into light gray (5Y6/1-7/1, 2.5Y7/2) marls and calcareous clays. These calcareous sediments may represent biogenic turbidites.

SMEAR SLIDE SUMMARY (%):

	1,34 D	1,57 M	1,96 D	2,62 D
TEXTURE:				
Sand	–	–	50	–
Silt	–	30	40	2
Clay	100	70	10	98
COMPOSITION:				
Quartz	–	10	Tr	1
Feldspar	–	5	–	1
Mica	Tr	–	–	Tr
Clay	90	30	–	92
Accessory Minerals (Opaques, Zircon)	Tr	–	–	Tr
Foraminifers	–	10	90	–
Nannofossils	10	40	10	6
Unspecified Carbonate (Foram debris?)	–	5	–	–

PHYSICAL PROPERTIES DATA:

	1,35	1,67	1,92	2,35	2,66
V_p (a)	1.59	–	–	1.30	–
V_p (b)	–	–	–	1.25	–
V_p (c)	–	–	1.29	1.52	–
ρ_b	1.89	–	1.76	1.90	–
Tc	–	2.77	–	–	2.51

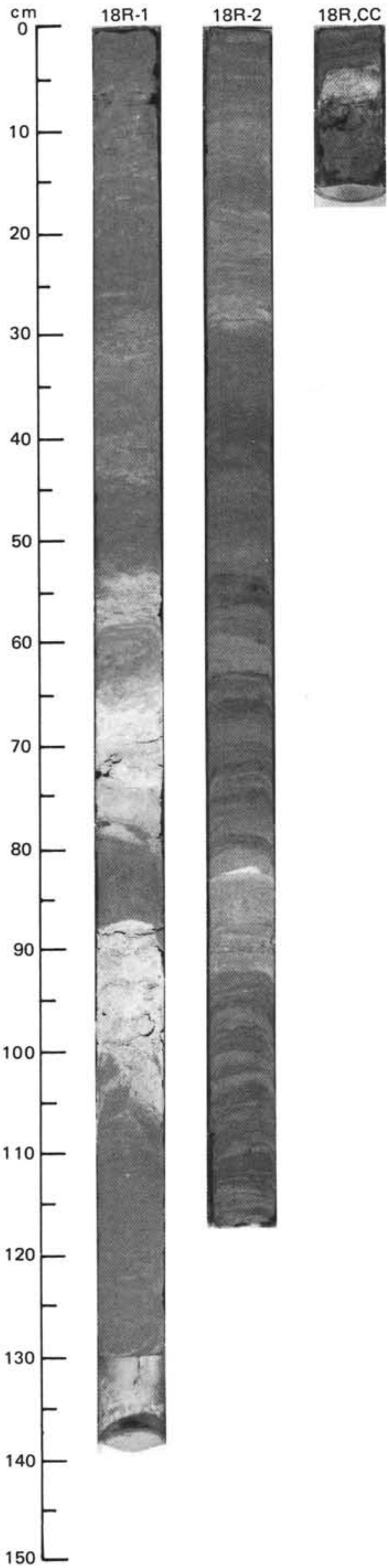
cm
0
10
20
30
40
50
60
70
80
90
100
110
120
130
140
150
18R-1
18R-2
18R,CC

SITE 637 HOLE A CORE 19 R CORED INTERVAL 5480.9-5490.4 mbsl; 170.4-179.9 mbsf

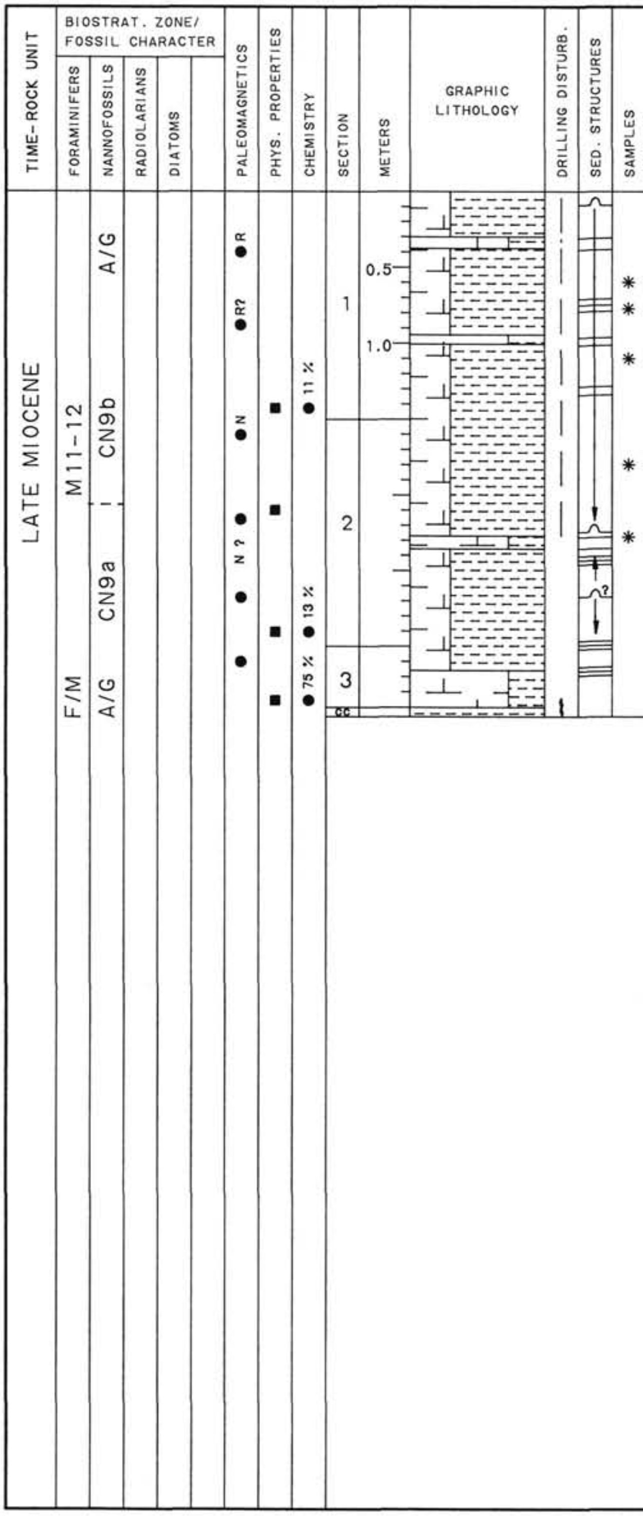

LITHOLOGIC DESCRIPTION

CALCAREOUS CLAYS and CLAYEY OOZES.

This core consists dominantly of contorted, convoluted and swirled, very dark gray (10YR3/1), dark gray (10YR4/1), pale brown 10YR6/3), and light yellowish brown (2.5Y6/3) calcareous clays. Faint bedding is present in the calcareous clays in Section 2. The calcareous clays are interbedded with layers of white (5Y8/1) clayey oozes, thin layers of black mangenese-rich clays, and minor lenses and layers of dark gray (5Y4/1) silt. We interpret the sediments recovered in this core to represent slump material.

SMEAR SLIDE SUMMARY (%):

	1,60 D	1,75 D	1,108 D	2,32 D	2,80 D
TEXTURE:					
Sand	20	–	–	Tr	–
Silt	40	10	10	30	10
Clay	40	90	90	70	90
COMPOSITION:					
Quartz	10	5	8	25	Tr
Feldspar	–	–	Tr	Tr	–
Mica	–	Tr	Tr	Tr	–
Clay	15	80	80	60	5
Calcite/Dolomite	35	–	–	Tr	–
Accessory Minerals (Opaques, Zircon, Glauconite)	Tr	10	1	3	Tr
Foraminifers	20	–	Tr	2	10
Nannofossils	20	5	10	10	85
Sponge Spicules	Tr	–	–	–	–
Fish Remains	–	–	–	Tr	–

PHYSICAL PROPERTIES DATA:

	1,141	2,57	2,141	3,35
$V\rho$ (a)	1.58	–	1.53	–
$V\rho$ (b)	1.26	–	1.44	–
$V\rho$ (c)	–	–	1.43	1.14
ρ_b	1.95	–	1.89	1.86
T_c	–	2.84	–	–

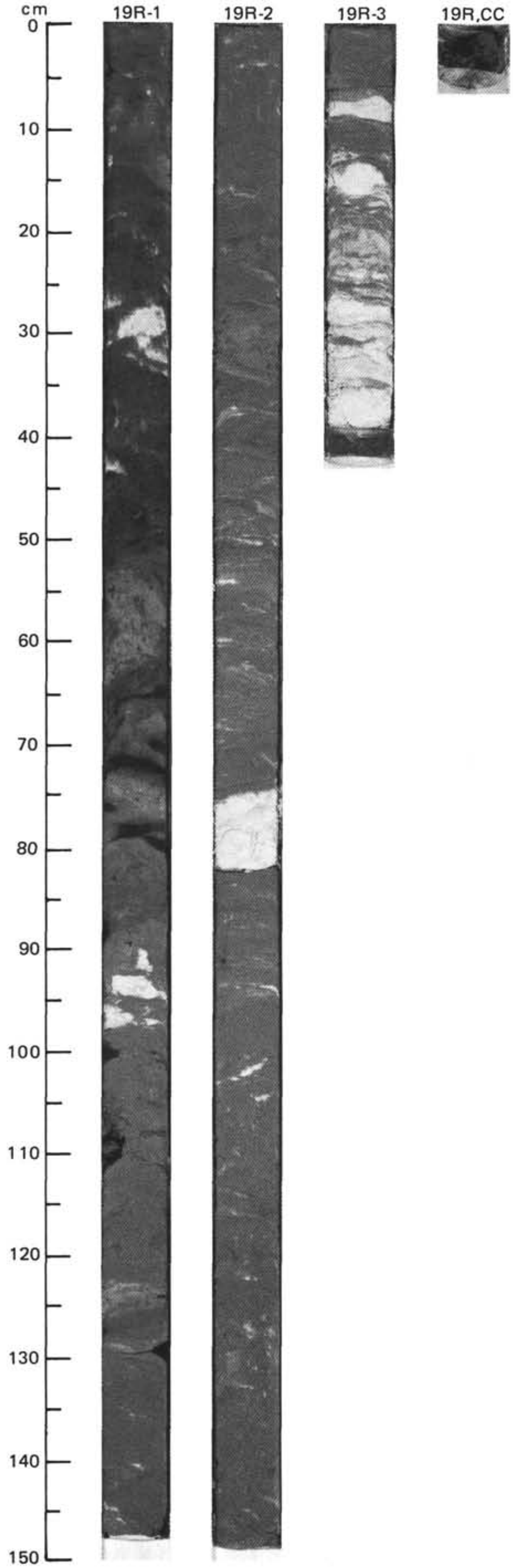
cm
0
10
20
30
40
50
60
70
80
90
100
110
120
130
140
150
19R-1
19R-2
19R-3
19R,CC

SITE 637 HOLE A CORE 20 R CORED INTERVAL 5490.4-5500.0 mbsl; 179.9-189.5 mbsf

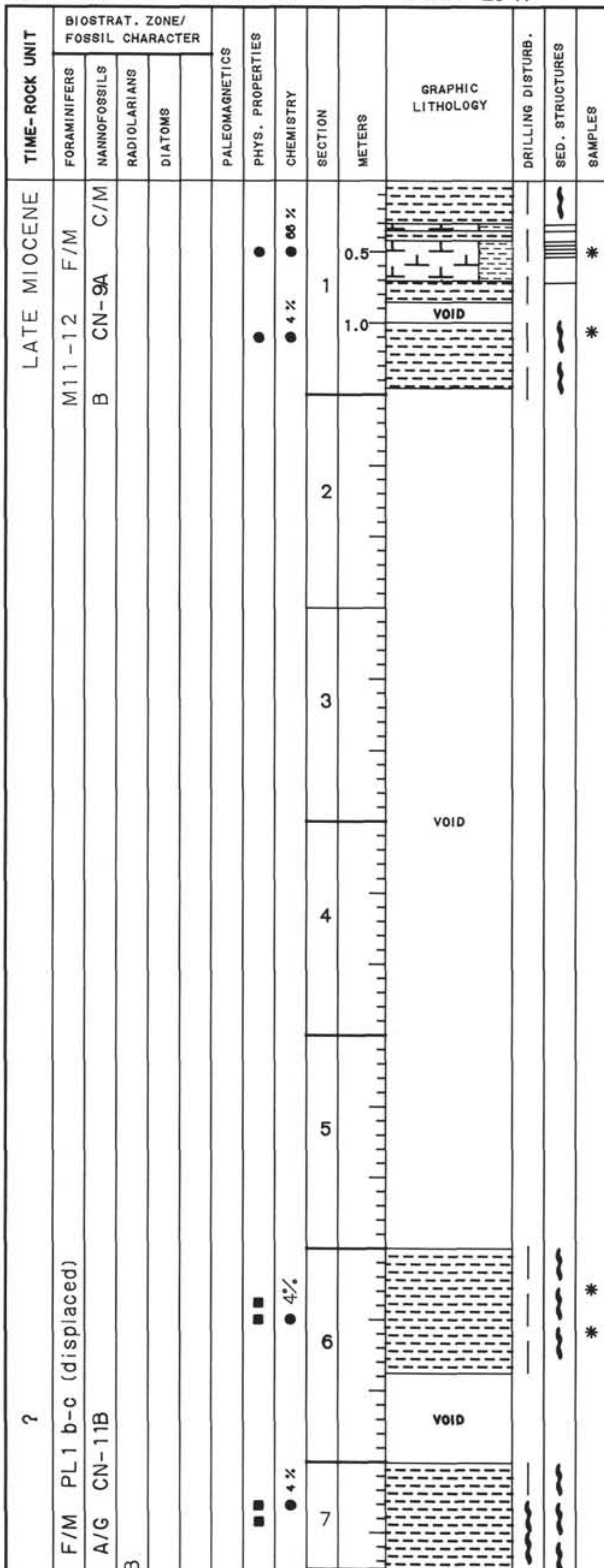

LITHOLOGIC DESCRIPTION

CLAY and CLAYEY OOZE.

This core consists dominantly of bioturbated and mottled, red (2.5YR4/2-5/2) clay in Sections 6, 7, CC and pale brown (10YR6/3), yellowish brown (10YR5/4), and dark grayish brown to grayish brown (2.5Y4/2-5/2) clay in Section 1. Mottles are light yellowish brown (10YR6/4). The clays contain dark specks which appear to be Mn-oxides coating detrital grains. The clays from the bottom portion of Section 7 and the CC are very deformed by drilling and include varigated white (5Y8/1), light yellowish brown (10YR6/4), and dark olive gray (5Y3/2) clays, interpreted to represent cavings from higher up in Hole 637A.

The clays in Section 1 contain interbedded white (5Y8/1) clayey oozes at 30-35 cm and 42-70 cm. The ooze at the top of the 42-70 cm interval includes irregular, fine laminae of yellowish brown (10YR5/4) clays.

A metamorphic (schist) pebble 1.5 cm in diameter occurs in Section 6, 78 cm.

SMEAR SLIDE SUMMARY (%):

	1,50 D	1,104 D	6,31 D	6,63 M
TEXTURE:				
Silt	40	10	10	30
Clay	60	90	90	70
COMPOSITION:				
Quartz	Tr	5	Tr	30
Mica	—	—	5	Tr
Clay	5	95	90	70
Accessory Minerals (Zeolites, Zircon)	—	Tr	5	Tr
Foraminifers	5	Tr	—	—
Nannofossils	90	Tr	—	Tr

PHYSICAL PROPERTIES DATA:

	1,51	1,111	6,40	6,40	7,31	7,40
V_p (a)	1.87	1,56	—	1.49	1.58	—
V_p (b)	—	1.39	—	1.17	1.15	—
V_p (c)	4.71	1.10	—	.55	1.60	—
ρ_b	1.99	1.85	—	1.94	1.94	—
T_c	—	—	2.89	—	—	2.34

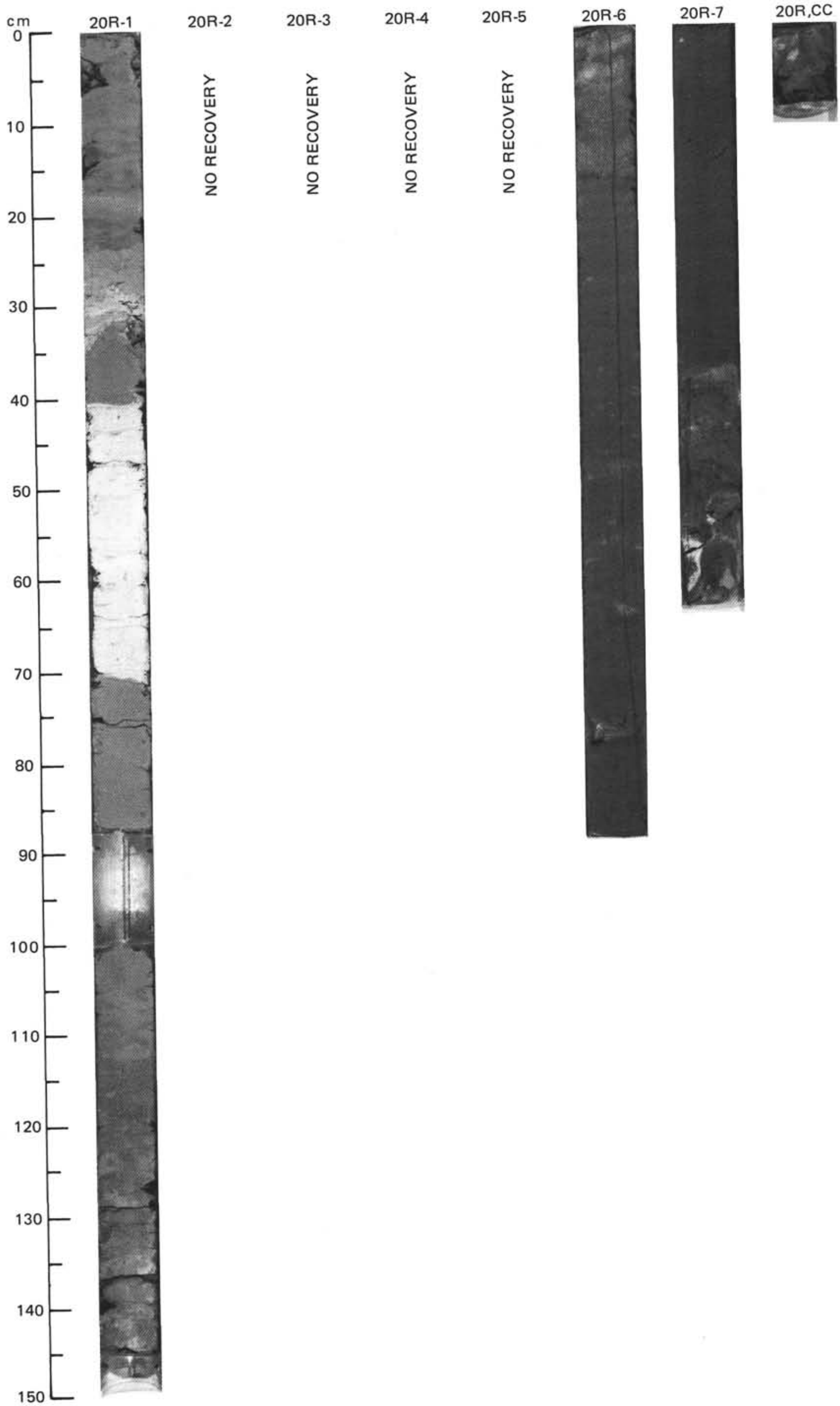
cm
0
10
20
30
40
50
60
70
80
90
100
110
120
130
140
150
20R-1
20R-2
NO RECOVERY
20R-3
NO RECOVERY
20R-4
NO RECOVERY
20R-5
NO RECOVERY
20R-6
20R-7
20R,CC

SITE 637 HOLE A CORE 21 R CORED INTERVAL 5500.0–5509.7 mbsl; 189.5–199.2 mbsf

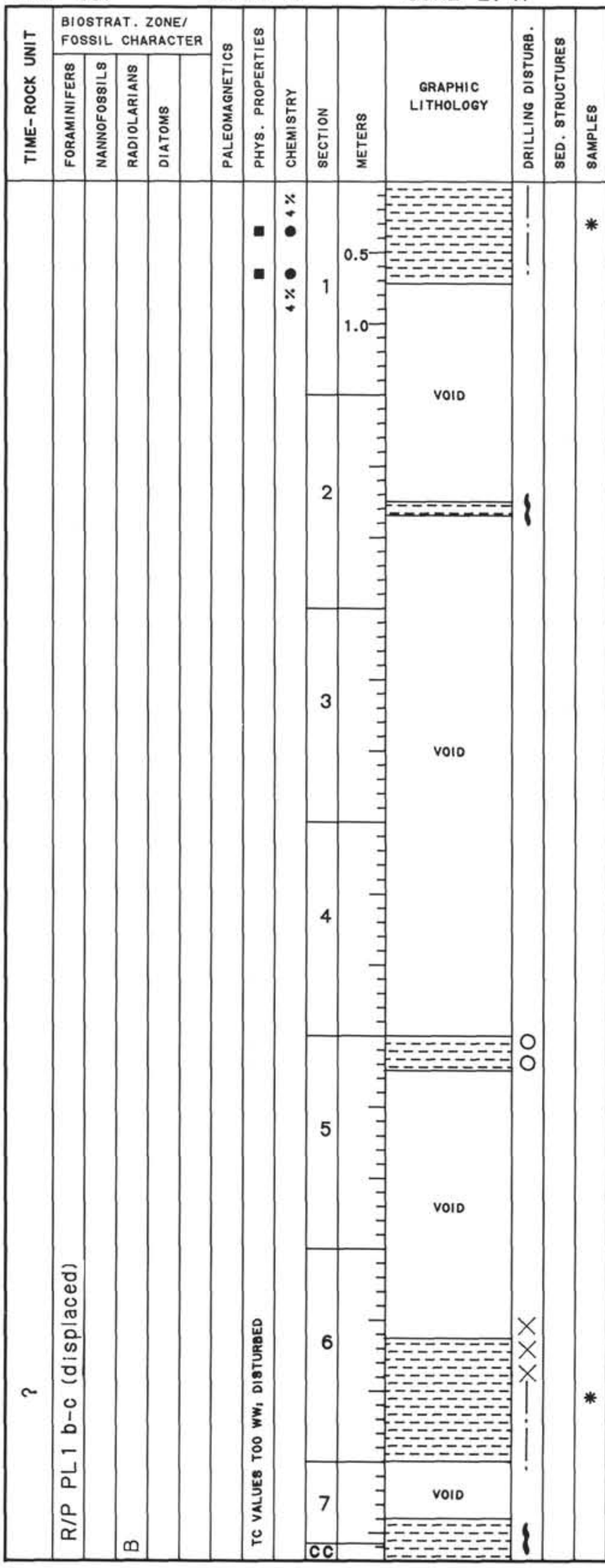

LITHOLOGIC DESCRIPTION

CLAY.

This core consists entirely of olive brown (2.5Y4/4) and reddish brown (2.5YR4/4, 5YR5/3) clay mottled with black specks. Where drilling has least disturbed these clays, they are very firm. The clays in Section 1 and Section 6 contain clasts of reddish, greenish, and white clay and dark manganese-stained(?) patches that may be interpreted to be deeply-altered breccia layers.

SMEAR SLIDE SUMMARY (%):

	1,32	6,106
	D	D
TEXTURE:		
Silt	–	6
Clay	100	94
COMPOSITION:		
Quartz	Tr	4
Mica	–	1
Clay	100	95
Accessory Minerals (Zeolite, Opaques, Fe Oxides)	Tr	Tr
Nannofossils	Tr	Tr

PHYSICAL PROPERTIES DATA:

	1,36	1,66
V_p (a)	–	1.70
V_p (b)	–	1.74
V_p (c)	1.67	2.23
ρ_b	1.52	1.60

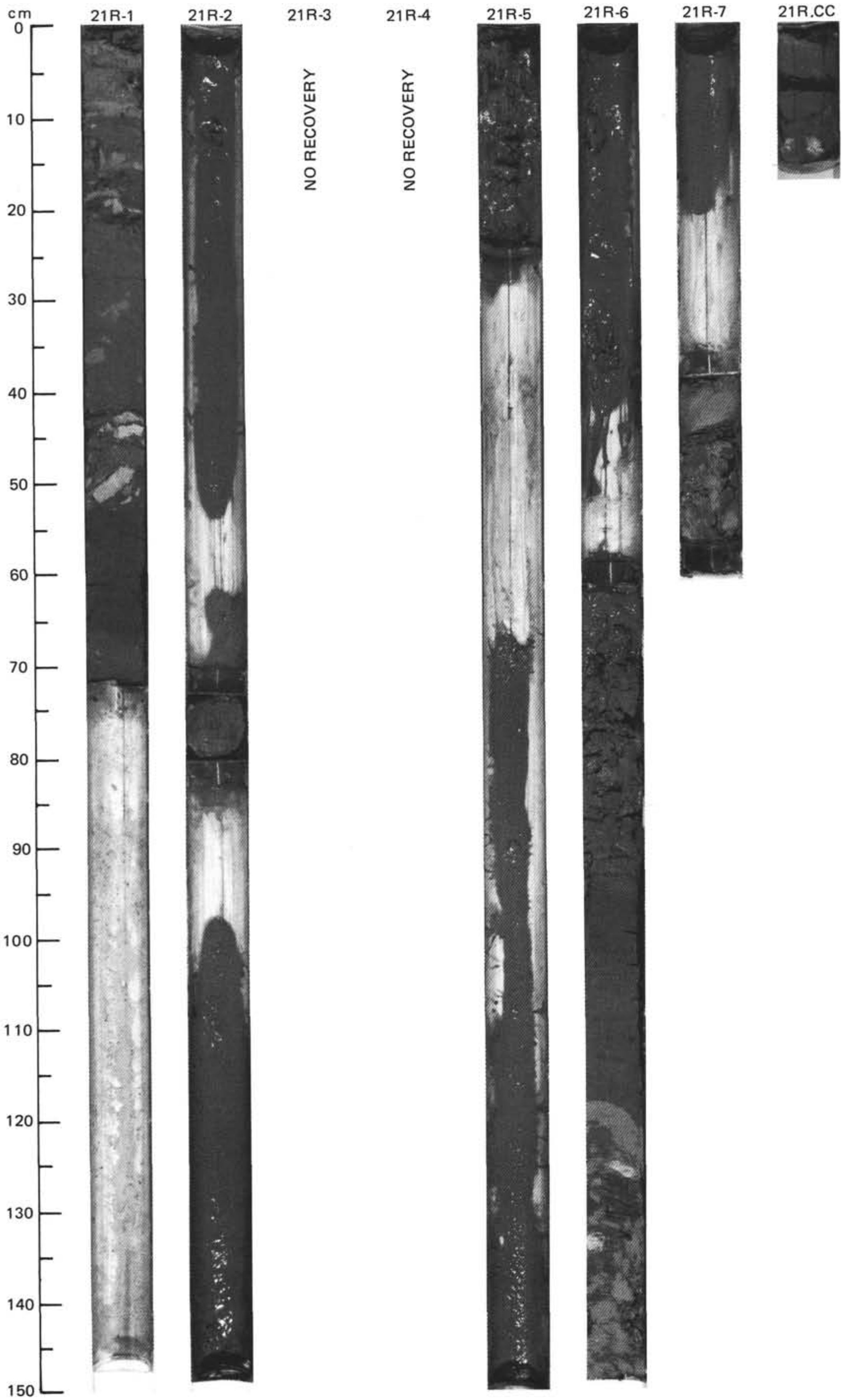
cm
0
10
20
30
40
50
60
70
80
90
100
110
120
130
140
150
21R-1
21R-2
21R-3
21R-4
21R-5
21R-6
21R-7
21R,CC
NO RECOVERY
NO RECOVERY

SITE 637 HOLE A CORE 22 R CORED INTERVAL 5509.7-5519.3 mbsl; 199.2-208.8 mbsf

TIME-ROCK UNIT	FORAMINIFERS	NANNOFOSSILS	RADIOLARIANS	DIATOMS	PALEOMAGNETICS	PHYS. PROPERTIES	CHEMISTRY	SECTION	METERS	GRAPHIC LITHOLOGY	DRILLING DISTURB.	SED. STRUCTURES	SAMPLES
?	PL1b-c (displaced)	B	B			■ ■	● 4%	1 2 3 4 5 6	0.5 1.0	VOID			* * *
	R/M							7 CC					*

LITHOLOGIC DESCRIPTION

CLAY.

This core consists entirely of moderately to very deformed, mottled, reddish brown (5YR4/4-5/4), brown (7.5YR5/4, 10YR5/3), and dark grayish brown (10YR4/2) clay with black specks. Least disturbed portion of core in Section 1, 50-95 cm exhibits faint banding. Small patches of quartz-rich silt occur in Section 1, 107 cm and Section 2, 38 cm.

SMEAR SLIDE SUMMARY (%):

	1,78 D	1,107 M	1,125 D	CC D
TEXTURE:				
Sand	–	20	–	1
Silt	8	80	2	7
Clay	92	Tr	98	92
COMPOSITION:				
Quartz	1	67	1	Tr
Feldspar	–	30	–	Tr
Rock Fragments	–	–	–	Tr
Mica	6	Tr	Tr	1
Clay	92	–	95	90
Calcite/Dolomite	–	1	4	5
Accessory Minerals (Opaques, Hematite, Epidote, Zircon)	1	2	Tr	3
Nannofossils	–	Tr	–	–

PHYSICAL PROPERTIES DATA:

	2,40	2,53
$V\rho$ (a)	–	1.84
$V\rho$ (b)	–	1.79
$V\rho$ (c)	–	1.80
ρ_b	–	1.74
T_c	2.38	–

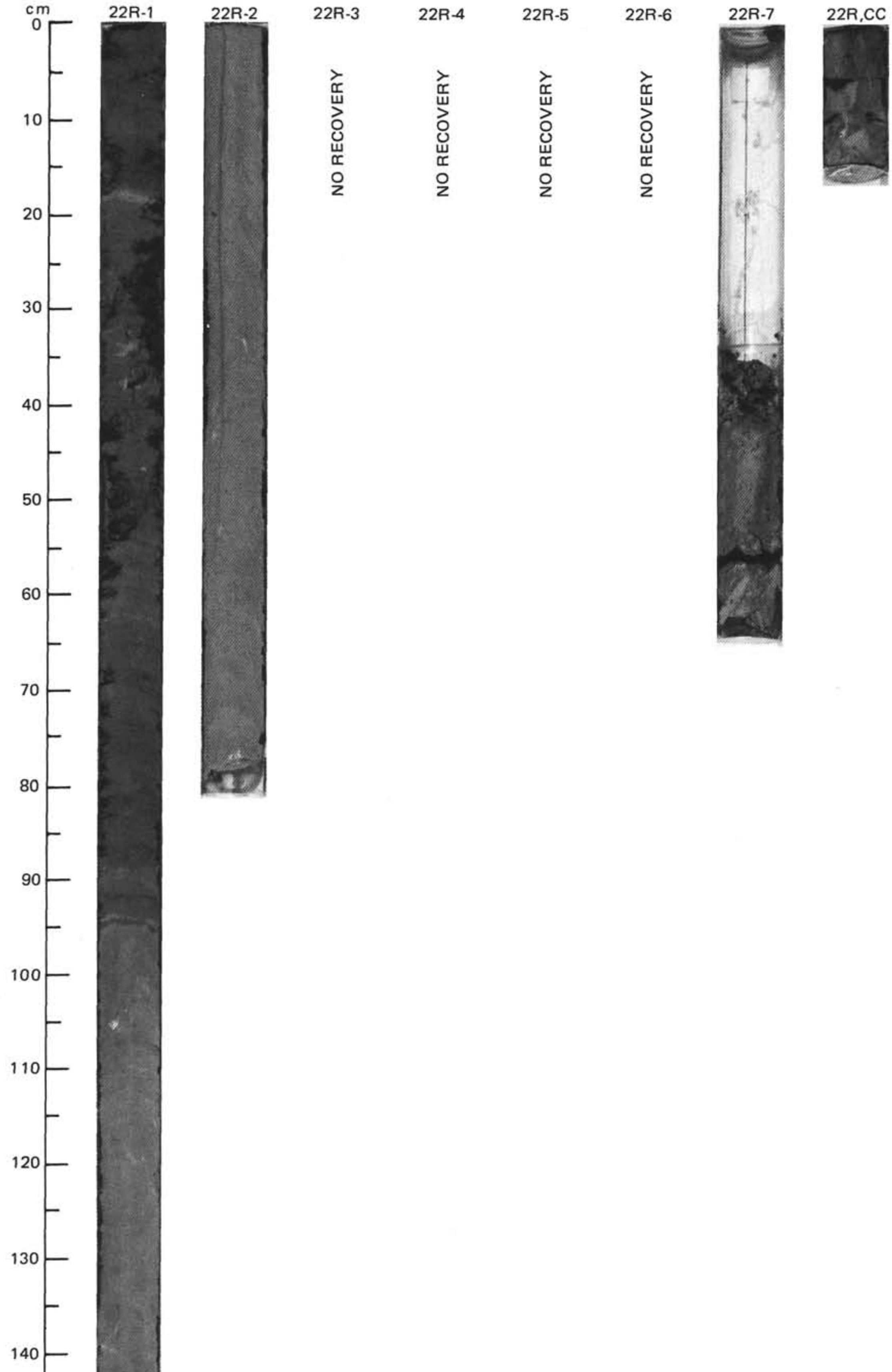
cm
0
10
20
30
40
50
60
70
80
90
100
110
120
130
140
150
22R-1
22R-2
22R-3
22R-4
22R-5
22R-6
22R-7
22R,CC
NO RECOVERY
NO RECOVERY
NO RECOVERY
NO RECOVERY

SITE 637 HOLE A CORE 23 R CORED INTERVAL 5519.3-5528.9 mbsl; 208.8-218.4 mbsf

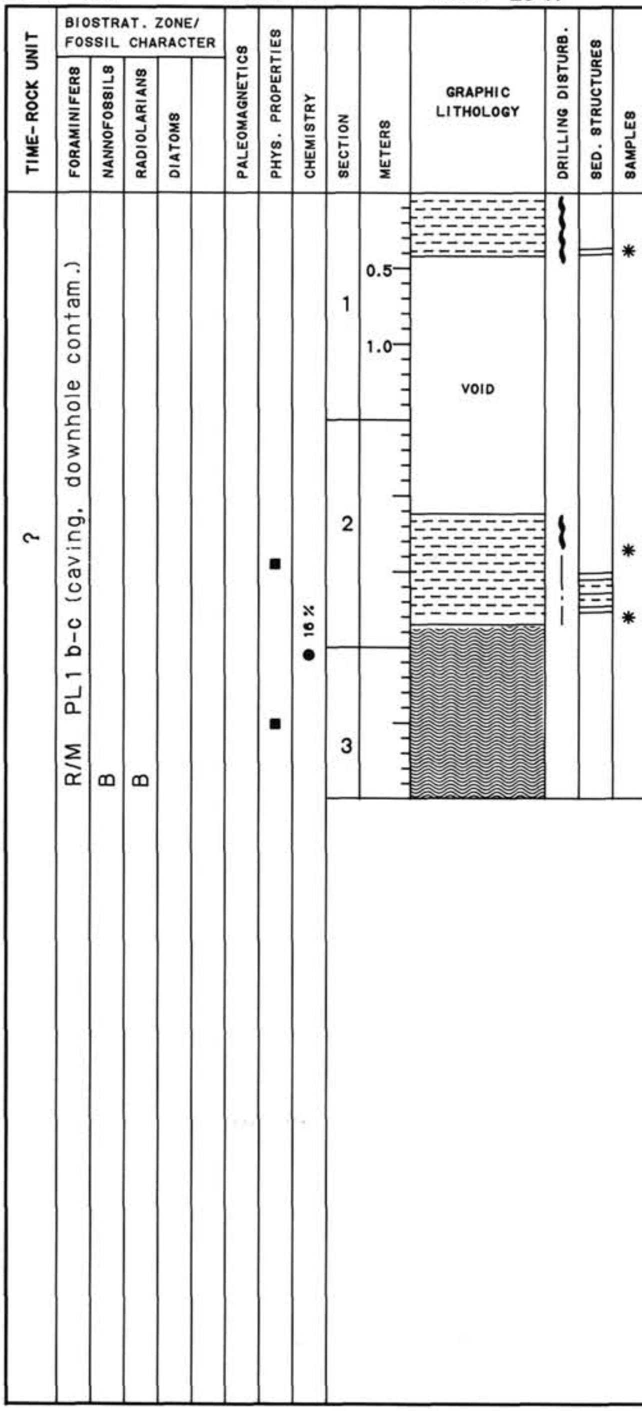

LITHOLOGIC DESCRIPTION

CLAY overlying PERIDOTITE.

The sedimentary section of the core, recovered in Section 1 through Section 2, 133 cm, consists of moderately to very deformed, pale brown (10YR6/3) and light reddish brown (5YR6/4) hematite-stained(?) clay that grades down into yellowish brown (10YR5/8) limonite-stained(?) clay at Section 2, 120 cm.

The clay/peridotite basement contact was recovered at Section 2, 133 cm, 211.63 m below the seafloor. However, based on drilling rate of penetration records, we estimate the actual depth of the contact to be at 215 m below seafloor, further down in the cored interval.

SMEAR SLIDE SUMMARY (%):

	1,38	2,81	2,127
	M	D	M
TEXTURE:			
Silt	12	6	20
Clay	88	94	80
COMPOSITION:			
Mica	1	Tr	Tr
Clay	88	94	53
Calcite/Dolomite	4	5	2
Accessory Minerals (Fe-Oxide, Limonite, Hematite, Spinel, Pyroxene, Opaque Minerals)	7	1	35

PHYSICAL PROPERTIES DATA:

	2,93	3,47
V_p (a)	–	3.56
V_p (b)	–	3.85
V_p (c)	–	3.66
ρ_b	–	2.53
T_c	2.00	–

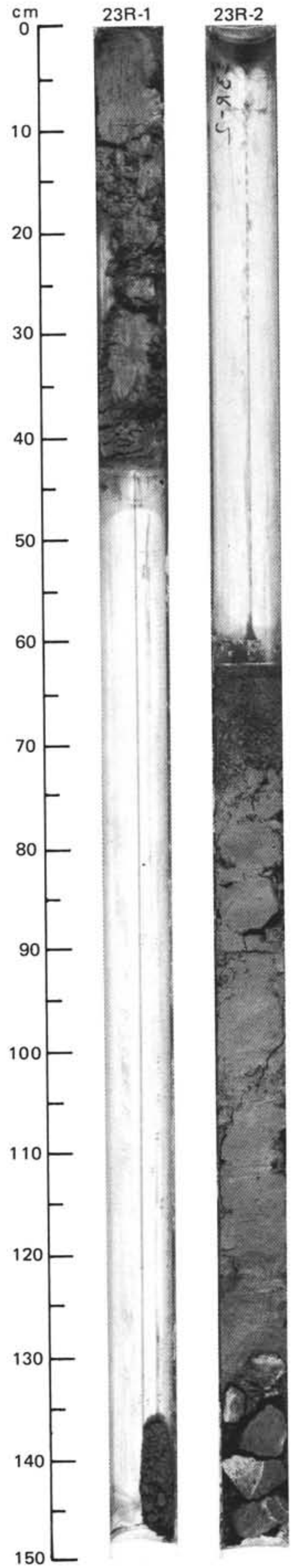
cm
23R-1
23R-2
0
10
20
30
40
50
60
70
80
90
100
110
120
130
140
150

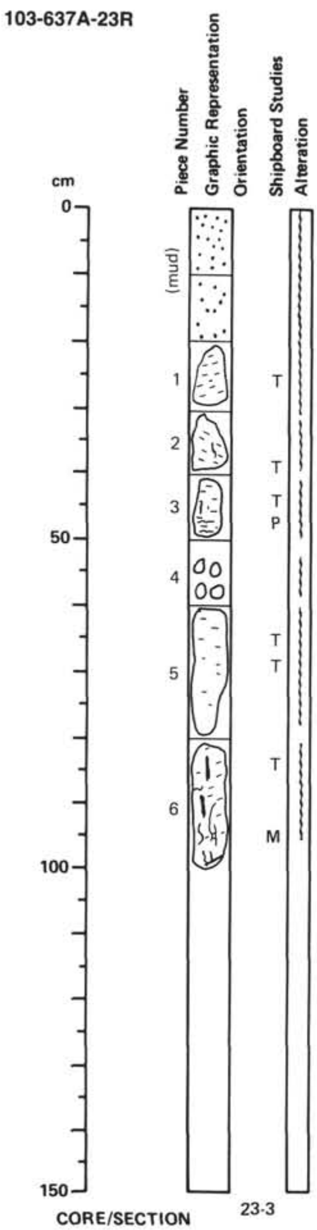

5519.3–5528.9 mbsl 208.4–218.4 mbsf

SERPENTINIZED PORPHYROCLASTIC HARZBURGITE

Basement rock was recovered at the bottom of this core in Section 637A-23R-3, which includes 20 cm of yellow-red mud overlying about 80 cm of extremely altered foliated harzburgite. The rock grades from a very leached yellow rock with elongated dissolution cavities along the foliation (at an angle of 30°) to a more massive, srongly foliated green-gray peridotite. The rock is almost completely serpentinized and extensively replaced by calcite (> 75% in the top few cm); vertical calcite veins are abundant near the bottom of the core, and calcite rims and replaces the pyroxene porphyroclasts. The freshest samples (637A-23R-3R, 37–40 cm and 46–48 cm) have a few relict mineral fragments (orthopyroxene, clinopyroxene, chromite). The rocks are 75–80% olivine, 10–15% orthopyroxene, 0–5% clinopyroxene and 1–2% chromium spinel.

Thin Section Description

637A-23R-3, 37–40 cm: Porphyroclastic, altered peridotite with approximately 80% olivine almost totally transformed into secondary serpentine, 10% orthopyroxene, 5% clinopyroxene, and 1% chromium spinel. The rock is completely serpentinized and replaced by calcite. However, elongate orthopyroxene pseudomorphs are recognizable. A few unaltered fragments of clinopyroxene are seen. The rock is pervasively dissected by calcite veinlets (< .5 mm thick) which are subparallel to the foliation.

	1, 47 (#3)
$V_p(a)$	3.56
$V_p(b)$	3.85
$V_p(c)$	3.66
ρb	2.53

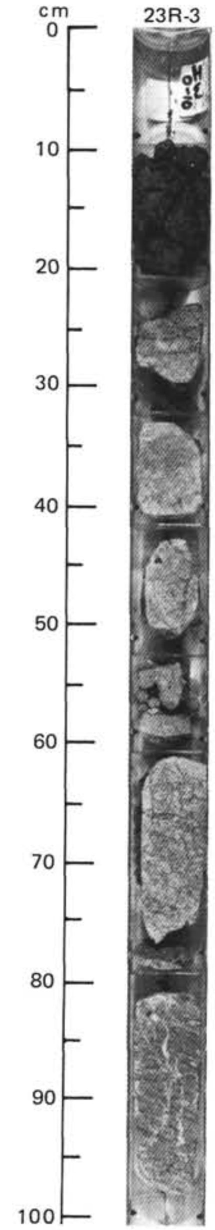

103-637A-24R

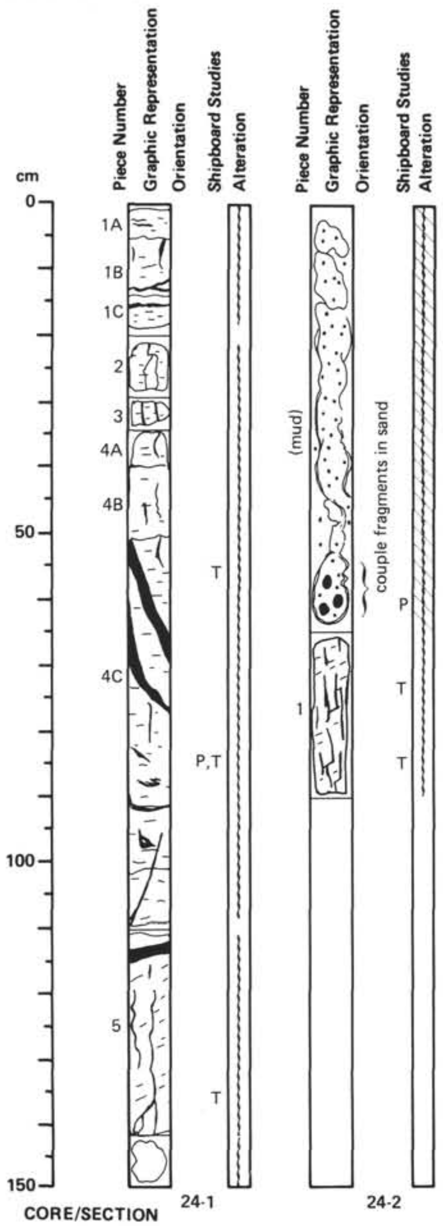

5528.9–5538.5 mbsl **218.4–228.0 mbsf**

SERPENTINIZED PORPHYROCLASTIC HARZBURGITE

Coarse porphyroclastic harzburgite with foliation defined by the alignment of oval-shaped orthopyroxene and chromium spinel. The rock is cut by thick (1–2.5 cm) diagonal and vertical calcite veins which appear to become more regularly spaced downcore. The bottom of Section 637A-1 and the top of Section 637A-2 include a pink-gray mud and sand with Miocene discoasters. The rock is almost completley altered (95%–100%) to serpentine. A few fragments of the pyroxene porphyroclasts remain. Abundant thin calcite veins dissect the rock. The rock is a pyroxene-poor harzburgite with 90% serpentine derived from olivine, < 10% orthopyroxene, 1–2% clinopyroxene, and 1% chromium spinel. It is sheared, as shown by the strong elongation of orthopyroxene pseudomorphs.

Thin Section Description

637A-24R-1, 55–58 cm: Porphyroclastic, foliated harzburgite, which is almost completely altered. Original mineralogy included 90% olivine (now serpentine), 10% orthopyroxene, 1% clinopyroxene, and 1% chromium spinel. The orthopyroxenes are oval, up to 7 mm in size, and are mostly altered to serpentine and replaced by calcite. However, the pseudomorphs preserve the original grain morphology, which includes curved and bent lamellae of clinopyroxene. Clinopyroxene occurs in rounded grains 1–2 mm in size. The chromium spinel is light brown in color, fractured, and elongated parallel to the foliation. Essentially none of the original mineralogy of the rock remains; the composition of the rock now consists of 70% serpentine and 25% calcite (both veins and replacing pyroxene), and about 5% Fe-oxides which occur as amorphous red material associated with some of the calcite veins.

	1, 83 (#4C)	2, 71 (#1)
V_p(a)	3.41	3.01
V_p(b)	3.37	3.33
V_p(c)	3.23	3.02
ρb	2.50	2.49

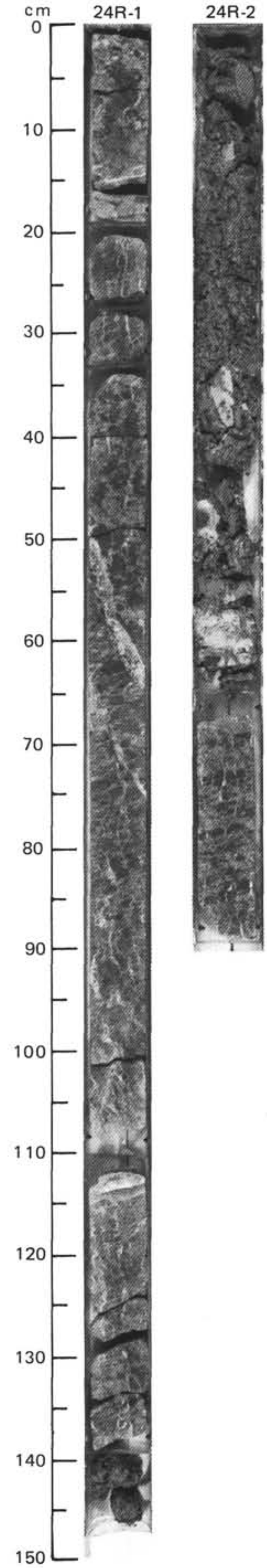

103-637A-25R

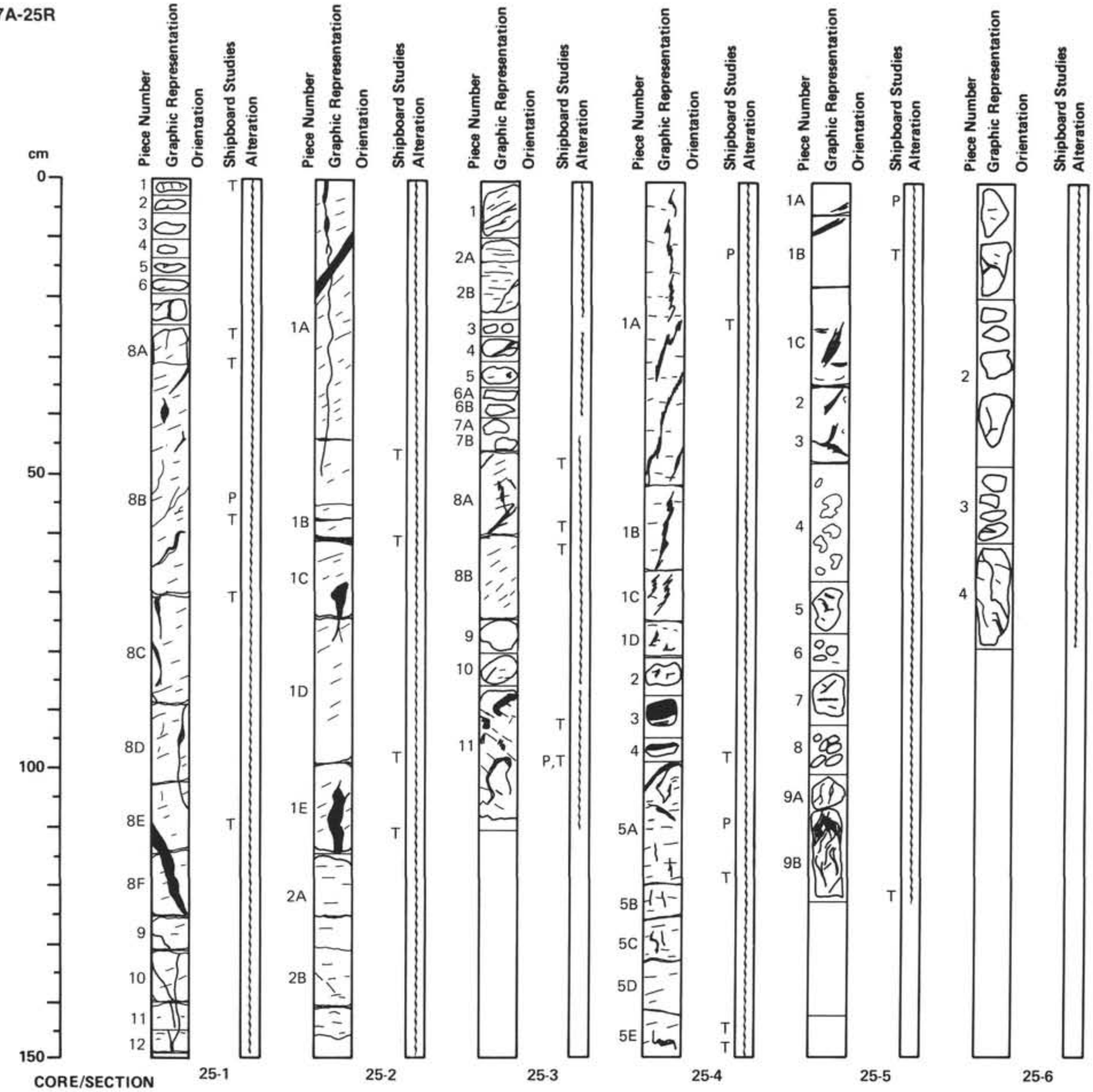

5538.5-5547.7 mbsl **228.0–237.2 mbsf**

SERPENTINIZED PORPHYROCLASTIC HARZBURGITE

The top of this core is composed of a gray-green homogeneous foliated peridotite which displays porphyroclastic textures. It is dissected by small calcite veins which are oriented at a high angle to the foliation. The calcite often contains small inclusions of magnetite. The degree of deformation, marked by the extreme elongation of orthopyroxene, increases downward to the middle of the core. This is also the case for the serpentinization of the peridotite, and almost no relict primary phases are preserved. Calcite veining is not as extensive, but increases again towards the base of the core. The bottom sections contain pyroxene-poor harzburgite which is highly serpentinized and brecciated; a lot of serpentine rubble was recovered, with large (2–3 cm) calcite veins.

Thin Section Description

637A-25R-4, 99–100 cm: This sample is a sheared peridotite displaying a mylonitic texture. The crystal size is generally small (< 5 mm). The original mineralogy of the rock included about 80% olivine, 15% orthopyroxene, 5% clinopyroxene, and 1% chromium spinel. The olivine is completely serpentinized. The orthopyroxene is extremely elongated (1 by 8–10 mm), and displays thin exsolution lamellae of clinopyroxene. The clinopyroxene constitutes either isolated rounded crystals or forms small lenses (.1–.5 mm) parallel to the foliation. The chromium spinel is elongate, fractured, and embayed. The rock is highly altered, and mostly replaced by serpentine. A few relict mineral fragments are observed in the serpentine mesh. This sample contains less calcite than most of the other samples. The calcite veins are small (.1–.5 mm), and are finely crystalline with abundant fine opaque inclusions.

	1, 60 (#8B)	2, 48 (#1A)	3, 91 (#11)	4, 25 (#1A)	4, 118 (#59)	5, 12 (#19C)
V_p(a)	3.31	3.47	3.01	3.74	4.34	4.18
V_p(b)	3.56	3.68	3.12	3.67	4.69	4.69
V_p(c)	3.61	3.71	2.94	3.74	4.56	4.44
ρb	2.51	2.48	2.79	—	2.57	2.91

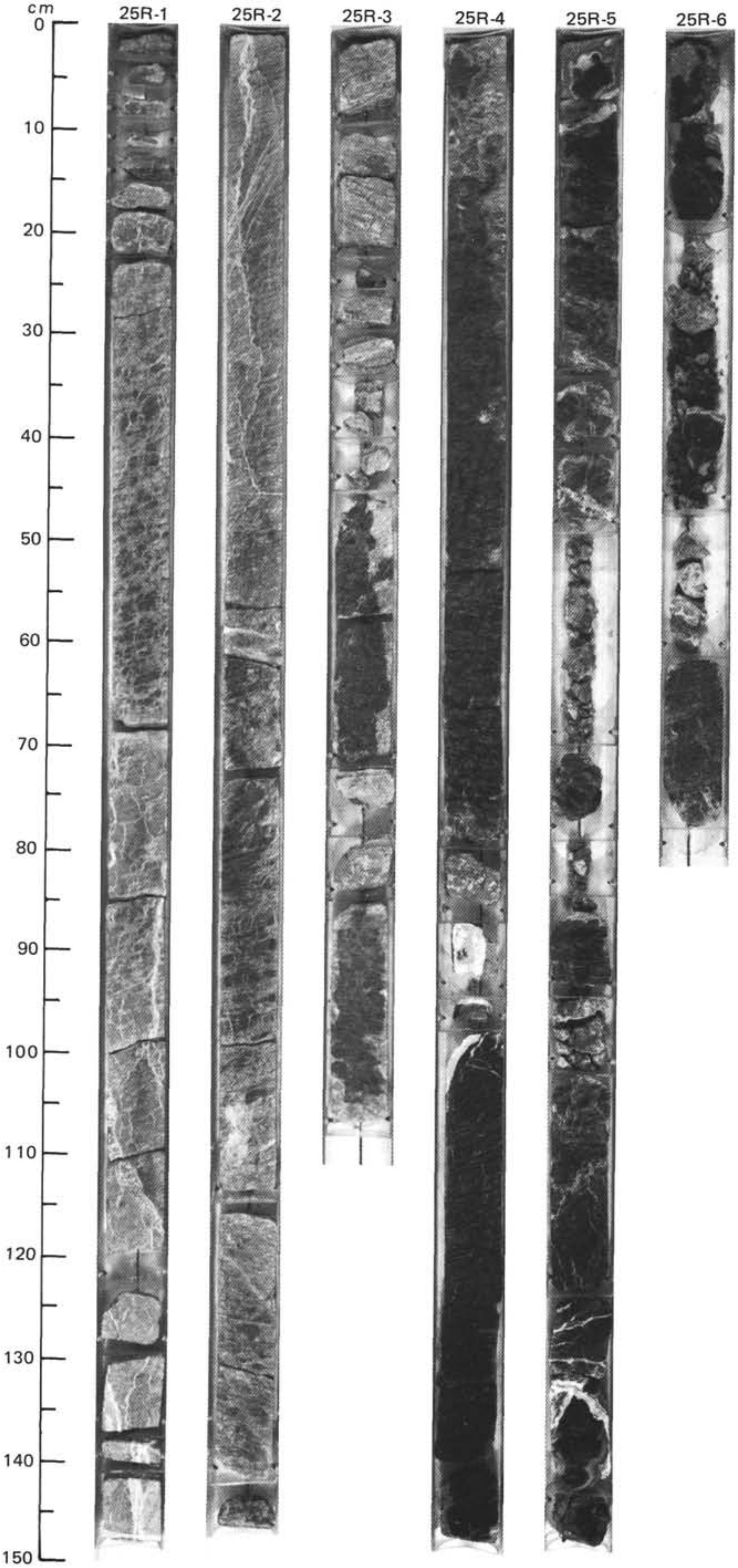
cm
0
10
20
30
40
50
60
70
80
90
100
110
120
130
140
150
25R-1
25R-2
25R-3
25R-4
25R-5
25R-6

103-637A-26R

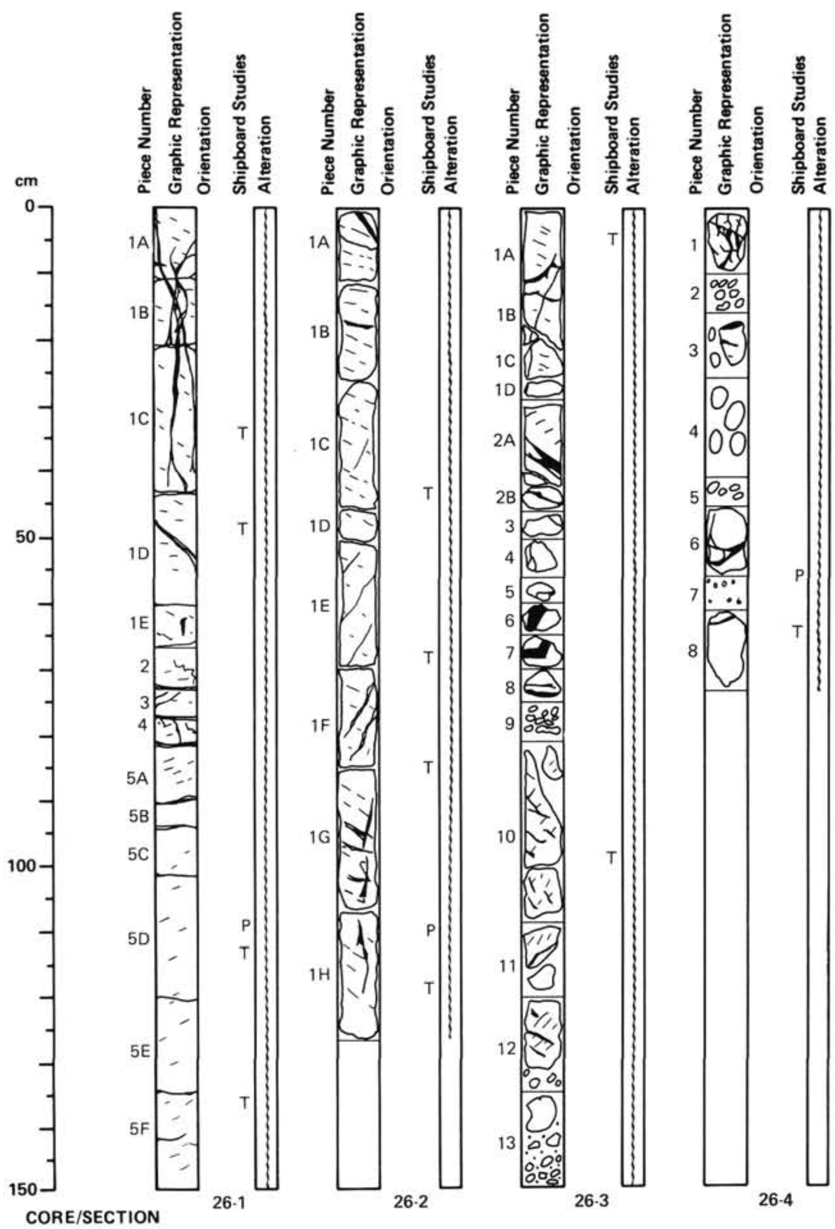

5547.4–5557.4 mbsl **237.2–246.9**

SERPENTINIZED PORPHYROCLASTIC HARZBURGITE

This core consists of highly altered peridotite which is variably veined by calcite. The veining is especially notable at the top and the bottom of the core. The veins are thick, zoned, and are coarsely crystalline with comb structures. Serpentine veining is also pervasive. The middle of the core includes massive, strongly altered and sheared, pyroxene-poor harzburgite. The orthopyroxene, which constitutes less than 10% of the rock, is highly elongate and strained; the clinopyroxene is rounded and often replaced by calcite. The base of the core contains brecciated serpentinite and black serpentine rubble. Many of the cobble-sized pieces contain large calcite veins.

Thin Section Description

637A-26R-1, 36–40 cm: This section is a highly altered harzburgite with an original mineralogy of 80% olivine (now serpentinized), 10% orthopyroxene, 3–5% clinopyroxene, and 1–2% chromium spinel. The rock has a relatively fine-crystalline, porphyroclastic texture (the largest orthopyroxene crystals are 5 mm). Olivine is completely serpentinized. The orthopyroxenes are oval-shaped with abundant thin exsolution lamellae, and are generally serpentinized but the pseudomorphs preserve the original crystal sizes, shapes and deformation (bent lamellae). The clinopyroxenes are small (1–2 mm), equant, and are relatively unaltered. The light brown chromium spinels are fractured and have irregular, embayed outlines. Alteration includes serpentine meshwork and more massive veins which dissect the rock irregularly. These veins may be partially replaced by calcite. Calcite also occurs in separate veins of coarse, radiating crystals.

	1, 111 (#5D)	2,118(#1H)	4, 69 (#6)
V_p(a)	3.25	3.27	4.71
V_p(b)	3.63	4.08	4.82
V_p(c)	3.32	4.05	4.82
ρb	2.74	2.59	2.76

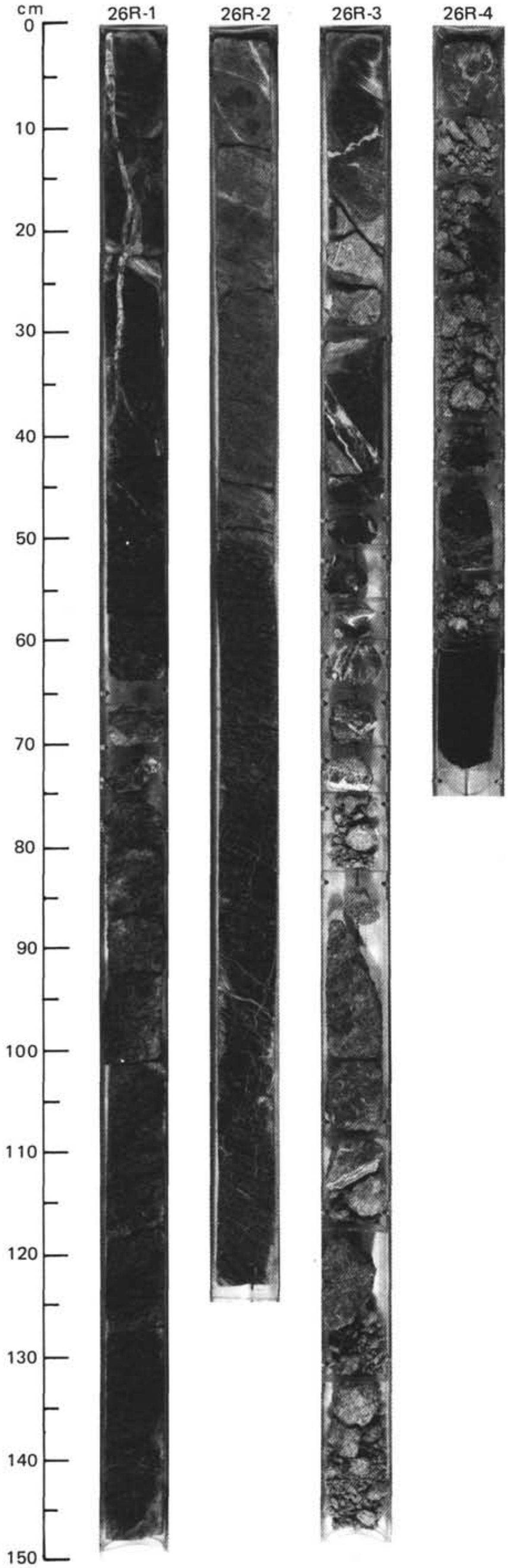
cm
0
10
20
30
40
50
60
70
80
90
100
110
120
130
140
150
26R-1
26R-2
26R-3
26R-4

103-637A-27R

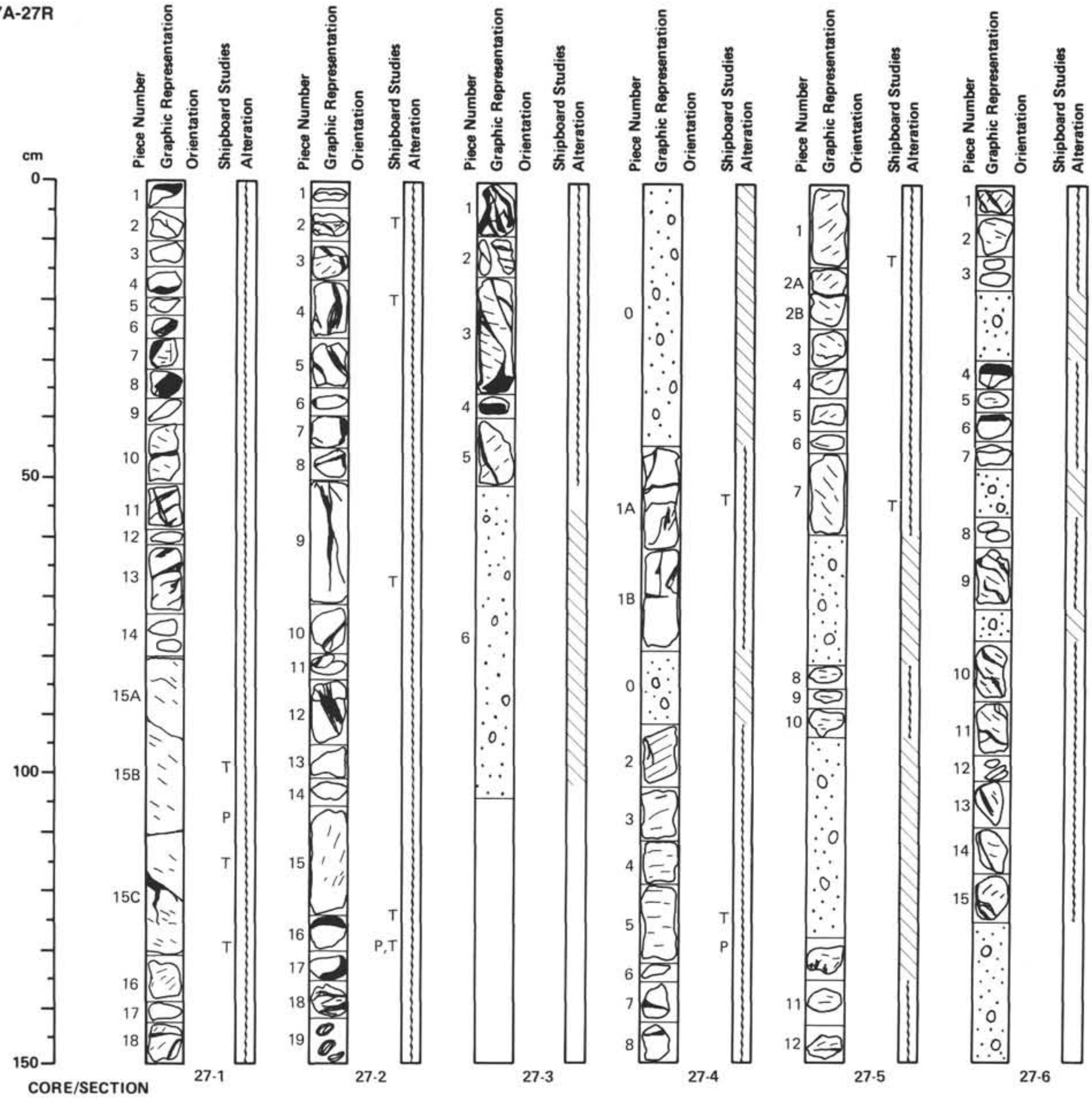

5557.4–5567.1 mbsl **246.9–256.6 mbsf**

SERPENTINIZED PORPHYROCLASTIC HARZBURGITE

This core consists of moderate to highly altered and sheared peridotite. Part of the recovered material includes some coarse-grained peridotite sand which was presumably a result of drilling. The top of the core includes cobble or smaller sized pieces of peridotite. This becomes more massive and less altered downward. Thin sections reveal the rock to be a pyroxene-rich harzburgite which contains more and larger fragments of the primary minerals (mostly orthopyroxene and clinopyroxene). The rock is black in color in the middle of the core, but is heavily veined with calcite. The rock grades into a pyroxene-poor (< 10%) harzburgite with local occurrences of pyroxene-rich layers (20–25% pyroxene). Some amphibole associated with the alteration of pyroxenes is observed. The abundance of shear zones increases downward. The base of the core is highly altered and friable; it contains pieces of peridotite with large calcite veins and breccias. The foliation of the rock increases to 45° at the base of the core.

Thin Section Description

637A-27R-1, 113–116 cm: This sample is a foliated, porphyroclastic, altered harzburgite with 75% serpentine derived from olivine, 15% orthopyroxene, 5% clinopyroxene, and 2% chromium spinel. The orthopyroxene crystals are about 5 mm in length, oval (with the long direction parallel to the foliation), highly altered to serpentine, and often rimmed by calcite. The pyroxenes seem to occur in bands in the peridotite. Small chromium spinel crystals are highly fractured and have very irregular morphologies. The rock comprises about 5% relict primary grains, 90% serpentine, and 5% calcite which is associated with altered pyroxene and also occurs in thin veins.

	1, 108 (#15B)	2, 124 (#16)	4, 127 (#5)
V_p(a)	4.00	4.89	3.39
V_p(b)	4.37	4.65	3.96
V_p(c)	4.40	5.03	3.84
ρb	2.53	2.87	3.36

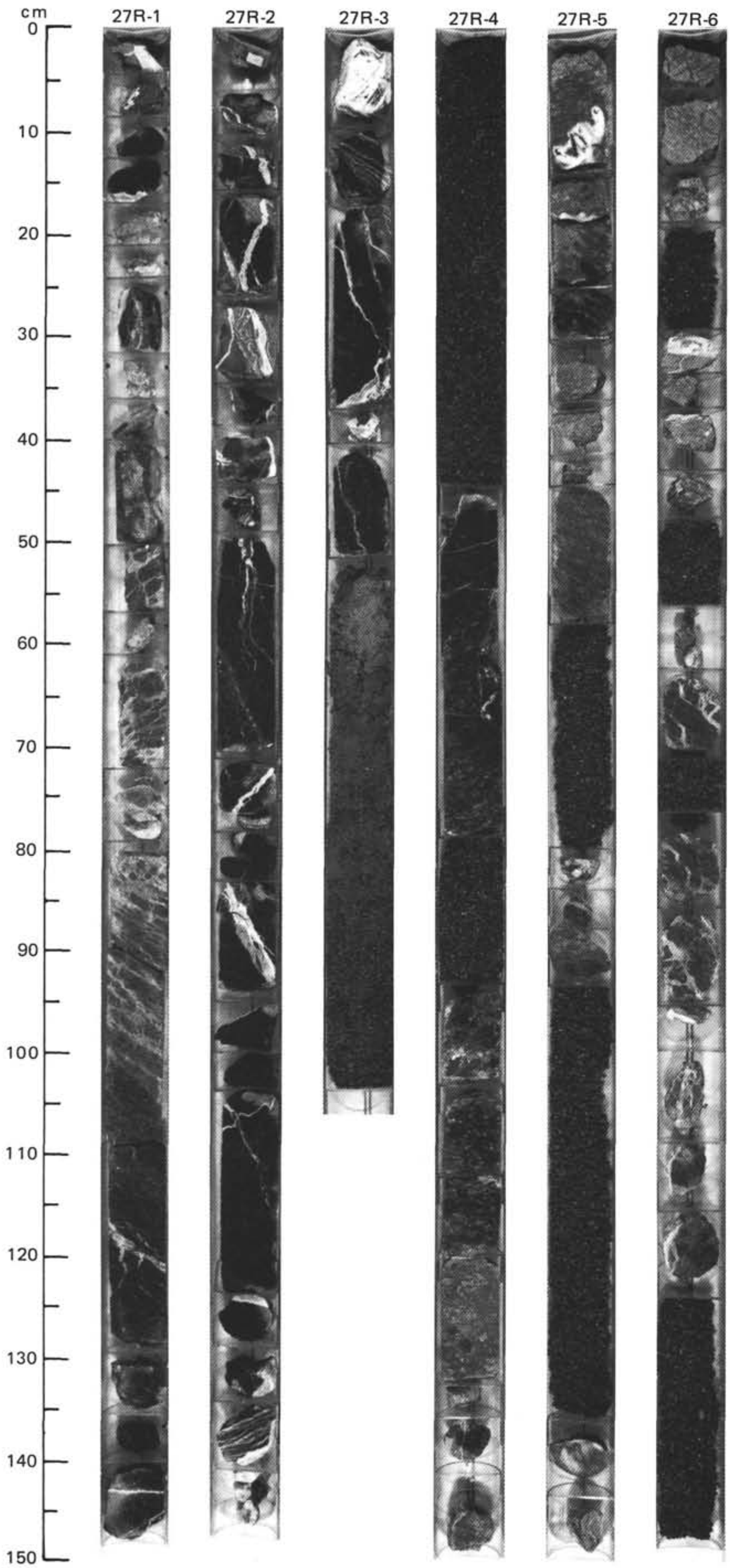
cm
0
10
20
30
40
50
60
70
80
90
100
110
120
130
140
150
27R-1
27R-2
27R-3
27R-4
27R-5
27R-6

103-637A-28R

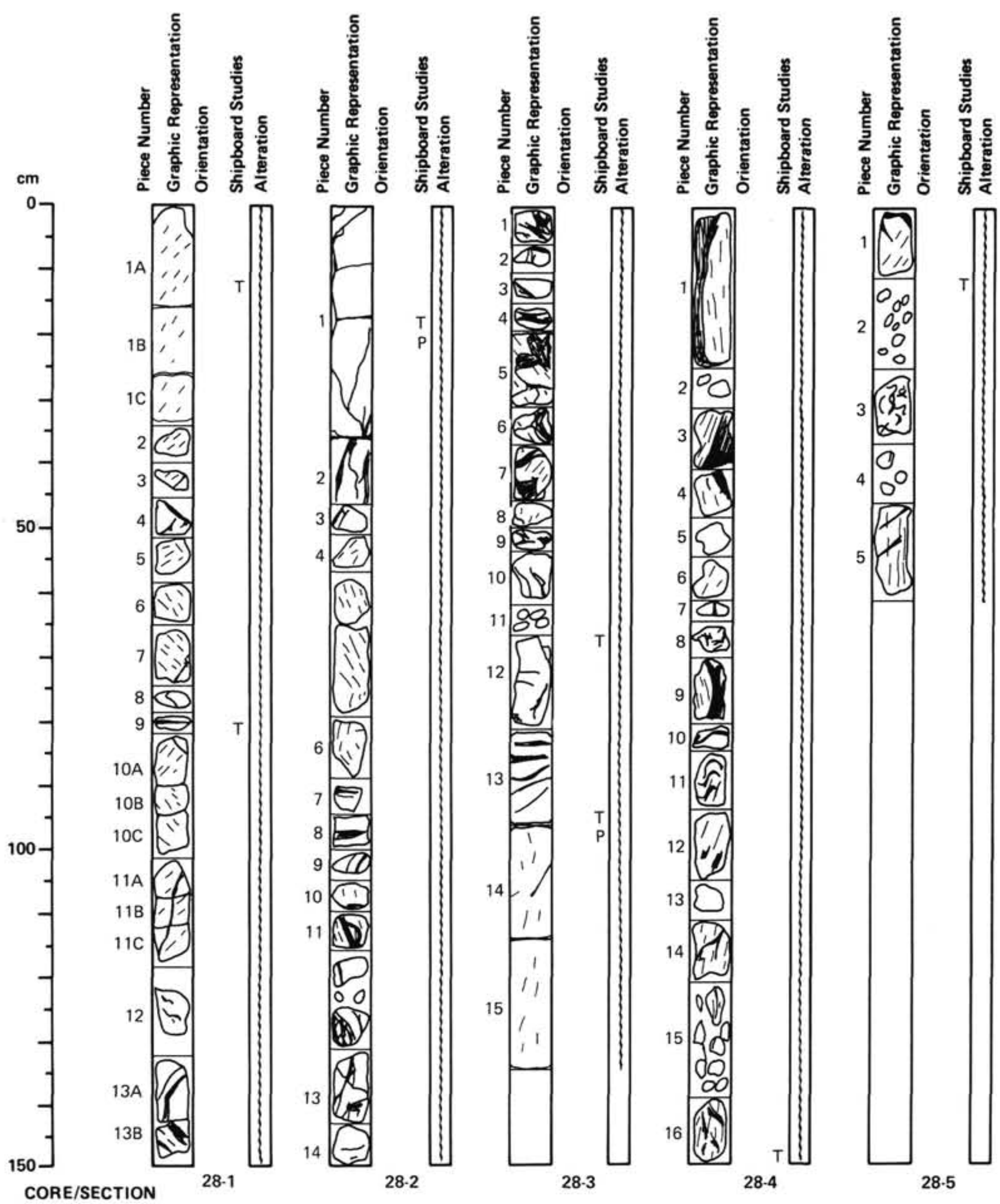

5567.1–5576.4 mbsl **256.6–266.3 mbsf**

SERPENTINIZED PORPHYROCLASTIC HARZBURGITE

This core consists of gray-green coarse to fine-grained porphyroclastic peridotites which are pyroxene-poor (10–15% pyroxene). The apparent foliation is about 45–50° at the top of the core, steepens to 75–80° mid-core, and is near vertical at the base. The rock has a well-developed foliation, which is evident in thin section (extreme elongation of orthopyroxene, fragmented clinopyroxene and chromium spinel crystals which are strung out along the foliation plane). The rock becomes increasingly altered and brecciated downsection, and virtually no relict fragments of the primary minerals are preserved. The color changes to red-green and black downsection. The peridotite is broken into many cobble-sized pieces which have thick calcite veins and fibrous serpentine veins.

Thin Section Description

637A-28R-1, 81–83 cm: This section is a sheared, porphyroclastic harzburgite with original mineralogy of 75% olivine, 20% orthopyroxene, 2–3% clinopyroxene, and 1% chromium spinel. The orthopyroxene crystals are stretched to lengths greater than 1 cm and show deformation by gliding. They are replaced by serpentine and calcite. Clinopyroxene crystals are equant, fractured, and are also rimmed and replaced by calcite. The pyroxenes seem to be associated in bands parallel to the sheared foliation. Chromium spinel crystals are small (< 1 mm), are highly brecciated, and the fragments are strung out along the foliation plane. The rock comprises about 80% serpentine, both as direct alteration of the mafic minerals and also as thin tension gashes (1 by 10 mm) which are perpendicular to the main foliation. About 15% of the rock is calcite which replaces pyroxene grains and occurs as relatively large (2–3 mm) veins. The remaining 5% of the rock includes relicts of the original mineralogy.

	2, 21 (#1)	3, 98 (#14)
$V_p(a)$	—	3.49
$V_p(b)$	—	3.62
$V_p(c)$	—	3.95
ρb	2.73	2.97

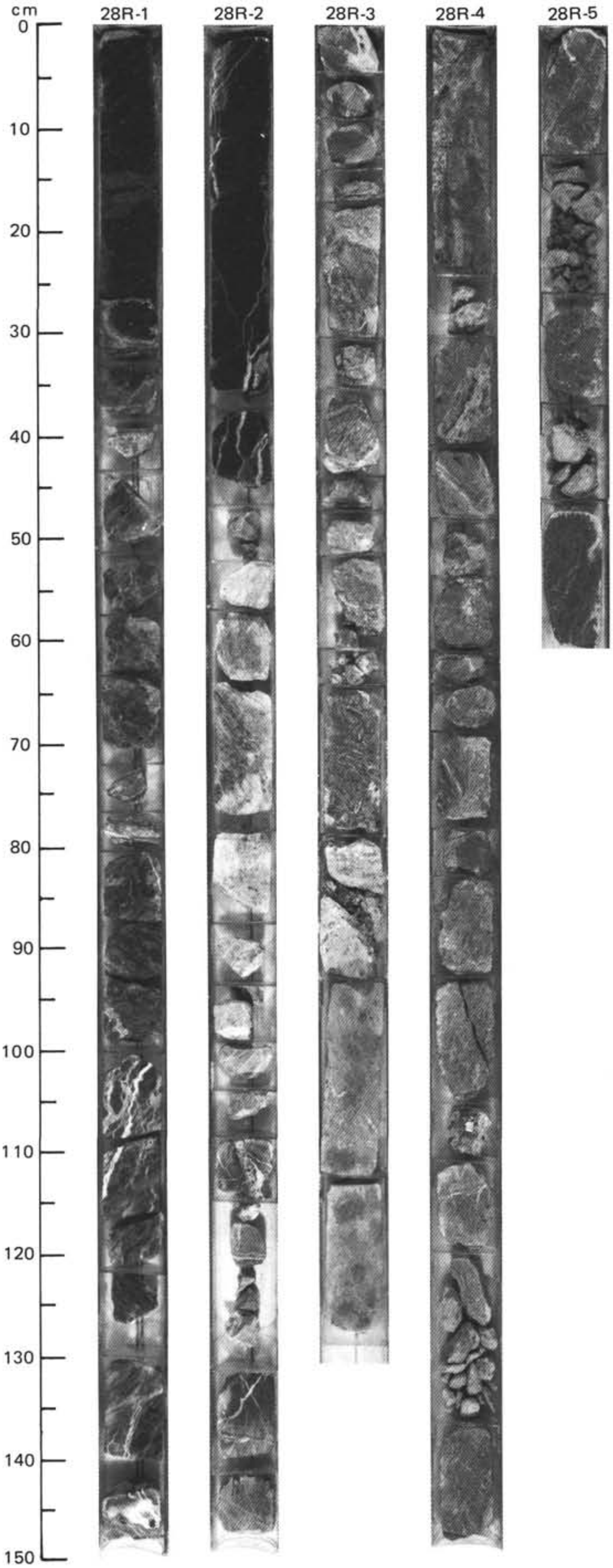
cm
0
10
20
30
40
50
60
70
80
90
100
110
120
130
140
150
28R-1
28R-2
28R-3
28R-4
28R-5

103-637A-29R

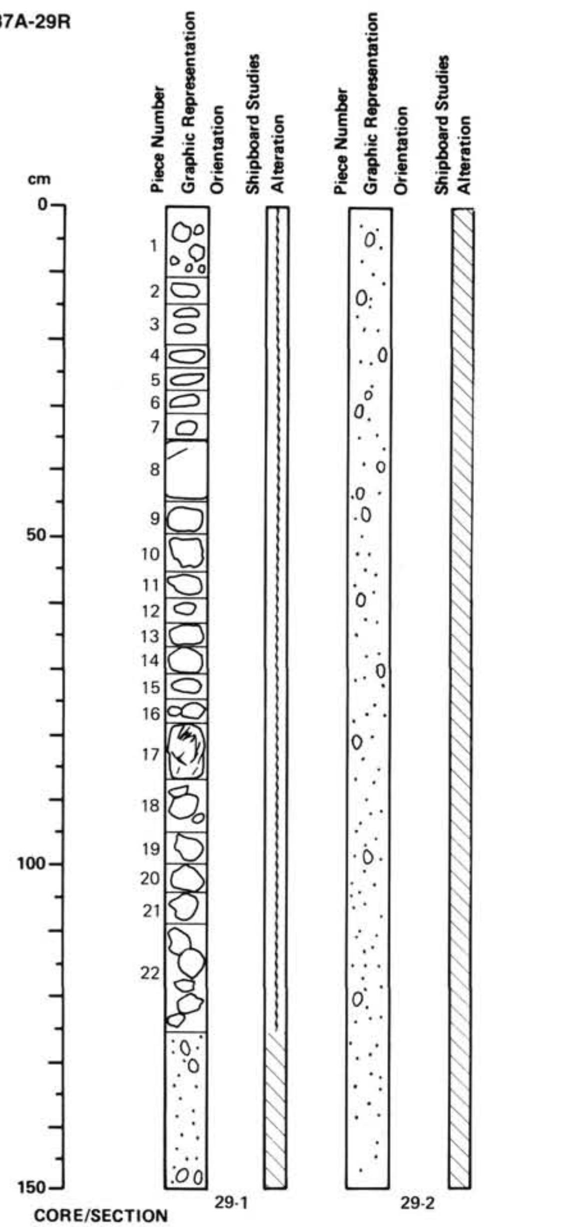

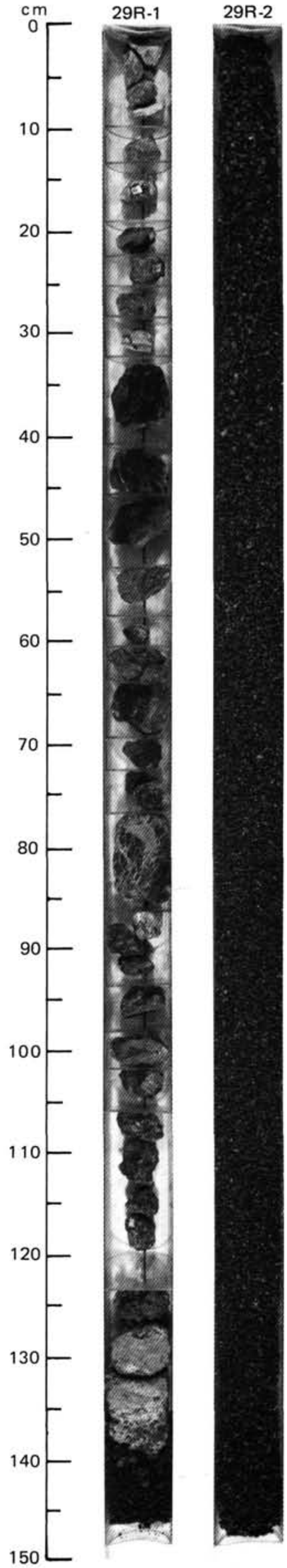

5576.4–5586.0 mbsl **266.3–275.9 mbsf**

ALTERED PERIDOTITE

Very friable and heavily altered peridotite was recovered in this core. It is broken up into many pieces. The color changes from red-green to black downcore. The upper part of the core contains pieces which are cut by abundant calcite veins, but this changes downwards into pieces with no calcite veins where the rock has a vertical foliation and is highly sheared. The base of the core recovered a coarse, poorly sorted peridotite sand, which is presumably the product of drilling. No shipboard thin sections were made.

103-637A-30R

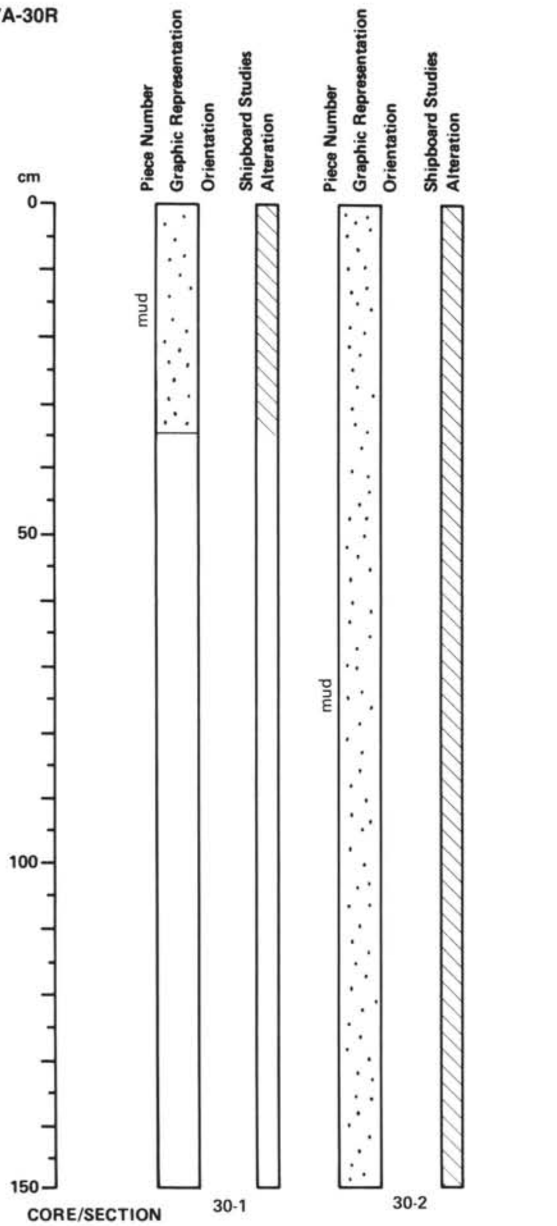

5586.0–5595.7 mbsl

275.9–285.6 mbsf

SERPENTINE MUD

Only a blue-gray mud was recovered in this core. It has the composition of serpentine (chrysotile and lizardite), and is presumably drill gouge material.